# Production and characterization of reinforced hydroxyapatite for bone replacement.

Parsons, Norah Sophienaz

# PRODUCTION AND CHARACTERIZATION OF REINFORCED HYDROXYAPATITE FOR BONE REPLACEMENT

NORAH SOPHIENAZ PARSONS

**THESIS SUBMITTED FOR THE DEGREE OF DOCTOR OF PHILOSOPHY**

**FEBRUARY 2001**


INTERDISCIPLINIARY RESEARCH CENTRE IN BIOMEDICAL MATERIALS, QUEEN MARY UNIVERSITY OF LONDON

UNIVERSITY OF LONDON

***I dedicate this thesis to the people who believed I could do it.***

*"The great tragedy of science-the slaying of a beautiful hypothesis by an ugly fact"*

**Thomas Huxley**

*"It is not always as easy as you might think to tell when a scientist is successful. But one sound practical indication that your efforts are being rewarded by a modicum of success is that other scientists start to hate you"*

**Brian Malpass**

## ABSTRACT

Hydroxyapatite(HA) is a highly biocompatible calcium phosphate material which in porous form, promotes rapid bone ingrowth and revascularisation. As such it has potential for use as a synthetic bone graft substitute. However, due to poor mechanical strength, its use has been limited to non-major load bearing applications. In response, secondary phase additions such as calcium/phosphate-based glasses have been used to reinforce HA. However, the improved mechanical properties obtained by secondary-phase reinforcement are often associated with decomposition of the HA to tricalcium phosphate(TCP), which may be undesirable due to the increased solubility and controversial biocompatibility of the latter. The aim of this thesis was to produce a calcium/phosphate-based additive for reinforcing HA and to investigate the mechanical and chemical stability of this composite in a physiological environment. Furthermore, the possibility of transferring this technology to porous structures was investigated.

Prior to investigating the effects of second phase addition on strength and phase stability, the HA used in this study was characterized as having a biaxial flexural strength (BFS) of 65±11MPa and being chemically stable up to sintering temperatures of 1350°C. Two calcium/phosphate-based additives were produced with Ca/P ratios of 0.5 (CAP1) and 0.8 (CAP2); CAP1 was found to be amorphous, whilst CAP2 was predominantly crystalline in nature where the crystalline phase was primarily $Ca_2P_2O_7$. The maximal BFS value found for HA doped with 2.5 wt% CAP1 (CAP1HA) was 27MPa with up to 73%TCP, whilst the CAP2-doped HA (with 2.5 wt% CAP2) achieved a maximal BFS of 102±21MPa with up to 13%TCP. Thus CAP2HA was judged to be a successful composite suitable for more comprehensive investigation. Studies were carried out to decipher the ideal wt% of CAP2 to promote mechanical reinforcement with a minimal presence of TCP, using 1, 2.5 ,3.25 ,4 and 5 wt % CAP2. The results indicated that 2.5 wt% CAP2HA was optimal in terms of both the mechanical and chemical criteria. For investigating mechanical and chemical stability, the HA and CAP2HA samples were soaked in 50% strength Ringer's solution for periods of 1-30 days. HA retained 60% of its original strength, whilst CAP2HA retained 78% of its original strength. In view of the success in using CAP2 as a reinforcing additive, a preliminary investigation was carried out using HA and CAP2HA. This involved development of a technique for producing porous HA, using a reticulated foam template, with a highly interconnected structure and mean porosities and strengths of 66% and 2MPa. Porous samples of CAP2HA were also successfully produced however, only mean porosities and strengths of 75% and 0.6MPa were achieved. This was attributed to processing complications arising from the solubility of $Ca_2P_2O_7$ in water leading to inhibited sintering, which may be overcome by the use of a different binder system.

# ACKNOWLEDGEMENTS

Firstly, I would like to express my gratitude to my supervisors, Karin and Serena, for their guidance, help, and support throughout my PhD, especially over the last few months, which were challenging to say the least. Furthermore, I would like to thank Tom and Iain for their time and admirable patience, without which I would still not know how to work machinery in the laboratory, and Jawwad for helping me through ICPMS. Liz, thanks for all the advice and listening to me with an open mind. I owe a big general thanks to everyone else in the IRC who I have hassled for one thing or another these past three years.

I would like to thank my family for all the unconditional love and support I have received since I can remember, without which I certainly would not have made it through further education, not to mention the rest. As for Gabs, Fabio, Mr +Mrs.V, you have given me more support than you can imagine, and thank you so much for always being there for me (and feeding me!). Paul, Nick, Nicky, John, Iain, and Michelle, thank you so much for all the laughter, good times, and for winding me up (revenge will be mine.....one day).

I would not be here if it wasn't for the Materials Department, where I was inspired during my undergraduate years to do a PhD, so I would like to say a very big thank you to Sandra, Cath, Paul H, Ray S, Craig D, Andy B, Mike R, Xiao G, John B, Zsofia L, Mick W, Bob W, and of course James "Hey, kid!""How's it goin' team?" B. As for the suffering PhD lot in Materials, to my equally insane friend Silv, thanks for the skating sessions and giving me insight into my husband's bizarre role-playing activities and Mediterranean lifestyle. Huge thanks to Chulee for putting a smile on Silv's face. Rob, I want your car, and thanks for that spin around Docklands and all the beer sessions. Simon, you need a faster car, and thanks for all the support and chats.

ZouZou and Tony, Num-Num, Bong, Samaa, Big John, Mark, Dora, Neven, Marco, and Nelesh, and Judith, big warm thanks for all the coffee breaks, the chats, the mutual tears/laughter/hysteria, and most of all, thank you for putting up with my

dramas/moods/stroppy moments. And let's remember to meet up in a couple of years for a conference and tear the town to shreds.

To Curist Steph, thanks for all the inspiration, the chats, and for feeling my pain as I felt yours during these last years of multiple dramas. I would also like to thank Mike, Justin, Chester, and Chidgey for entertaining my husband with all your little toys and keeping him sane. As for my sanity these past few years, I owe a great deal of that to QMW Aikido club, without whom I would have had hypertension and angina by now if it had not been for the relaxation (thanks Femi!) and aggression-venting provided by Rick, Shane, Joanne, Ed, Oscar, Pete, John, Greg, Siam, Rishi, Kiaran, and Anna.

Last but definitely not least, I would like to thank Raff for loving me, making me very happy, and helping me to understand myself, and goodness knows that's not an easy task.

# TABLE OF CONTENTS

# LIST OF FIGURES

# LIST OF TABLES

# INTRODUCTION

The sintering characterisitics of hydroxyapatite ($Ca_{10}(PO_4)_6(OH)_2$) have an important role in affecting its' physical and mechanical properties. The temperature at which hydroxyapatite (HA) is sintered will affect the phase composition, which influences the solubility, and the degree of densification, which influences the strength. Extensive studies carried out on HA have revealed that it is a highly biocompatible material, which may stimulate boneingrowth in-vivo. However, the mechanical properties of HA, in dense and porous form, have been reported as relatively low. Therefore, in order for HA to display higher strength, so as to increase its potential for use in high load-bearing applications, it requires reinforcement in the form of a sintering aid. Calcium/phosphate-based glasses are ideal sintering aids because at high temperatures, they achieve viscosities low enough for enhancing densification by means of a liquid-assisted sintering process. However, glassy materials are calcium-deficient and will therefore affect the ionic behaviour of the composite during sintering.

Phase decomposition, which may occur at high sintering temperatures, involves the loss of hydroxyl ($OH^-$) ions. Calcium-deficient materials tend to lose more $OH^-$ at high temperature and decompose to form a biphasic material containing tricalcium phosphate (TCP), a highly resorbable material. Reinforcing HA with a calcium-deficient additive will reduce the overall Ca/P ratio, and will therefore cause it to promote decomposition at elevated temperatures, as opposed to its' stoichiometric counterpart, which has a Ca/P ratio of 1.67 and does not experience decomposition at high temperature. Bone substitute materials that behave as scaffolds, into which bone must grow, must not resorb too quickly in-vivo. Therefore it is fundamental to add an appropriate amount of the additive to achieve a balance between the amount of liquid-assisted sintering and the decomposition to TCP.

This thesis details a systematic study of the production and characterization HA, reinforced with glassy phases, in the hope of improving the strength, whilst minimising the decomposition to TCP. The chemical, mechanical and microscopical properties of the HA and its' reinforced composites were investigated in addition to the in-vitro assessment of biocompatibility. Following the identification of the composite with ideal physical and mechanical properties, an investigation into transferring this technology to porous structures was carried out.

# CHAPTER 1
# STRUCTURE AND PROPERTIES OF BONE

*This thesis is concerned with the production and characterization of materials used to replace bone, and the purpose of this chapter is to provide insight into the constituents, structure, and function of the original tissue to be replaced.*

## 1.1 INTRODUCTION

The skeleton is the structural and supportive framework of the body, which enables motion in vertebrates. The structure consists of bone, which is a hard, connective tissue that has a complex heirarchy of organised structures. Bone consists of cells embedded in mineralised tissue which, in turn, is composed of an organic matrix of collagen fibres reinforced by a mineral filler, hence bone is a composite. Furthermore, by delving deeper into the micro- and ultrastructural levels of bone, it can be shown that bone is a composite on many levels.

The functions of bone are mechanical and metabolic in nature. The former refers to the protection of vital organs as well as the provision of structural support, whilst the latter refers to the fact that bone acts as a reservoir for the calcium and phosphate ions needed for metabolism. The different structures of bone are adapted to the variety of mechanical functions that bone fulfills, hence the existence of structure-function relationships, which will be discussed in this chapter.

## 1.2 CONSTITUENTS OF BONE

The main constituents of bone are cells embedded in an extracellular matrix. There are two phases present in the extracellular matrix, namely an inorganic phase and an organic phase. The inorganic phase is composed of a calcium/phosphate mineral similar to hydroxyapatite. The organic phase is composed, primarily, of collagen (90-95%) (Vaughan, 1970) and the remainder is a homogeneous medium called ground substance, or cement (Pritchard, 1972), containing extracellular fluid and proteoglycans (Black et al, 1998). This ground substance is considered to be the phase in which discrete fibrils and crystals are embedded amongst mucopolysaccharides, glycoproteins, lipids, carbonate, citrate, sodium, magnesium, and fluoride (Pritchard, 1972), resulting in a mixture of proteins and mineral salts.

### 1.2.1 ORGANIC COMPONENT

Collagen is a protein that occurs in calcifying as well as non-calcifying tissues, and is found in several varieties. The form of collagen found in bone is referred to as *type I* and is comprised of three polypeptide chains that make up the collagen molecule, which are arranged in a triple-helix formation. Each collagen molecule, termed tropocollagen, measures about 300 nm in length, and together they are organised in highly ordered fibrils, which are held together by inter- and intra-molecular cross-links. This tough organic matrix provides a framework upon which the mineral component is deposited within the bone. There is much argument as to the way in which the collagen fibrils are arranged. One model which seems to be the most commonly accepted is that proposed by Grant et al (1965) in which filaments 2800 nm (28000 Å) in length are divided into five bonding zones and four non-bonding zones with respective approximate lengths of 26.5 nm (265Å) and 37.5 nm (375Å) (Figure 1.1). The remaining 5 % of the organic matrix consists of non-collagenous proteins, which are closely associated with bone collagen, in terms of promoting the initial deposition of apatite mineral and regulating the size,

orientation and growth rate of bone mineral crystals. These non-collagenous proteins are phosphoproteins, glycoproteins, gamma carboxy-glutamic acid proteins, and proteoglycans.

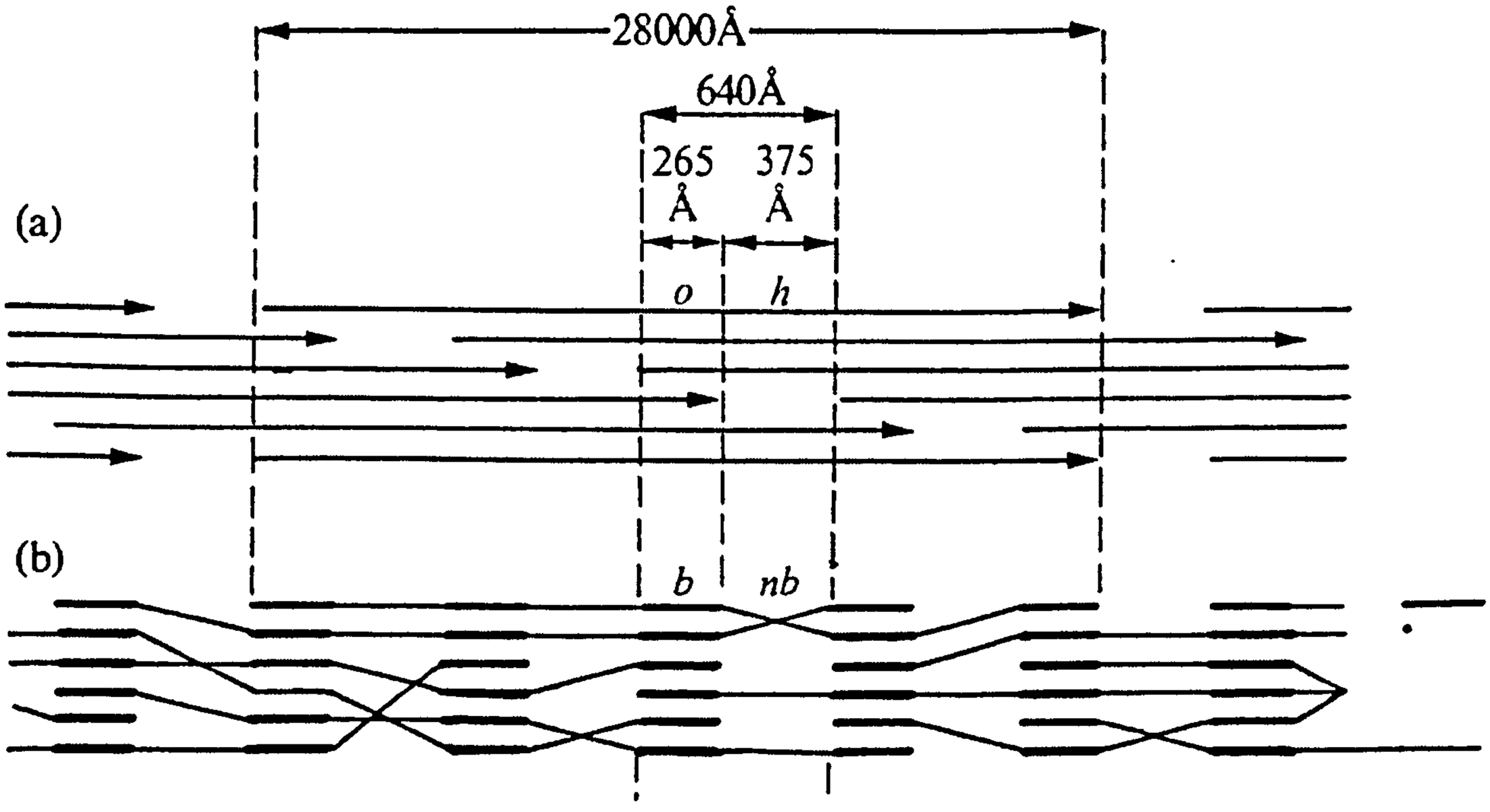


**Figure 1.1** Diagrammatic scheme proposed for the organization of tropocollagen molecules into fibrils (o = overlap zone; h = 'hole' zone) (Grant et al, 1965)

### 1.2.2 INORGANIC COMPONENT

The mineral/inorganic phase of bone is incorporated into the organic matrix, and is principally composed of calcium phosphate crystals. The major crystalline salt present in bone is similar to hydroxyapatite ( $Ca_{10}(PO_4)_6(OH)_2$ ). Fernandez-Moran (1957) found that deproteinated bone, when observed at high magnification using electron microscopy, exhibited myriads of tightly packed, minute crystals 3 – 5 nm wide and up to 60 nm long. Engstrom (1960) discovered that these crystals gave an X-ray diffraction pattern similar

to that of the above-mentioned hydroxyapatite, hence the inorganic component of bone is often referred to as hydroxyapatite. However, this is strictly incorrect as natural bone mineral is a calcium deficient carbonate substituted apatite additionally containing other ions such as $Na^+$, $Mg^{2+}$, $F^-$, and $Cl^-$. The mixture of soft, organic collagen and hard, crystalline phases provide bone with elastic properties, whilst maintaining mechanical strength. Collagen provides ductility and bone mineral provides the mechanical integrity sufficient to sustain body weight and to enable motion. Together, collagen and mineral make a biological composite with unique properties that shall be discussed later in section *1.6*.

## 1.3 STRUCTURE OF BONE

### 1.3.1 MACROSTRUCTURE

In the mature skeleton, two types of bone structure are seen macroscopically:

- Compact, or *cortical* bone, is mostly situated in the long shafts of the long bones, eg. femur, tibia, humerus, and radius, where it surrounds the marrow cavities, and covers the ends of the shaft.
- Spongy, trabecular, or *cancellous* bone, is found largely in the flat bones, in the vertebrae, and in the ends of long bones, and consists of a foam-like structure of pores and struts. Cancellous bone has been classed as a foam (Gibson and Ashby, 1988) with a mixture of open and closed porosity, whereby the open foams have interconnecting cells and the closed foams consist of cells, which are separate from their neighbouring cells.

The following diagram illustrates the relative structural organization between cortical/compact bone, cancellous/spongy bone and the marrow cavities between both the trabeculae and within the cortical bone:

# CHAPTER 1
# STRUCTURE AND PROPERTIES OF BONE

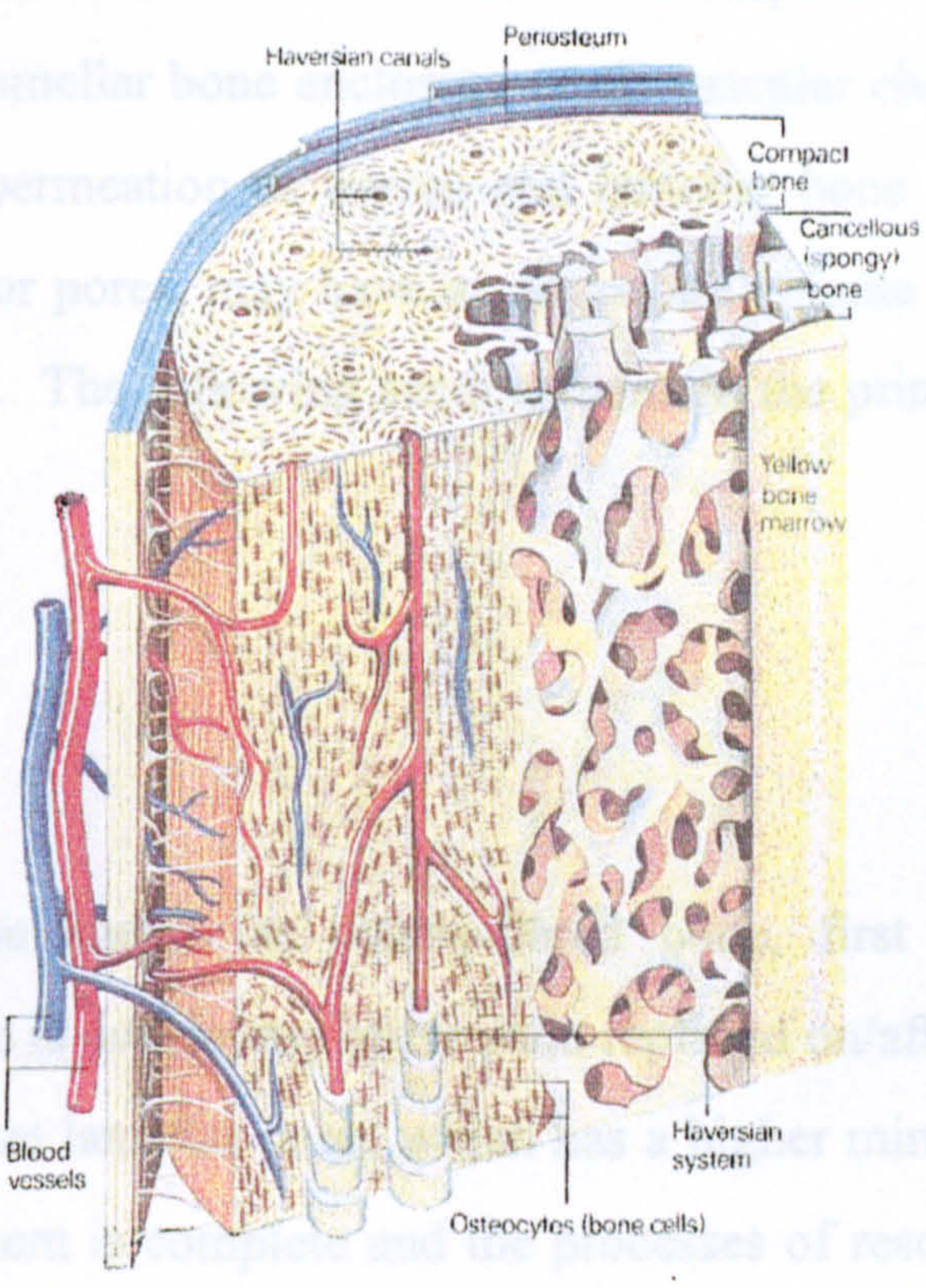


**Figure 1.2** Structure of long bone shaft showing the location of the compact and spongy bone (Weston 1985)

Cortical bone may be regarded as the hard outer skin of the long bone, encapsulating the marrow cavity in the shaft and cancellous bone in the epiphyseal regions. The cellular encapsulating medium of long bone is the periosteum, which consists of two layers; an inner, cellular, osteogenic layer, and an outer, fibrous connective tissue layer conveying the blood vessels and nerves supplying the bone. A further layer of cells lines the inner layer of the central medullary canal, i.e. the endosteum.

### 1.3.2 MICROSTRUCTURE

As mentioned in the previous section, bone is categorised as either cortical or cancellous, on a macrostructural scale. However, there are two chief microstructural types of bone; woven or coarse-fibre, and lamellar or fine-fibre bone respectively. Cortical bone arises from both woven and lamellar bone enclosing small vascular channels, while cancellous bone results from the permeation of woven and lamellar bone by many large vascular spaces. These spaces, or pores, may have an aggregate volume equal to or greater than that of the bone matrix. The following sections contain the principal features of woven and lamellar bone.

#### 1.3.2.1 Woven bone

Woven bone, otherwise known as coarse-fibred bone, first appears in embryonic development as the bone is developing but is soon replaced on/after birth by another type of bone, known as mature lamellar bone, which has a higher mineral content. After two or three years, replacement is complete and the processes of resorption and replacement are initiated. The mature lamellar bone generally replaces the woven bone except at certain sites such as the tooth socket, at cranial sutures (Cowin et al 1986), and near tendon insertions and ligament attachments (Vaughan, 1970). Woven bone is also characteristic of early fracture callus at fracture sites due to its association with rapid formation and active growth.

As stated previously, woven bone may enclose small channels or large spaces, but in its commonest form, it consists of an irregular array of spaces separated by walls of substance of varying thickness, much like a porous structure containing pores separated by struts. These strut-like walls are referred to as trabeculae, within which they contain coarse collagenous fiber bundles, which interweave in a random manner, thereby running in all spatial directions, unlike the characteristically ordered arrangement of lamellar

bone. These fibre bundles are commonly referred to as osteogenic fibres and between them and the calcified bone matrix lies "osteoid", a zone whereby the fibres are not yet calcified. Another characteristic of woven bone is the random distribution of osteocytes in the bone matrix (Figure 1.3), and the random orientation of osteocytes with respect to the vascular channels, as opposed to the relative order of such in lamellar bone.

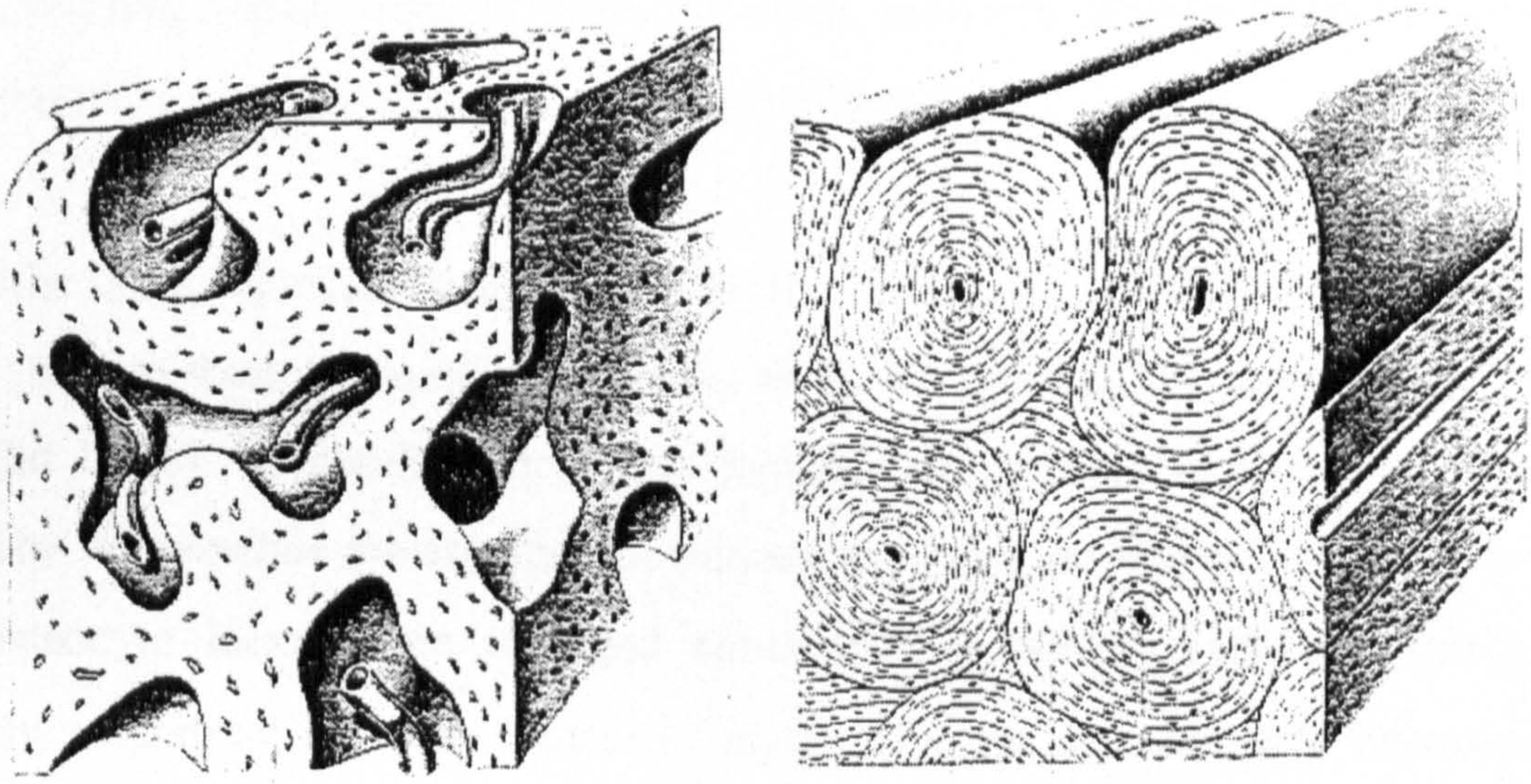

**Figure 1.3** 3-D representation of differences between (a) Woven bone and (b) Lamellar Bone (Hancox, 1972)

In terms of appearance, the particular plane of section of woven bone can affect its perceived structure. For example, in some sections the bony structure may resemble a mesh of wire whilst in other sections, the impression is given of a series of parallel trabeculae with few cross connections (Pritchard, 1972). However, the overall three-dimensional appearance reveals a honeycomb-like structure with the majority of the blood vessels running in a parallel fashion.

### 1.3.2.2 Lamellar Bone

Lamellar bone, otherwise known as mature bone, is a more slowly forming tissue which differs from woven bone mainly because it has fine, organised collagen fibres in the form of sheets, i.e. the lamellae, and an ordered, regular array of osteocytes (Figure 1.4). Numerous layers of lamellar bone may accumulate on the outer or periosteal surface of bone, forming a thick, cortical plate. However, only two or three layers of lamellar bone are present in the inner or endosteal surface of bone.

Lamellar bone is present in three main forms. Firstly, the lamellae may just lie on top of each other, in stack-like extended parallel arrays of lamellae (often called circumferential lamellar bone). Secondly, concentric lamellae are present in the form of cylinders, whereby the lamellae are arranged in concentric circles around each other. Furthermore, the osteocyte lacunae are arranged concentrically, within each concentric lamella. Thirdly, interstitial lamellae consist of layers of lamellae interposed between osteons, often as a remainder from the normal turnover of bone resorption.

With regards to the concentric lamellae, the above mentioned cylinders are referred to as osteons, which may fill spaces left as a result of the rapid growth of woven bone to form a mixed bone type called fibrolamellar bone (Weiner et al, 1999). This constitutes so-called highly elongated primary osteons. Osteons may alternatively be produced secondarily, following bone remodelling whereby earlier formed bone is removed. Secondary osteons are of cylindrical form and surround what is called a Haversian canal; this constitutes a Haversian system.

The purpose of the Haversian canal is to act as a conduit for the blood vessels that nourish bone. As seen in Figure 1.4 (Vaughan, 1970), osteocytes surround each Haversian system and communicate to one another through their canaliculi, up until the

cement line, after which communication stops. The cement line contains each Haversian system, and is the characteristic end feature of an osteon. Another important feature of Figure 1.4 is the variably sized Haversian canals, whereby the larger canals are indicative of bone resorption and have an irregular edge. These types of canals are called resorption cavities where bone mineral and matrix may be removed whilst osteoid tissue is being laid down in another area of the cavity. The osteoid tissue becomes mineralized as it is laid down in the Haversian system.

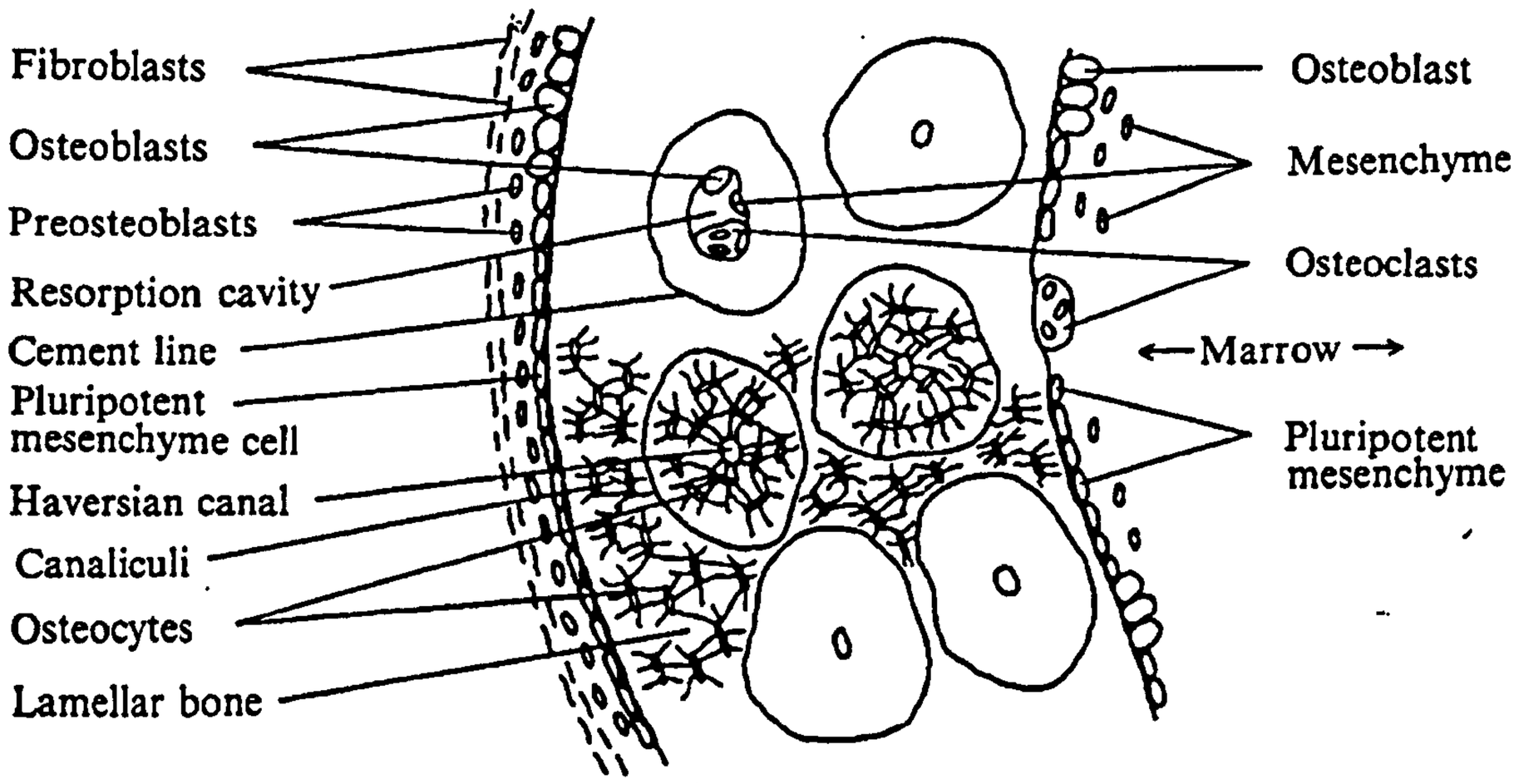


**Figure 1.4** Cross-section of adult cortical bone to show the arrangement of Haversian canals, resorption cavities, osteocytes with connecting canaliculi and cells lining the surfaces (Vaughan, 1970)

According to Riqles et al (1991), only large animals have a tendency to produce mature bones almost entirely composed of osteons, whereas in smaller animals, the bone remains composed of initially deposited primary lamellar bone. In cases where there are concentrated areas of osteons in smaller animals, they are often associated with points of ligament or tendon attachment.

### 1.3.3 ULTRASTRUCTURE

The ultrastructure of bone refers to the intimate arrangement of collagen fibers and bone mineral crystals. There are many hypotheses in the literature as to the bone mineral crystal shape, the mechanism and site of nucleation, and how collagen fibres and bone mineral crystallites are related to each other. However, there are significant difficulties associated with deciphering these parameters, which lead to variable results and general disagreement; as a result, currently the nature of the ultrastructure of bone is unresolved. However, there is general agreement that there are many complex processes involved in the mechanism of the mineralisation of the collagen, which mostly depend on enzymatic reactions that result from ion/matrix interactions. Unfortunately, it is very difficult to investigate the crystal organization of bone due to the difficulties in preparing thin specimens containing mineral for transmission electron microscopical examination without incorporating preparation artefacts.

In 1966, Pautard proposed that ionic calcium/phosphate was originally bound to a non-collagenous component of the matrix; bone mineral crystals were then thought to nucleate on the collagen. In terms of orientation, White et al (1977) proposed that within the collagenous matrix, the bone mineral crystals evolve in a way such that the c-axis of its' crystal is always parallel to the fibre axis of the collagen. This is consistent with earlier findings determined with electron microscopy (Fitton-Jackson et al, 1956; Fernandez-Moran, 1957). Furthermore, the way in which the collagen fibrils are woven influences the calcifiability of bone collagen, thereby regulating mineralisation, and controlling the size of the mineral crystallites. This highlights the importance of collagen for bone formation and development.

Despite the various theories, it is safe to assume that the key to determining the ultrastructure of bone is to investigate the manner in which the crytals are arranged in the mineralized collagen fibril, the basic building block. More recently in 1986, Weiner et al showed that the crystals are arranged in parallel layers through the fibril, which is consistent with not only the authors mentioned in the previous paragraph, but also with the findings of Landis et al (1993) who confirmed his data with TEM tomographic studies and also with Erts et al (1994) who used atomic force microscopy to study mineral orientation. Rho et al (1998) also advocates the theory that the mineral crystals grow with a specific crystalline orientation, i.e. that the "c" axis of the crystals are roughly parallel to the long axis of the collagen fibrils. Furthermore, they reported that the plate-like apatite crystals of bone occur within the discrete spaces within collagen fibrils, as demonstrated in Figure 1.5 (Rho et al, 1998).

The question of whether the layered arrangement of the crystals in one collagen fibril is alligned with neighbouring fibrils has yet to be established.

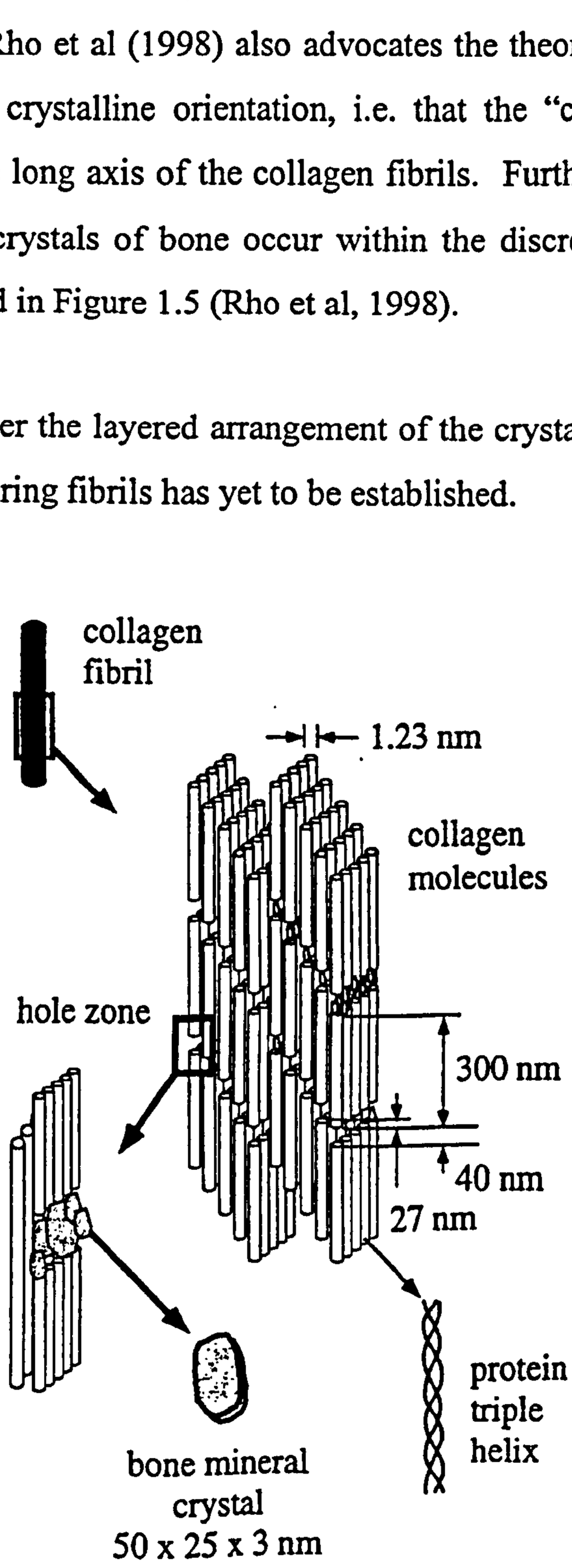

**Figure 1.5** The organization of bone mineral crystals within each collagen fibre and between collagen fibrils (Rho et al, 1998)

## 1.4 BONE CELLS AND THEIR FUNCTION

There are three groups of bone cells, namely the osteoblasts, osteocytes, and the osteoclasts. The osteoblasts and osteoclasts are involved with the remodelling of bone, in the sense that the osteoblasts are responsible for bone deposition while the osteoclasts are involved in bone resorption, and the osteocytes are said to play an important role in mineral homeostasis and the maintenance of the bone matrix; the location of these cells is illustrated in Figure 1.6.

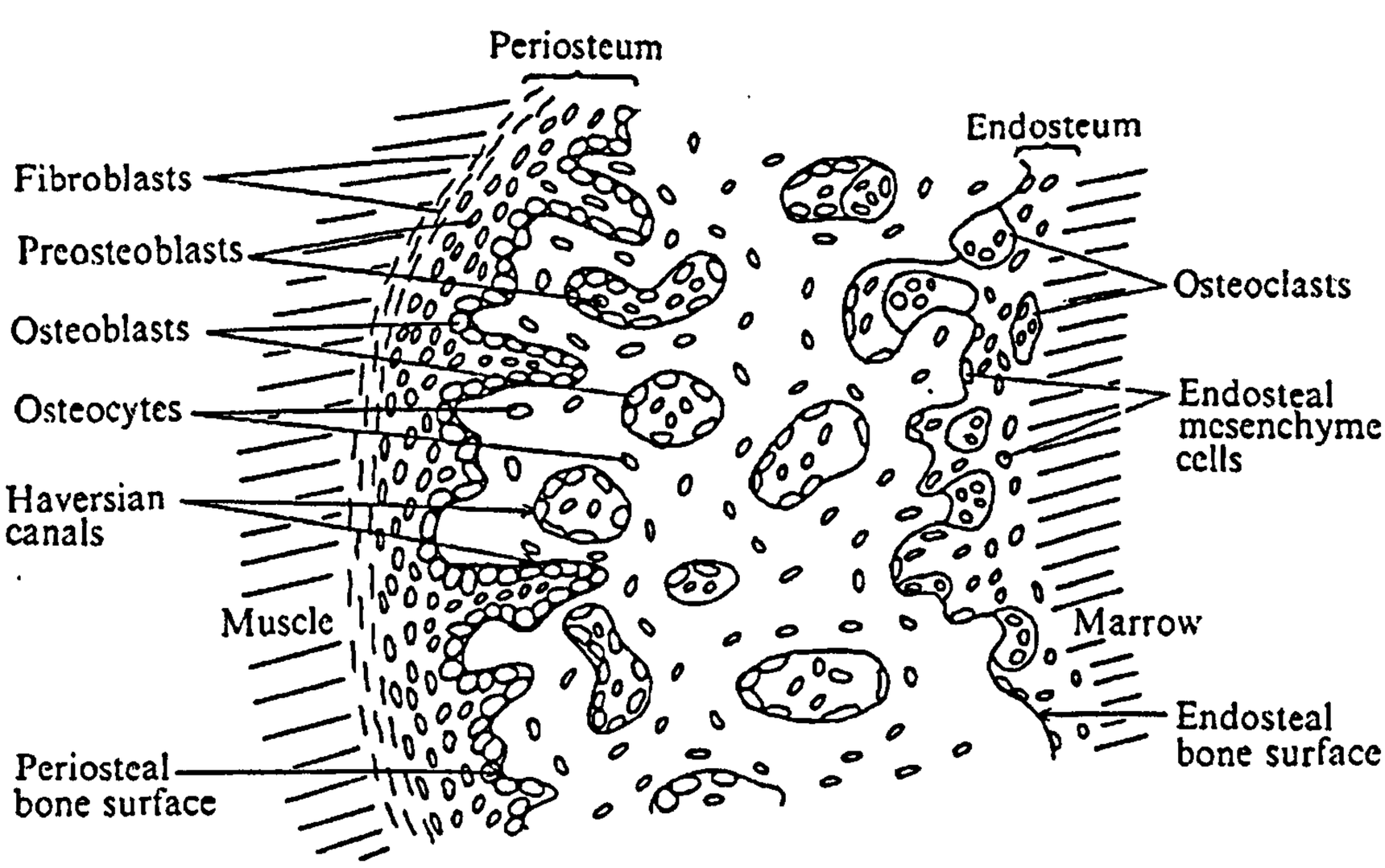


**Figure 1.6** Location of cells associated with bone formation (periosteal surface) and bone resorption (endosteal surface) (Vaughan 1970)

Osteogenic precursor cells, known as pre-osteoblasts or osteoprogenitor cells, are situated in the periosteum and give rise to osteoblast formation. The osteoblast is a differentiated

functional cell, which may further differentiate into an osteocyte. Previous theories stated that osteoblasts may also fuse with other cells to become part of an osteoclast, however it is now generally known that the fusion of separate monocyte cells results in the formation of an osteoclast.

Osteoblasts in actively growing bone tend to be cuboidal in shape, with an irregular contour, particularly on the matrix surface where long processes called canaliculae penetrate the adjacent osteoid and mineralised matrix. The osteoblasts are involved in the mechanism of bone deposition/apposition, and are therefore required to balance out bone resorption by the osteoclasts. Initially, the osteoblasts secrete collagen monomers and ground substance (mainly proteoglycans). These collagen molecules polymerise rapidly to form collagen fibers, resulting in the production of osteoid (newly formed organic bone matrix prior to calcification). During the formation of the osteoid, osteoblasts may become trapped within the matrix, and then differentiate into osteocytes. Calcium salts start precipitating on the surface of these collagen fibers, several days after osteoid formation, which provide nucleation sites. During a period of 7-14 days, the growing precipitates mature into bone mineral (substituted apatite) crystals via crystallite growth and ageing.

Within the skeleton, osteoblasts are continually depositing bone tissue, at the same time as bone is being resorbed where osteoclasts are active. During periods of large growth rates, such as childhood, more bone is being deposited than resorbed, resulting in increases in the total bone mass, due to a higher activity in the osteoblasts. When adulthood is reached and growth is finished, there is normally an equilibrium maintained between the activity of the osteoblasts and the osteoclasts. As a result of the hormone imbalance during the ageing process, the osteoclasts become more active, and more bone is resorbed than deposited, resulting in a reduction in the total mass of bone. Osteoclasts are large, phagocytic, multinucleated cells that are normally active on less than 1 % of the bone surfaces, whose absorptive activities are controlled by the parathryoid hormone. Bone absorption occurs at the ruffled border of the osteoclasts, where they secrete

enzymes that digest/dissolve the bone matrix, and acids that cause dissolution of the bone salts.

As mentioned earlier, osteoblasts differentiate into osteocytes when they become trapped within the surrounding osteoid during bone apposition. Osteocytes occupy cavities in bone tissue called lacunae, and they have cytoplasmic processes that extend into canaliculae with which they can make contact with other osteocytes. If there is a break in the canalicular network, osteocyte death may occur, which is often associated with bone death, where the area of bone in which osteocyte death has occurred becomes necrotic and is then removed by osteoclasts. The osteocytes are located in the inner, osteogenic layer of the periosteum, and in young woven bone they are present as closely but irregularly packed cells that are almost indistinguishable from the osteoblasts from which they were derived. The relationship between the osteocyte and the surrounding mineralized matrix is complex in that the osteocyte mediates the continuous exchange of both mineral and organic components between the blood and the matrix.

## 1.5 BONE BIOMECHANICS

### 1.5.1 RESPONSE OF BONE TO MECHANICAL LOADING

The discipline of mechanics can be applied to bones, which are objects that obey the laws of mechanics. Mechanics is a physical science that deals with the effects of forces on objects, and Sir Isaac Newton in 1707 defined three laws of motion, which alongside the laws of Robert Hooke in elasticity, form the foundation of the mechanics of elastic objects such as bone. Newton's third law of motion, i.e. every action has an equal and opposite reaction, underlines the basis of bone remodelling.

The way in which bone responds to a mechanical environment was described by Wolff in 1892 and is known as Wolff's law (Wolff, 1892). Wolff desribed bone biomechanics as

an extrapolation of Newton's third law of motion in that when a stress is imposed on bone, more bone is laid down (the action being the stress, the equal and opposite reaction being the bone deposition), and when a stress is not imposed, the bone is resorbed. Bone shows a bioelectric response to mechanical stresses, which is reminiscent of piezoelectricity, yet studies by Pollack et al (1984) suggest that piezoelectric phenomena do not play a significant role in wet bone. Pollack et al (1984) suggested that streaming potentials generate the transmission from electric signals and mechanical stress to bone formation. Nevertheless, bone has different mechanical properties depending on location, i.e. strong in areas that undergo large stresses, which are discussed further in section 1.6.

### 1.5.2 STRESS MEDIATION IN REMODELLING

The continual remodelling of bone is extremely valuable because it allows bone to respond to changes in the stress patterns imposed on the bone. This feature enables bone to change its strength in response to the loads/strains to which it is exposed, such as thickening when subjected to heavy loads. Stress patterns determine the amount of remodelling and therefore the resulting shape of the bone as a function of osteoblastic activity, i.e. the amount of bone deposition, which increases with the amount of stress/strain that the bone experiences. For example, athletes tend to have heavier and larger bones than people who do little, regular exercise. Hoshi et al (1998) studied the effects of exercise training on the bone density of mice of various ages and discovered that exercise-training at every age suppresses age-associated loss of bone density, such as in osteoporosis. These results suggested that mechanical stimulation does affect osteoblastic activity and therefore, that osteoblastic deposition and calcification of bone may be stimulated by regular patterns of exercise, whether continual or oscilating.

Bone's ability to remodel is also beneficial with respect to fracture healing, for example if a long bone is broken in its centre and heals at an angle, there is increased deposition in the 'inside' under of compression, and bone absorption in the outside area of tension (see

Figure 1.7). So, bone mechanically responds to stress by means of an adaptive remodelling mechanism. In young children who experience rapid bone remodelling, this adaptive behaviour can eventually straighten out the leg. This sort of fracture healing is common amongst minor fractures; however, when a major fracture has occurred which neccessitates the use of fracture fixation devices, sometimes the adaptive healing process includes side effects. Cattermole et al (1997) investigated the degree of bone mineralization around fracture sites along the tibia held by fracture fixation devices, and discovered that the patients who were immobilised suffered from "dis-use osteoporosis", whereby there was a large decrease in proximal and distal bone density along the entire tibia.

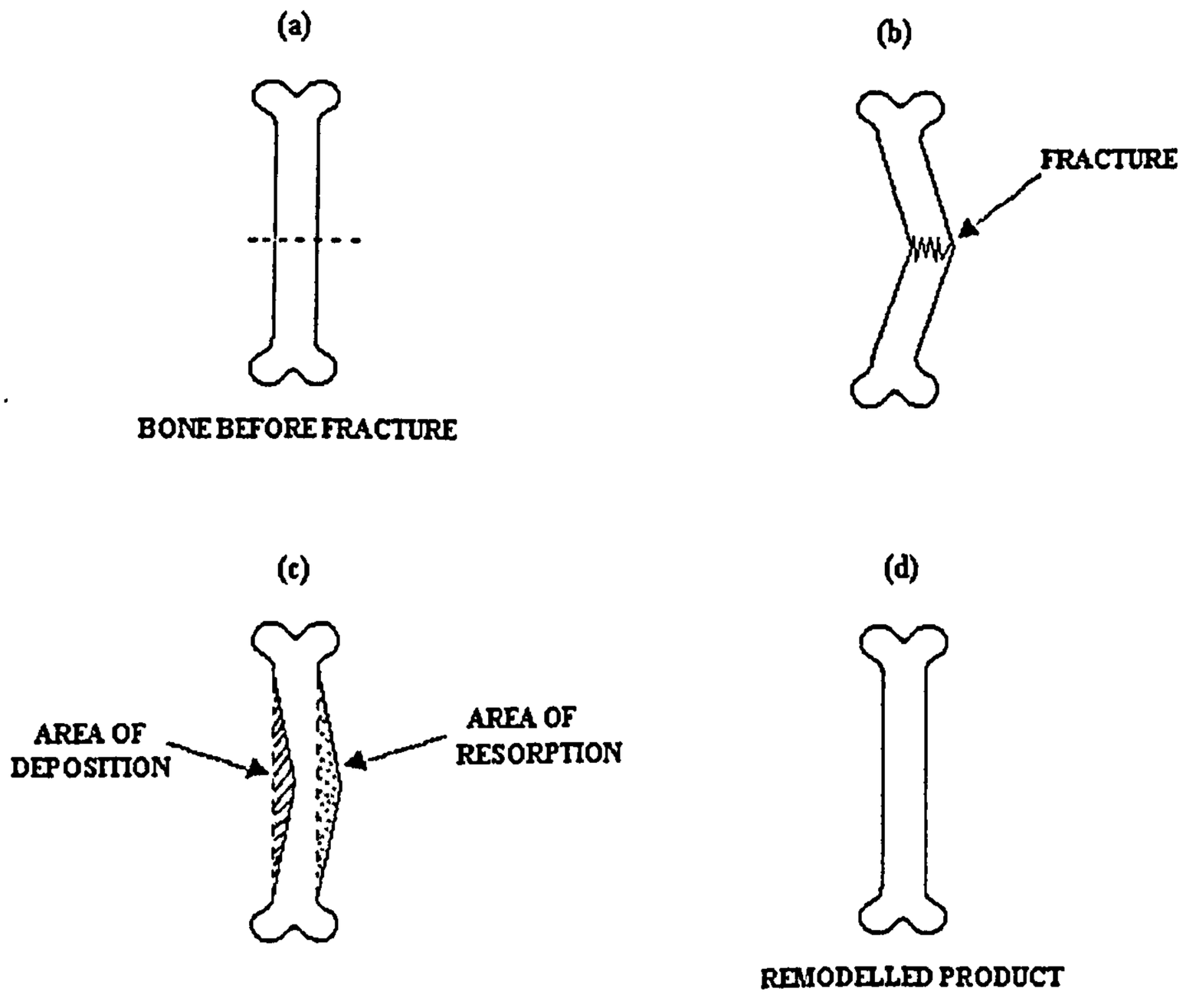


**Figure 1.7** Stage of bone remodelling with respect to fracture healing. (a) original bone with location of area to be fractured (b) bone after fracture (c) simultaneous deposition of bone in inside/resorption of bone on the outside (d) final product/straight bone.

### 1.5.3 STRESS THERAPY IN FRACTURE HEALING

Another feature Cattermole et al (1997) found common to all tibial fracture sites was bone resorption in response to the actual fracture, termed *post-traumatic osteoporosis*. Cattermole et al (1997) discovered an accurate, precise and minimally invasive means of quantifying the extent of mineralization at the fracture site, i.e. dual energy x-ray absorptiometry, which could be useful in prediciting healing potentials. This sort of technique is very helpful for patients experiencing posttraumatic or disuse osteoporosis because it serves as an indication that perhaps subjecting the patients' leg to minor loads may speed up the healing process. Inman et al (1999) reinforced this idea in their studies with immobilized rats who were experiencing bone loss due to disuse. They found that subjecting the rats' tibias three times a week to variable loads prevented the decline in bone density seen in the control rats attenuated decreases in ultimate load and stiffness. Periosteal mineralization was stimulated by the loading regime, which helped to maintain the bone density. Of course, human patients may object to having their healing legs in plaster subjected to stresses on frequent basis but it may be benenficial in the long term.

### 1.5.4 TISSUE DIFFERENTIATION IN RESPONSE TO MECHANICAL STIMULUS

There is confusion in the literature concerning the influence of mechanical loading on tissue differentiation as a result of confliding biological observations. Much of this confusion results from trying to identify and understand the associated physical environment as well as the full description of the mechanical stimuli applied to the tissue. Carter et al (1991) summarized the concepts of tissue differentiation in terms of distortional strains and hydrostatic stresses in Figure 1.8. This figure indicates that the complete loading history will determine tissue response. Extending these theories and applying them to bone implant materials, under typical conditions, the tissue at the bone-

implant interface is oxygenated enough to fall to the right of the "vascularity" line in the model, therefore preventing the differentiation to cartilage because of a low oxygen supply.

Taking these theories further, one can postulate that in a porous bone replacement material, control of porosity becomes critical to the formation of bone tissue. In a highly porous material, tissue differentiation to bone will be ensured by the nature of the open structure promoting vascularization and oxygenation, while a low porosity, closed structure will favour the formation of cartilagenous tissue.

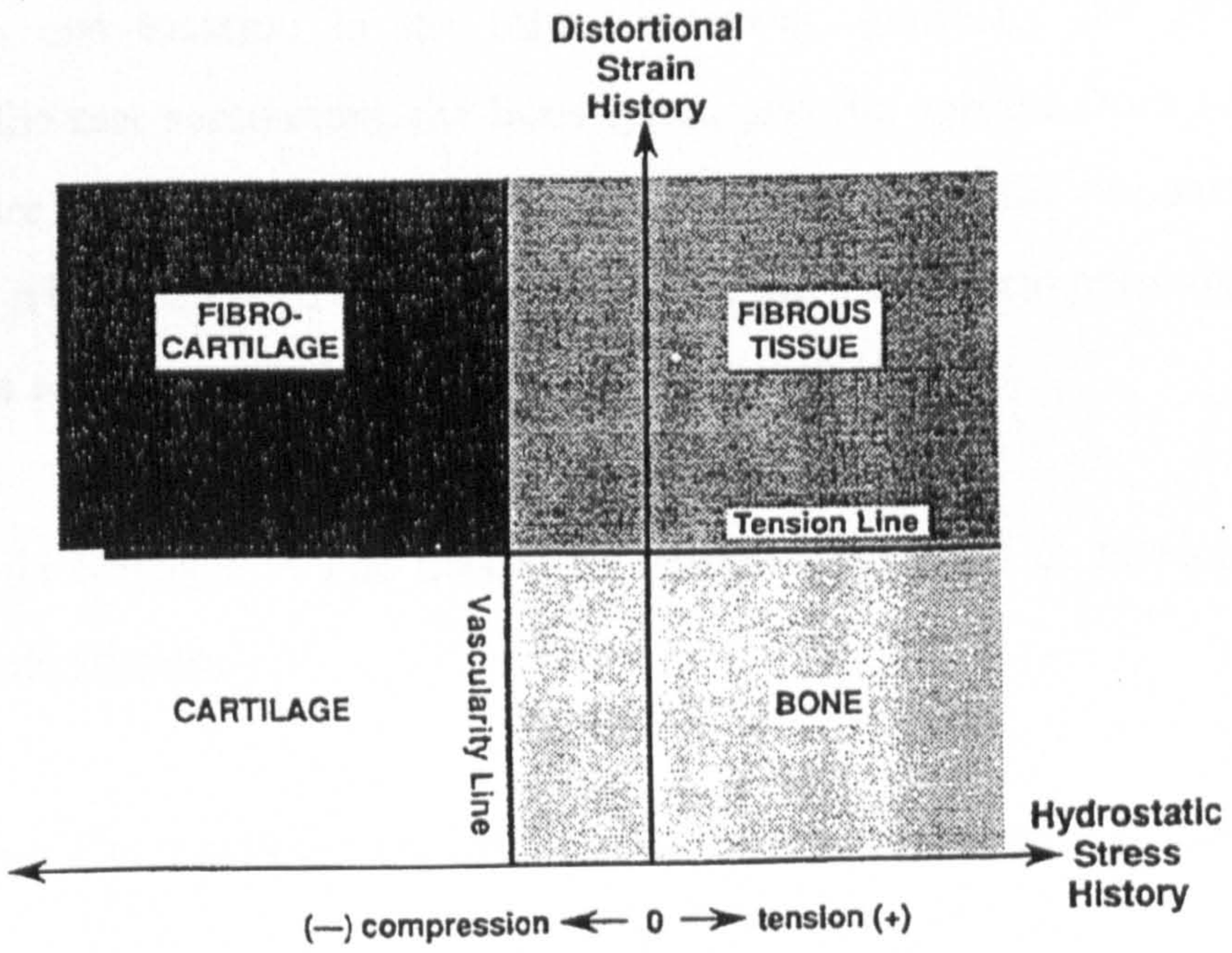


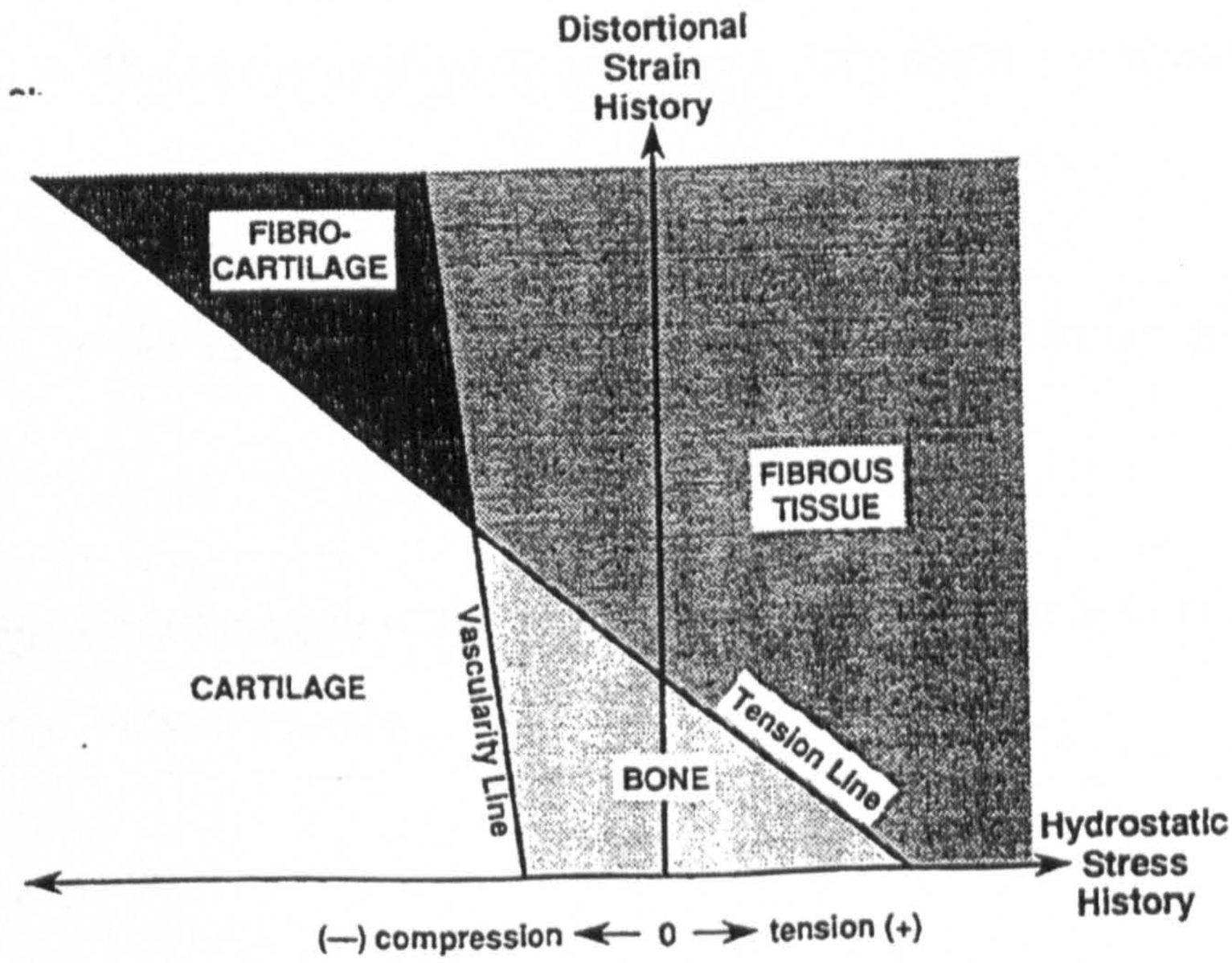


**Figure 1.8** The effect of mechanical stimulus on the tissue differentiation of bone (Carter et al, 1991)

## 1.6 MECHANICAL PROPERTIES OF BONE

Many studies have been carried out to provide a broad under-study of the mechanical properties of bone as there are no set of definite properties due to the degree of structural variation from one location to the other. However, generally the properties under investigation, the test parameters, the bone types, and the species from which the bone was derived, are specific to each study, almost eliminating valid comparisons between investigations, which can be frustrating. However, the mechanical properties that will be regarded in this section are defined as follows (Callister, 1994):

Ultimate Tensile Strength = The maximum engineering stress in tension that may be sustained without fracture

Shear Strength = The maximum engineering stress in shear that may be sustained without fracture.

Yield Strength = The stress required to produce a very slight yet specific amount of plastic strain.

Shear Modulus = The ratio of shear stress to shear strain; otherwise an indication of rigidity.

Ultimate Compressive Strength = The maximum engineering stress in compression that may be sustained without fracture.

Fracture Toughness = Critical value of the stress intensity factor for which crack extension occurs.

Impact Energy = A measure of the energy absorbed during the fracture of a specimen of standard dimensions and geometry when subjected to rapid (impact) loading.

Apparent Density = The mass divided by the total volume of bone matrix (i.e. total volume is indicative of open and closed pore spaces).

### 1.6.1 CORTICAL BONE

Much literature has been published regarding the mechanical properties of cortical bone, the general consensus being that the mechanical properties are dependent on the bone mineral content. The data gathered by various authors shall be organised as follows:

Table 1.1 – General comparison of mechanical properties
Table 1.2 – Comparison of age effects on mechanical properties
Table 1.3 – Effect of immobilisation on mechanical properties
Table 1.4 – Effect of differing ion solutions on mechanical properties

In cortical bone, there is a periodic array of segments within each collagen fibre, and bone mineral crystals lie adjacent to and are bound tightly to each segment. This close bonding prevents shear, in which the bone mineral crystals and collagen fibres move and slip out of place; this is important to the maintenance of bone strength. Furthermore, the segments of adjacent collagen fibers overlap each other, hence the bone mineral crystals overlap each other. The degree of bonding between the bone mineral and collagen fibers gives the bone tissue versatile properties; the collagen fibres have good tensile strength, while the bone mineral crystals have good compressive strength.

With reference to Table 1.1, cortical bone appears to be a stiff material with high compressive strength. The compressive strength of cortical bone is higher than the tensile strength, both of which are higher than the shear strength. Therefore, one can conclude that cortical bone is strongest in compression, and weakest in shear. The stresses involved in compression, tension, and shear are multidirectional, and therefore because the strength values differ according to the type of stress induced, it can be concluded that cortical bone is anisotropic, i.e. it has different physical properties in different directions.

The general trend of the data inTable 1.2 demonstrates that cortical bone becomes weaker and stiffer with age, with regards to the ultimate tensile strength, the fracture toughness, and the yield stress. Gaynor-Evans (1975) attributed bone weakness in general to stress concentrations around the cement lines in the osteons; he found that older men had many more osteons per $mm^2$ than the younger men (despite the fact that the osteons were much smaller), hence more likely sites for stress concentrations leading to loss of strength. Gaynor-Evans (1975) also noticed that the Haversian canals in older men were larger than that of younger men, which increases porosity and decreases density, all of which attribute to the marked lower mechanical properties; Ueshira had reported similar results in 1960. From this literature, it appears that despite the fact that Haversian canals do not have sharp corners, they may create areas of higher stress concentration at which microfractures may occur.

As evident in Table 1.3, Kaneps et al (1997) found that immobilisation caused the ultimate tensile strength and the Young's Modulus of canine bone to decrease. This is consistent with section *1.5.2*, which discusses the effect of stress on bone tissue, whereby bone grows in response to stress, and loses density when the stress is taken away, hence the lesser the ability to sustain loads.

As demonstrated in Table 1.4, Kotha et al (1998) found that placing bone tissue in an environment of fluoride ions decreased the mechanical properties of cortical bone in tension. It was hypothesised that the fluoride treatment decreased the Young's Modulus, the yield stress, and the ultimate tensile strength by converting small amounts of bone mineral to mostly calcium fluoride. This in turn decreased the amount of structurally effective bone mineral content and possibly effected the interface bonding between the organic matrix and the bone mineral. This data suggests that perhaps there are ways of substituting ions in bone mineral that may have an opposite effect and be advantageous with regards to the mechanical properties.

**Table 1.1** General comparison of the mechanical properties of cortical bone

| Author | Year/ Bone Type | Young's Modulus (GPa) | Ultimate Compressive Strength (MPa) | Ultimate Tensile Strength (MPa) | Yield Strength (MPa) | Shear Modulus (GPa) | Shear Strength (MPa) | Fracture Toughness ($MN.m^{-3/2}$) |
|---|---|---|---|---|---|---|---|---|
| Colberg et al | 1999 monkey | 9 - 16 | | 155 – 208 | | | | |
| Zysset et al | 1999 human | 25.0 ± 4.3 | | | | | | |
| Currey et al | 1998 human | | ~180 | ~158 | | | | 2.4 – 5.3 |
| Wohl et al | 1998 sheep | 86 - 1385 | | 30 – 80 | | | | |
| Jepsen et al | 1997 human | | | | 55.8 ± 3.8 | 5.0 ± 0.2 | 74.1 ± 3.2 | |
| Cezayirlioglu | 1985 human | | 213 ± 10.1 | 158 ± 8.5 | | | 71 ± 7.8 | |
| Bonfield et al | 1976 bovine | | | | | | | 2.2 – 4.6 |

**Table 1.2** Comparison of age-effects on the mechanical properties of human cortical bone

| Author | Year | Ultimate Tensile Strength (MPa) | Young's Modulus (GPa) | Real Density ($gcm^{-3}$) | Fracture Toughness ($MPa.m^{1/2}$) | Impact Energy ($KJm^{-2}$) | Yield Strength (MPa) |
|---|---|---|---|---|---|---|---|
| Wang et al | 1998 | | 4.89 ± 0.8 *(11-16)*<br>5.03 ± 1.47 (*>16*) | 1.29 ± 0.01 *(11-16)*<br>1.35 ± 0.02 (*>16*) | 2.28 ± 0.3 *(11-16)*<br>1.73 ± 0.25 (*>16*) | | |
| Courtney et al | 1996 | | 15.69 ± 1.66 *(~26)*<br>14.78 ± 1.55 *(~72)* | | | | 81.6 - 10.6 *(~26)*<br>49.3 - 5.5 *(~72* |
| Currey et al | 1996 | | | | | *5* (~40)<br>*70* (~7) | |
| McCalden et al | 1993 | 120 *(20)*<br>65 *(65)* | 11 *(20)*<br>20 *(65)* | | | | |
| Gaynor-Evans | 1975 | 102 *(41.5)*<br>68 *(70)* | 14.90 *(41.5)*<br>13.60 *(70)* | 1.91 *(41.5)*<br>1.85 *(70)* | | | |

**NB/** The age of the patients are in italics

**Table 1.3** Effect of immobilisation on the mechanical properties of canine cortical bone (Kaneps et al, 1997)

| Condition | Ultimate Tensile Strength (MPa) | Young's Modulus (GPa) |
|---|---|---|
| Immobilised | 70.34 ± 25.4 | 2.62 ± 0.33 |
| Control | 193.23 ± 35.2 | 2.66 ± 0.01 |

**Table 1.4** Effect of differing ion solutions on the mechanical properties of bovine cortical bone (Kotha et al, 1998)

| Group | Young's Modulus (GPa) | Yield Strength (MPa) | Ultimate Tensile Strength (MPa) |
|---|---|---|---|
| NaCl | 19.8 ± 1.6 | 113.6 ± 4.9 | 116.1 ± 6.9 |
| NaF | 16.8 ± 1.7 | 83.0 ± 13.1 | 91.6 ± 11.6 |

### 1.6.2 CANCELLOUS BONE

Cancellous bone, structurally an open cell foam, is weaker than cortical bone. This is due to the reduction in apparent density resulting from a high degree of macroporosity, due to the increased size and frequency of the vascular channels, as opposed to the microporosity found in cortical bone. Lindahl (1976) and Galante (1970) reported a linear relationship between the compressive strength of cancellous bone and the apparent density, i.e. the lower the apparent density, the lower the strength. Currey (1998) similarly reported that the mechanical properties of cancellous bone are mainly a function of variation in apparent density in addition to the structure of the trabeculae, i.e. the texture and degree of macroporosity. Kang et al (1998) found that the apparent density and strength of canine cancellous bone correlate well, as seen in Table 1.5. A mathematical relationship was used by Rice et al (1988) to describe this relationship, in that the strength/elastic modulus of bone are proportional to the square of the apparent density.

There is considerable data available describing the mechanical properties of cancellous bone in compression, where the anisotropy of cancellous tissue results in well-defined anatomical variations in strength. A recent study by Sugita et al (1999) highlighted the importance of mechanical anisotropy in osteoporotic bone in the proximal femur and observed a strong dependence of mechanical properties on the loading direction. It was concluded that the osteoporotic proximal femur was more prone to fracture when stress was applied in the longitudinal direction compared to when stress was applied in the transverse direction.

The following tables list the mechanical properties of bone when subjected to compressive stresses in a longitudinal direction. The lack of data in the literature regarding other mechanical properties reflects the practical difficulties associated with specimen preparation and clamping when dealing with brittle porous materials.

Table 1.5 – Strength and density of canine cancellous femoral bone

Table 1.6 – Mechanical properties of cancellous femoral bone

Table 1.7– Mechanical properties of human cancellous vertebral bone

Table 1.8 – Mechanical properties of human miscellaneous cancellous bone

From the tables, it can be seen that cancellous bone is strong in the femoral regions and much weaker along the vertebrae. This is consistent with the theory that the strength of bone correlates with its' demands. The femur is subjected to much higher loads than the bone around the spine, due to walking, running, etc; therefore the difference in strength is inevitable and expected. It is often interesting to compare the mechanical properties of human cancellous bone to that of other species. For example, Kang et al (1998) discovered that the compressive strength of canine cancellous bone in the femoral head was 29±4 MPa. The strength difference compared to that of human bone highlights the fact that the strength of bone is also subject to its function in that bone grows and strengthens in response to stress; an average human leg only experiences short periods of running and walking, whereas canine bone suffers much more impact and fatigue, hence has stronger cancellous bone.

Recently, Rho et al (1998) made several unsuccessful attempts at predicting the mechanical properties of bone by applying the composite rule of mixtures formulae. It was decided that an accurate model needed to include the molecular interactions or physical mechanisms involved in the transfer of load across the bone material subunits, which of course would be particularly challenging as the bonding mechanisms between the organic and inorganic components, on an ultrastructural level, have not as yet been clearly established. In 1997, Rho et al did construct a successful model for predicting the mechanical properties of bone whereby Broadband Ultrasound Attenuation and Fractal Analysis was used; a significant correlation was found between fractal dimension and density, which was promising because density plays an important role in determining the mechanical properties of trabecular bone. However, bone macrostructure was not considered in this study and in order for the mechanical properties of bone to be fully

understood, further investigations at the constituent and structural level of bone are required. Recently, Nicholson et al (1999) demonstrated that quantitative ultrasound could be applied clinically in the measurements of sound velocity and bone mineral density as good predictors of the elastic modulus in calcaneal cancellous bone.

**Table 1.5** Strength and density of canine cancellous femoral bone

| Bones | Apparent Density ($g.cm^{-3}$) | Ultimate Compressive Strength (MPa) |
|---|---|---|
| Femoral Head | 1.17 ± 0.17 | 29 ± 4 |
| Medial Femoral Condyle | 0.89 ± 0.12 | 24 ± 4 |
| Lateral Femoral Condyle | 0.69 ± 0.13 | 14 ± 4 |
| Medial Tibial Plateau | 0.52 ± 0.11 | 10 ± 3 |
| Anterior Tibial Plateau | 0.41 ± 0.11 | 5 ± 2 |

**Table 1.6** Mechanical properties of cancellous femoral bone

| Author | Year/ Type | Area | Compressive Modulus (MPa) | Ultimate Compressive Strength (MPa) | Apparent Density ($g.cm^{-3}$) |
|---|---|---|---|---|---|
| Kang et al | 1998 canine | Femoral Head | 428 ± 237 | 29 ± 4 | 1.17 ± 0.17 |
| Kang et al | 1998 canine | Femoral Condyle | 317 ± 98 | 19 ± 5 | 0.89 ± 0.12 |
| Shoenfeld et al | 1974 human | Femoral Head | 344 ± 28 | | |
| McElhaney | 1965 human | Femoral Head | 1518 ± 1172 | | |
| Gaynor-Evans et al | 1961 human | Femoral Head | 581 ± 17 | | |
| Gaynor-Evans et al | 1961 human | Femoral Head | 287 ± 9 | 3.8 ± 1.1 | 0.75 ± 0.18 |

**Table 1.7** Mechanical properties of human vertebral cancellous bone

| Author | Year | Area | Young's Modulus (MPa) |
|---|---|---|---|
| Zysset et al | 1999 | Neck | 6.9 ± 4.3 |
| Nicholson et al | 1997 | Spine | 43-165 |
| Knese | 1988 | Spine | 57 |

**Table 1.8** Mechanical properties of miscellaneous human cancellous bone

| Author | Year | Area | Ultimate Compressiv eStrength (MPa) | Compressive Modulus (MPa) | Yield Strength (MPa) |
|---|---|---|---|---|---|
| Anglin et al | 1999 | Glenoid | 10.3 | 99 | |
| Li et al | 1997 | Femoral Head | | OA ~ 450<br>Normal ~ 400<br>OP ~ 350 | OA ~ 7.2<br>Normal ~ 6.8<br>OP ~ 4.6 |
| Odgaard et al | 1991 | Proximal Tibia | | 689 | |

**NB/** OA denotes those affected with osteoarthritis; OP denotes those affected with osteoporosis

## 1.7 SUMMARY

Bone is a highly complex biological composite in several senses as described by Martin (1999); it is a polymer-ceramic mixture, a lamellar material with a plywood structure-type (fibril-matrix mixture), and an intimate mixture of mineral crystals and collagen fibres. This reinforces the theory that bone is a composite of a composite of a composite. The composite structure of bone repairs any damage through the normal remodelling actions of its' cells, as well as growing in response to stress, all of which highlights its' continual adaptive modelling mechanism. Mechanically speaking, cancellous bone is weaker than cortical bone due to its' evident macroporosity. However, the areas where cancellous bone are present in large quantities are not as mechanically demanding as those composed of cortical bone, which is indicative of mechanical matching and the balancing of mechanical requirement with density.

# CHAPTER 2
# BIOCERAMICS –TYPES AND APPLICATIONS

*This chapter aims to define bioceramics and to compare and contrast the different types used in orthopaedic applications.*

## 2.1 INTRODUCTION

The skeleton first appeared in the evolutionary pattern of life in the Paleozoic era, approximately 500 million years ago (Hollinger et al, 1996). This evolutionary development was unique not only because of its advantages towards motion but also because of the ability of bone to repair itself. Bone regeneration is helpful in situations where the tissue has suffered slight damage or micro-fracture but in space-filling situations, or rather in large defects, an alternative is necessary.

## 2.2 BIOCOMPATIBILITY IN BIOCERAMICS

Materials used to replace bodily parts, otherwise known as biomaterials, ideally exploit the skeleton's ability to regenerate and repair. A bioceramic is a biomaterial used in the repair or reconstruction of parts of the musculoskeletal system. There has been increasing interest in the use of bioceramics because they can achieve stability and achieve differing levels of biocompatibility, which puts them at an advantage against other biomaterials. The biocompatibility of a material indicates the degree to which a material is accepted by the host tissue as well as the interactions. Hench (1991) categorised materials/tissue interactions, as listed on the next page:

| | |
|---|---|
| **Type 1** | The material is toxic and causes the surrounding tissue to die |
| **Type 2** | The material is non-toxic and resorbable and is replaced by surrounding tissue |
| **Type 3** | The material is non-toxic and inactive, resulting in the formation of a non-adherent fibrous capsule of variable thickness |
| **Type 4** | The material is non-toxic and biologically active, resulting in the formation of an interfacial bond with surrounding tissues |

The three most important types of bioceramics are:

- Resorbable (*Type 2*)
- Inactive (*Type 3*)
- Bioactive (*Type 4*)

Resorbable bioceramics degrade over a period of time, during which they are replaced by the original tissue. Due to the constant turn over of new tissue, a very thin interfacial layer exists between the implant and the tissue. In order for the material to be efficient, it must maintain the stability and strength of the relatively small interface during the degradation/replacement period. Furthermore, the rate of resorption must match the rate of bone apposition. The resorption products must also be metabolically acceptable.

Type 3 bioceramics, such as alumina and zirconia, are nearly inert biomaterials. Following the implantation of this type of bioceramic, a thin fibrous layer forms around the implant separating it from the surrounding tissue which may cause movement of the implant, resulting in failure. However, this problem can be overcome by press-fitting such an implant into the bone tissue, thereby achieving stability due to the limited amount of movement.

Bioactive ceramics are biomaterials that attach themselves to bone by means of a chemical bond, otherwise known as an interfacial bond. Examples include bioactive glasses, glass-ceramics, and hydroxyapatite. Following implantation, the surfaces of these implants form a biologically active hydroxycarbonate apatite (HCA) layer, thereby providing the bonding interface with tissues. The interfacial layer is more

resistant to mechanical fracture than the surrounding bone or implant, and failure almost never occurs at the interface. Hench (1986) attached a strong philosophy to this bonding mechanism, in that "the knowledge that substances can be made by man that will bond chemically to living tissue has broad philosophical implications." Hench believed that the fundamental principles of impant-tissue bonding were not discovered, but uncovered. Therefore, by defining these bonding mechanisms, the principles responsible for the creation of living matter from non-living matter may be uncovered.

### 2.2.1 BIOCERAMICS-TISSUE ATTACHMENT

The way in which a bioceramic attaches to a tissue is related to the type of response the implant elicits. When the bioceramics are non-toxic and dissolve (*Type 2*), they are termed resorbable ceramics which are designed to be slowly replaced by bone. Ideally the rate of bone re-growth should equate to the rate at which the material is resorbed; examples of these dense, nonporous materials are calcium sulphate and tricalcium phosphate. For dense, nonporous, nearly inert ceramics (*Type 3*), such as alumina ($Al_2O_3$), the interface between the implant and tissue is not biologically or chemically bonded, causing some movement which results in the formation of a non-adherent fibrous capsule. Bioceramics of this type are attached by means of cementing the device into tissues or press-fitting into a defect, otherwise known as morphological fixation. However, for porous polycrystalline $Al_2O_3$, bone ingrowth occurs after implantation, therefore achieving stability by means of a mechanical attachment between the implant and bone; this type of biological fixation is also experienced by hydroxyapatite-coated porous metals. When the biomaterial is non-toxic, dense, and surface-reactive (*Type 4*), a chemical reaction occurs between it and the bone, forming an interfacial bond; materials that experience this sort of bioactive fixation are bioactive glasses, bioactive glass-ceramics, and hydroxyapatite. Of course, if *Type 4* bioceramics are porous, the attachment mechanism could possibly be a combination of morphological fixation and chemical bonding.

### 2.2.2 MICROMOTION VS BIOCOMPATIBILITY

At this point, it is important to mention that the function of the bone-biomaterial interface is to provide safe and effective transfer of load from implant to bone. There are a number of variables that may affect the integrity of the interface. One biomechanical factor that affects interface biology is micromotion, which was described by Brunski et al (1991) as a dominant interfacial factor. Micromotion has never been precisely defined but generally refers to displacements of the implant relative to the bone at the interface, such as sliding, opening of gaps, and wobbling. Brunski described stages in bone healing after implantation in the Figure 2.1.

Referring to Figure 2.1, if excessive micromotion occurs, the tissue scaffold upon which bone tissue is laid down is destroyed. This disrupts the events of normal bone healing and therefore bone repair is initiated as opposed to bone regeneration, resulting in the formation of fibrous scar tissue at the interface. Theoretically, a ceramic bone replacement material should not instigate the formation of scar tissue, but rather bone regeneration, seeing as the role of a bioactive ceramic is to act as a scaffold for bone tissue to grow into.

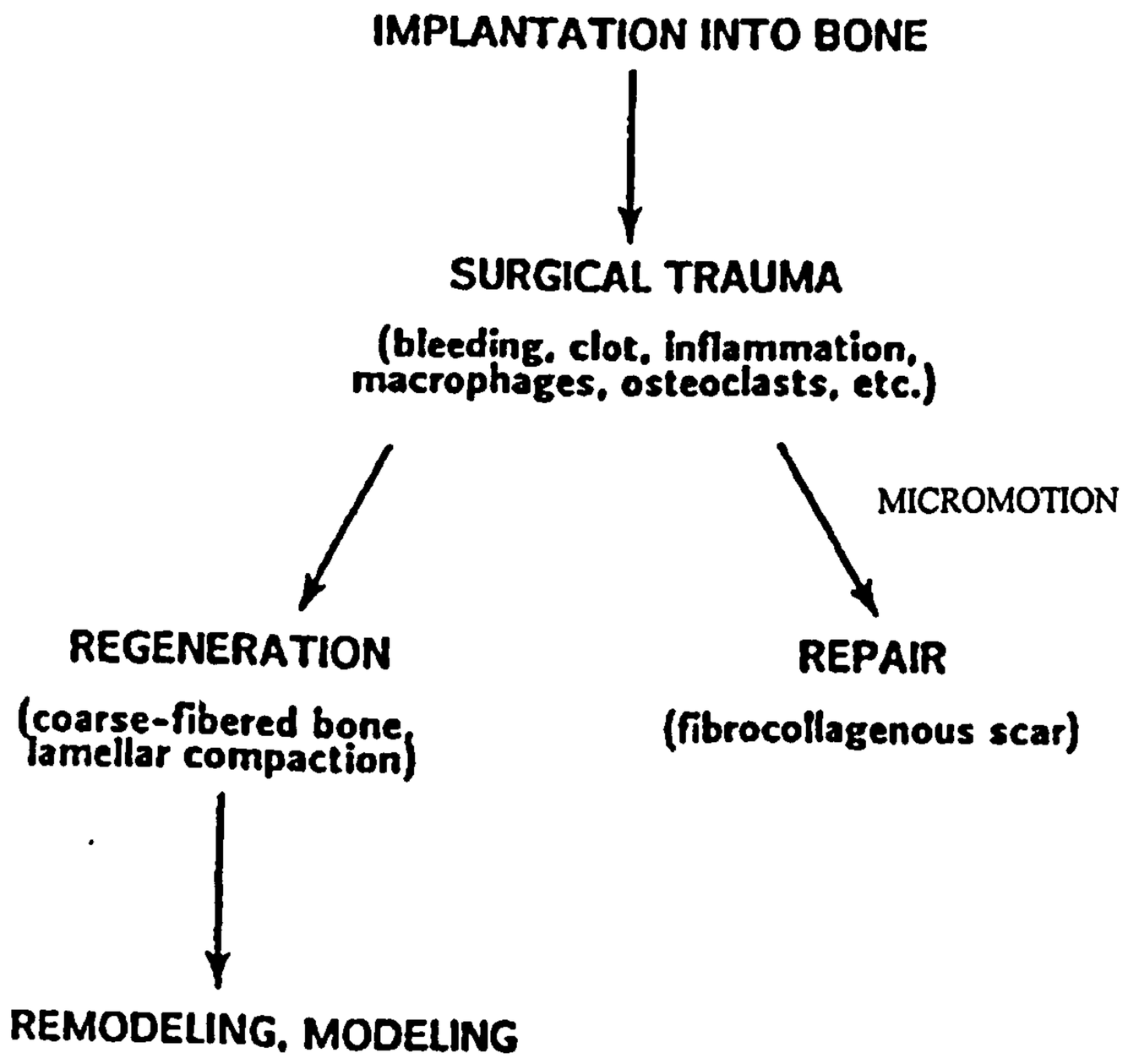


**Figure 2.1** The diverse stages of bone healing after implantation (Brunski et al, 1991)

However, in porous implants, micromotion has been seen to have an advantageous effect. Pilliar et al (1991) produced a quantitative report on micromotion which suggested that relative shear displacement greater than 150 μm can result in fibrous tissue ingrowth into porous materials, leading to good impant fixation into bone. Despite this report, there is a general lack of quantitative information on the effect of micromotion on interface biology and until more information is available with perhaps the development of a model, one can only rely on speculative measures.

Porous bioactive ceramics are advantageous due to the mechanical stability of their implant/tissue interface that develops following the ingrowth of bone tissue into the pores of the ceramic. However, porous ceramics have poor mechanical strength, due to the existence of macropores, which restricts their use to non major load-bearing applications, such as alveolar ridge augmentation and in maxillofacial surgery (Frame, 1987), for the treatment of simple bone cysts (Inoue et al, 1991), and as a filling device for bone defects (Ylinen, 1994). After implantation, porous ceramics serve as a structural bridge for bone formation, as the bone grows into the pores. Pore size is important to the process of this mechanical interlocking, as the pore size must be a minimum of 100 μm for bone to grow within the interconnecting pore channels near the implant's surface (Hench, 1991), and at least 200 μm in order for osteoconduction to occur (Liu, 1996*). Despite the beneficial attributes of these macropores with respect to bone ingrowth, they do have detrimental effects on the strength of the material, i.e. the material's strength decreases rapidly as the porosity increases.

Hollinger et al (1996) proposed in their review of bone substitutes that an ideal bone substitute material should promote bone regeneration. Bioceramic materials based on calcium phosphates seem ideal for this role. However, in order to understand the mechanical limitations of ceramics such as calcium phosphates, it is necessary to become familiarized with the dynamics of ceramic processing, which affect the microstructure, hence the mechanical properties of the biomaterial.

## 2.3 SINTERING AND MICROSTRUCTURE

On a macro and micro scale, the shape of a bioceramic will determine the type of response that it elicits. The geometry of a porous or dense implant will determine the amount of bone that will grow into the implant, mechanically interlocking the two together (discussed in section 2.2.1). Furthermore, the ceramics processing involved in the preparation of the implant may affect the overall properties.

### 2.3.1 SINTERING

The use of powder is fundamental to ceramics technology and plays an important role in the properties of the final product. The final microstructure of a ceramic refers to the size and shape of the individual ceramic powder particles. By controlling the morphology of the particles, the sintering characterisitics can be controlled, hence the porosity and the specific surface areas of the ceramic material. Sintering is a process involving the coalescence of powder particles at high temperature into a dense mass, so experiencing a reduction of porosity and an improvement in mechanical integrity (Figure 2.2). At first, the sintering mechanism involves the formation of necks along the contact regions between adjacent particles, and the formation of a grain boundary within each neck; the spaces between particles, the interstices, become pores. Eventually, the pores decrease in size and become more spherical in shape as the sintering process continues.

The way in which powder particles are packed and the amount of contact that they experience within a green compact will affect the sintering characteristics. Powder contact is affected by the compaction pressure of the powders (in the production of a green compact) and the powder morphology. The compaction pressure will affect the particle contact and therefore will control the area available for sintering. As for the morphology, powder compacts that have a low surface area, and irregular particle sizes and shapes, have a lower packing density in the green state, and therefore do not sinter very well. Therefore, one can say that it would be advantageous to be able to control powder morphology in order to produce samples with good density, mechanical properties, and porosity. The reduction of porosity as a result of the

sintering process is fundamental to strengthening the ceramic, yet, must not be completely eliminated for achieving biological union with the surrounding tissue.

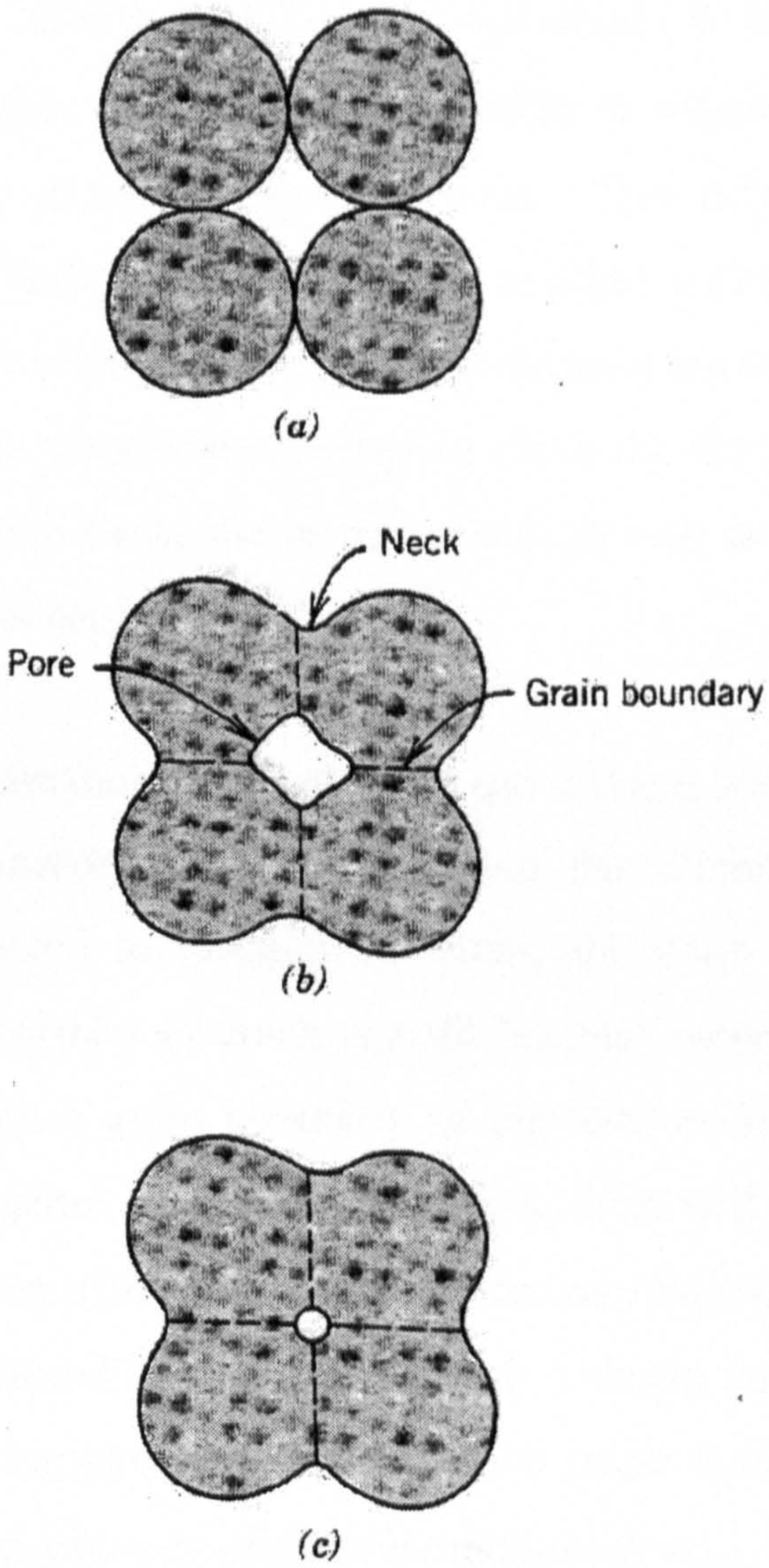


**Figure 2.2** Microstructural changes that occur during sintering (Callister, 1994)

The overall driving force for sintering is a reduction in free-energy, i.e. the reduction in total particle surface area and lowering of surface free energy by elimination of solid-vapour interfaces. The local driving force is the free energy change and pressure differences across a curved surface that gives rise to material transfer. As the particle size decreases, i.e. the particle radius of curvature is small, the overall driving force for densification increases, hence the amount of sintering.

### 2.3.2 MICROSTRUCTURE

The sintering process does result in the reduction of porosity, yet at the expense of the grain growth, which may be detrimental to the mechanical properties of the material. When the pores have shrunk and become spherical in shape, and no longer interconnecting, it becomes energetically favourable to reduce internal (solid:solid) interfaces as opposed to external (solid:gas) ones. This reduction in surface area results in grain growth. Therefore it is important to select a sintering temperature that allows the pores to shrink without causing too much grain growth. Too low a sintering temperature will result in insufficient energy to drive the densification process, and too high a temperature will cause the grain growth as well as decomposition of the ceramic (discussed later in section 3.1.4).

The microstructure of a ceramic is related to the mechanical properties. Therefore the ability to control the microstructure by selecting the correct sintering regime is important. When subjected to mechanical stress, the grain boundaries in an as-sintered ceramic act as barriers to crack growth because more energy is required to propogate a crack through a grain boundary as opposed to through the grain itself. Therefore if the microstructure is fine (small grains), there will be more grain barriers present per length of given crack flaw than in a coarse microstructure (large grains). As a result, the stress required to propogate a crack through, for example, four sets of grain boundaries (fine microstructure) will be much larger than the stress required to propogate a crack through two sets of grain boundaries (coarse microstructure), given that the crack length is similar. Griffith flaw theory (1920) described this phenomena (eq.2.3.2) in which the stress required to propogate a fracture across a grain boundary is inversely proportional to the square root of the length of fracture.

$$\sigma = \sigma_o + Kd^{-1/2} \qquad (2.3.2)$$

Where $\sigma$ = strength, $\sigma_o$ = applied stress required to move dislocations along a glide plane, K = empirical constant and d = grain size

Therefore large grains result in structures that are mechanically weaker than fine microstructures, because less energy is required for cracks to propogate along the larger grains than fine grains. The ceramics processing technology that has been discussed in this section may also be applied to the production of bioceramic materials such as calcium phosphate-based bioceramics, whereby not only the mechanical properties must be controlled, but also the biocompatibility.

## 2.4 BIOCERAMIC MATERIALS

### 2.4.1 CALCIUM PHOSPHATE-BASED BIOCERAMICS

Ever since the discovery that the mineral phase of bone and teeth contain calcium phosphate salts, a great deal of research has been put into the potential use of calcium phosphates as bioceramic bone replacement materials. The preparation of biomaterials from calcium phosphate powders started in the end of the 1960's (de Groot, 1983), using standard ceramics processing technology (i.e.pressing and sintering), which is still used today. As stated in chapter 1, the mineral found in bone is similar to calcium hydroxyapatite, a biological apatite. According to McConnell (1973) apatite is found in great abundance in nature, out of the phosphatic minerals, as well as in the hard tissue of humans. The similarity between calcium phosphate (Ca-$PO_4$) materials to the mineral found in bone is often used to justify its use today in orthopaedic applications.

The calcium to phosphorus (Ca:P) ratio is an important issue in the field of Ca-$PO_4$ bioceramics. This factor is believed to affect not only the physiochemical but also the mechanical properties, as well as the biocompatibility. The two Ca-$PO_4$ materials which receive the most attention for bioceramic applications are hydroxyapatite (HA) due to its' similarity to the mineral content of bone (discussed later in Chapter 3) and tricalcium phosphate (TCP), because it is resorbable. HA has a Ca/P ratio of 1.67 (PDF card no.9-432) whilst the more calcium-deficient TCP has a Ca/P ratio of 1.5 (PDF card no.9-438/9-169). There are two polymorphs of TCP (refer to Figure 2.3), known as α-TCP and β-TCP, the latter being more stable at high sintering

temperatures (LeGeros et al, 1993). Both polymorphs are resorbable, but higher solubility is found in α-TCP than β-TCP (Kuroyama et al, 1991).

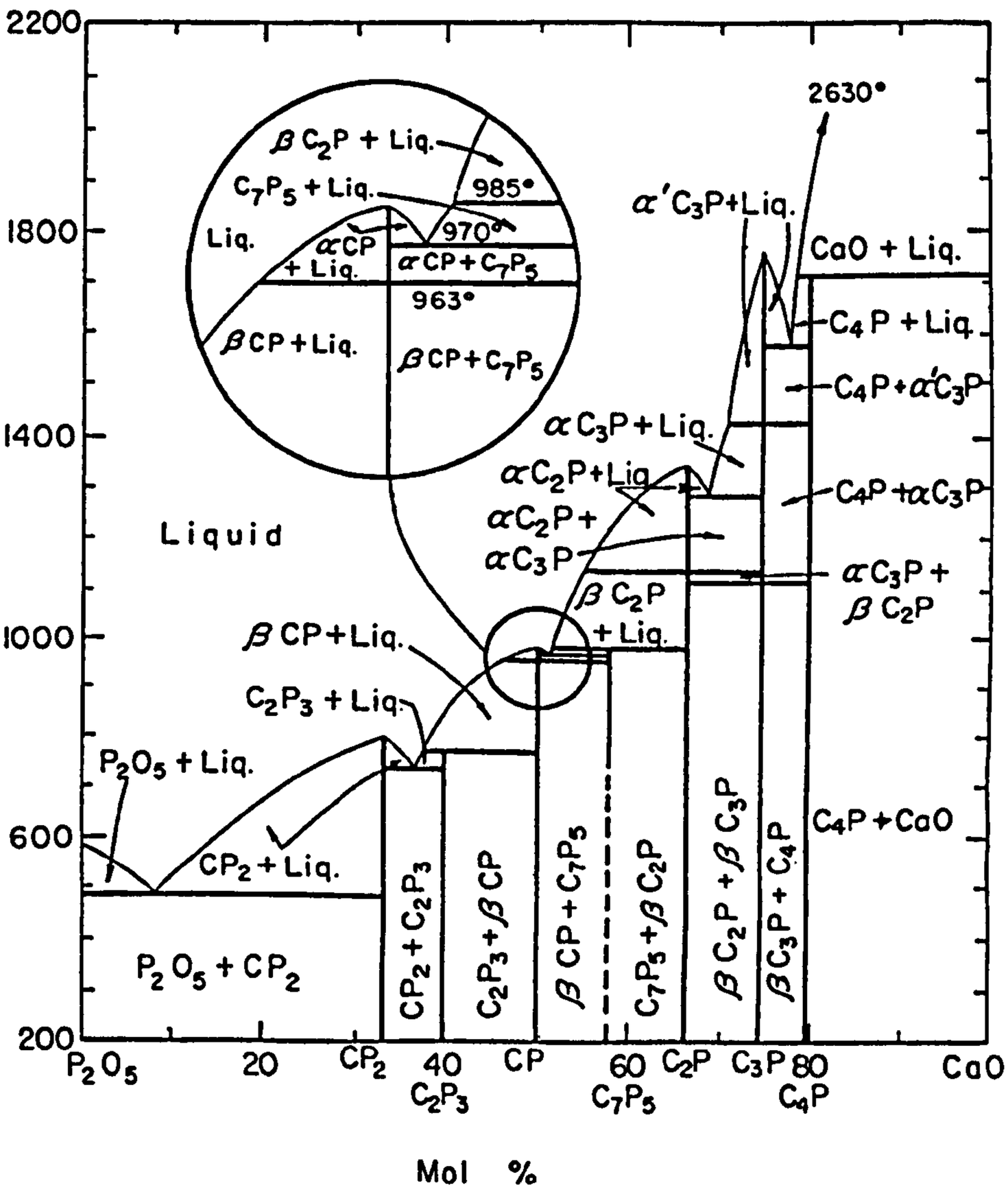


**Figure 2.3** $CaO/P_2O_5$-based phase diagram

The phase diagram in Figure 2.3 demonstrates that the more Ca-deficient a species is (such as TCP), the greater the potential to be biphasic at high temperatures.

### 2.4.1.1 Mechanical Properties

Raynaud et al (1998) discovered that the highest mechanical properties were obtained for calcium phosphates having a Ca/P ratio close to 1.65 (Ca-deficient HA), whilst the stoichiometric HA with a Ca/P ratio of 1.67 had the lowest fracture strength and toughness. Both materials were prepared for mechanical testing as polished,

rectangular specimens. The fracture strength was determined by 3-point bending, and the fracture toughness by a Vicker's indentation technique. The strength and toughness values found in this study are in Table 2.1. Evidently, lowering the Ca/P ratio appeared to improve the mechanical properties.

**Table 2.1** The effect of differing Ca/P ratios on the strength and toughness of calcium phosphate materials (Raynaud et al, 1998)

| Ca/P ratio | Fracture Strength (MPa) | Fracture Toughness ($MPa.m^{1/2}$) |
|---|---|---|
| 1.65 (Ca-deficient HA) | 150 | 1.00 |
| 1.67 (HA) | 70 | 0.85 |

Akao et al (1982) found that β-TCP displayed relatively good mechanical properties at different temperatures which can be see in Table 2.2. The β-TCP was produced in the laboratory and was prepared for mechanical testing as flat square specimens. The compressive strength/modulus values were determined by compression tests and the bending strength/modulus values were determined by 3-point bending.

**Table 2.2** The mechanical properties of β-TCP at different temperatures (Akao et al, 1982)

| Temperature (°C) | Compressive Strength (MPa) | Bending Strength (MPa) | Compressive Modulus (GPa) | Bending Modulus (GPa) | Relative Density (%) |
|---|---|---|---|---|---|
| 1150 | 459 ± 37 | 138 ± 11 | 82.6 ± 4.6 | 89.2 ± 5.3 | 98.6 |
| 1200 | 436 ± 35 | 119 ± 12 | 77.2 ± 3.6 | 72.7 ± 6.2 | 99.4 |
| 1250 | 599 ± 57 | 153 ± 10 | 79.4 ± 4.2 | 84.6 ± 6.1 | - |
| 1300 | 648 ± 38 | 137 ± 10 | 77.5 ± 4.4 | 83.5 ± 5.9 | - |

*NB/ The density values were calculated by assuming a theoretical density of 3.07 $g.cm^{-3}$*

The material at 1150°C had a finer grain size than that at 1200°C, which may explain in part the difference in strength. The greatest compressive strength at 1300°C (the

material was 93% β-TCP, 7 % HA) was probably due to the increased presence of a secondary phase.

It is also interesting to compare the mechanical properties of HA and TCP to other apatites, in particular fluoride-substituted apatites. Sax et al (1999) characterised hydroxyapatite (HAP), fluorapatite (FAP) and tricalcium phosphate (TCP); the mechanical properties are shown in Table 2.3. The specimens were produced in the laboratory and were mechanically pressed into green compacts, sintered, and polished, yet the resulting shape of the specimens was not reported. A Vicker's indentation technique was used for determining the mechanical properties. The Young's Modulus appears to be much higher in this investigation than the values reported in Table 2.2. However, the fact that the specimen shape was not reported in addition to the fact that the specimens were polished (which eliminates surface stress concentrations, hence improves strength during testing) renders the comparability of these results questionable.

**Table 2.3** The mechanical properties of various calcium phosphate ceramics (Sax et al, 1999)

| Ceramic (sintered at 1250°C) | Relative Density (%) | Poissons Ratio | Young's Modulus (GPa) | Shear Modulus (GPa) |
|---|---|---|---|---|
| HA | 98.1 | 0.15 | 106.06 | 46.17 |
| FAP | 95.9 | 0.28 | 114.35 | 44.66 |
| TCP | 99.3 | 0.45 | 103.97 | 35.94 |

NB/ *The results associated with a sintering temperature of 1250°C was chosen because it correlated with the highest densities, which were calculated with regards to the corresponding theoretical densities.*

It appears that the densification of fluorapatite seemed more difficult. Previously, it has been suggested that the lack of polar moment associated with Ca and F in fluorapatite may contribute to its crystallinity (Jha et al, 1997) and its chemical stability (Young et al, 1966) over hydroxyapatite, where such polar moments do occur. These advantages may explain the lower density in that the increased stability

and crystallinity indicate a larger amount of energy for sintering to occur, hence the poorer the densification at the temperature where HAP and TCP densify more.

### 2.4.1.2 Biocompatability

Calcium phosphate materials are mostly osseoconductive and bioresorbable materials with great potential in clinical applications (Hing et al, 1998). Oreffo et al (1998) and Passuti et al (1989) both carried out studies on calcium phosphates and found that osteoblastic activity, hence bioactivity, occurred on the surfaces of the materials, with no cytotoxicity recorded. In terms of bioresorbability, the actual application determines the type of bioceramic required. In non load-bearing applications, such as space-filling in maxillofacial surgery, the bioceramic in question may have a higher rate of resorption because it is a temporary material serving as a scaffold for bone remodelling. However, rapid biodegradation is undesirable for implants used in higher load-bearing applications, where the implant should retain some structural integrity during remodelling.

A recent attempt was made (Denissen et al, 2000) to control the resorbability of dense calcium phosphate materials such as hydroxyapatite (discussed in the next chapter). The assumption was that adding an agent such as biphosphonate solution would inhibit resorption. However, the results indicated that after one year, dense hydroxyapatite implanted in the mandibles of goats with and without the bisphosphonate solution experienced the same degree of osteoconduction, biocompatibility and bone ingrowth.

Whatever the application, it is important to find an ideal rate of resorption, which is determined by the calcium to phosphorus (Ca/P) ratio. LeGeros et al (1993) defined Ca-deficient materials such as TCP as more soluble than materials with a higher Ca/P ratio. Solubility in biological fluids is often a good indication of biodegradability as found by Knabe et al (1997), who discovered that the most rapidly resorbable calcium phosphates had lower Ca/P ratios, as indicated by their high phosphate ion releases in solution. So at this point it is safe to assume that the lower the Ca/P ratio, the more resorbable the material. De Groot (1987) found that β-Tricalcium Phosphate (TCP)

(Ca/P ratio of ~1.5) had a much higher rate of resorption than hydroxyapatite ( Ca/P ratio of ~1.67). According to de Groot (1987), biodegradation of calcium phosphate ceramics is caused firstly by physicochemical dissolution and secondly by disintegration into small particles, whereby the disintegration is dependent on the solubility product of necks connecting the powder particles after sintering. De Groot (1987) discovered that hydroxyapatite ceramics hardly disintegrate while macro- and micro- porous β-TCP disintegrate very rapidly into particles which may be found in neighbouring lymph nodes.

Ducheyne et al (1991) and Kuroyama et al (1991) also found that the more Ca-deficient the material was, the more resorbable. The order of solubility of various calcium phosphates were found as follows:

α -TCP > oxyhydroxyapatite > β -TCP > hydroxyapatite

Ducheyne et al's (1991) studies furthermore revealed that despite the fact that β-TCP exhibits greater dissolution than HA, carbonated apatite does not precipitate on its' surface as readily as it does on that of HA. Given that the precipitation of carbonated apatite is important to the issue of bone ingrowth and deposition of bone in the interfacial area, it is questionable whether β-TCP is a sufficiently stable substrate upon which cell activity may occur.

### 2.4.2 INERT BIOCERAMICS

#### 2.4.2.1 Alumina

Alumina is an inactive bioceramic and a nearly inert biomaterial, therefore it does not stimulate osteoblastic activity or form a bond with surrounding bone tissue. However, it is biologically compatible, i.e. does not instigate cytotoxic reactions, and has high mechanical strengths, both of which are favourable characteristics for use in fabricating prostheses of the knee (Oonshi et al, 1981), the ankle (Murasawa et al, 1982), and of the elbow (Kurata et al,1983). Alumina, in porous form, has also

proven to be a successful and "interesting" material for drug-delivery (Krajewski et al, 1998).

Yamamuro et al (1991) investigated the effects of different surface characteristics on the bonding behaviour of various materials, one of which was bead-coated alumina, whereby the beads were bonded to the alumina substrate using an identical alumina ceramic binder. Pull out tests showed that after 24 weeks, the interface shear strength of the bead-coated alumina was ~ 0.047 MPa while that of uncoated and unbeaded alumina was ~ 0.015 MPa. So, perhaps using bead-coated alumina in load bearing applications may prevent loosening of the prosthesis, which happens frequently when there is a lack of bone-implant fixation. The only disadavantage in this potential application that Yamamuro et al (1991) pointed out was that alumina ceramic has an extremely high elastic modulus in comparison to metallic materials, which prevents near-net shaping.

Mechanically, alumina is strong and, as pointed out by Seidel et al (1997), the mechanical reliability of alumina is determined by the fracture strength as well as the Weibull modulus. Table 2.4 shows various mechanical properties of alumina ceramics.

**Table 2.4** Mechanical properties of various alumina ceramics (authors stated in table)

| Material | Fracture Strength (MPa) | Weibull Modulus | Bending Strength (MPa) |
|---|---|---|---|
| As-sintered alumina (Seidel et al, 1997) | 460 (cold isostatic pressing)<br>925 (cast slip) | 8-12<br>8-12 | |
| In-Ceram<br>In-Ceram Spinell<br>(Magne et al, 1997) | | | 530<br>283.1 |

### 2.4.2.2 Zirconia

Zirconia, like alumina, is a nearly inert biomaterial. There is interest in the orthopaedic community in using zirconia as ball heads for total hip replacements; the first paper concerning its use in this application was introduced by Christel et al (1988). Burger et al (1999) listed mechanical properties of different kinds of zirconia in Table 2.5. The main advantage that zirconia has over other biomaterials is the transformation toughening mechanisms operating in its' microstructure. Stabilising oxides such as CaO, MgO, and $Y_2O_3$ (yttria) may be added to pure zirconia to produce Partially Stabilised Zirconia (PSZ), and yttria combined with zirconia alone results in finely grained microstructures known as Tetragonal Zirconia Polycrystals (TZP) or Y-TZP. TZP stabilised with yttria is mechanically more favourable as described by Burger et al (1997) who discovered that Y-TZP materials show bending strengths of more than 1000 MPa, a Weibull Modulus of up to 20, and a fracture toughness of 9 $MPa.m^{1/2}$. This mechanical advantage of TZP over PSZ is also evident in Table 2.5.

**Table 2.5** Mechanical characteristics of different types of zirconia (Burger et al, 1997)

| Property | Mg-PSZ | TZP |
|---|---|---|
| Density ($g.cm^{-3}$) | 5.74 – 6 | > 6 |
| Bending Strength (MPa) | 450 – 700 | 900 – 1200 |
| Compressive Strength (MPa) | 2000 | 2000 |
| Young's Modulus (GPa) | 200 | 210 |
| Fracture Toughness ($MPa.m^{-1}$) | 7 - 15 | 7 - 10 |

## 2.4.3 GLASSES

### 2.4.3.1 Definition

Glass is an archetypal brittle solid, of which several definitions have been proposed, the most widely accepted definition at present being that proposed by the ASTM:

" a glass is an inorganic product of fusion which has cooled to a rigid condition without crystallising"

Zarzycki (1991) proposed a more general definition that does not neglect polymeric glasses as well as glasses produced via techniques such as sol-gel:

" a glass is a non-crystalline solid exhibiting the phenomenon of the glass-transition"

The glass transition, *Tg*, occurs at a characteristic temperature (Figure 2.4), during which the elastic solid starts behaving as plastic material. Below the *Tg*, the material is considered to be a glass, above it is considered to be a supercooled liquid, and finally a liquid. These phase changes are related to the viscosity of the system. As the temperature increases above the *Tg*, there is continuous decrease in viscosity until the glass is a liquid. The melting point, *Tm*, corresponds to the temperature at which the viscosity is such that the glass is fluid enough to be considered a liquid. For non-crystalline material such as glass, there is continuous volume change upon cooling (Figure 2.4), unlike crystalline materials who undergo a characteristic discontinuous volume change.

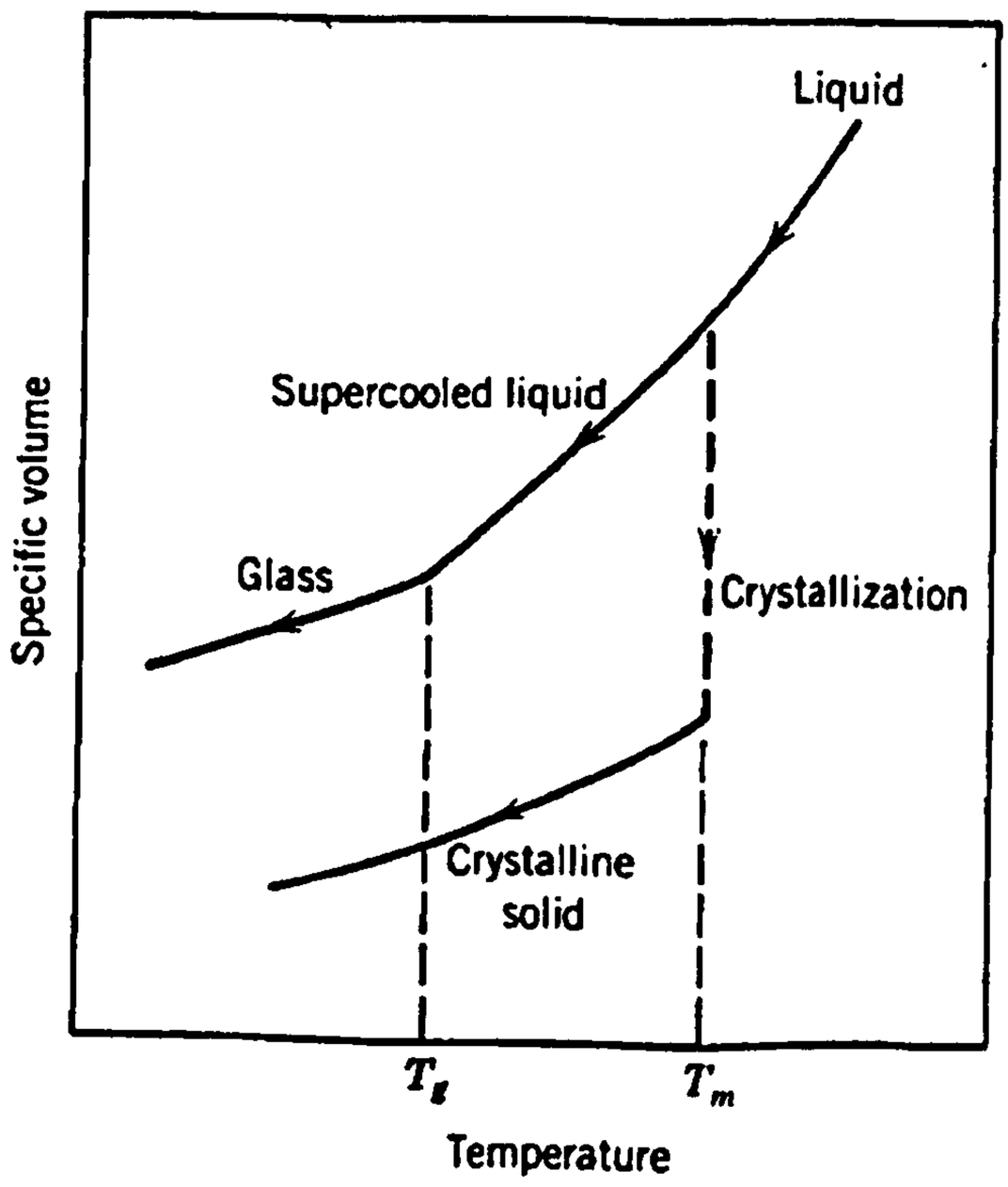


**Figure 2.4** Temperature-volume changes in crystalline non-crystalline materials (Callister, 1994)

### 2.4.3.2 Structure and Formation

Several structural theories of glass formation have been developed since that of Goldschmidt's in 1926, who proposed that glasses are formed in systems where the ratio of a cation radius to that of an anion radius is between 0.225 and 0.414, with a tetrahedral coordination polyhedra (i.e. a coordination number of 4). Zachariasen (Callister, 1994) proposed the random network model whereby glasses are viewed as 3-D networks or arrays, lacking symmetry and periodicity, i.e. no structure repeated at regular intervals. In the case of oxide glasses, these networks are composed of $O_2$ polyhedra. Figure 2.5 (Kingery, 1976) illustrates the difference between structures of crystalline form and glassy form.

Adopting the hypothesis that a glass should have an energy content similar to that of the corresponding crystal, W.H.Zachiaresen (Callister, 1994) considered conditions for constructing a random network and proposed four rules for the formation of an oxide glass:

- Each oxygen ion should be linked to not more than 2 cations
- The coordination number of oxygen ions about the central cation must be small (4 or less).
- Oxygen share polyhedra corners, not edges or faces
- At least 3 corners of each polyhedron should be shared

In practice, glass-forming $O_2$ polyhedra are planar triangular units; tetrahedra and cations forming such coordination polyhedra have been termed Network Formers. Network Modifiers break up the 3-D glassy network by the addition of monovalent anions; the anions occupy random positions distributed through the structure and provide local charge neutrality. Cations of higher valence and lower coordination number than network modifiers may contribute to the network structure and are called network intermediates; a 3-D glass network will form when an intermediate is added to a glass-forming oxide.

As for glass formation, the crystal nucleation and growth in glasses is an active area of investigation because there are many parameters that determine which melts form glasses upon cooling. Many solutions have appeared, based on viscosity-temperature relationships, diffusion rates, thermodynamic barriers, or structural requisites (Gustow, 1990). Glasses are deliberately fabricated such that bulk crystallisation is avoided. However, most glasses exhibit surface crystal nucleation. In order to promote internal nucleation within the volume of a glass, it is usually necessary to add a nucleating agent, which may for example consist of metallic particles or another oxide (James et al, 1997); this results in the production of a glass-ceramic, which will be discussed in the next section. An example of a nucleating agent is that described by Reaney et al (1996) who identified $TiO_2$ and $Al_2O_3$ as volume-nucleating agents in calcium phosphate-based glasses.

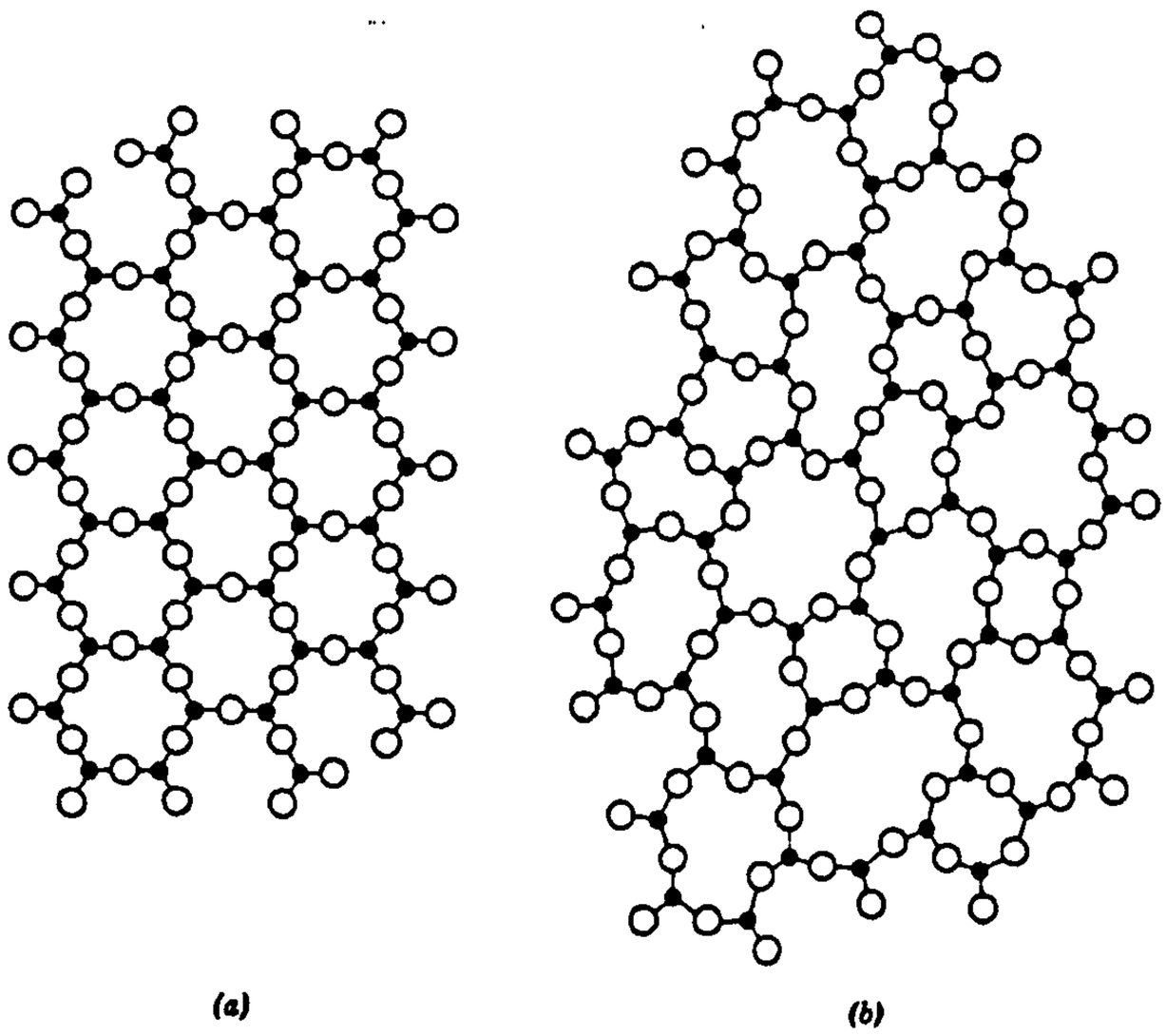


**Figure 2.5** Schematic representation of (a) ordered crystalline form (b) random-network glassy form of the same composition (Kingery, 1976)

### 2.4.3.3 Bioactivity

The criterion that determines whether or not a glass is bioactive is such that a calcium phosphate surface layer must form on the surface of the glass when it is surrounded by body fluid. The implant therefore obtains a new surface, which may bind with bone through osteoblastic deposition and thereby protect the glass from further

dissolution. The solubility of phosphate glasses contribute to its potential as a material for bone substitution. Clement et al (1998) evaluated the influence of chemical composition on the solubility of a range of phosphate glasses in the $P_2O_5$-CaO-$Na_2O$ system. The solubility was dependent on the $Na_2O$ content, as indicated by the fact that mass loss per unit time increased as the mol % of sodium in the glass decreased. These findings contradict Salin et al (1998) who claimed that the solubility of calcium phosphate based glasses is related to that amount of CaO present whereby glasses containing less than 20 % are very soluble and those containing more are much less soluble. However, in the presentation of data in Salin et al's paper, it appears that the solubility increases with increasing amounts of $Na_2O$. The theory behind this is that both CaO and $Na_2O$ are both network modifiers, hence they reduce the stability of the glass and therefore both will result in increased solubility in solution; increased ionic mobility results in increased reactivity of the system. Nevertheless, Salin et al found that the phosphate based glasses that were prepared were not cytotoxic following in-vitro studies and therefore have potential in the use of bone repair systems.

Silicate-based glasses, such as the commercially used Bioglass®, also display bioactive behaviour and have proven to be capable of bonding to bone and connective tissue (Hench, 1990) (Vogel et al, 1987). Furthermore, Bioglass® has been shown to be very easily manipulated (Wilson et al, 1992) when being packed into a defect in-vivo.

### 2.4.4 GLASS CERAMICS

#### 2.4.4.1 Definitions

A glass-ceramic is an inorganic product of fusion, which can be made to transform from a noncrystalline state to one that is crystalline by means of a process called devitrification. This process may not be desirable in many cases since devitrified polycrystalline glass may contain residual stresses as a result of the discontinuous volume changes that attend the transformation, which may yield a mechanically poor

material. For some glasses, however, the devitrification process can be controlled such that a fine-grained material is produced which is devoid of any in-built stresses. These materials, called glass-ceramics, can achieve relatively high mechanical strengths. A glass-ceramic that has been used in spine and hip surgery since 1983, as a bone filler and a major load-bearing material is apatite-wollastonite (A-W); the success of A-W glass ceramic is due to its excellent bioactivity and mechanical properties (Kokubo et al, 1985)(Nakamura et al, 1985).

### 2.4.4.2 Formation and Properties

The production of a glass-ceramic is a controlled crystallisation process, which involves the conversion of a glass to a crystalline material by the addition of nucleating agents and crystallisation heat treatment. Glasses are heat-treated to produce a glass-ceramic through two or more steps; firstly, a lower temperature step for promoting nucleation, and one or more higher temperature treatments to induce crystal growth and the desired microstructure (Zarzycki, 1991). This product of crystallisation typically consists of fine grains (<10μm) and contains approximately 2 % residual glass at the grain boundaries (Hanson et al, 1993).

One of the advantages of glass-ceramic materials is that their microstructure can be tailored to gain certain properties by controlling the heat treatments. The ability to control microstructure is very advantageous because microstructure directly affects the mechanical properties in all engineering materials. McDermott et al (1997) identified large differences in the microscopy of calcium phosphate glasses at range of temperatures; at high temperatures, the material appeared coarser which lowers the mechanical integrity of the system. Another advantage is that glass-ceramics are very easily machined. Boccacini et al (1997) identified a means of measuring how machinable a glass-ceramic is; a "brittleness index" (B) was suggested and it was found that this index should be lower than $B \approx 4.3\ \mu m^{-1/2}$. Other authors such as Hockin et al (1996) preferred to use the depth of penetration experienced during indentation as an indication of machinability.

### 2.4.4.3 Bioactivity

Glass-ceramics of the $CaO-P_2O_5-SiO_2$ system demonstrated biocompatibility at the in-vitro level as determined by the studies of Laczka-Osyczka et al (1998). AW glass-ceramic was shown by Ohgushi et al (1996) to indicate in-vitro biocompatibility; the data obtained in this study indicated that the surface of the glass ceramic promoted osteoblastic differentiation. Glass ceramics have also been shown to be bioactive at an in-vivo level. Gross et al (1985) found that in order for bone-bonding to occur, the glass-ceramic must not release substances such as polyphosphates, which may inhibit the mineralisation processes at the bone-implant interface.

Vogel et al (1987) condoned the use of crystalline as opposed to non-crystalline material in biomedical applications, in that glass-ceramics are both bioactive and biocompatible. Glass-ceramics may be accepted by tissues of the human body and may further establish firm intergrowths with bone tissue. Andronescu et al (1995) carried out in-vitro and in-vivo tests on $Na_2O-CaO-SiO_2-P_2O_5$ glass ceramic systems to determine biocompatibility and bioactivity respectively and found that the glass-ceramics showed no cytotoxicity in-vitro and no bone necrosis of the surrounding tissue in-vivo.

A commercially available bioactive glass-ceramic, which has been used widely to replace the iliac bone segment in the vertebral column, is known as Cerabone® (an AW glass-ceramic), and has been shown to shorten the recovery time for a patient in spinal and other reconstructive surgery. Cerabone® is a high strength glass-ceramic that, due to its additional biocompatibility and bioactivity, may be used in major load-bearing medical applications. More recently, Duskova et al (2000) launched an investigation into the potential of oxyfluorapatite and wollastonite glass-ceramics for use in facial augmentation surgery for post-traumatic and congenital disorders. The glass-ceramics were chosen on the basis of their low resorbability and performed successfully. Furthermore, it was concluded that bioactive glass-ceramics have better mechanical properties and more stable chemical features (i.e. lower resorbability) than hydroxyapatite, for example.

## 2.5 SUMMARY

The bioceramics industry has shown great interest in using synthetic HA as a bone replacement material, as a result of its bioactivity in an osseous environment. Of course, there are a number of other bioceramics available in the prosthetics industry that are biocompatible but undergo different mechanisms of bioceramic-tissue attachment. The mechanism that a bioactive bioceramic or bioglass undergoes appears to be more beneficial to the long-term stability and mechanical integrity of the bone in question, especially if the implant is porous and allows significant bone ingrowth to compensate for the weaker mechanical properties of a porous structure. The material must be reactive enough to initiate a biological reaction, yet not too reactive that it resorbs too rapidly. HA is a highly biocompatible option, which is not as resorbable as TCP, but not as strong as glasses and glass-ceramics. The ideal bone replacement for high load-bearing applications must be strong and slightly resorbable, which may be achieved by perhaps reinforcing HA with a strong material that instigates some decomposition. The next chapter focuses on the calcium phosphate material, hydroxyapatite, for bone replacement, which is also the focus of the practical portion of this thesis.

# CHAPTER 3

# HYDROXYAPATITE CERAMICS FOR BONE REPLACEMENT

*This chapter aims to discuss hydroxyapatite, an osteoconductive calcium phosphate ceramic, and the concept of reinforcing hydroxyapatite as a means of improving the mechanical properties, followed by the effect of biological solution on hydroxyapatite-based composites.*

## 3.1 PROPERTIES OF HYDROXYAPATITE

### 3.1.1 INTRODUCTION

Hydroxyapatite (HA), a calcium phosphate ceramic, is similar to the mineral component of bone and has the following stoichiometric formula:

$$Ca_{10}(PO_4)_6(OH)_2$$

Depending on the preparation routes, HA can have a *dense* or *porous* structure. The "dense" structure is likely to contain micropores, while the "porous" structure contains macropores as well as micropores and depending on the particular preparation route may have the physical characteristics of an open cell foam.

This chapter contains information on both dense and porous HA. Despite the fact that this overall aim of the laboratory work is to produce porous reinforced HA, it is important to know basic information about dense HA because before a porous HA composite is produced, a dense HA composite must be produced, characterised, and optimised.

### 3.1.2 CRYSTAL STRUCTURE

Calcium hydroxyapatite has a well-defined crystallographic structure, which was refined by Kay et al (1992), showing the exact atomic positions in the crystal. HA has a hexagonal structure and with a space group $P6_3/m$, which is characterised by a six-fold c-axis perpendicular to three equivalent a-axes ($a_1$, $a_2$, $a_3$), all of which constitutes a three-dimensional network of calcium, hydroxyl, and polyhedral phosphate ions. The smallest building unit of the structure is the unit cell, which in this case consists of Ca, $PO_4$, and OH groups closely packed together. The ten calcium ions are present in either an octahedral site (Ca(I)), or a seven-co-ordinate site (Ca(II)); four occupy the Ca(I) positions, while six occupy the Ca(II) positions. The apatite structure is arranged such that substitutions of many other ions are allowed; when substitutions in the apatite structure for $Ca^{2+}$, $PO_4^{3-}$, or $OH^-$ groups occur, changes in properties occur as a result of changes in unit cell dimensions to accommodate different sized ions.

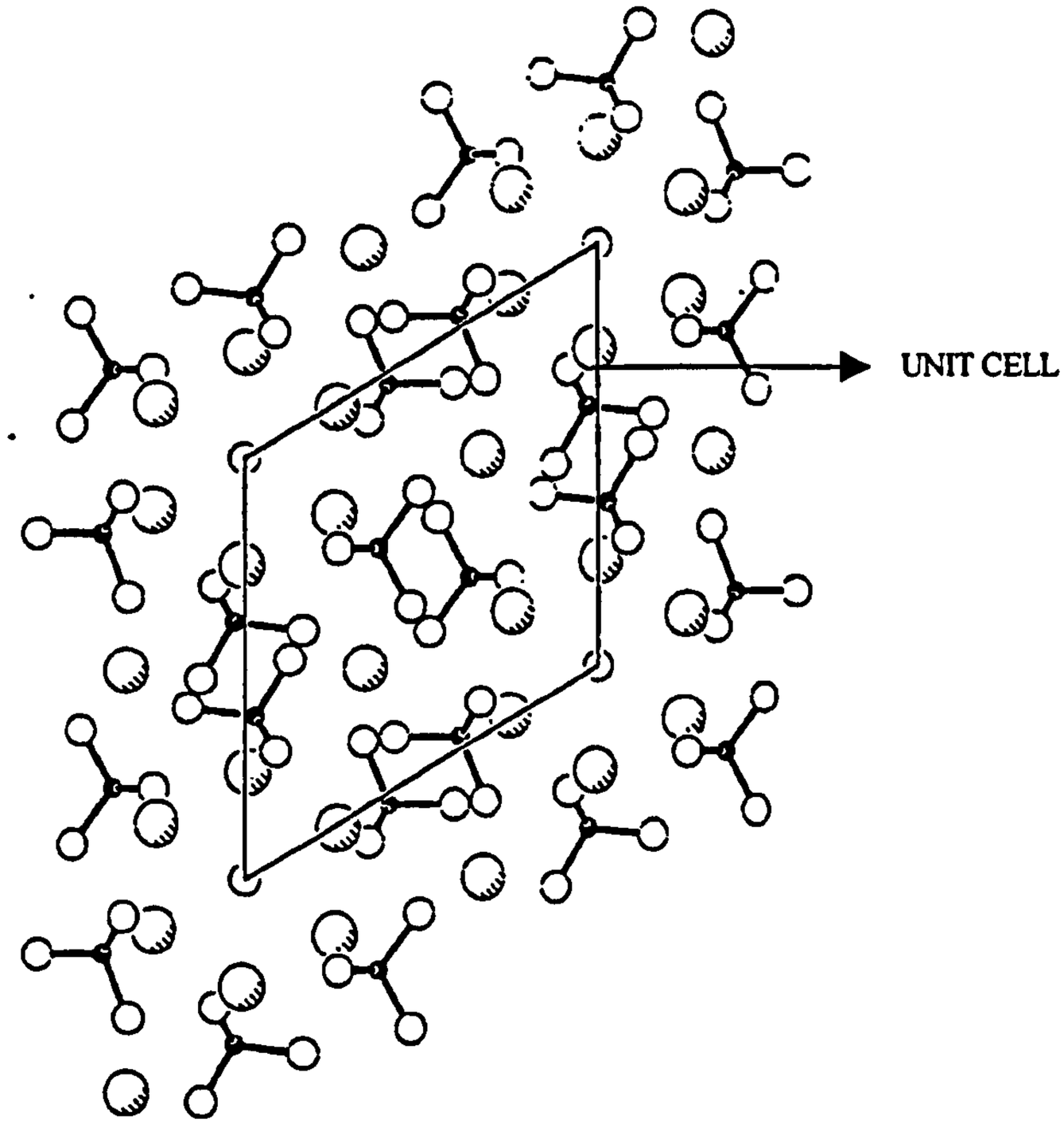


**Figure 3.1** Projection down c-axis of HA showing P(black circles), O(open circles), Ca(shaded circles) (Abrahams et al, 1994)

The unit cell, the smallest building unit of the apatite crystal, is shown in Figure 3.1 (Abrahams et al, 1994) and demonstrates how the Ca (II) atoms are arranged such that they form channels running parallel to the c-axis; the hydroxy ions may be found within these channels.

### 3.1.3 COMPOSITION

LeGeros (1993) found that pure, stoichiometric HA, $Ca_{10}(PO_4)_6(OH)_2$, has the following theoretical composition:

**Table 3.1** Composition of HA (LeGeros et al,1993)

| Element | Wt % |
|---|---|
| Ca | 39.68 |
| P | 18.45 |

(Wt. Ratio of Ca/P = 2.151, Molar ratio of Ca/P = 1.667)

Commercial or non-commercial dense HA materials may vary in their Ca/P ratio which will in turn affect the phase composition on sintering. If the Ca/P ratio is lower than 1.67, it will partially decompose to β-TCP and become a biphasic material; furthermore, β-TCP may be transformed to α-TCP at temperatures above 1300°C. At Ca/P ratios higher than 1.67, CaO will occur. However, if the Ca-P ratio is 1.67, only HA will be present and the precise phase compositin can be detected using X-ray diffractometry (Figure 3.2).

An X-ray diffraction pattern indicates the presence and percentage of phases within a material. The diffractometer apparatus (Figure 3.3) consists of an x-ray source which generates beams at point T towards the sample, and the intensities of diffracted beams are detected by a counter, labelled C in Figure 3.3. The counter moves at a constant angular velocity, during which the diffracted beam intensity is automatically plotted by a recorder, as a function of 2θ ( the diffraction angle). As a result a trace or rather a diffraction pattern is obtained.

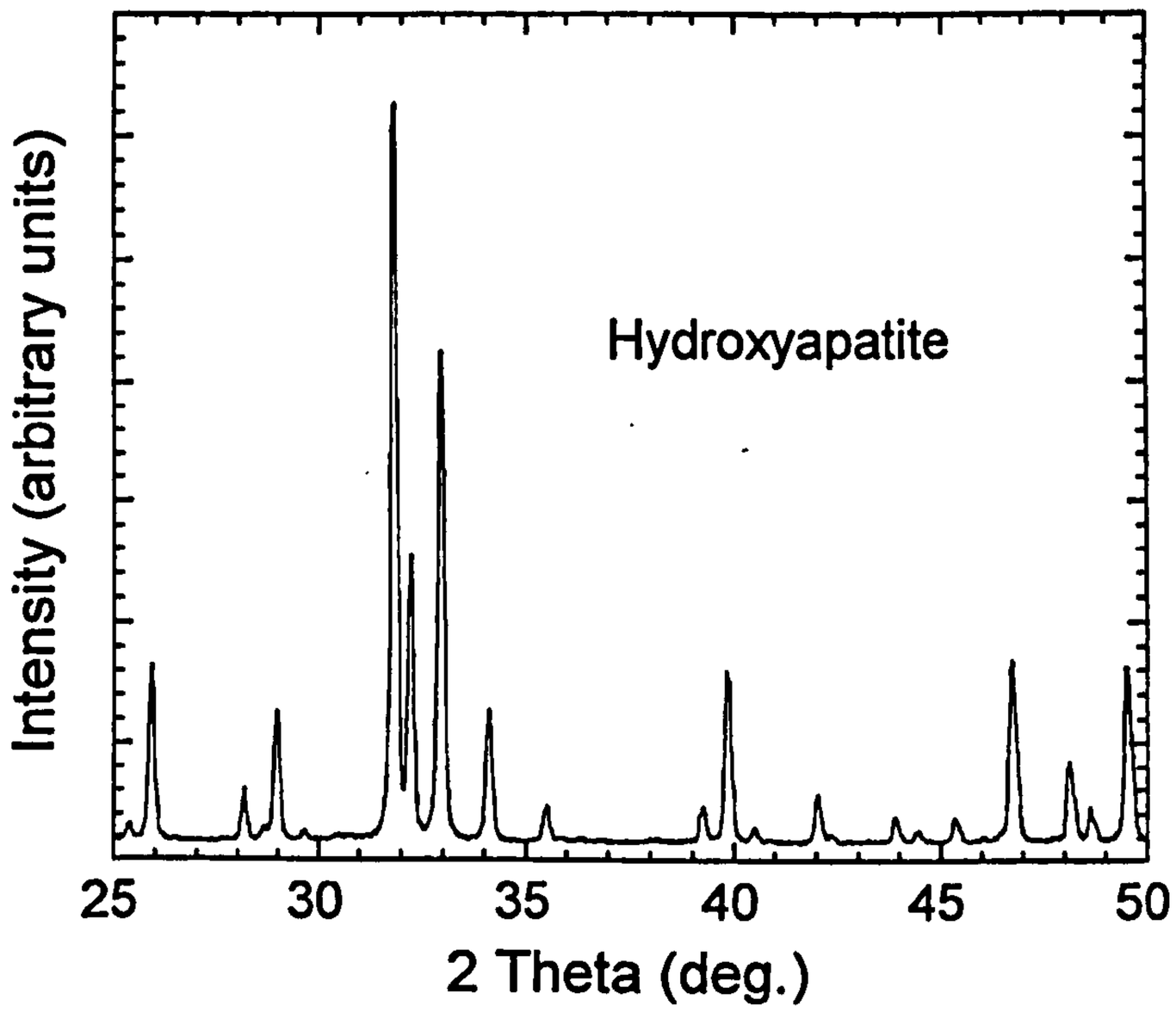


**Figure 3.2** X-Ray Diffraction pattern of powdered dense HA showing only the presence of the HA phase (PDF Card no. 9-432)

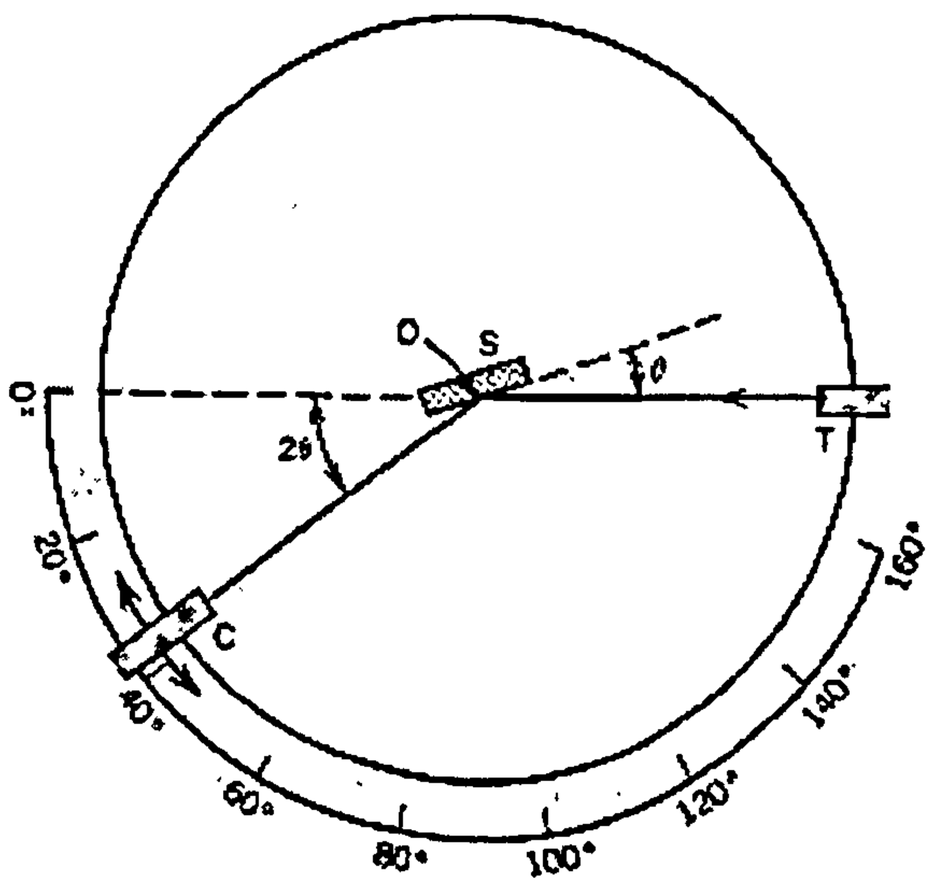


**Figure 3.3** Schematic diagram of an x-ray diffractometer (Callister, 1994)

At this point, it is very important to mention that HA is very sensitive to the sintering temperature used in densification. Different sintering regimes may result in the decomposition of HA to produce different phases, which will affect the mechanical and biological properties. Tampieri et al (1997) described this phenomenon very well where it was stated that at high temperatures (~1200°C), HA becomes unstable and tends to eliminate $OH^-$ groups and form decomposition products such as TCP, a highly resorbable material mentioned in the previous chapter. Their studies also demonstrated that α-TCP is more stable at high temperatures than β-TCP. The following diagram indicates the stable phases found present at increasing temperatures:

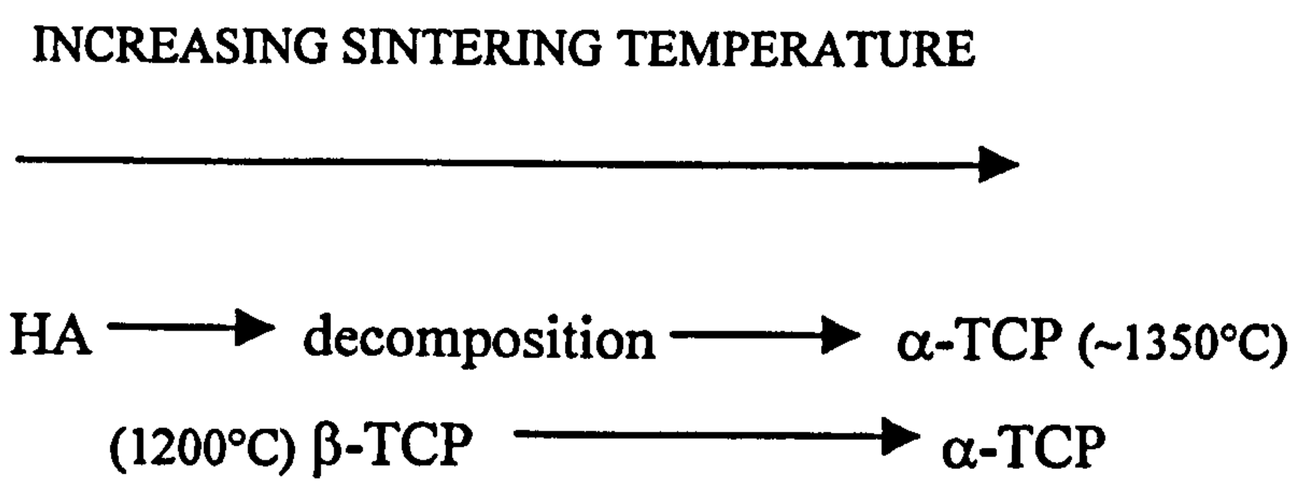


## 3.2 PRODUCTION OF POROUS HA

### 3.2.1 INTRODUCTION

Bone replacement materials should be fundamentally similar in structure to the bone in question in order for the implant to initiate bone integration and hence the stabilisation of the implant. Cortical bone contains Haversian systems, or osteons, that average 190-230 μm in diameter and intercommunicate through Volkmann canals. Therefore an ideal cortical bone substitute would be structurally similar to osteon-evacuated cortical bone with interconnectivity of similar dimensions. Klawitter et al (1971) established a minimum pore size (100μm) for bone in-growth into ceramic structures such as dense HA. However, Chang et al (2000) recently discovered through their findings (Table 3.2) that it is not the optimum pore size that is fundamental for optimising osteoconduction in porous HA produced via burn-out (discussed later in section 3.2.3), but rather the size of the interconnections between

each pore. However, this conclusion is questionable because the study did not clearly state whether both variables were tested simulataneously or separately which ultimately effects the viability of the relationship between the interconnection size and the degree of osteoconduction.

**Table 3.2** Effect of pore and interconnection size on osseoconduction (Chang et al, 2000)

| Pore Size (μm) | Interconnection Size (μm) | Degree of Osteoconduction |
|---|---|---|
| 50 | 20 | Basic |
| 300 | 250 | Optimal |

Cancellous bone is trabecular and contains macropores and micropores (both of varying porosity) within its' struts unlike cortical bone which is restricted to microporosity. In the trabeculae, the osteons appear as planar lamellae whose thickness permits the nutrition of its osteocytes from blood vessels in the large macroporous trabecular spaces. Therefore an ideal cancellous bone substitute would be structurally similar to that of osteon-evacuated cancellous bone with a thin lattice interconnected by pores ranging between 500 and 600 μm in diameter (Figure 3.4).

(a)

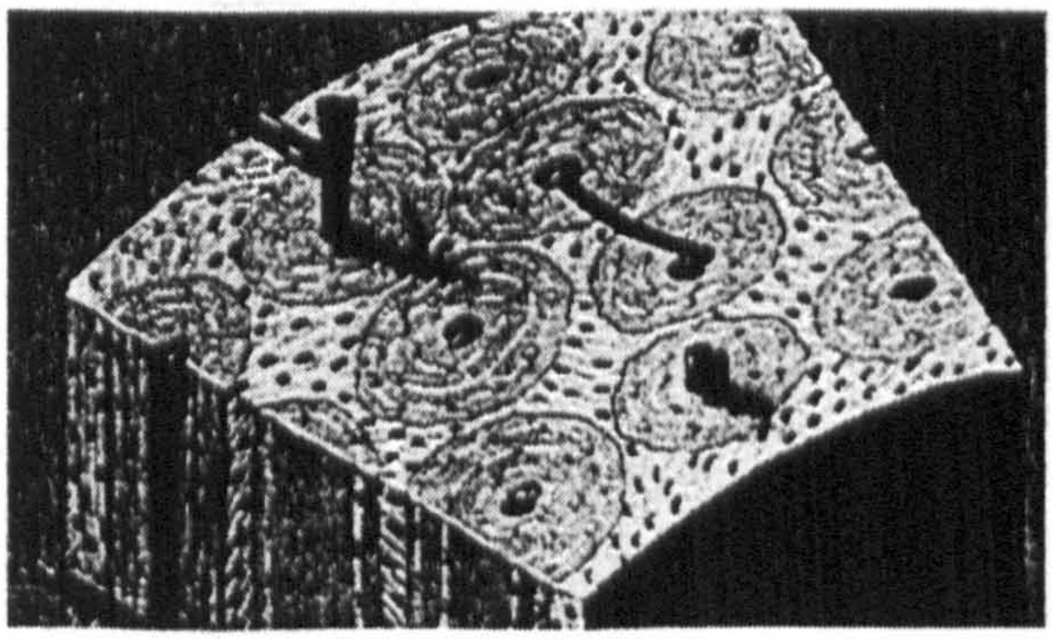

(b)

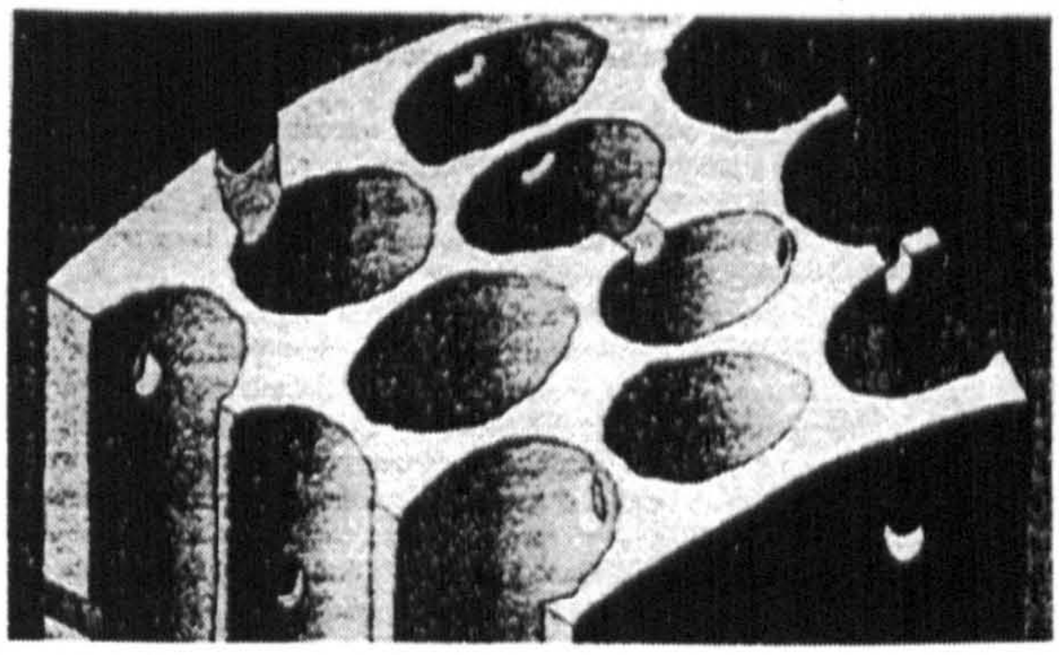

**Figure 3.4** (a) Microstructure of human cancellous bone (b) Idealized microstructure for cancellous bone regeneration (Shors et al, 1993)

Simske et al (1997) paid a great deal of attention to the engineering considerations of material property matching, especially in terms of the macroporous structure of ceramic bone substitute materials. An ideal structure was suggested whereby a gradient of porosity should exist; the greatest porosity should exist at the bone/implant interface and continually decrease until the implant material becomes either of optimal porosity or solid. This favoured quick bone ingrowth at the surface whilst still maintaining a degree of mechanical integrity. Whilst this idea may be advantageous to bone ingrowth, it may be mechanically detrimental to not only the implant, but the surrounding bone. A gradient of strength indicates that stress shielding may occur where the ceramic is strongest (taking into consideration that the ceramics are stiffer than bone), causing the implant to move and possibly microfracture, and therefore become weaker (not to mention necrosis of the surrounding osteoid tissue due to dis-use). This would ultimately result in a structure that is highly porous at the surface (hence weak by default) and weak in the center due to the presence of cracks/flaws as a consequence of stress shielding. Nevertheless, there are a variety of ways of producing porous ceramic bone substitute materials, which will be discussed in the following sections.

### 3.2.2 REPLAMINEFORM PROCESS

One of the early techniques for fabricating porous HA was developed by White et al (1972), called the replamineform process. This process involves using the skeletal structure of marine invertebrates, such as coral, as a template in the production of porous structures such as a porous HA. Coralline HA derives from the corals of the order Scleratinia, which includes a large group of marine invertebrates with skeletons of a porous nature (Weber et al, 1973; Wells, 1967). The coral is hydrothermally converted to porous HA by means of reacting the calcium carbonate skeleton with diammonium hydrogen phosphate, which involves a hydrothermal exchange of carbonate and phosphate , resulting in the formation of HA (Roy et al, 1974):

$$10CaCO_3 + 6(NH_4)2HPO_4 + 2H_2O \Rightarrow Ca_{10}(PO_4)_6(OH)_2 + 6(NH_2)CO_3 + 4H_2CO_3$$

In a study to characterize coralline HA, Piecuch (1982) found that the macrostructure resulting from the replamineform method consists of good pore interconnectivity and pore sizes suitable for bone ingrowth.

The great advantage of the replamineform process is that the raw materials, the coral organisms themselves, are easily accessible and the hydrothermal exchange is less time consuming than other conventional porous production methods (which will be discussed in the later sections of this chapter). The fact that these coral structures exist in nature give hope to dealing with the increasing demand for porous materials in medical applications. The disadvantage of producing porous coralline HA using this technique is the fact that porosity cannot be controlled by altering parameters in the process. In order to achieve an average pore diameter of 200μm, the correct species must be harvested with that specification such as the case with Interpore-200 (Yoshikawa et al, 2000), and to achieve an average pore diameter of 500μm, a species with macrostructural similarities must be harvested as in the case with Interpore-500 (White et al, 1996).

Coralline HA has also been proven to be biocompatible (Holmes, 1978) which reinforces its potential use as a bioceramic. Holmes et al (1987) carried out further

studies on the biocompatability of coral, in particular the colonial reef building coral of the family Poritae, which is known for the very interconnected porosity of its exoskeleton; it was reported that the implant demonstrated a great deal of bone ingrowth (51.2 % ) over 4 years. Salyer et al (1977) carried out studies on the biocompatibility of replamineform porous HA and found uniformly grown mature bone through the pores of the HA at 4 months after implantation, which highlighted the potential of replamineform HA in medical applications. More recently, porous coralline HA was proven to not only experience complete bone ingrowth in the dorsal regions of rats, but also lamellar bone formed followed by osteoclastic resorption and then new bone formation after 52 weeks (Yoshikawa et al, 2000). The fact that bone remodelling occurred was very promising; the fact that bone marrow stromal cells were previously cultured on their surface enhanced the process. However, one year is a very long time to wait for significant remodelling. Liao et al (2000) took biological studies on marine invertebrates one step further by crushing *Margaritifera* shells into granules (2mm diameter) and implanting them into the muscles and femurs of rats, and found that they were biocompatible, biodegradable, and osteoconductive. The shell granules experienced a dynamic interaction with the surrounding tissue, in which the bonding between the natural argonite and bone seemed to occur via a phosphorus-rich intermediate layer as opposed to mechanical interlocking.

Thermal treatment of materials has also recently been applied to human and bovine cortical bone (Catanese III et al, 1999) due to its success with coralline materials. It was discovered that cortical bone heat-treated at 350°C has excellent mechanical properties in compression, but very poor mechanical properties in tension, thereby limiting its applications.

### 3.2.3 Addition of Materials that Burn Out

A widely used technique for creating porous structures is the addition of particles to HA that are volatile and burn out during the sintering process, leaving a porosity that consists of spherical voids separated by narrow struts. If the pores do not exceed a minimum size of 100 μm (Shors et al, 1993), bone ingrowth does not occur, leaving empty channels and discontinuities in the bone. Liu (1996) used a drip-casting process

for fabricating porous HA. This process involved adding sythesized HA powder to de-ionized water and extensive mixing; this slurry was further mixed with poly(vinyl butyral) powders (PVB) of the following sizes: 95 μm, 250 μm, 400 μm. The slurry was then cast into a plaster mould of semispherical geometry by dripping onto the mould's surface with a pipette device. The dried, spherical-shaped casts were of granular appearance and were then heated at 500°C to burn out the PVB material, and followed by sintering at 1200°C for two hours. The resulting porous HA granules had a porosity from 24 to 76 % and pore sizes ranging from ~95 to ~400 μm (no mechanical properties were reported), which according to Shors et al (1993) meant that bone ingrowth will occur. Liu used another fabrication method in 1997* that involved adding PVB particles to the HA powder, which were then die-pressed, followed by sintering at 1200 ° C for two hours, resulting in macroporous structures of up to 55 % porosity (no mechanical properties reported). Huang et al (1995) adopted a similar method for fabricating porous alumina supports, whereby he added polyvinyl alcohol (PVA) binder to alumina in a slip-casting process; he discovered that the porosity of the resultant alumina support increased with PVA dosage (2-10%) from ~33% to ~40%. Shaw (1996) incorporated a different material altogether (graphite particles) into the green state, which were burnt out during sintering leaving voids and resulting in a porous structure.

More recently, burn-out routes have been optimised such that the resulting pore morphology and porosity could be controlled to produce structures even more similar to cancellous bone. In 1998, Liu et al fabricated a porous HA bioceramic via a slip-casting route; ceramic slurry was prepared at a desired rheology and then mixed with polymeric powders of controlled quantity and particle size. Investigations into the mechanical properties of the final structure revealed that the flexural strength decreased with increased macropore size. Rodriguez-Lorenzo et al (1998) reported similar findings in their porous HA ceramics processed via starch consolidation. This new method is based on the ability of starch to gellate in water, and in the process the starch is used as a consolidator, a binder, and a pore former. The end porosities obtained ranged from 45-67%. However, the most macroscopically identical synthetic implant processed via burn-out to date was fabricated by Tancred et al (1998). The procedure, shown in Figure 3.5, involved burning out the organic matrix

from cancellous bone and immersing the resulting inorganic matrix in wax, followed by decalcifying, leaving a wax negative replica of the bone. The wax mould is then dipped in ceramic slurry, left to dry, and the wax is then burned off leaving a ceramic positive replica of the original bone. So far this process has been successfully completed using HA, β-TCP, and HA/ β-TCP.

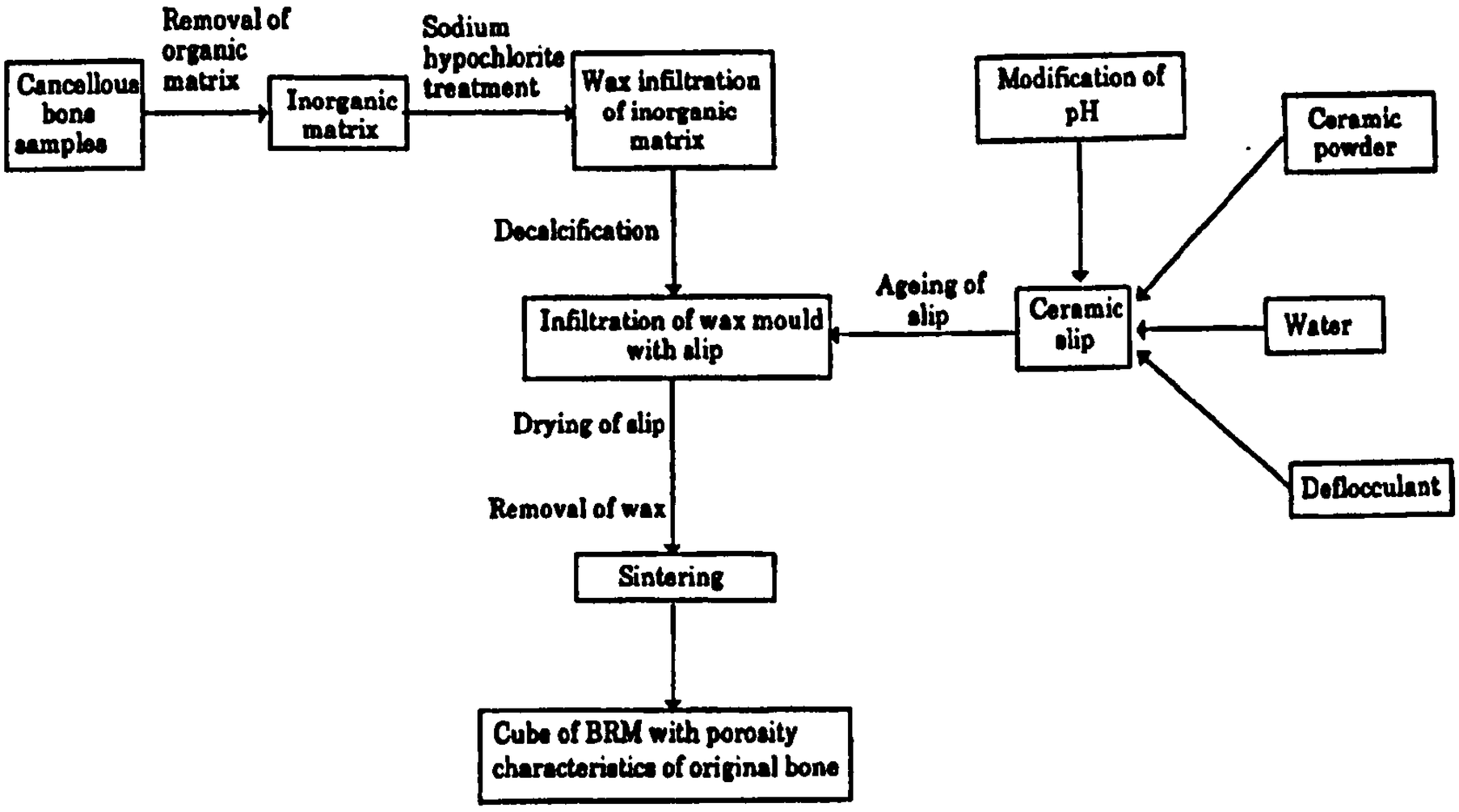


**Figure 3.5** Process flow chart for producing porous apatite ceramics (Tancred et al, 1998)

### 3.2.4 PRE-TREATMENT WITH GAS

A successful method (Peelen et al, 1980) (Shaw, 1996) has been used for creating a macroporous structure by adding $H_2O_2$ solution to a cast HA slip, allowing it to effervesce with the aid of a platinum catalyst, and leaving it to dry overnight. When the samples were removed from the mould, bubbles were trapped in the dried slip. Arita et al (1995) used a gas-forming agent, $CaCO_3$, to react with dibasic calcium phosphates ($CaHPO_4$) at a calcination temperature of 1000 ° C:

$$6CaPO_4 + 4CaCO_3 \Rightarrow Ca_{10}(PO_4)_6(OH)_2 + 2H_2O + 4CO_2$$

The evolution of gaseous $CO_2$ and gaseous $H_2O$ during the reaction results in the creation of voids whose sizes are controlled by the particle size of the original $CaCO_3$.

Unfortunately, Arita et al (1995) only mentioned porosity in a qualitative manner and referred to densities (50% theoretical achieved) as an indication of the degree of porosity.Yang et al (1998) similarly found that $CaCO_3$ and $CaHPO_4.2H_2O$ serve as pore-forming agents due to the evolution of $CO_2$ and water during the reaction and further found that it was possible to achieve porosity (up to 42 %) control by mixing the two powders in various proportions; pore volume was not mentioned. The fact that the authors do not state all the facts in their studies, such as porosities and pore sizes achieved, makes it very difficult to compare and contrast the data in order to decipher the most efficient preparation conditions and properties.

### 3.2.5 FOAM METHODS

A foam may be defined as "*a structure that consists of material domain separated by voids which may be filled with gases*," (Williams et al, 1989). Most commercially available, low-density organic polymer foams consist of the blown foam type with cell sizes typically ranging from 100 to 1000 μm where the cells are closed due to the use of gases in the production of the foam. Furthermore, scanning electron microscopy has shown that these commercial foams have relatively thick walls (> 10 μm) in order to provide maximal mechanical properties at a given density, as well as well-defined cells.

The ideas behind the methods for fabricating a variety of ceramic foams can be applied to the production of ceramic foam composites. HI-POR Ceramics, a division of Dytech Corporation Limited ( owned subsidiary of J & J Dyson plc) has been formed to manufacture a foamed ceramic product, the patent of which is owned by the Dytech Corporation Ltd. The route taken to produce a final foamed ceramic product is shown in Figure 3.6. In 1997, Binner characterised some of the foams patented as a result of joint collaboration between the University of Nottingham and Dytech Corporation and found that the foams could be manufactured in a variety of near-net shapes and sizes and they were easily machinable. Binner identified a very fundamental criterion in the manufacture of foamed ceramics, i.e. the ability to produce a stable ceramic suspension.

The process starts with the addition of organic binders and dispersing agents to ceramic powder, resulting in an aqueous dispersion to which a foaming agent is added. The organic binder must then undergo gelation to stabilise the foamed structure, forming a strong cross-linked polymer-water gel, thereby trapping the ceramic and water in the foamed structure. After drying, the gelled structure is heated to burn out the organic binder and then sintered to obtain the required foamed ceramic material. Recently, a system for manufacturing porous HA in this way has been developed by Dytech (Sambrook et al, 1993).

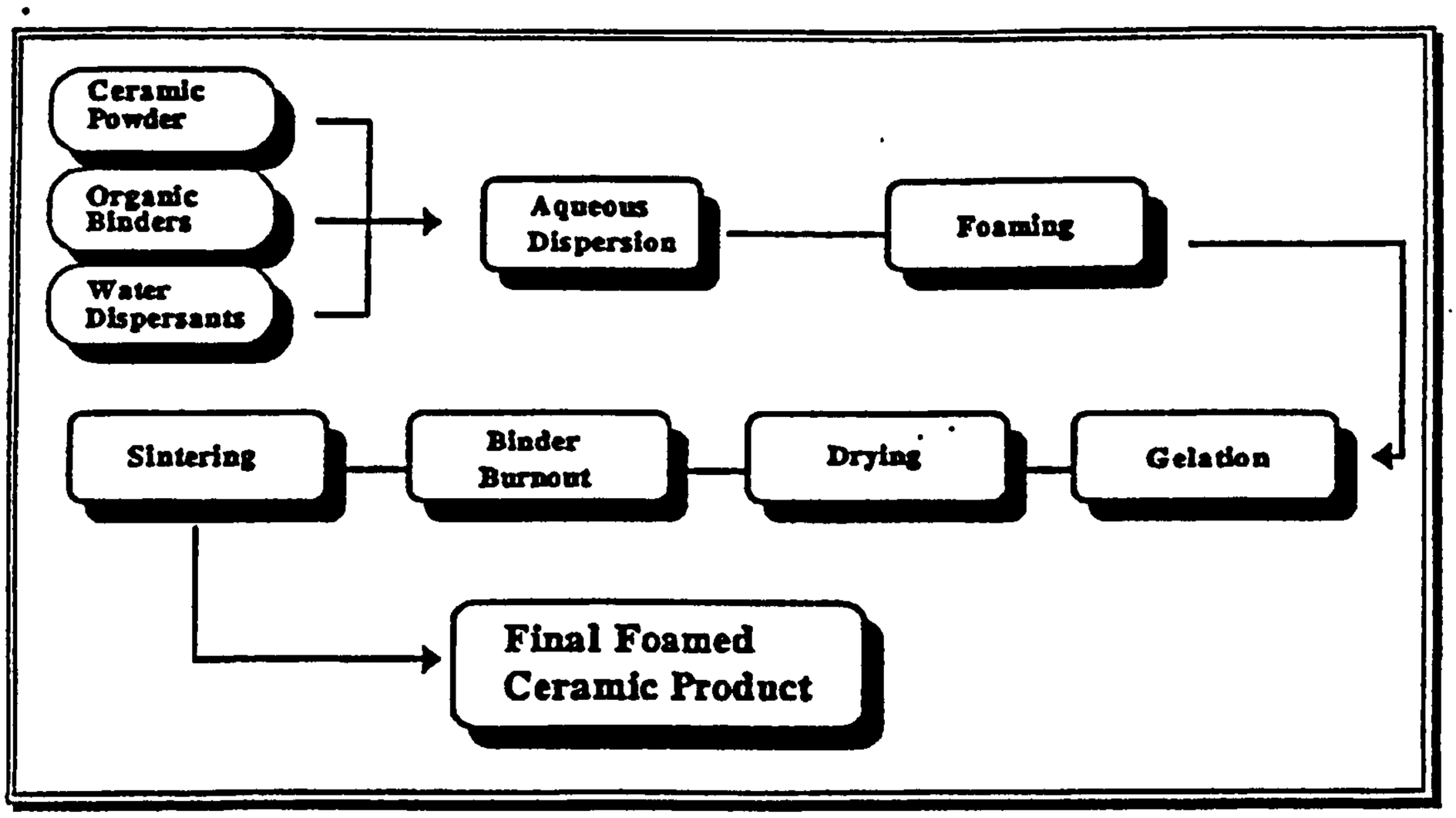


**Figure 3.6** Simplified flow diagram of manufacturing process (Sambrook et al, 1993)

In 1999, Engin et al manufactured macroporous HA in a similar manner, whereby HA powder was mixed vigorously with methyl cellulose binder, dried, cut, and then followed by sintering. The difference in this investigation was that the porous foam did not undergo "binder burn-out", according to the findings, but were slowly heated to the optimum sintering temperature. The sintered structure may be seen in Figure 3.7 and appears to show good macrostructural integrity. However, it seems odd that such a good macroporous structure could result from a heating regime that omits a burn-out phase. Theoretically, the continual increase in temperature would cause the polymer to pyrolyse and expand, whilst the ceramic shrinks due to the sintering process, resulting in compression-induced cracks in the macrostructure. Unfortunately, there were no high magnification images included in this paper.

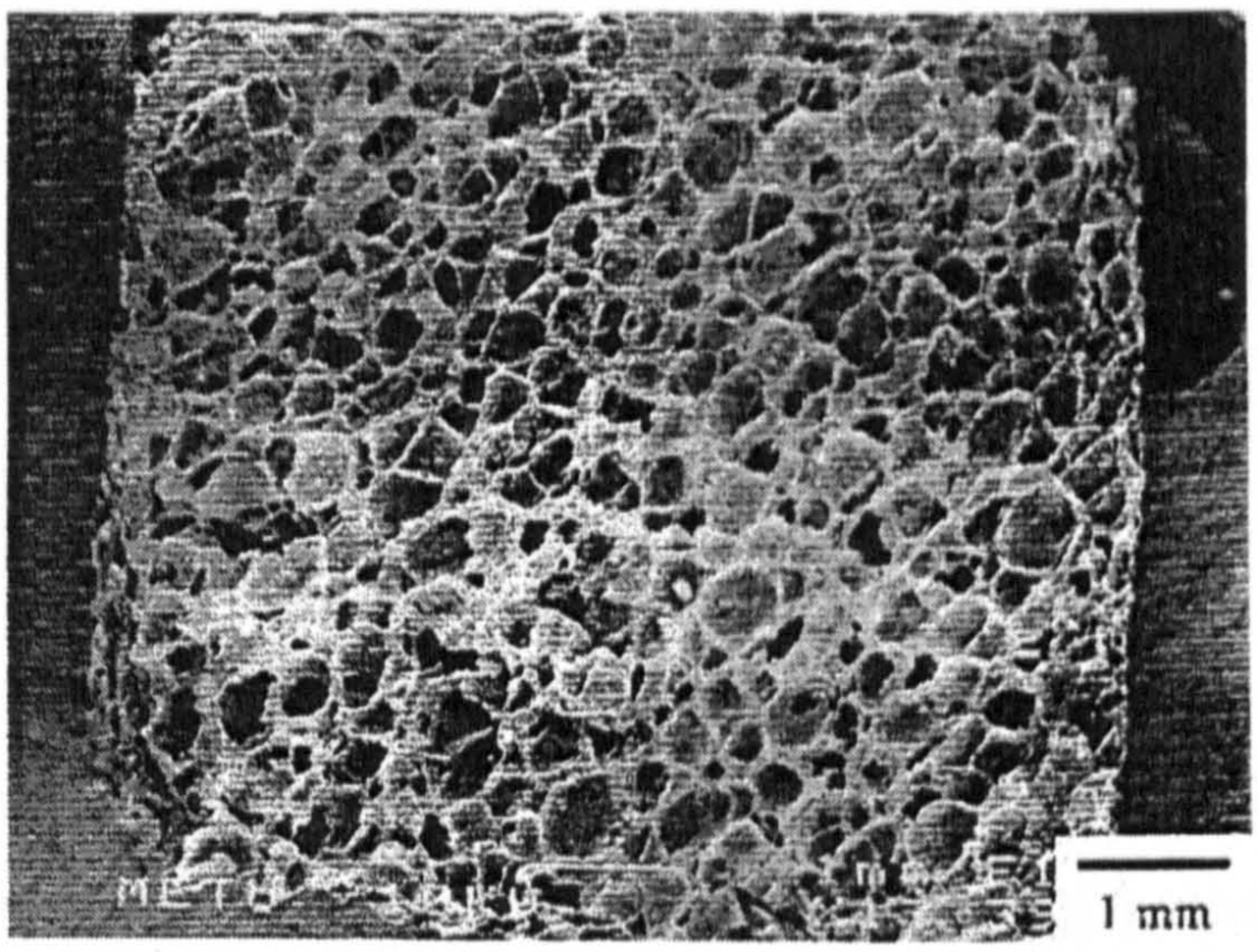


**Figure 3.7** SEM micrograph of HA bioceramics of 60 % porosity (Englin et al, 1999)

Twigg et al (1995) prepared a ceramic foam that had a sponge-like porous structure by pouring a ceramic slurry of ceramic particles onto an open-cell organic polymer foam (the organic precursor was polyurethane). The plastic foam was burnt off during heat treatments and the ceramic was then sintered to achieve either a positive or negative replica of the original polymer foam. The positive replica resulted from the removal of excess low-viscosity slurry by blowing air through the foam or compressing the foam. This was followed by drying, calcining, removing the organic precursor through vaporisation and combustion, and then sintering, resulting in a ceramic foam which was a positive image of the plastic foam skeleton with high porosity (up to 85 %), but low bulk density ($0.75 g.cm^{-3}$). The negative replica procedure involved pouring a slurry with increased viscosity onto the foam, which was then shaken or vibrated to remove any excess slurry; so ensuring that the organic pores remained filled with the ceramic slip. Removing the binder and organic foam upon calcination resulted in pores that corresponded to the original foam structure. The resulting ceramic foam had a lower porosity (up to 61%), but higher density($1.54 g.cm^{-3}$) than that obtained by the positive replica method. In order to optimise the processing technique, it is necessary to create a slurry that has the correct ratio of binder: water: powder, hence an appropriate viscosity.

A slightly different technique using burn-out is the mixing of ceramic powder and polymer pellets, as opposed to pouring a ceramic slurry on the pre-cursor. Williams

et al (1996) described an inexpensive route for manufacturing moulded porous ceramics by incorporating alumina powder into polystyrene by high shear mixing and immersing the pelletized product in pentane. This was followed by a single-stage steam treatment, resulting in low-density foam mouldings that retained their shape during pyrolysis of the polystyrene. The foams were then sintered, yielding a ceramic with ~84 % porosity. This technique results in porosity adequate for bone ingrowth.

More recently in 1998, company by the name of Ultramet developed and patented a biocompatible, cellular, 80 % porous material called Hedrocel for bone substitution. The manufacturing process involved the pyrolysis of a polymer foam into a reticulated vitreous carbon (RVC) foam with up to 50% theoretical density. Following this was the chemical vapour deposition and chemical vapour infiltration processing, resulting in the fabrication of ceramic foams such as silicon carbide. This biocompatible material is currently being used in the fabrication of artificial hips, vertebral bodies, and spinal discs, and has also been used to develop cell growth systems.

The three burn-out methods mentioned (i.e. foaming the slurry followed by heating, pouring the slurry onto a foam followed by heating, and then mixing the powder with polymer powder and heating) resulted in 60 –80 % porosity, which is adequate for bone ingrowth in-vivo. However, in terms of optimising the mechanical properties, perhaps the technique involving pouring the slurry over the foam is the most efficient, especially if an ideal burn-out temperature and burn-out time is used, hence avoiding compression cracks from polymeric expansion.

A more promising area of foam technology is that of porous biodegradable composite scaffolds, whereby porous ceramic/polymer composites are used not as bone substitutes but more so as biological scaffolds for bone to grow into. In an ideal situation, the composite scaffold biodegrades at a similar rate to the ingrowth of bone. Zhang et al (1999) used a thermally induced phase-separation/sublimation of solvent technique to create a highly porous composite scaffold, i.e. a polymer/HA composite skeleton, and reported good mechanical properties (compressive modulus of ~11MPa and yield strength of up to ~0.40MPa) as well as up to 95 % porosity and pore sizes of up to 100μm. Considering how high the porosity was, i.e. how low the density, the

mechanical properties obtained were very promising. Thomson et al (1998) similarly produced a biodegradable polymer/HA scaffold, the only difference being the use of HA short fibres as opposed to powder. The mechanical properties from Thomson et al's (1998) investigation revealed a compressive modulus of ~80MPa and a yield strength of ~2.8MPa. Unfortunately, the porosities and pore volumes were determined using mercury porosimetry and therefore the values are incomparable those of Zhang et al (1999). This inconsistency of data therefore makes it difficult to state whether the strengths achieved were good in terms of the porosity.

## 3.3 MECHANICAL PROPERTIES OF HYDROXYAPATITE

### 3.3.1 DENSE HYDROXYAPATITE

Hydroxyapatite is often chosen as a bone substitute material due to its similarity to the mineral naturally found in bone. The important contribution that this bone mineral makes towards the overall mechanical properties of bone was highlighted by Kotha et al (1998). Bovine bone was treated with fluoride ions and mechanical tests indicated a reduction in strength; the fluoride action reduced most of the structurally effective bone mineral content to calcium fluoride. Hence changing the amount of bone mineral present varies the mechanical properties of bone tissue. Due to the obvious role of the mineral content in maintaining the mechanical integrity of bone tissue, it is important to mechanically characterize a potential bone-replacement material which is very similar to bone mineral, i.e. commercial hydroxyapatite.

Hydroxyapatite is structurally brittle, but strong in compression, behaviour which is typical of ceramics in general at room temperature. Fracture almost always occurs before any plastic deformation can occur in response to an applied tensile load. Like most brittle ceramics, the fracture process of HA consists of the formation and propogation of cracks through the cross-section of material in a direction perpendicular to the applied tensile load. In crystalline ceramics, crack growth occurs through the grains (transgranular) and along specific crystallographic (cleavage) planes (Callister,1994). Fracture occurs due to the presence of very small and omnipresent flaws (microcracks, internal pores, grain boundaries) which serve as

stress-raisers, thereby increasing the magnitude of the applied stress. Fracture toughness ($K_{IC}$) is used to measure a ceramic's ability to resist fracture when a crack is present. However, for compressive stresses, stress amplifications are not associated with any existent flaws, which explains why ceramics have much higher strengths in compression than in tension. When ceramics are subjected to both tensile and compressive stresses, i.e. in three or four-point bending, the stress at fracture corresponds to the bending/flexural strength.

### 3.3.1.1 Mechanical Properties

Table 3.3 lists some general mechanical properties of HA, with an inclusion of TCP for comparison. In this table, it can be seen that dense HA is not as strong as cortical bone in compression (comparing the values to those found in the literature in Table 1.1.), with lower fracture toughness than bone (refer to Table 1.1 and 1.2),and weaker in bending than in compression. However, dense HA displays good stiffness (similar Young's moduli to that of cortical bone, listed in Table 1.1 to 1.4). In comparison to HA, TCP is stronger, less stiff, and tougher according to Metsger et al's (1999) results. It was concluded that by increasing the sintering temperature of HA, hence increasing the amount of TCP present from the decomposition of the HA, the overall mechanical integrity of HA increases. Aoki (1991) found a strong relationship between the sintering temperature of HA and its respective compressive and flexural strengths, as shown in Table 3.4. The compressive strengths were much higher than values found for bone. This may be due to the absolute accuracy of the cutting of the rectangular specimens used in his study, not to mention the likelihood of polishing, which is traditionally never mentioned; these factors will eliminate surface imperfections and increase flexural strength due to elimination of stress concentrations.

**Table 3.3** General mechanical properties of hydroxyapatite (authors stated in table)

| Material | Density ($g.cm^{-3}$) | Flexural Strength (MPa) | Vicker's Hardness (MPa) | Compressive Strength (MPa) | Young's Modulus (GPa) | Fracture Toughness ($MPa.m^{1/2}$) |
|---|---|---|---|---|---|---|
| HA (Metsger et al, 1999) | | | | 70 | 9.2 | 0.36 |
| TCP (Metsger et al, 1999) | | | | 315 | 21 | 2.34 |
| HA (Lu et al,1998) | 3.12 | 110 | 820 | | | |
| HA (Tampieri et al, 1997) | | 130 | | | | |
| HA (Willman 1996) | 3.16 | < 100 | | 100 - 200 | 100 | < 1 |
| HA (De With et al, 1981) | | | | 115 | 112 | 1.0 |

**Table 3.4** The effect of sintering temperature on the mechanical properties of HA (Aoki 1991)

| Temperature (°C) | Compressive Strength (MPa) | Flexural Strength (MPa) |
|---|---|---|
| 1150 | 308 ± 46 | 61 ± 8 |
| 1200 | 415 ± 46 | 104 ± 11 |
| 1250 | 465 ± 58 | 106 ± 10 |
| 1300 | 509 ± 57 | 113 ± 12 |

### 3.3.1.2 Effect of Granule Size on the Mechanical Properties of HA

Granules are useful for the filling of irregular-shaped defects. Furthermore, the use of granules increases the surface area of the material which may favour the transfer of load from bone to implant. Reducing the HA granule size is also advantageous for improving its' mechanical properties. When the granule size is decreased, the specific surface area increases, which increases the bonding capacity between implant and bone. Furthermore, a decreased granule size results in more contacting surface areas, hence greater frictional forces, all of which improves the mechanical properties of a packed column, as well as the uniform pore distribution. Figure 3.8. (Luo et al, 1996) demonstrates the effect of the smaller spheres in comparison to the traditional and conventional spheres. Reduced particle size results in closer packing, i.e. increased surface area for biological reactions (greater biocompatibility) and better load distribution.

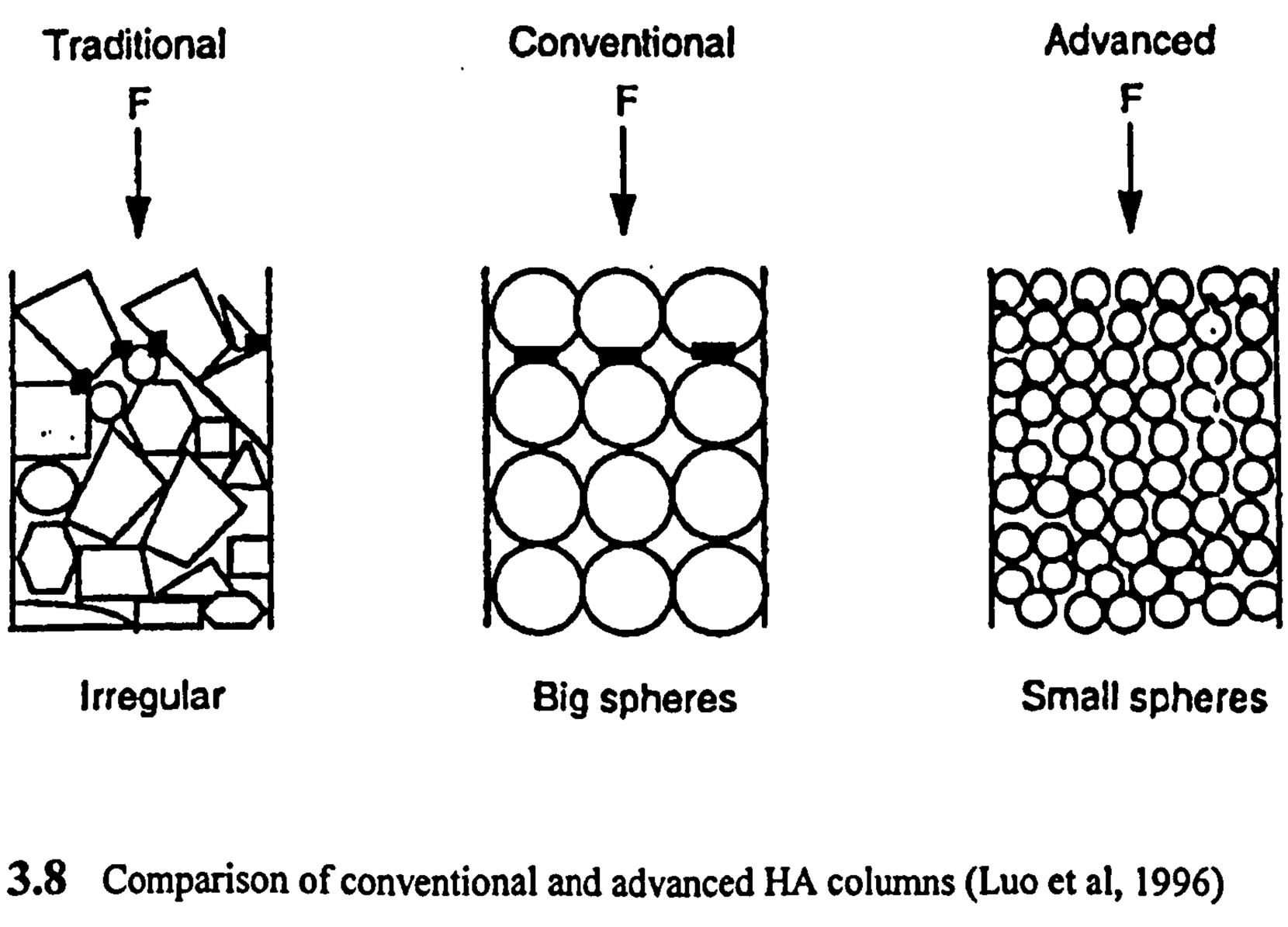


**Figure 3.8** Comparison of conventional and advanced HA columns (Luo et al, 1996)

Shareef et al (1993) studied the effect of decreasing individual granule size on the mechanical properties of HA, the results of which are shown in Table 3.5. The granules in this investigation were sieved to produce "pressbodies", from which ring-shaped test pieces were produced by double-ended uniaxial compression in a steel die

at 45MPa. The tensile strengths were determined using the Stanford ring bursting test, in which the test piece was pressurized internally to generate a tensile hoop stress in the ring.

**Table 3.5** The effect of granule size on the strength and toughness of HA (Shareef et al, 1993)

| | Maximum Granule Size (μm) | | | |
|---|---|---|---|---|
| **Property** | **710** | **500** | **250** | **100** |
| Tensile (MPa) | 20 – 24.2 | 23.5 – 29.3 | 29.2 – 33.3 | 31.8 – 37.1 |
| Fracture Tougness ($MPa.m^{1/2}$) | 0.48 – 0.55 | 0.51 – 0.62 | 0.61 – 0.68 | 0.69 – 0.73 |

These results are consistent with Luo et al's opinion in that the smaller the granule size, the better the mechanical properties. Biologically speaking, the high surface area created by using granules may be exploited in order to achieve rapid biological fixation. Burstein et al (1997) used porous granular HA in secondary orbitocranial reconstruction and found that the facial contour corrections induced by the implantation were long lasting, without evidence of granular resorption.

### 3.3.2 POROUS HYDROXYAPATITE

#### 3.3.2.1 General Properties

Porous HA bioceramics display lower strengths than dense bioceramics due to a combination of the existence of larger pores, hence more stress concentrations (i.e. macropores, as opposed to just micropores) combined with the thin lattice of struts. Table 3.6 contains the mechanical properties of various porous HA bioceramics before bone ingrowth. Unfortunately, different authors carry out different mechanical tests on their materials so there isn't a consistent means of comparing data, yet it is still informative. Furthermore, the test parameters such as sample size, cross-head velocity (on the testing apparatus), and test apparatus vary considerabely.

**Table 3.6** Mechanical properties of various commercial porous HA bioceramics (authors in table)

| Author | Year | Material | Mechanical Property | Value |
|---|---|---|---|---|
| White et al | 1986 | Interpore-200® (Commercial porous HA) (50 – 75 % porosity) | Compressive strength | 9.25 MPa |
| Holmes et al | 1984 | Coralline HA (Goniopora) (~66 % porosity) | Ultimate compressive strength | 2.3-5 MPa |
| Fabbri et al | 1995 | Commercial HA (70 – 80 % porosity) | Flexural strength | 1 – 2 MPa |
| Morgan et al | 1997 | Carbonated Apatite-Cancellous Bone Cement | Flexural Strength | ~0.468 MPa |
| Haddock et al | 1999 | Coralline HA | Ultimate Stress | 5.87 MPa |
| Engin et al | 1999 | HA (60-90 % porosity) | Fracture Strength | 5-10 MPa |
| Sepulveda et al | 1999 | HA (80.2-80.7 % porosity) HA (76.7 % porosity) | Compressive Strength | 4.4-4.7 MPa 7.4 MPa |
| Metsger et al | 1999 | HA TCP | Compressive Strength + Young's Modulus | 9.3 MPa/1.2 GPa 13 MPa/1.6 GPa |

### 3.3.2.2 Relationships between Strength and Porosity, Pore Size and Pore Geometry

Liu (1997) demonstrated that the compressive strength of porous HA decreases (from~37-1MPa) with increasing porosity (from ~47-77%) in an exponential manner (Figure 3.9); this is related to the decrease in the quantity of solid material present in each specimen (i.e.real density). Liu (1996*) previously reported that the compressive strength behaves linearly with macropore size; the larger the macropore, the lower the compressive strength (Figure 3.10). Liu (1996*) also reported a relationship between pore geometry and compressive strength; porous HA containing spheroidal/ellipsoid pores showed higher strength than that containing oblate pores (Figure 3.11). LeHuec et al (1995) found similar trends with porous HA ceramics, and concluded that even though it would be desirable to minimise porosity and pore size

for optimum mechanical properties, there would be limited integration by surrounding tissue, hence the necessity of a compromise between pore size and cellular integration. Therefore it is important to be able to control the porosity of the final structure; Arita et al(1995) managed to achieve and control intermediate porosities of HA (reported using density as an indication; 12-22% theoretical density) by mixing uncalcined and precalcined powders. The $CaCO_3$ used in that study served as a gas-forming agent, which led to the development of porous structures of up to 62% (this was the only porosity value mentioned in the investigation).

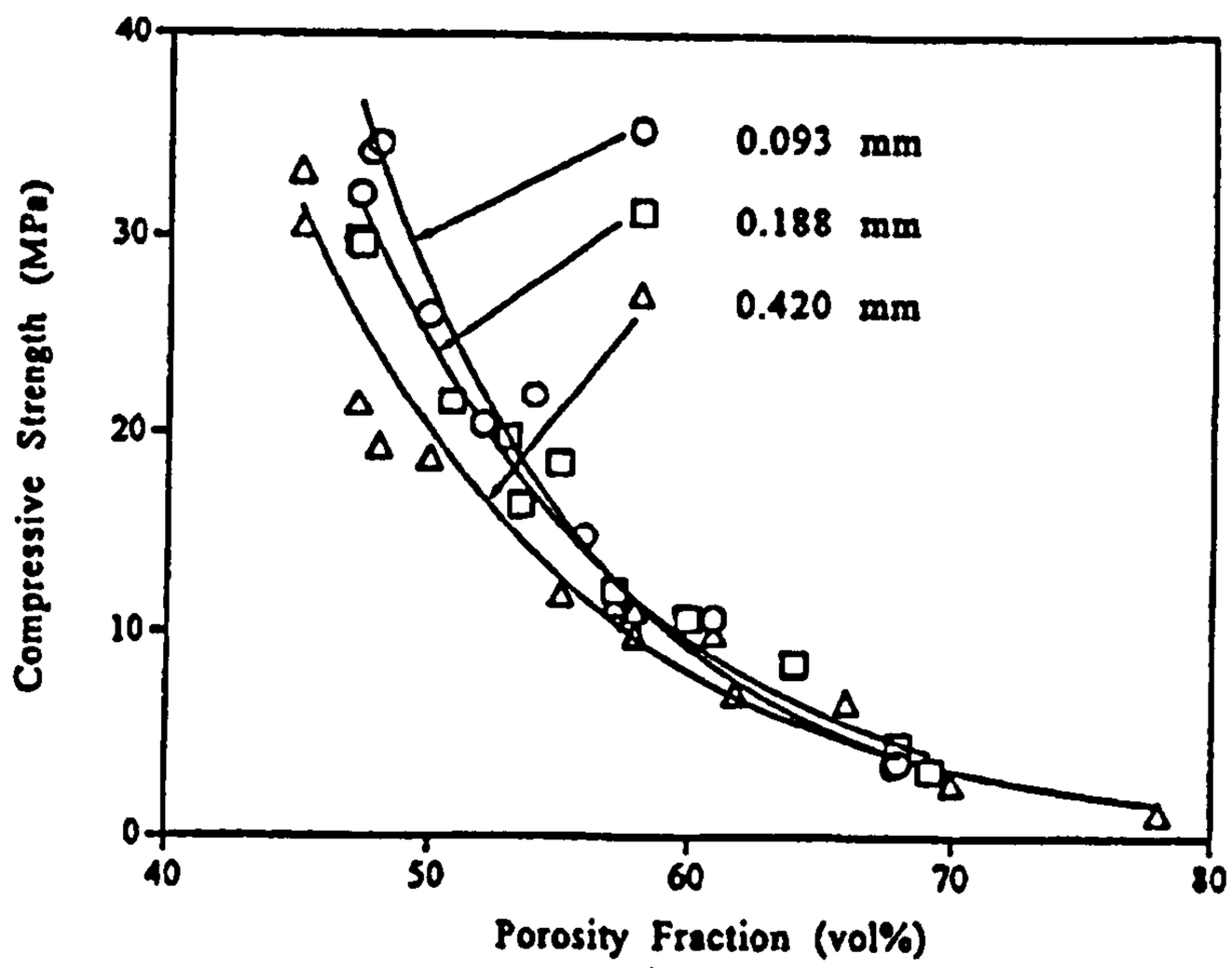


**Figure 3.9** The compressive strength of porous HA decreases linearly with increasing macropore size for a given total porosity (Liu, 1997)

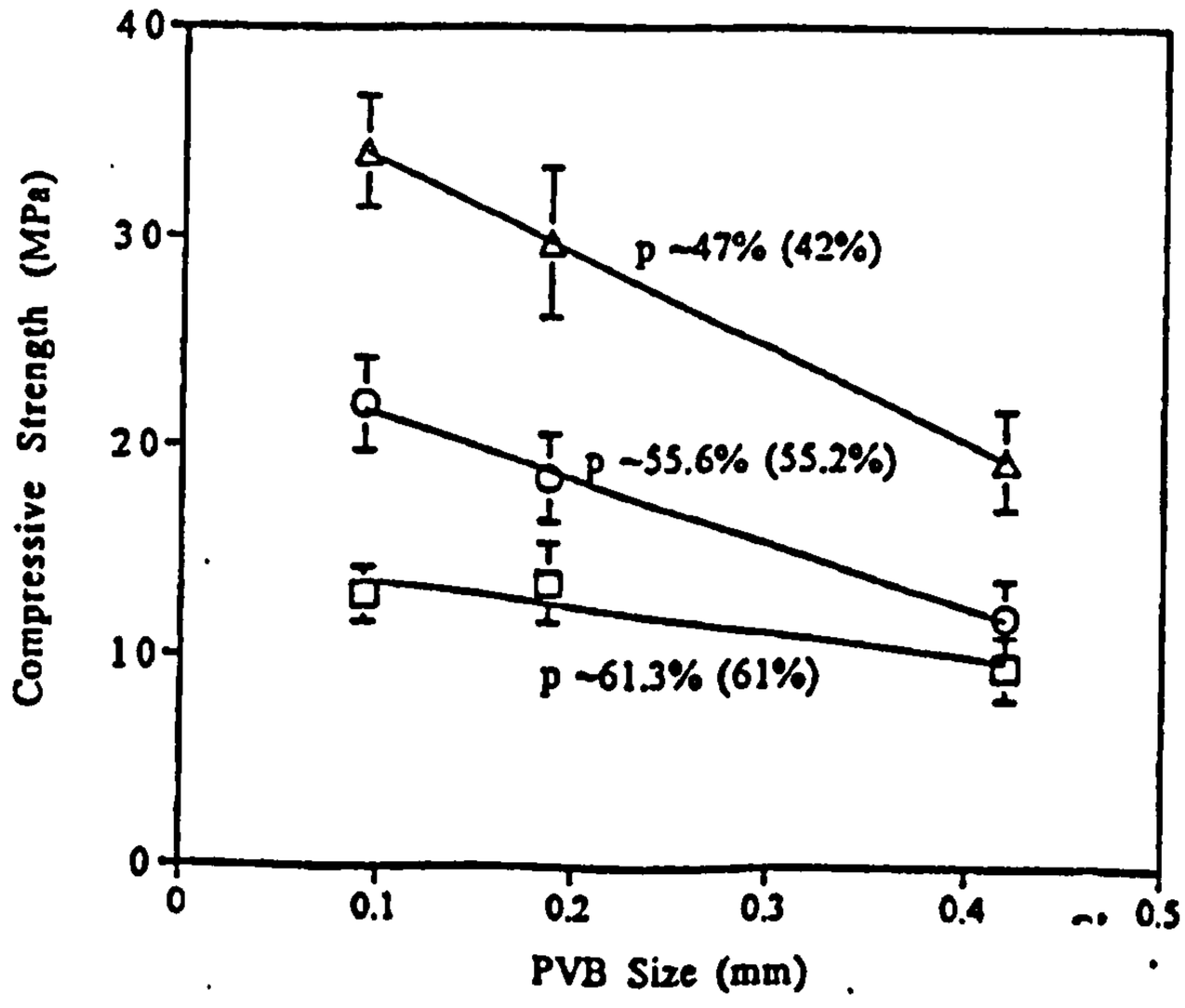


**Figure 3.10** The porosity-compressive strength behaviour of the porous HA ceramics in terms of different sizes of starting PVB particles (Liu, 1996*)

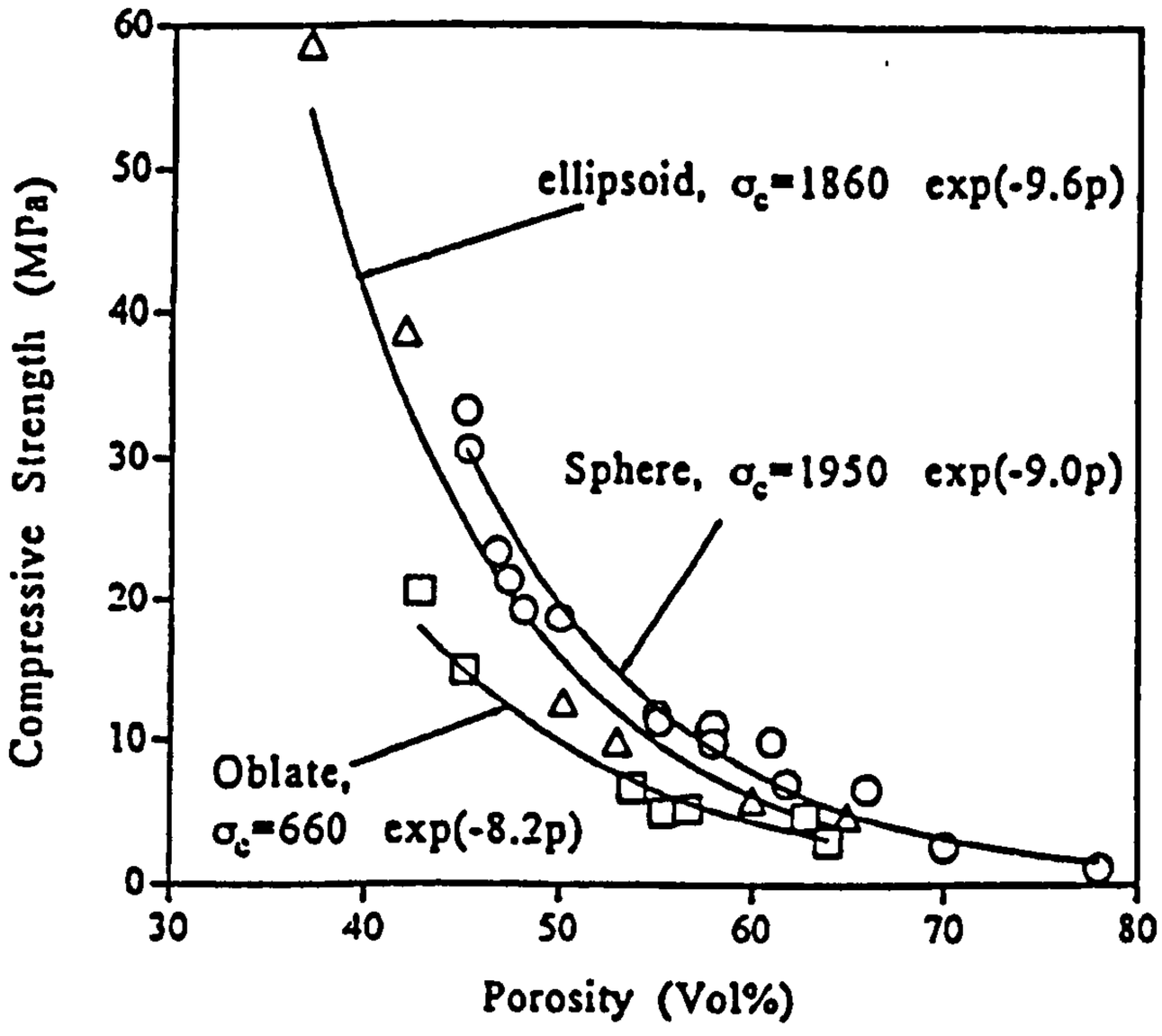


**Figure 3.11** The compressive strength-porosity behaviour of porous HA ceramic with different pore geometries (Liu, 1996*)

Liu et al (1998) discovered that the flexural strength of porous HA decreased with increased pore size (Figure 3.12), yet the pore size was roughly equal to the starting size of the polymer burnt out to produce the pore. This suggested the feasability of obtaining porous structures with optimal mechanical properties by controlling the quantity and particle size distribution of the polymer used in the burn-out.

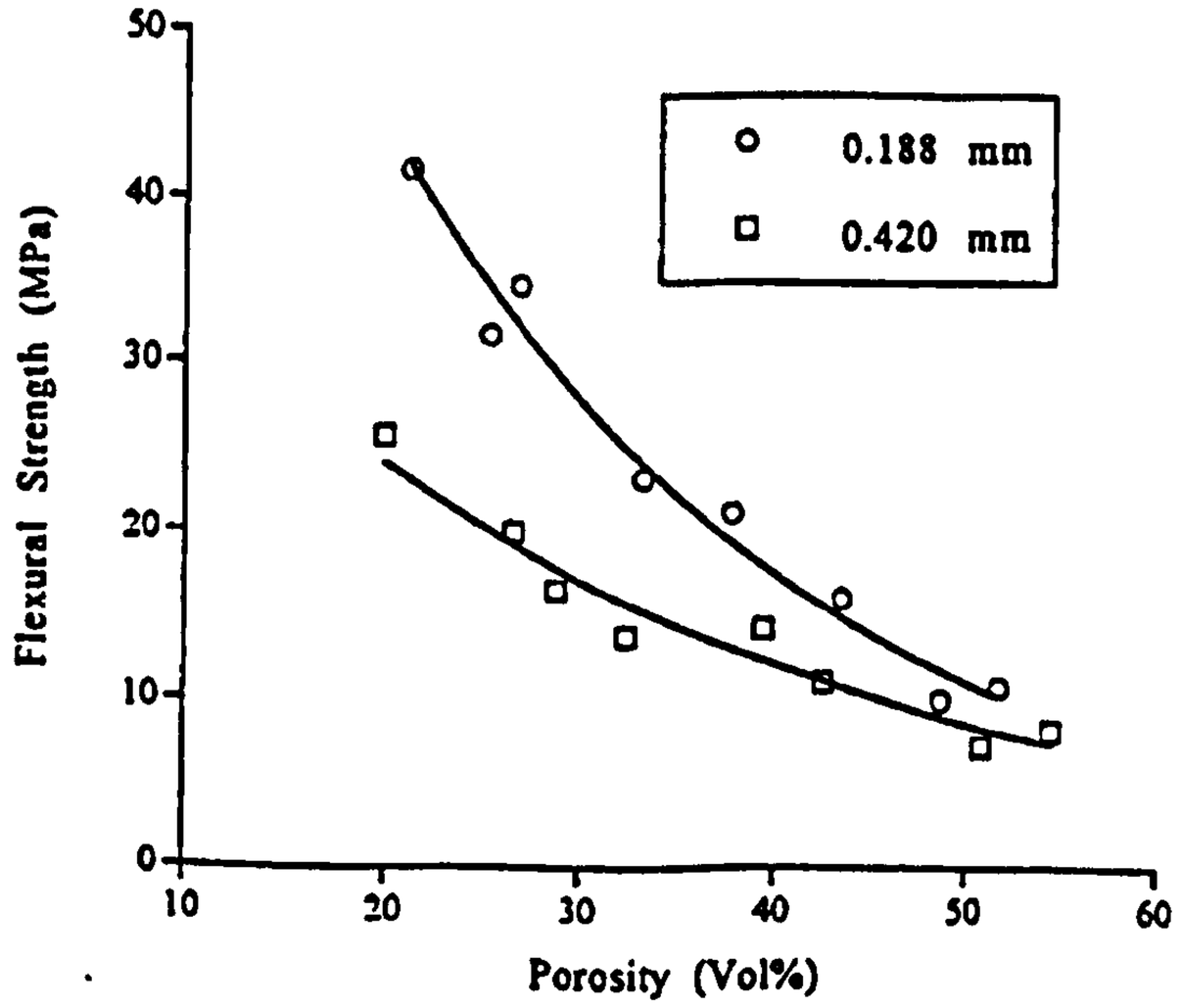


**Figure 3.12** The effect of porosity and macropore size on the flexural strength of porous HA (Liu, 1998)

A linear relationship between porosity and mechanical properties were also uncovered by Ono et al (1998), who reported a decrease in load value at fracture during a "crush test"with an increase in porosity (Figure 3.13); it was also reported, expectedly, that the load value increased with increased specimen dimensions (as indicated by the legend in Figure 3.13). Rodriguez-Lorenzo et al (1998) reported a similar trend in which the flexural bending strength of porous HA decreased with increasing porosity (Figure 3.14), with resulting spherical pores of ~80μm.

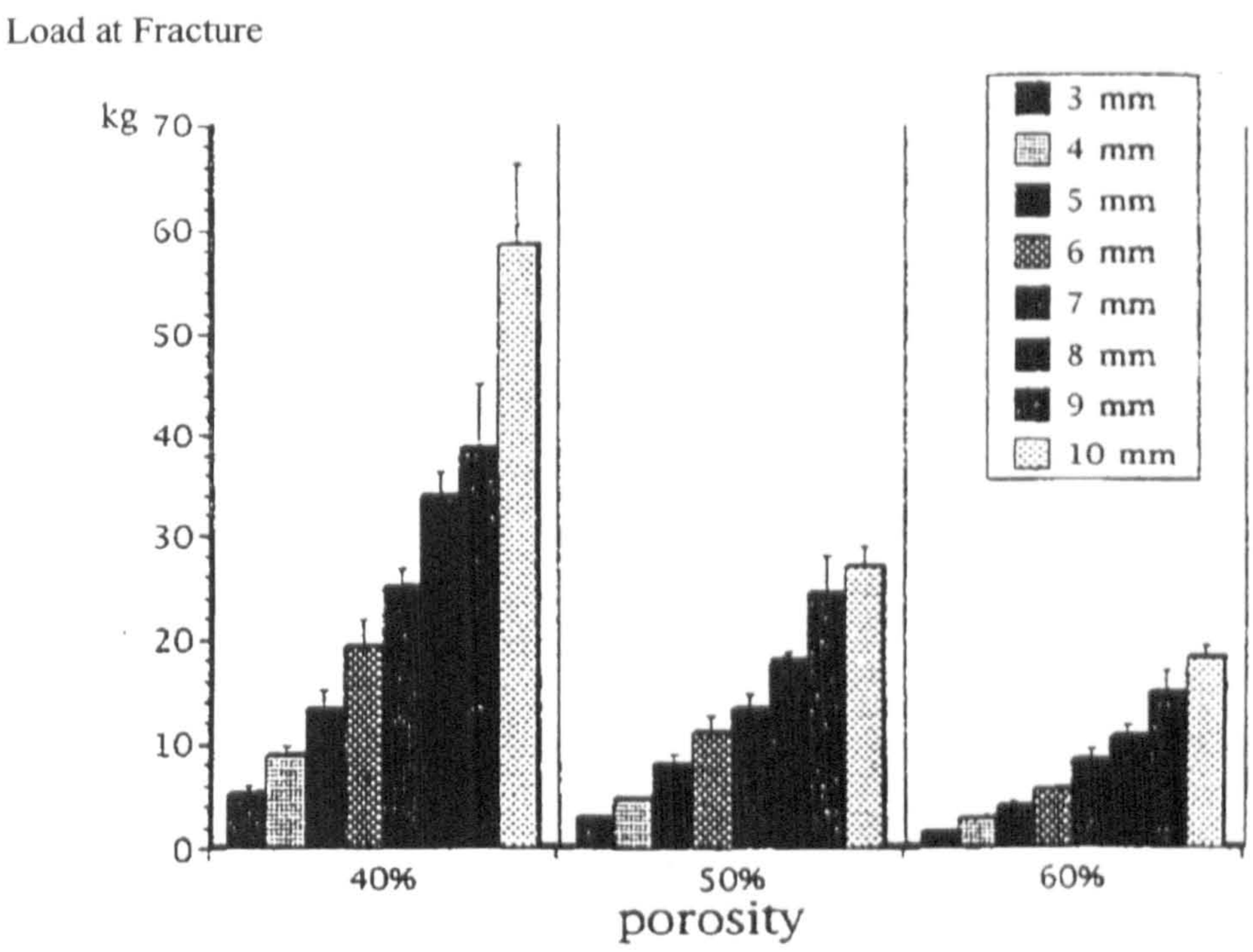


**Figure 3.13** The effect of varying porosity and specimen thickness on the load fracture of porous HA (Ono et al, 1998)

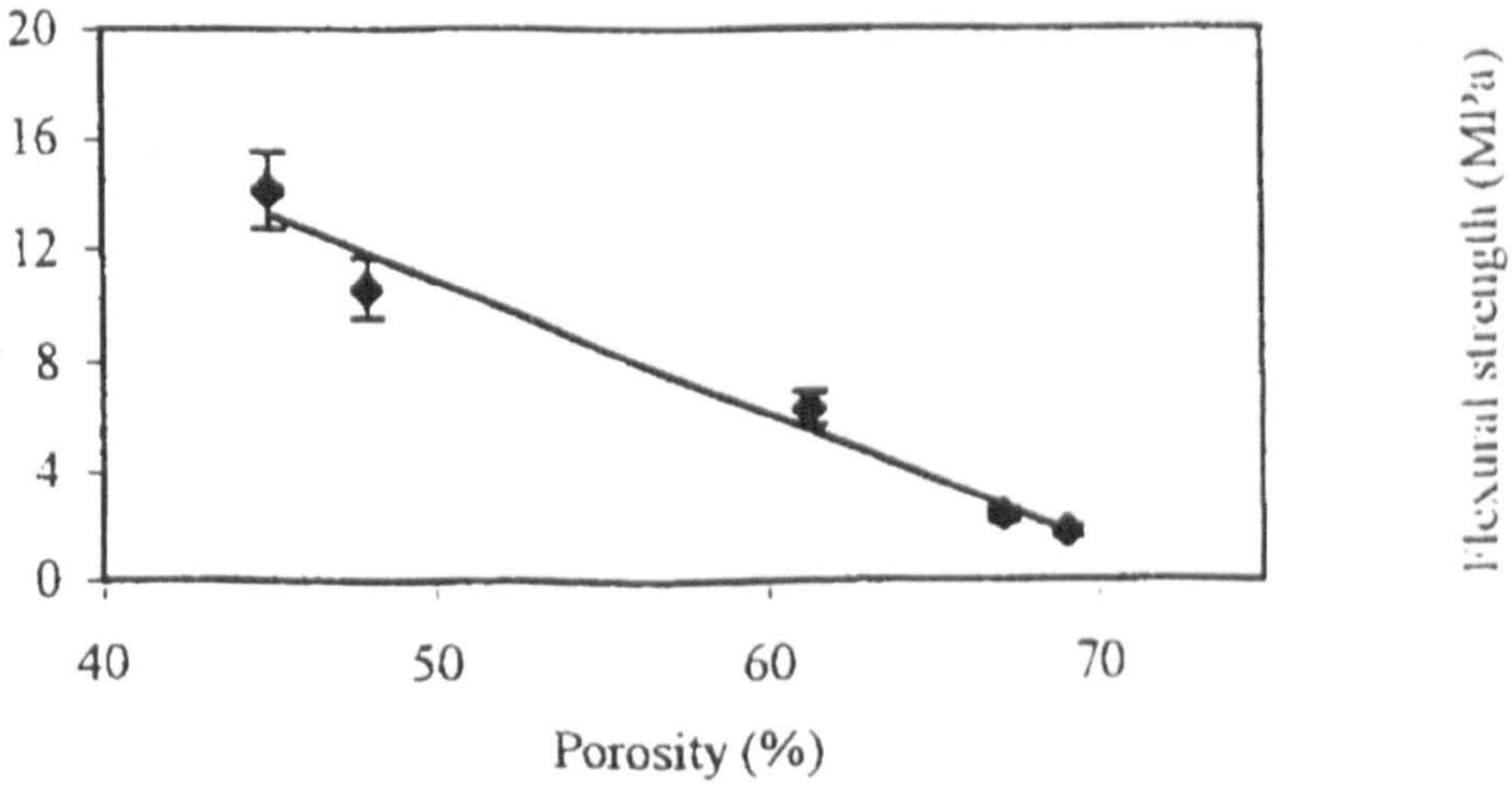


**Figure 3.14** The influence of porosity on flexural strength (Rodriguez-Lorenzo et al, 1998)

## 3.4 BIOACTIVITY OF HYDROXYAPATITE AND BONE INGROWTH

In some bioactive ceramics following implantation, the surfaces form a biologically active carbonate-substituted apatite layer, which provides a bonding interface with tissues. Surfaces such as these may further facilitate osteoblastic growth (Knabe et al, 1997) (Zyman et al, 1998). Dense bioceramics that contain only micropores should theoretically undergo this process; however, unlike the biological response elicited by dense HA, porous HA is inherently better for biological fixation because of the opportunity for bone ingrowth. Gauthier et al (1998) recently identified an optimum pore diameter (565 μm) and degree of macroporosity ( 40 %) for homogeneous and abundant bone ingrowth, which is in direct contradiction to Klawitter et al (1971) and Hench (1991) who reported the pore sizes necessary for bone ingrowth as 100μm. Gauthier et al's (1998) proposed optimum pore diameter seems toolarge and would probably result in a very poor mechanical properties (which were conveniently not reported in their investigation).

However, the disadvantage (if the application is relatively high load-bearing) of a porous structure as opposed to a dense structure is the larger surface area, hence an increased potential for the material to degrade in-vivo. A recent study (Benhayoune et al, 2000) into the in-vivo behaviour of dense vs porous HA ceramics indicated that once the dense and porous cylinders were implanted into cortical sheep femurs, the dense HA experienced little to no degradation due to resorption, unlike its porous counterpart. According to Behayoune et al (2000), the explanation lies in the lack of immature bone present in at the dense implant/tissue interface. When the resorption cavities of immature bone are in contact with a dense ceramic surface, resorption on this surface occurs. Therefore, it was assumed that when the resorption cavities of immature bone are in contact with a dense ceramic surface, resorption occurs, but only in the early periods of bone development before woven bone is converted to lamellar bone ( period in which the remodelling rate is high). However an alternative explanation may lie in differences in surface area. This cellular mechanism of calcium phosphate ceramic degradation was previously suggested by Heymann et al (1999), in which it was suggested that osteoclasts resorb calcium phosphate ceramics similarly to natural bone and hence possess a phagocytic capability. This is quite believable

because HA is similar to the mineral found in bone, therefore it is reasonable to assume that the osteoclasts would resorb HA in a similar manner.

Nevertheless, regardless of the mechanism, the deposition and integration of bone should enhance the strength of the implant by bonding with the host bone tissue (Hing et al, 1997). The key factors determining the amount and type of ingrowth are porosity and interconnectivity. Radin et al (1994) compared the in-vitro reaction kinetics of porous and dense bioactive ceramics and discovered that dense HA and calcium deficient HA led to immediate precipitation and direct apatite formation whereas the porous ceramics showed a lag time that depended on their structure and composition. It was also concluded that the composition, crystal structures and ultrastructure of ceramics with identical porosity were the key factors in controlling the reaction kinetics.

In comparing the bioactivity of HA to other calcium-phoshate based materials, Fujishiro et al (1997) carried out an investigation into the quantitative rates of in-vivo bone generation for Bioglass® and HA particles, and discovered that the bone growth rate constants of Bioglass® at the periphery and centre of the implant site were approximately twice that of the HA particles. Wilson et al(1992) similarly found that Bioglass® materials were more osteoconductive than two HA-based materials when implanted in the alveolar bone of patus monkeys. This leaves room for thought on combining HA with a bioactive glass for improving the overall bioactivity. However, if that were the case, the amount of bioactive glass added would have to be strictly controlled because bioactive glasses have lower Ca:P ratios than HA and therefore resorb at a higher rate (as discussed previously in section 3.1.4), which may be undesirable for high load-bearing applications in which the scaffold material must remain intact for as long as possible until adequate bone ingrowth has occurred.

Various attempts have been made to improve the bioactivity of HA, some successful and others providing no overall benefit. Radin et al (1996) found that placing serum proteins into simulated physiological solution did not significantly affect the solution/precipitation reactions on the surface of the HA. Yoshikawa et al (1996) found that osteogenic HA (containing pre-inserted stem cells) showed immediate

bone forming capability in-vitro; the results highlighted the inherent osteogenic ability of marrow stromal stem cells from rat femur in the pore regions of the HA, therefore proving that in an in-vivo situation, HA can promote rapid osteoblastic activity. Gundle et al (1997) similarly combined porous calcium phosphate ceramics with cultured marrow stromal cells in-vivo from human cancellous bone, and found the composite to have good osteogenic and osteoconductive properties. In 1999, Oreffo et al indentified the potential for using osteogenic stem cells in bioceramic technology as huge. Anselme et al's (1999) work further reinforced this idea as the advantages of culturing pre-implantation were demonstrated by the ability of the cultured stromal cells to differentiate on the implant surface. Furthermore, studies have been made (Flautre et al, 1999) into how to control cell culture medium in order to affect the depth of bone penetration within the implant in-vivo.

In fabricating a bioactive ceramic like HA as a scaffold for bone ingrowth, it is important to focus on not only pore size/pore geometry/porosity, but also balancing the rate of bone ingrowth and any possible biodegradation. Increased porosity indicates increased surface area, i.e. a larger area for resporption to occur. Tricalcium phosphate displays high rates of resorption therefore it would be advantageous to limit the amount of tricalcium phosphate present in an as-sintered material, given the application, especially if it is high-load bearing. It is fundamental to minimise the amount of TCP present in a porous HA ceramic in order to avoid this type of situation.

## 3.5 REINFORCED HYDROXYAPATITE

Section *3.3* revealed that the mechanical properties of both dense and porous hydroxyapatite are much lower than the strength values of cortical and cancellous bone as described in section *1.6*, yet bioactivity is displayed by hydroxyapatite. Biologically, hydroxyapatite is efficient in terms of being accepted into the body and stimulating bone ingrowth, yet its' mechanical properties need improvement. Reinforcing the HA with a material that is strong and biocompatible would solve this problem. Bioceramic materials may be used to reinforce each other, to form a bioceramic composite, in order to maximise the use of particular properties from each

respective material. This section desribes various dense reinforced hydroxyapatite composites.

### 3.5.1 HYDROXYAPATITE/HA-WHISKER-FIBRE COMPOSITES

Fibres and whiskers are reinforcement materials whose reinforcement mechanism is based on crack-stopping. If the toughening mechanism occurs in the crack-wake, it requires more energy for the crack to propogate through the material, thereby increasing the mechanical integrity of the system. Suchanek et al (1996) described the use of pure HA whiskers, which were single fine crystals. These were mixed with HA powder and then sintered or hot-pressed to produce the composites. The mechanical characterization results of HA/HA-Whisker composites carried out by Suchanek et al (1996, 1997) are shown in Table 3.10.

**Table 3.10** The mechanical properties of HA/HA-Whisker Composites (authors stated in table)

| Author | Year | Density (% Theoretical) | Fracture Toughness ($MPa.m^{1/2}$) |
|---|---|---|---|
| Suchanek et al | 1996 | 90-97 | 1.4 |
| Suchanek et al | 1997 | 97.0-99.5 | 1.4-2.0 |

The fracture toughness in both cases was relatively poor in comparison to bone, and only a slight improvement over dense hydroxyapatite (≤1). This attempt at reinforcing HA, in the hope of improving the mechanical properties, was unsuccessful. Despite the mechanical disadvantages of this composite, there are biological advantages due to its' bioactivity and biocompatibility from solely containing HA (the biocompatibility and bioactivity of which has been discussed in section *3.4*).

When hydroxyapatite is reinforced with short fibres such as alumina, 316-L stainless steel, or titanium, the significant factor affecting the success of the composite is the processing technique (Knepper et al, 1997,1998). Knepper et al (1997, 1998) found that sintering in air, and hot-isostatic pressing caused the HA matrix of the composites

to decompose to undesired TCP, which apparently mechanically weakened the material by decreasing the density (values were not reported). The decomposition was suggested to derive from chemical interactions between the matrix phase and the fibre-reinforcement phase, resulting in a reaction zone. In 1997, Knepper et al found no reaction zone around the alumina fibres which was accounted for by hot isostatic pressing during the sintering process, which apparently suppressed the decomposition of the HA matrix in the composites at elevated temperatures. This technique is indicative of producing reinforced HA with better mechanical viability than by reinforcing with HA whiskers; however, alumina was desribed in section *2.4.2.1* as an inert bioceramic, which means that it may not display as good a biocompatibility as the whisker-reinforced HA.

### 3.5.2 CALCIUM PHOSPHATE/POLYMER COMPOSITES

As mentioned previously in Chapter 1, the major phases of bone are an organic phase (collagen) and an inorganic phase (mineral similar to hydroxapatite). Therefore, a bone analogue material composed of calcium phosphate and a polymer such as collagen would be a very suitable composite for bone replacement, due to its appropriate biological and mechanical compatibility . Bonfield et al (1988) pioneered a composite bone replacement material of this description, which has subsequently been given the trade name HAPEX™; this composite material consists of hydroxyapatite and high density polyethylene. In 1994, Ladizesky et al discovered that powderizing, recompacting, and then hydrostatically extruding HA/chopped high modulus polyethylene (HMPE) fibre composites creates materials with the highest stiffness and strength as of yet with HA/PE composites. In 1998, Lawson et al produced a polymer/ceramic composite whereby calcium phosphates were precipitated onto collagen; the mechanical properties of their material are shown in Table 3.11.

**Table 3.11** Mechanical properties of collagen and collagen-calcium phosphate composites with varying mineral contents (Lawson et al, 1998)

| Mineral (wt %) | 0 | 29 | 32 | 34 | 39 |
|---|---|---|---|---|---|
| Failure Stress (MPa) | 34 | 49 | 53 | 53 | 49 |
| Elastic Modulus (GPa) | 0.44 | 1.25 | 1.58 | 2.48 | 2.82 |

These types of composites have similar strength to cortical bone and therefore appear to have potential for bone substitution in high load bearing areas in the skeleton; yet the modulus is much lower than that of cortical bone and slightly lower than values recorded for hydroxyapatite. Marra et al (1999) recently produced a porous composite consisting of polycaprolactone (PCL)/poly (D,L-lactic-co-glycolic acid) (PCGA) in a ratio of 10:90 with 10 % HA, with lower moduli than Lawson et al's (1998) composite, as shown in Table 3.12.

**Table 3.12** Mechanical properties of porous scaffolds (Marra et al, 1999)

| Material | Tensile Strength (MPa) | Young's Modulus (MPa) |
|---|---|---|
| Trabecular Bone | 1.2 | 100-900 |
| PCL | 1.1 ± 0.1 | 11.8 ± 4.0 |
| PLGA | 0.45 ± 0.08 | 2.4 ± 0.7 |
| 10/90 | 0.4 ± 0.1 | 2.5 ± 0.7 |
| 10/90 + 10 % HA | 0.51 ± 0.08 | 12.5 ± 3.2 |

### 3.5.3 GLASS-REINFORCED HYDROXYAPATITE

Glass is incorporated into the HA structure by a liquid-assisted sintering process (discussed later). The pressure-less sintering of ceramic composites requires the presence of a liquid phase to obtain a desired degree of chemical homogenisation. The addition of glass to HA is advantageous due to its bioactive nature which has been previously discussed. Conversely, glass on its own has one main drawback, i.e. its poor mechanical properties due to its very brittle nature (Andersson et al, 1988), whereas glass-ceramics have better mechanical properties and are more machinable, therefore would appear to be more appropriate for reinforcement. However, in small quantities, glass can improve the sinterability of HA through liquid-assisted sintering

and hence the overall mechanical integrity of the system. Glass-ceramics too can undergo liquid assisted sintering. Reinforcing materials such as glass or glass-ceramics may be added in an attempt to enhance the mechanical properties and bioactivity of the HA. This chapter will focus on the literature regarding glass-reinforced HA only, seeing as there is currently no literature published on glass-ceramic reinforced HA.

### 3.5.3.1 Mechanism of Reinforcement

Liquid assisted sintering is a process whereby a material is sintered in the presence of a reactive liquid. The liquid is in fact a sintering aid as it improves the sinterability of the starting material. The systems which undergo liquid phase sintering contain a solid phase that shows limited solubility in the liquid at sintering temperature. The essential part of this process is the solution of the starting material in the liquid phase, followed by the reprecipitation of solids to give changes in grain size and density.

In order for liquid phase sintering to take place, there are three requirements that the system must have (Kingery et al, 1976):

- An appreciable amount of liquid phase
- An appreciable solubility of the solid in the liquid
- Wetting of the solid by the liquid

In this case, the capillary pressure of the liquid phase located between the fine solid particles is the driving force for densification, as shown in Figure 3.15(Kingery et al, 1976). The liquid phase wets the particles, and in doing so, attracts the particles closer together due to the capillary created in this interparticle space. Hence the increased potential for atomic and vacancy movement between two particles during sintering.


**Figure 3.15** (a) Contact between solid and liquid (b) Particle attraction due to capillary action (Kingery et al, 1976)

There are four stages involved in the densification experienced during liquid-assisted sintering:

1. Particles rearrange themselves on formation of the liquid phase to allow better and more effective packing
2. In the bridges between the particles at the contact points, high local stresses develop, leading to plastic deformation and creep, thereby rearranging the particles further.
3. The smaller particles go into solution in the liquid phase and reprecipitate into larger particles by material transfer through the liquid phase.
4. In the situations where the liquid penetrates between particles forming a capillary, the increased capillary pressure at contact points results in an increased solubility which enhances stage 3. This further causes the material to transfer in a direction

away from contact areas, therefore particle centres approach, and shrinkage results.

This liquid assisted sintering process increases strength because it creates greater particle contact prior to the sintering temperature. The reinforcing glass reaches the viscosity of a liquid ($T_m$) at a low temperature and results in greater particle contact as shown in Figure 3.15, which is maintained during the sintering process at higher temperature. Increased contact results in a greater amount of atomic diffusion across the grain boundaries, which ultimately enhances the densification process, hence strength is improved.

### 3.5.3.2 Phase Composition

During the sintering process for a glass-reinforced hydroxyapatite composite, the glass has a low viscosity and is highly reactive in its liquid phase, which occurs roughly between 1200-1350°C (Knowles et al, 1993). In this form, the glass pulls ions out of the HA, namely OH- ions, which causes an imbalance and results in phase changes. Knowles et al (1993) further found that by increasing the glass wt % in the composites, an increase in the phase change from HA to TCP would occur. Reinforcing HA results in the production of a biphasic material because glass enhances ionic mobility, hence the reactivity of the material, and therefore $OH^-$ ions are more readily released during sintering, resulting in the presence of TCP.

In 1994, Knowles et al indentified the temperatures at which different forms of TCP would be present:

- Between 1200-1350°C, HA would decompose to β-TCP.
- Above 1350°C, β-TCP would transform further to α-TCP resulting in ~ 40 % α-TCP in the composite.

Therefore it was deduced that an increase in temperature above 1300°C was associated with a decrease in the amount of β-TCP and an increase in the amount of α-TCP. Lopes et al (1998) were in full agreement with this and further added that the

higher the glass additions, the more likely β-TCP is to contain more residual ions from glass and be unstable, hence the ease at which α-TCP is formed. Knowles et al (1994) also discovered that the transformation from β-TCP to α-TCP involved a larger volume change than the transformation from HA to β-TCP, therefore disrupting the overall structure of the material; therefore the presence of α-TCP is often associated with a decrease in mechanical strength.

In 1996, Knowles et al's studies showed that the phase changes that occur may not only be detrimental to the mechanical integrity of the composite system ( in terms of the volume change associated with the β-TCP to α-TCP transformation) but may also be advantageous. The phase change from HA to β-TCP was described as a reinforcing mechanism by Knowles et al (1996), comparable to the transformation toughening mechanism of Partially Stabilized Zirconia. The HA to β-TCP transformation was reported to cause a decrease in volume, therefore eliminating porosity and increasing strength. But, of course, after 1350°C when the β-TCP to α-TCP transformation occurs, the associated increase in volume relates to a decrease in strength, which contradicts Knowles et al's results. Santos et al (1996) justified their results by describing the same mechanism as above and further adding that the highest bending strength of their glass-reinforced composite samples was associated with significant amounts of β-TCP present.

The general concensus from these findings are that the presence of β-TCP is related to an increase in mechanical strength in these composites. Of course, this is very useful if the presence of TCP is a desirable requirement for the particular application. However, TCP has been described previously in Chapter 2 as a highly resorbable material with high rates of biodegradation. In high load-bearing applications where the bioceramic behaves as a scaffold for allowing bone ingrowth at the same time as maintaining strength, a highly resorbable component such as TCP is undesirable. Therefore, it is necessary in these applications to produce a composite, which has an even balance of resorption rate and strength.

### 3.5.3.3 Mechanical Properties

Table 3.13 summarises the findings of several authors concerning the highest biaxial flexure strengths of G-R-HA composites, according to glass type, wt % of glass, and sintering temperatures. The flexural strengths from all findings appear to be generally similar if not lower than the flexural strengths of unreinforced hydroxyapatite, whose strengths lie between 100-130 MPa as found in Tables 3.3 and 3.4. The authors all found that the liquid phase of the glass at high temperature inhibited grain growth which resulted in increased densification and better mechanical properties.

| Author | Year | Glass System | Wt % Glass | Sintering temperature (°C) | Highest Flexural Strength (MPa) |
|---|---|---|---|---|---|
| Kokubo et al | 1985 | $MgO-CaO-SiO_2-P_2O_5$ | 0.5 | 1200 | 213 ±1 7 |
| Santos et al | 1992 | $CaO-P_2O_5$ | 2.5 | 1300 | 73 ± 13 |
| | | $CaO-P_2O_5$ | 5 | 1350 | 96 ± 17 |
| Knowles et al | 1993 | $CaO-P_2O_5$ | 2.5 | 1350 | ~69 |
| Knowles et al | 1993 | $CaO-P_2O_5$ | 2.5 | 1350 | ~124 |
| Santos et al | 1994 | $CaO-P_2O_5$ | 2.5 | 1300 | 73 ± 13 |
| | | $CaO-P_2O_5$ | 5 | 1350 | 96 ± 17 |
| Knowles | 1994 | Na2-P2O5 | 5 | 1250 | ~60 |
| Santos et al | 1996 | $CaO-P_2O_5-Na_2O-MgO$ | 2 | 1350 | 107 ± 21 |
| | | $CaO-P_2O_5-Na_2O-K_2O$ | 4 | 1350 | 93 ± 27 |
| Knowles et al | 1996 | $CaO-P_2O_5-Na_2O$ | 2 | 1350 | ~103 |
| | | $CaO-P_2O_5-Na_2O$ | 4 | 1250 | ~94 |
| Tancred et al | 1996 | $CaO-P_2O_5$ | 2.5 | 1250 | 32.3 ± 4.0 |
| | | | 5 | 1350 | 61.9 ± 7.5 |
| | | | 10 | 1300 | 50.5 ± 2.6 |
| Wang et al | 1998 | $SiO_2-Na_2O-CaO-P_2O_5$ | 1.5 | 1200/1250 | ~75/~77 |
| | | | 2.5 | 1200/1250 | ~76/~91 |

**Table 3.13** Highest Biaxial Flexural Strengths of Various Glass-Reinforced HA System

### 3.5.4 MECHANICAL DEGRADATION OF REINFORCED HYDROXYAPATITE

HA has excellent biocompatibility and can directly bond to bone by forming a biologically active bone-like apatite layer on its surfaces. .Therefore, composite materials that contain HA combined with another bioactive component should theoretically also experience a degree of biocompatibility. Not only is the ability to form an apatite layer important towards the behaviour in-vivo/-vitro, but also the ability to maintain structural hence mechanical integrity. However, the material must not be too strong and stiff and incapable of resorption; a balance must be reached in order to optimise bone ingrowth and strength maintenance.

There is very little in the literature regarding the in-vivo/-vitro mechanical degradation of bioceramic materials. Furthermore, the authors mentioned in this section did not all immerse their materials in the same biological mediums for the same length of time, therefore solid comparisons were difficult to achieve. Nevertheless, the following information reports on investigations into the in-vivo/-vitro degradation of various composites.

In 1997, Huang et al immersed HAPEX™ in simulated biological fluid (SBF) for 3 months, a solution which closely resembles the inorganic ion concentrations in blood plasma, and found that the mechanical properties were not really affected by contact with physiological solution (Figure 3.16). HAPEX™ also appeared to to provide a favourable environment for cell attachment, cell proliferation, and cell differentiation. Later in 1998, Huang et al found again that there was little to no decrease in the tensile strength, Young's Modulus, and fracture strain of HAPEX™, as opposed to polyethylene reinforced with Bioglass®, whose strength decrease was correlated to the reactivity of the Bioglass® in SBF. The reactivity of a component within a composite may be advantageous for low-load bearing applications but disadvantageous for high-load bearing applications, where a degree of structural integrity must be maintained in order for the composites to act as a scaffold.

Xiaodong et al (1998) immersed poly-DL-lactide/HA composites in a degradation medium (pH 7.4 phosphate buffer) and found that the PDDLA experienced less

degradation when HA was incorporated into its' structure (Figure 3.17). It was suggested that this may be due to a thick layer of apatite crystals acting as a hydrolysis barrier and therefore delaying the penetration of water, hence preventing the release of particles. Furakawa et al (2000) similarly discovered this trend, whereby the resorption of TCP within a composite scaffold correlates with the remaining material becoming more crystalline; it was found that the HA/PLLA composite rods implanted in-vivo were stronger the less crystalline they were, which also indicates that the presence of TCP enhances strength. Figure 3.18 and 3.19 show the differences in strength and crystallinity of calcined and uncalcined HA/PLLA composites, in which the less crystalline composite appeared to be stronger in-vivo.

Wang et al (1998) found that most of the α-TCP within a α-TCP/ HA composite (70%/30%, respectively) disappeared after a month in-vivo, according to XRD analysis, which may limit this composites' applications due to its high resorbability from containing a large amount of α-TCP.

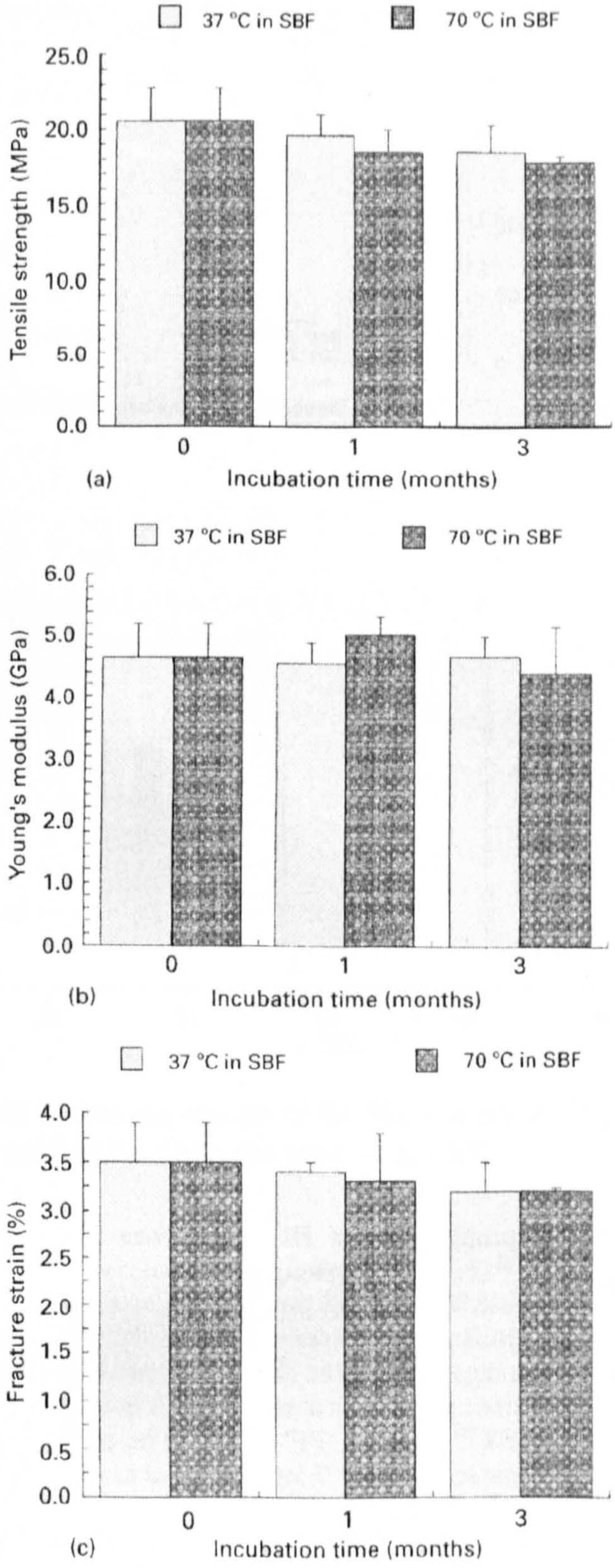


**Figure 3.16** Comparison of the mechanical properties of HAPEX™: (a) tensile strength (b) Young's modulus and (c) strain to failure before and after immersion in SBF at 37 and 70°C for 1 and 3 months (Huang et al, 1997)

| Time (week) | Bending strength (MPa) | | Shear strength (MPa) | |
|---|---|---|---|---|
| | HA/PDLLA | PDLLA | Ha/PDLLA | PDLLa |
| 0 | 120.3 | 109.7 | 84.5 | 78.1 |
| 2 | 82.5 | 68.7 | 69.2 | 60.3 |
| 4 | 73.5 | 56.5 | 58.4 | 46.7 |
| 6 | 66.8 | 47.9 | 50.2 | 30.9 |
| 8 | 57.4 | 36.7 | 42.4 | 19.8 |
| 10 | 42.9 | 20.1 | 36.3 | 12.4 |
| 12 | 34.0 | 11.3 | 30.2 | 7.5 |

**Figure 3.17** Strength of HA/PDLLA Composite and Unfilled PDLLA (Xiaodong et al, 1998)

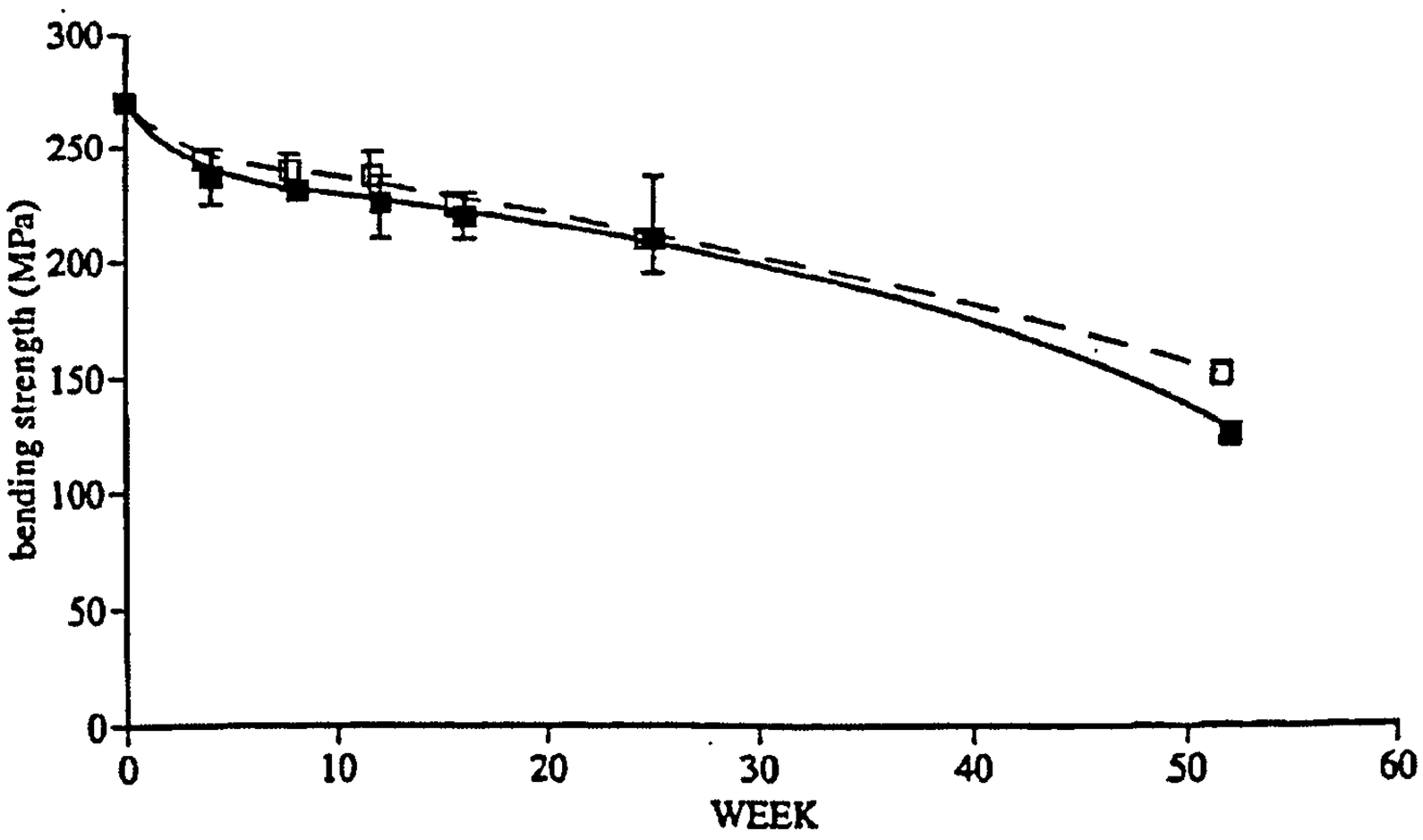


**Figure 3.18** Changes of the bending strength of HA/PLLA composite rods with time in vivo. (■) uncalcined HA/PLLA (□) calcined HA/PLLA (Furakawa et al, 2000)

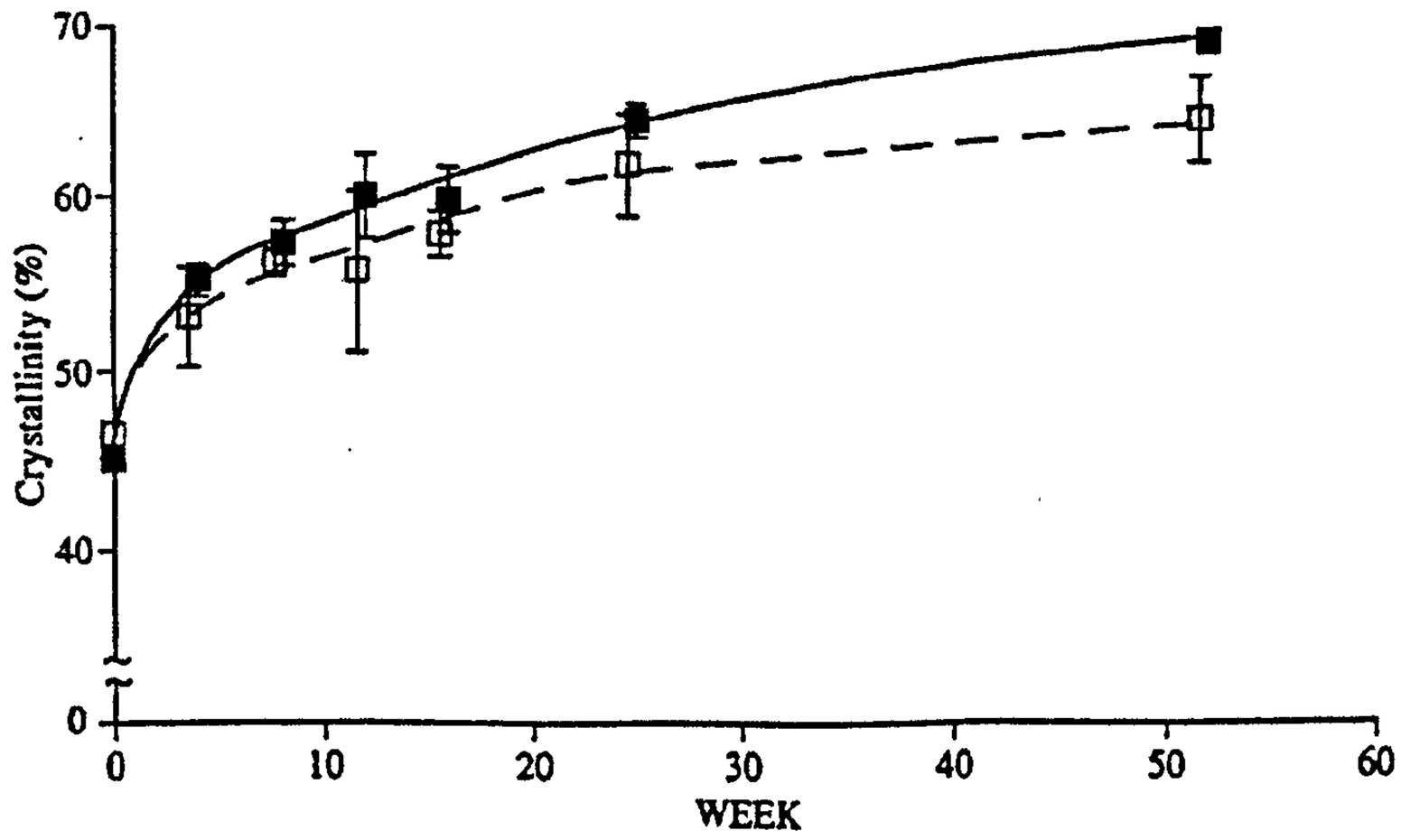


**Figure 3.19** Changes in the crystallinity of HA/PLLA compsite rods. (■) uncalcined HA/PLLA (□) calcined HA/PLLA (Furakawa et al, 2000)

The resorbability of filler glasses such as $CaO-SiO_2-P_2O_5-CaF_2$ have also been shown to affect the strength of resin-based composite cements in SBF due to their high reactivity, in comparison to resins without filler as shown in Figure 3.20 ( Miyata et al, 1999).

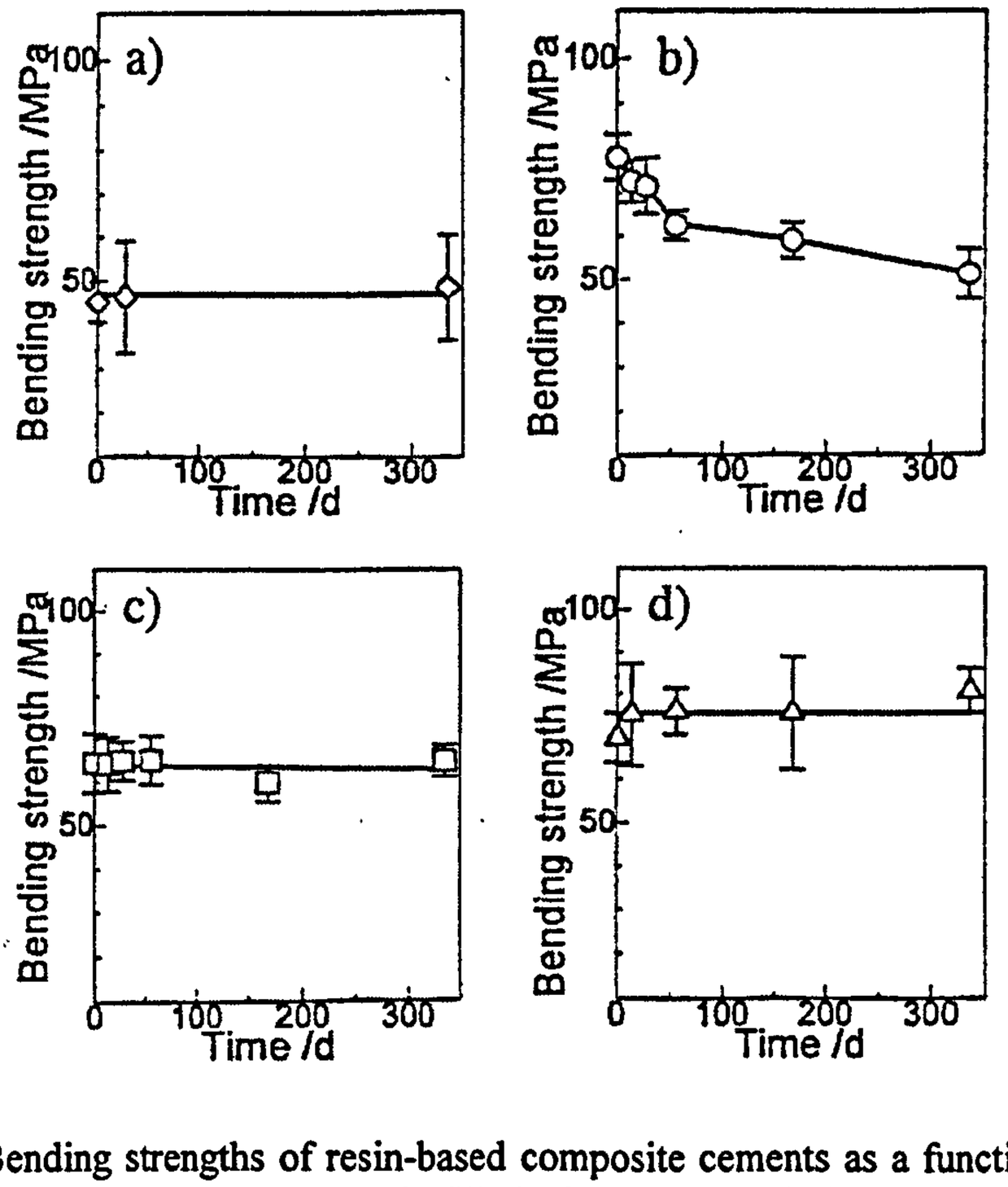


**Figure 3.20** Bending strengths of resin-based composite cements as a function of soaking time in SBF at 50°C: (a) resin without filler (b) resin filled with CaO-based glass (c) resin filled with AW glass (d) resin filled with silica glass (Miyata et al, 1999)

## 3.6 SUMMARY

HA is a brittle ceramic, which has been used extensively in the medical industry as a synthetic bone replacement material. Dense HA has poor mechanical properties on an absolute scale but good mechanical properties relative to porous HA. However, it lacks the level of bioactivity achieved by porous HA whose porous structure allows bone ingrowth, thus stabilising the implant; yet, porous HA lacks the level of mechanical integrity shown by dense HA. Therefore in order to construct a porous bioceramic that displays the bioactivity shown by porous HA and the mechanical strength of dense HA, it is necessary to construct a composite material, such as porous glass-reinforced-hydroxyapatite, whereby the glass strengthens the porous HA

structure. It is important to maintain the porous structure and interconnectivity ( for maintaining vascular support between pores) so it may function as a scaffold for bone regeneration, whilst controlling the rate of degradation in-vivo, so as not to compromise the biocompatibility or in-vivo mechanical integrity.

Composites are useful for increasing the mechanical properties of a bone-substitute material in high load-bearing applications. Hydroxyapatite has shown improved strength when combined with calcium-phosphate based glassy materials, at the expense of the phase decomposition which is undesirable for high load-bearing applications.

The practical investigation in this report focuses on comparing the effect of different $Ca\text{-}PO_4$ materials on the sintering behaviour of hydroxyapatite, followed by an analysis of their mechanical degradation in-vitro.

# CHAPTER 4

# METHODS AND MATERIALS

## 4.1 MATERIALS

- Commercial hydroxyapatite powder (P201) (Plasma Biotal Ltd., U.K.)
- Glass pre-cursors: $CaCO_3$, $P_2O_5$, $Na_2CO_3$, $K_2CO_3$, $MgCO_3$ (BDH Company, Merck Ltd., U.K.)
- Polyvinyl alcohol powder (mol wt.= 115,000) (BDH Company, Merck Ltd., U.K.)
- BU Foam (Foam Engineers Ltd., U.K.)
- YU Foam (IRC in Biomedical Materials, U.K.)
- Ringer's solution tablets (quarter strength) (BDH Company, Merck Ltd., U.K.)

## 4.2 AIMS AND OBJECTIVES

The aim of this thesis is firstly to investigate the reinforcement of HA by the addition of a low melting point 2$^{nd}$ phase, which, as a composite, will not lose strength on immersion in physiological solution. Once this is established, the ultimate aim is the production of porous ceramic structures with enhanced mechanical properties. The characterization process involves investigations of particle size and distribution, phase composition, mechanical properties, and microstructure.

The experimental work was set out in three stages:

**Stage 1** ⇒ *Development of a reinforced hydroxyapatite composite*

- Characterise the commercial HA(P201) used in the composite
- To synthesize reinforcing phases with varying Ca:P ratios

- To reinforce dense P201 HA with the secondary phases and compare and contrast the results of their characterisations with that of pure P201 HA
- To select the best wt % 2nd phase addition for mechanical reinforcement and minimized phase decomposition

**Stage 2** ⇒ *Investigation into the mechanical degradation of reinforced hydroxyapatite in physiological solution*

- To carry out an in-vitro study of the composites in Ringers' solution in order to determine the effect of a biological environment on the mechanical and crystallographic properties of the composite.

**Stage 3** ⇒ *Production of reinforced porous hydroxyapatite*

- To develop a protocol for a foam burn-out technique using P201 hydroxyapatite.
- To reinforce porous P201 with a secondary phase, based on the consitituents of the dense composite that displayed optimum mechanical and physical properties.

This chapter firstly describes the ways in which the materials were produced and prepared for characterisation, followed by the actual characterisation techniques used for each study.

## 4.3 PRODUCTION AND PREPARATION OF TEST MATERIALS

### 4.3.1 PREPARATION OF DENSE P201 HA DISCS FOR CHARACTERISATION

The P201 powder (100 g) was milled for 24 hours in a ceramic ball mill (Pascall Eng.Co.Ltd, Sussex) that had a pot volume of 1 litre; milling media (containing 18 alumina 25 mm diameter balls weighing ~25 g each, and 20 alumina 20 mm diameter balls each weighing ~ 13 g) were used to mill the powder which was then mechanically sieved through a 75 μm mesh. The powder was then pressed uniaxially in a steel die (30 mm diameter), to 85 MPa (6 Tonnes), using 5 grams of powder for

each specimen. This pressure was selected on the basis that it was the optimum pressure for achieving maximal compaction of powder in a 30 mm die without capping, cracking, or delamination of the powder compacts. At lower pressures, one could not ensure adequate packing for maximising densification during sintering. The discs were then sintered at temperatures of between 1000°C and 1350°C under the following regime:

| | |
|---|---|
| Ramp 1 | + 5°C.min$^{-1}$ |
| Level 1 | Sintering temperature (1000°C – 1350°C) |
| Dwell 1 | 2 hours |
| Ramp 2 | - 10°C.min$^{-1}$ |
| Level 2 | 20°C |
| Dwell 2 | End |

### 4.3.2 MELT PROCESSING OF CAP1 AND CAP2 ADDITIVES

Two secondary reinforcing calcium-phosphate (Ca/P) based additives were produced via melt processing of the precursors. CAP1, whose composition in mol % and wt % is shown in Table 4.1 and 4.2 respectively, had a Ca:P ratio of 0.5 and, when quenched from a melt at 1100°C, yielded a glass. CAP2, whose composition in mol % and wt % is shown in Table 4.3 and 4.4 respectively, had a Ca:P ratio of 0.835 and, when quenched from a melt at 1300°C, yielded a material with a predominantly crystalline content. The CAP2 material could not be classed as a classic glass ceramic as the crystallization did not occur via a pre-determined crystallization step, but rather via spontaneous crystallization upon cooling during quenching.

The raw materials were mixed in a pestle and mortar for approximately five minutes; safety precautions were taken due to the volatile nature of one of the precursor powders, $P_2O_5$. The mixed powder (~117 g for CAP1 and ~115 g for CAP2) was then placed in a platinum-rhodium crucible and placed in the pre-heated glass furnace for ~1-2 hours at a temperature high enough to ensure melting of the precursors (1100°C for CAP1 and 1300°C for CAP2). The crucible was removed from the furnace and the melt poured onto a steel plate, upon which a cold iron was immediately used to

quench the melt. Once cool, the additives were crushed in a pestle and mortar until a particle size of ~1mm was achieved.

**Table 4.1** Composition of CAP1 in mol %

| Oxide | Mol % |
|---|---|
| CaO | 35 |
| $P_2O_5$ | 35 |
| $Na_2O$ | 5 |
| $K_2O$ | 12.5 |
| MgO | 12.5 |

**Table 4.2** Composition of CAP1 in wt %

| Chemical | Mass (g) | Wt % |
|---|---|---|
| $CaCO_3$ | 35.0315 | 29.73 |
| $P_2O_5$ | 49.679 | 42.16 |
| $Na_2CO_3$ | 5.298 | 4.49 |
| $K_2CO_3$ | 17.276 | 14.66 |
| $MgCO_3$ | 10.538 | 8.94 |

**Table 4.3** Composition of CAP2 in mol %

| Oxide | Mol % |
|---|---|
| CaO | 58.45 |
| $P_2O_5$ | 35 |
| $Na_2O$ | 2.18 |
| $K_2O$ | 2.18 |
| MgO | 2.18 |

**Table 4.4** Composition in CAP2 in wt %

| Chemical | Mass (g) | Wt % |
|---|---|---|
| $CaCO_3$ | 58.50 | 50.72 |
| $P_2O_5$ | 49.68 | 43.07 |
| $Na_2CO_3$ | 2.31 | 2.00 |
| $K_2CO_3$ | 3.01 | 2.61 |
| $MgCO_3$ | 1.83 | 1.58 |

### 4.3.3 PRODUCTION OF COMPOSITE POWDER AND DENSE COMPACTS

Composite powders (CAP1-HA and CAP2-HA) were prepared by wet-milling commercial HA (P201) with the reinforcing additive in 300 ml of methanol for 24 hours in a ceramic ball mill containing ceramic milling media (as described in section *4.3.1*). Powders containing 1, 2.5, 3.25, 4, and 5 wt % of additive were prepared (for CAP2-HA only):

1 wt % ⇒ 1 g of additive + 99 g of P201 HA

2.5 wt % ⇒ 2.5 g of additive + 97.5 g of P201 HA

3.25 wt % ⇒ 3.25 g of additive + 96.75 g of P201 HA

etc.

The mixed powders were then dried and mechanically sieved through a 75 μm mesh. The resulting composites were uniaxially pressed at 85 MPa in a steel die using 5g of powder to produce 30 mm diameter discs. The discs were placed in a furnace on an alumina tile and then fired using the same protocol as that of P201 HA.

### 4.3.4 POROUS P201 PRODUCTION USING FOAM BURN-OUT

Two grades of polyurethane foam were used in this study:

- YU (IRC in Biomedical Materials)
- BU (Foam Engineers Ltd.)

The foams were cut into rectangular shapes with the following dimensions; ~ 4.5 cm × ~1.5 cm × ~1.5 cm. A ceramic slurry was prepared for pre-soaking the foams and consisted of the following:

- 20 ml 5 wt% Polyvinyl alcohol(PVA) solution (prepared by adding 5 g of PVA to 95 ml of distilled water at 35°C under conditions of continuous stirring until dissolution was complete)
- 80 ml Distilled Water
- 25 g Powder (P201 HA or Composite powder with 2.5 wt % additive)

The binder, water and powder were placed in a large plastic bowl and stirred thoroughly yet slowly, to avoid the creation of a slurry foam. The slurry mixture contained 20 wt % powder and 1 % concentration of PVA. The YU and BU foams were then dipped into the ceramic slurry and manipulated, squeezed to encourage the slurry to wet all of the surfaces of the foam (soaking time ranged from 1-2 minutes). After soaking, the samples were hung by metal hooks in a drying cabinet overnight at a temperature of 70°C ± 10°C.

The dried foams were then placed in the furnace and heat-treated under a regime that would allow the PVA to burn out, followed by sintering:

| | |
|---|---|
| Ramp 1 | + 1°C.min$^{-1}$ |
| Level 1 | 500°C |
| Dwell 1 | 3 – 4 hours |
| Ramp 2 | + 5°C.min$^{-1}$ |
| Level 2 | Temperatures ranging between 1200°C and 1400°C |
| Dwell 2 | 2 hours |
| Ramp 3 | - 5°C.min$^{-1}$ |
| Level 3 | 20°C |
| Dwell 3 | End |

The result was a positive replica of the porous foam structure (Figure 4.1).

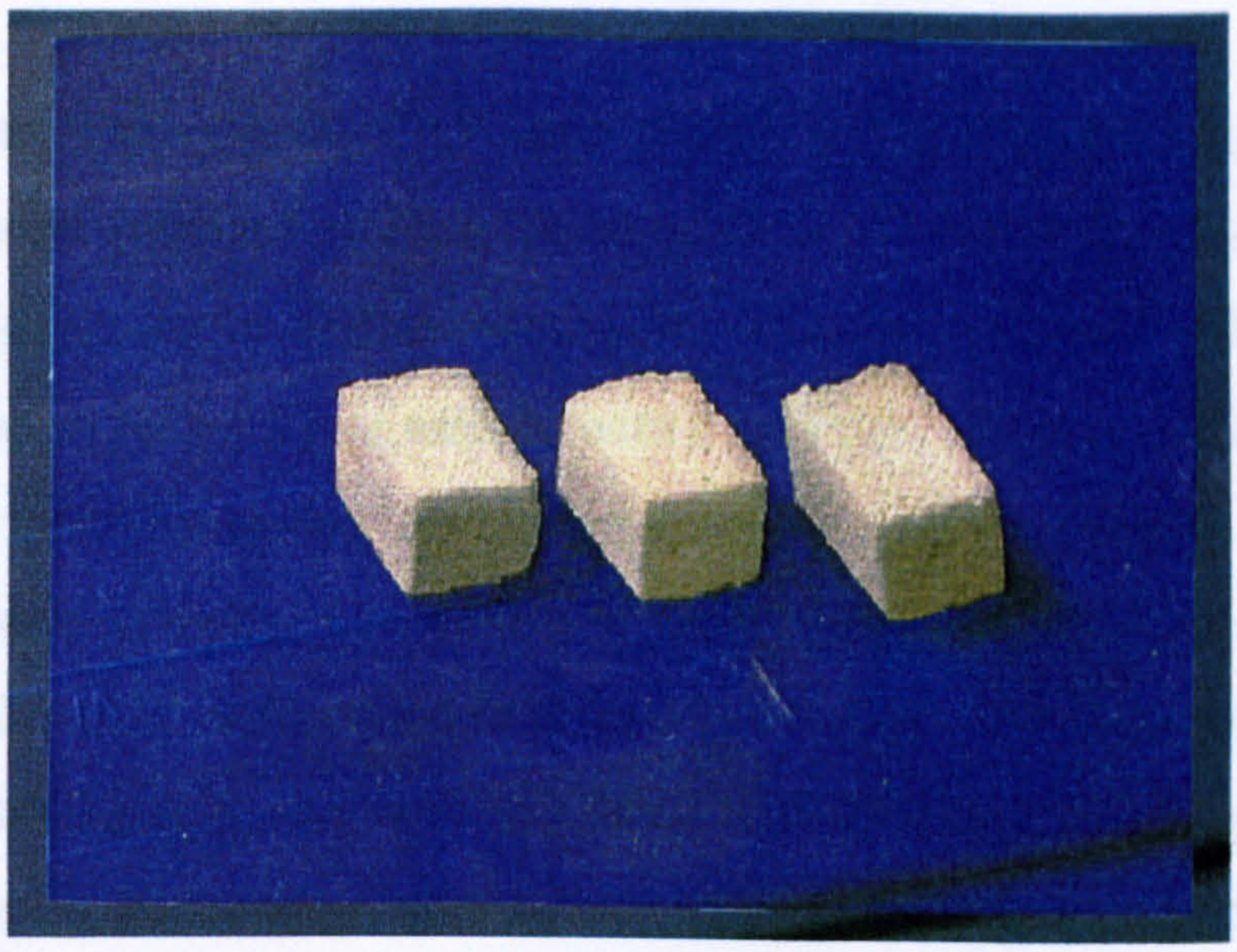

**Figure 4.1** Porous ceramic specimens produced by burn-out

## 4.4 CHARACTERISATION TECHNIQUES

### 4.4.1 PARTICLE SIZE ANALYSIS

The Malvern Mastersizer (Malvern Instruments) was used for particle size analysis. A 100μm lens was used which analysed particles within the 0.2 - 180μm size distribution. Approximately 1 g of powder, obtained after milling, was used for each analysis, for which it was necessary to disperse the powder in distilled water. The sample presentation unit was cleaned with distilled water before and after each reading to ensure accuracy. The powder was added under constant conditions of mixing to ensure uniform powder dispersion, after which the data was retrieved. At least two repeats were carried out for each sample to ensure representative results were obtained. The data was displayed in the form of a histogram of particle size distribution and values of median particle size ($D_{0.5}$), $D_{0.1}$, and $D_{0.9}$ were also calculated.

### 4.4.2 X-RAY FLUORESCENCE (XRF)

XRF was used to determine the Ca:P ratio of all dense specimens used in this thesis. Sample preparation involved making fused glass disks out of specimens in powder form, using a glass fluxer (Fluxy Model 30, Claisse, Canada). The preparation process consisted of fusing 1 g of sample with 6 g of flux (lithium tetraborate) to form a homogeneous melt (controlled heating/agitation cycle up to 1000°C). The melt was spun in the fluxer to provide good mixing and then automatically poured into a mould (Pt/Au 5 %) and cooled (using fans) to form a glass disk. The disks were then placed in the sample holding unit, and were irradiated with an unfiltered X-ray beam, which in turn caused each element to emit a characteristic fluorescence pattern. The raw data was analysed using the program CAPFLUX, from which percentages of Ca and P were obtained, hence the Ca:P ratios.

### 4.4.3 DIFFERENTIAL THERMAL ANALYSIS (DTA)

DTA was used to characterize any thermal events exhibited by the CAP1 and CAP2 additives on heating/cooling, i.e. exotherms and endotherms that occur due to the release or take-up of latent heat during structural changes such as crystallization, glass transition, and melting. The analysis was performed using a Setaram Labsys DSC/DTA with a 1600°C sensor rod, at a ramp rate of $10°C.min^{-1}$ under a nitrogen atmosophere where the furnace was flushed with nitrogen for 25 minutes prior to the test. The analysis was carried out on ~ 80 mg of sample in powder form with a particle size < 75 μm. The samples were placed in platinum crucibles for heating and reached temperatures of 1200°C, during which time thermal events such as the glass transition point were recorded.

### 4.4.4 X-RAY DIFFRACTION

X-Ray diffractometry (XRD) was performed to determine the crystalline phase composition of all dense and porous specimens used in the investigations described in this thesis. The dense specimens were analysed as sintered compacts whereas the

porous specimens were crushed to a fine consistency and analysed in powder form. The measurements were made using a Siemens D-5000$^{TM}$ X-ray diffractometer. Data was collected from 25 to 40° 2θ with a step size of 0.02° and step time of 2.5 seconds. Intensity data was collected using a scintillation counter, and the results were compared with PDF Ca-P standards to determine the crystalline phase composition, such as HA, α-TCP, and β-TCP. The amounts of α-TCP and β-TCP were semi-quantified as relative percentages between the 100% intensity peak for HA and the 100% intensity peak for either α- or β-TCP as follows:

$$\text{Relative Intensity}\,\alpha - TCP, or \beta\text{ - TCP} = \frac{I_{\alpha/\beta}}{I_{HA}} \times 100 \qquad (4.1)$$

where: $I_{\alpha/\beta}$ = Intensity of α/β-TCP

$I_{HA}$ = Intensity of HA

### 4.4.5 Density Measurements

The density of the dense specimens was calculated by dividing the mass of the specimen (measured on an electronic balance to 4 decimal places) by the volume,

$$\text{Density} = \frac{M}{V} \qquad (4.2)$$

The volume was calculated by assuming the specimen was a perfect cylinder:

$$\text{Volume} = \pi r^2 t \qquad (4.3)$$

where t = specimen thickness

r = specimen radius

All dimensional measurements (diameter, thickness, width) for the dense and porous specimens were taken as an average of three measurements for each dimension. The apparent and real densities of the porous specimens were obtained using Archimedes principle. The apparent density, as defined when applied to cancellous bone, describes the open and closed porosity of a structure, i.e. the value obtained when including the volume of the pores as well as the struts. Apparent density was given by:

$$\text{Apparent density} = \left(\frac{W_{dry}}{(W_{sat} - W_{sub})}\right)\rho H_2O \qquad (4.4)$$

where $\rho H_2O$ = Density of deionised water.

Archimedes' principle was also used to determine the real density of specimens, i.e. the density of the individual struts, as an indication of the extent of closed porosity present in a structure, (assuming the theoretical density of HA to be 3.156 $g.cm^{-3}$).

$$\text{Real density} = \left(\frac{W_{dry}}{(W_{dry} - W_{sub})}\right)\rho H_2O \qquad (4.5)$$

$$\text{Closed porosity} = \left(1 - \frac{\text{real density}}{3.156}\right) \qquad (4.6)$$

### 4.4.6 BIAXIAL FLEXURAL STRENGTH TESTING

#### 4.4.6.1 Testing Procedure

The dense sintered discs were mechanically tested in biaxial flexure(in their as-sintered, unpolished state), using a concentric ring jig (Figure 4.2) with a load ring diameter of 4 mm and an outer support ring diameter of 17 mm. Specimens were tested to failure on an Instron Desk Standing testing machine (Instron 4464) at a crosshead speed of $1mm.min^{-1}$ using a 2 kN load cell. The flexural strengths (in MPa) were calculated using the peak load at failure and the following relationship:

$$\textbf{BFS (MPa)} = \sigma_{BFS} = \left\{\left(\frac{3P}{2\pi t^2}\right)\cdot\left(1.25\ln\frac{d_s}{d_l}\right)\cdot\left(0.75\frac{d_s^2 - d_l^2}{2d^2}\right)\right\} \quad (4.7)$$

where $\sigma_{BFS}$ = biaxial flexural strength (BFS) in MPa

$P$ = load at failure in N

$d_s$, $d_l$, $d$ and $t$ = support ring diameter, the loading ring diameter, the specimen diameter and the specimen thickness respectively, in mm.

For the mechanical degradation study, the discs were tested in an improvised environmental chamber, as shown in Figure 4.3. The chamber contained the half-strength Ringers' solution, which allowed the test to be performed under solution. The immersed discs were transferred from the metal-free polyethylene containers with tweezers to the biaxial flexure jig within the chamber.

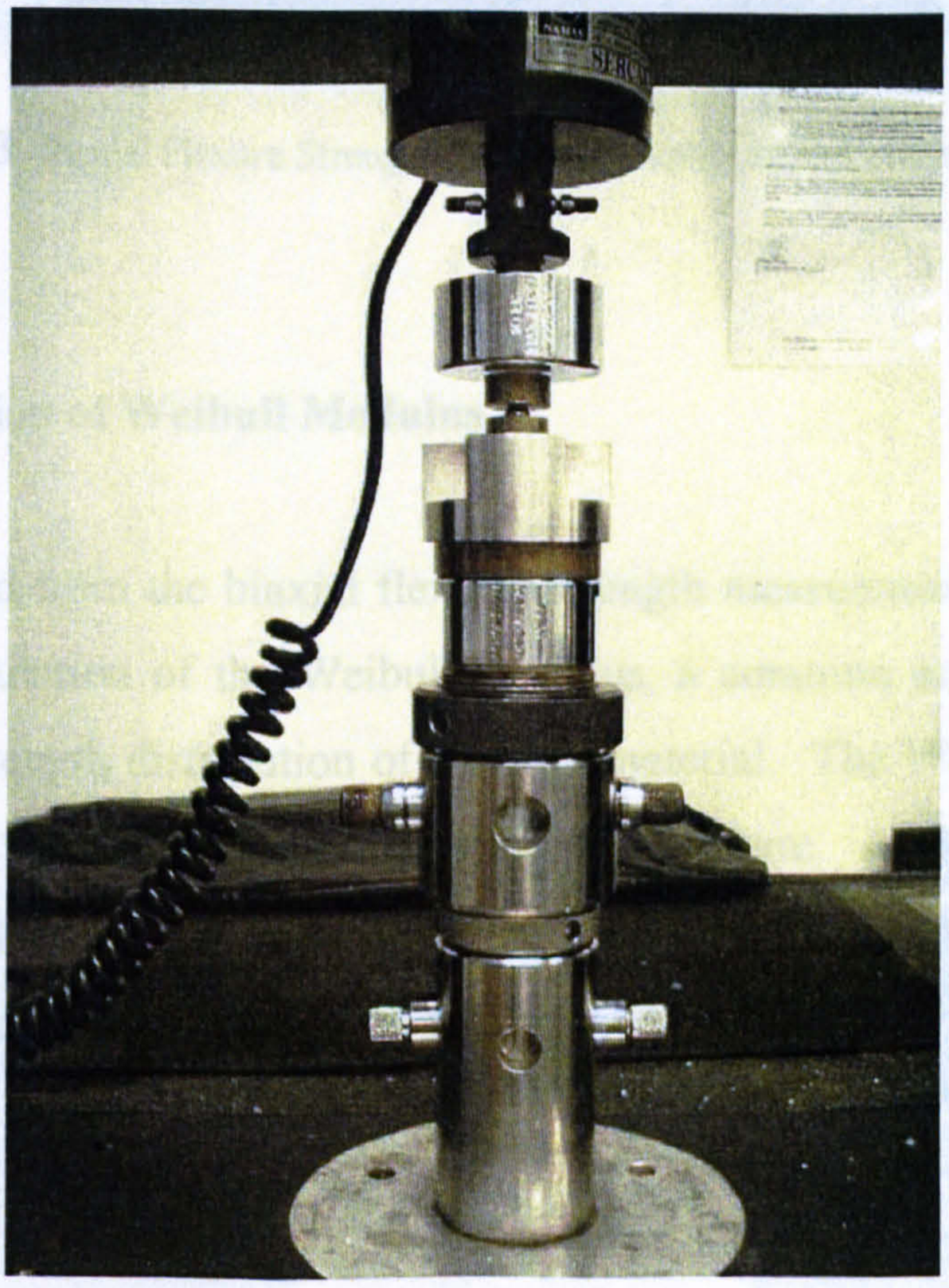

**Figure 4.2** Biaxial Flexure Strength Testing Jig

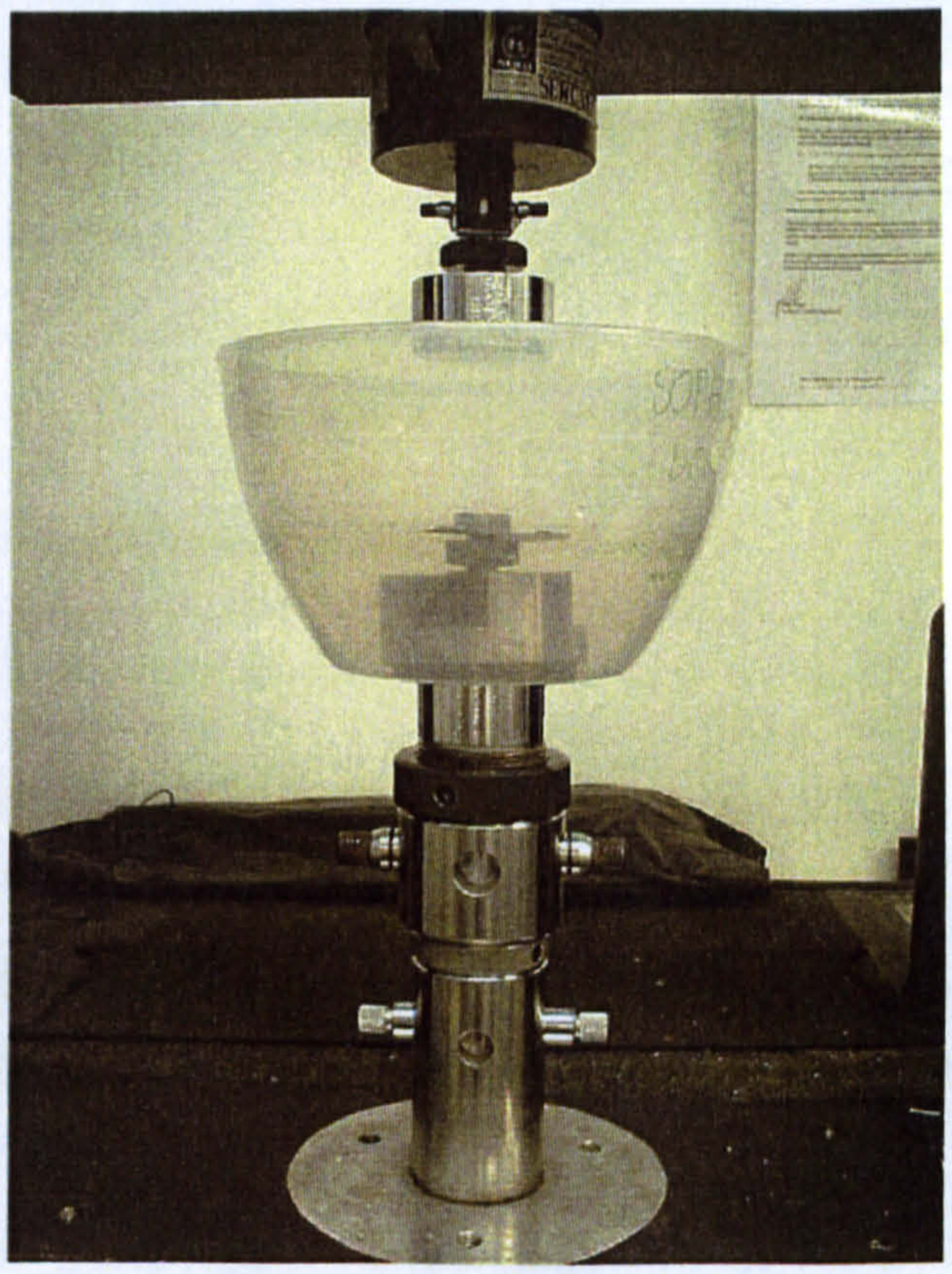

**Figure 4.3** Biaxial Flexure Strength Testing Jig within an Environmental Chamber

### 4.4.6.2 Calculation of Weibull Modulus

The data obtained from the biaxial flexural strength measurements were statistically analysed by calculation of the Weibull modulus, a common empirical approach to describing the strength distribution of a brittle material. The Weibull modulus is an indication of the reliability of a brittle material in failure. A high Weibull modulus suggests that failure of the material is predictable and reproducible whilst a low moduli suggests large variations in the failure strength.

Weibull modulus is determined as follows:-

The probability of survival of a sample in a given set of data is given by:

$$S = \exp-\left(\frac{X}{X_o}\right)^m \qquad (4.9)$$

where X = value of the variable (BFS)

Xo = value of the variable for which $S = \frac{1}{e} = 0.37$

m= Weibull Modulus

Therefore the specimens are ranked in the order in which they failed, 1,2,3,.....j, j + 1, .....n, where the probability of survival of the jth specimen was given by:

$$Sj = 1-\left(\frac{(j-0.3)}{(n+4)}\right) \qquad (4.10)$$

where j = rank number

n = number of specimens

The straight line version of the Weibull distribution declares:

$$LnLn\left(\frac{1}{S_j}\right) = mLn\left(\frac{X}{X_o}\right) \qquad (4.11)$$

By plotting $LnLn\left(\frac{1}{S_j}\right)$ against $Ln\left(\frac{X}{X_o}\right)$, m can be obtained by calculating the gradient of the graph.

### 4.4.7 COMPRESSION TESTING

#### 4.4.7.1 Preparation for Testing

In order for the porous ceramics to be tested under compression, it was necessary to ensure the surfaces in contact with the upper and lower platens of the testing machine were plane parallel to one another, otherwise surface inconsistencies (asperities) would lead to pressure gradients and premature fracture. The assembly for compression testing is shown in Figure 4.4.

Initially, silicon carbide paper was used to flatten the surfaces; however this proved to be unsuccessful and inefficient. Instead, the samples were wax-mounted onto a flat sample holder and a diamond Accutom™ blade was used to slice off sections from the ends of each sample to obtain two flat surfaces. The advantages of smoothing the surfaces as opposed to leaving the asperities prior to mechanical testing were noticable during pre-load, as both the upper and lower platens were in contact with the specimens' surfaces.

#### 4.4.7.2 Testing Procedure

Mechanical testing of the porous ceramic materials was performed in compression on an Instron 4464 screw driven test machine, fitted with a 2 kN load. Specimens were placed, unconstrained, on the lower platen of the mechanical test equipment and a pre-load of 5 N applied with the upper platen, at a cross-head velocity of 0.1 $mm.min^{-1}$.

Testing was performed under computer control using a test template created on Series IX Automated Testing System v 1.21. The load was applied axially to the specimens with a crosshead velocity of 0.1$mm.min^{-1}$ until catastrophic brittle failure occurred. The test data (load and displacement) was digitally recorded at a sample rate of 0.5 $point.s^{-1}$.

The compressive stresses applied to the sample throughout the test were calculated using equation 4.4.7:

$$\sigma c = \left( \frac{\text{Applied Load}}{\text{Width} \times \text{Thickness}} \right) \qquad (4.12)$$

The ultimate compressive stress (UCS), defined as the maximum value of stress supported by the specimen before significant loss of structural integrity or structural densification, was determined for each specimen from this data.

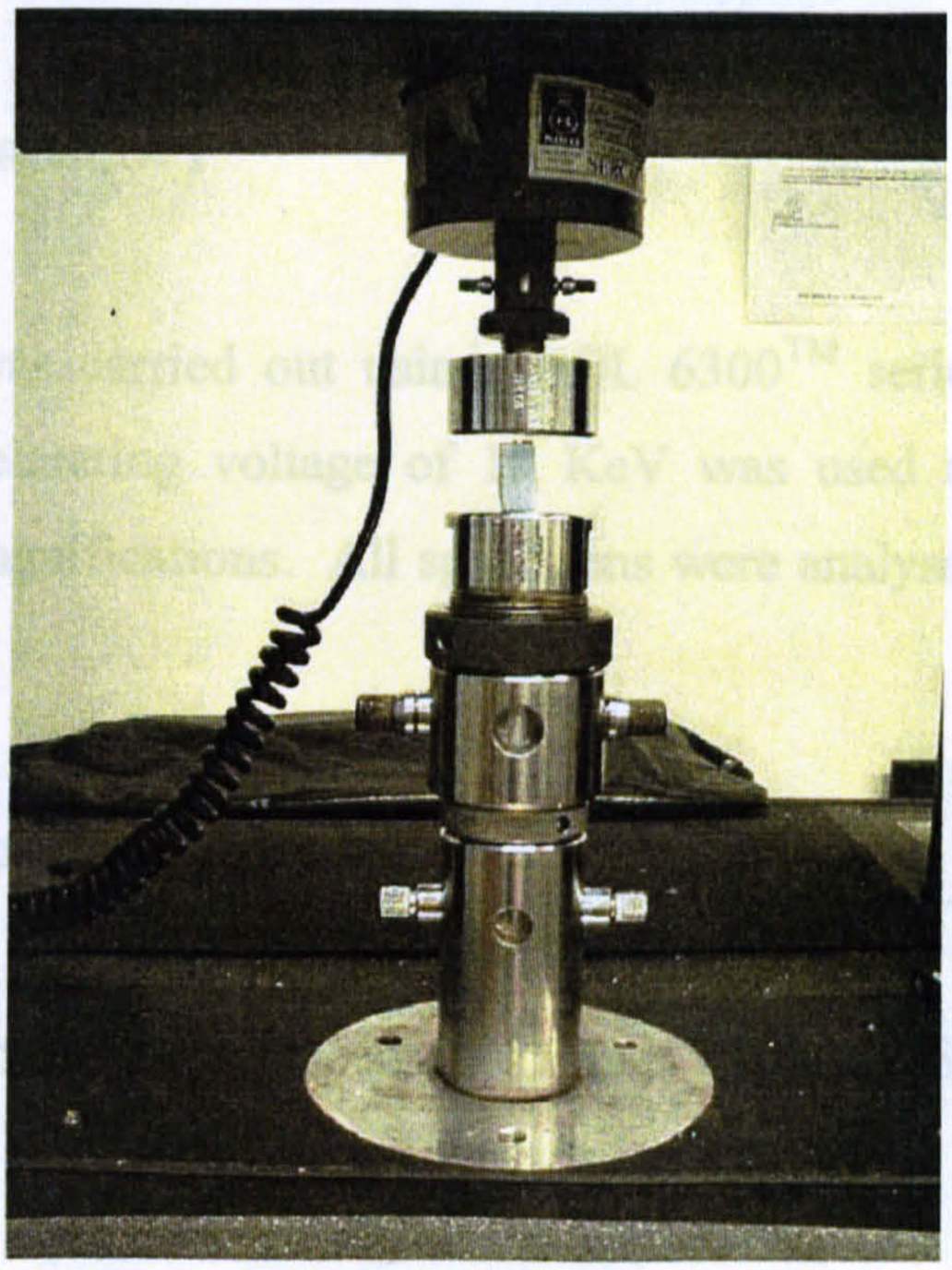

**Figure 4.4** Compression jig holding a porous ceramic sample

### 4.4.8 INDUCTIVELY COUPLED PLASMA MASS SPECTROMETRY (ICPMS)

Inductively coupled plasma mass spectometry (ICPMS) was used to analyse the calcium and phosphorus content of Ringer's solution collected after having HA/CAP2-HA discs soaked in it. The Spectromass 2000$^{TM}$ machine measured the content of the liquid by transporting it via a nebulizer through a spray chamber to a plasma torch containing inductively coupled plasma (ICP), which acts as an efficient ion source. The combination of the ICP and a mass analyser as a spectrometer enabled multi-element analysis.

Before the analysis, the Ringer's solution samples were prepared by dilution with high-purity de-ionised water followed by the addition of nitric acid to ensure ionic dispersion. From each polyethlene container, 1 ml of solution was taken and added to 97 ml of high-purity de-ionised water and 2 ml of nitric acid (69 % strength), all of which were placed in high-purity 100 ml polyethylene volumetric flasks. Before and after each analysis, the analysis chamber was cleaned out with an acid blank containing roughly 4 % nitric acid.

### 4.4.9 ELECTRON MICROSCOPY

Electron microscopy was carried out using JEOL 6300™ series scanning electron microscopes. An accelerating voltage of 10 KeV was used and specimens were studied at a range of magnifications. All specimens were analysed after sintering and mechanical testing.

The specimen preparation was as follows:

- Embedding- Specimens were placed in 25 mm diameter Struers™ embedding moulds.

- A mixture of Epofix resin (Struers) and hardner in a ratio of 25 parts (volume) of resin to 3 parts (volume) of hardner was then introduced into the moulds. This was then left to harden for 24 hours. For porous specimens, the resin/hardener mixture was introduced into the structure by vacuum embedding, using the Stuers Epovac™ vacuum embedding machine.

- Polishing- After the hardened specimens were removed from the moulds, they were polished using the Struers Abramin™. A 75 μm diamond wheel was first used to level off the surface, and then 63, 30, and 10 μm diamond wheels were used to remove any scratches. Duration of grinding for each grit wheel depended on the sample and was repeated as necessary.

- Etching- An orthophosphoric acid solution (0.1 – 2.5 % strength) was used for etching specimens (when necessary) for approximately 10 seconds.

- Gold Coating of Embedded Specimens- Specimens were cleaned in methanol, mounted on clean SEM stubs with a conductive element and gold coated using a Balzers High Vacuum™ sputter coater.

# CHAPTER 5

# INVESTIGATION INTO THE SINTERING BEHAVIOUR OF P201 HA

The P201 HA was uniaxially pressed and the green compacts were sintered at 1000°C, 1100°C, 1200°C, 1250°C, and 1300°C, and the following chapter reports the results from analysing the P201 HA in this range. Two batches of 10 specimens were made for each temperature category.

## 5.1 PARTICLE SIZE ANALYSIS

All the batches in the HA study came from the same source, i.e. P201 from Plasma Biotal. Prior to the preparation of powder compacts, the P201 was milled for 24 hours (as stated in section *4.3.1*). Particle size analysis was performed on milled and unmilled powder. The results from this analysis are shown in Table 5.1.

**Table 5.1** Results from particle size analysis on milled/unmilled P201 HA

| Sample | $d_{0.1}$ (μm) | $d_{0.5}$ (μm) | $d_{0.9}$ (μm) | mode (μm) |
|---|---|---|---|---|
| Milled P201 Run 1 | 4.14 | 37.44 | 63.02 | 43.73 |
| Milled P201 Run 2 | 3.58 | 37.11 | 62.63 | 43.40 |
| Unmilled P201 Run 1 | 3.78 | 37.95 | 65.80 | 43.77 |
| Unmilled P201 Run2 | 3.59 | 37.57 | 65.81 | 43.52 |

The histograms in figure 5.1 and 5.2 display the particle size distribution for milled/unmilled P201 HA respectively. Both are clearly bimodal distributions with modes at ~3μm and ~43μm. As for particle size reduction, milling appeared to have little effect by comparing the unmilled/milled particle sizes.

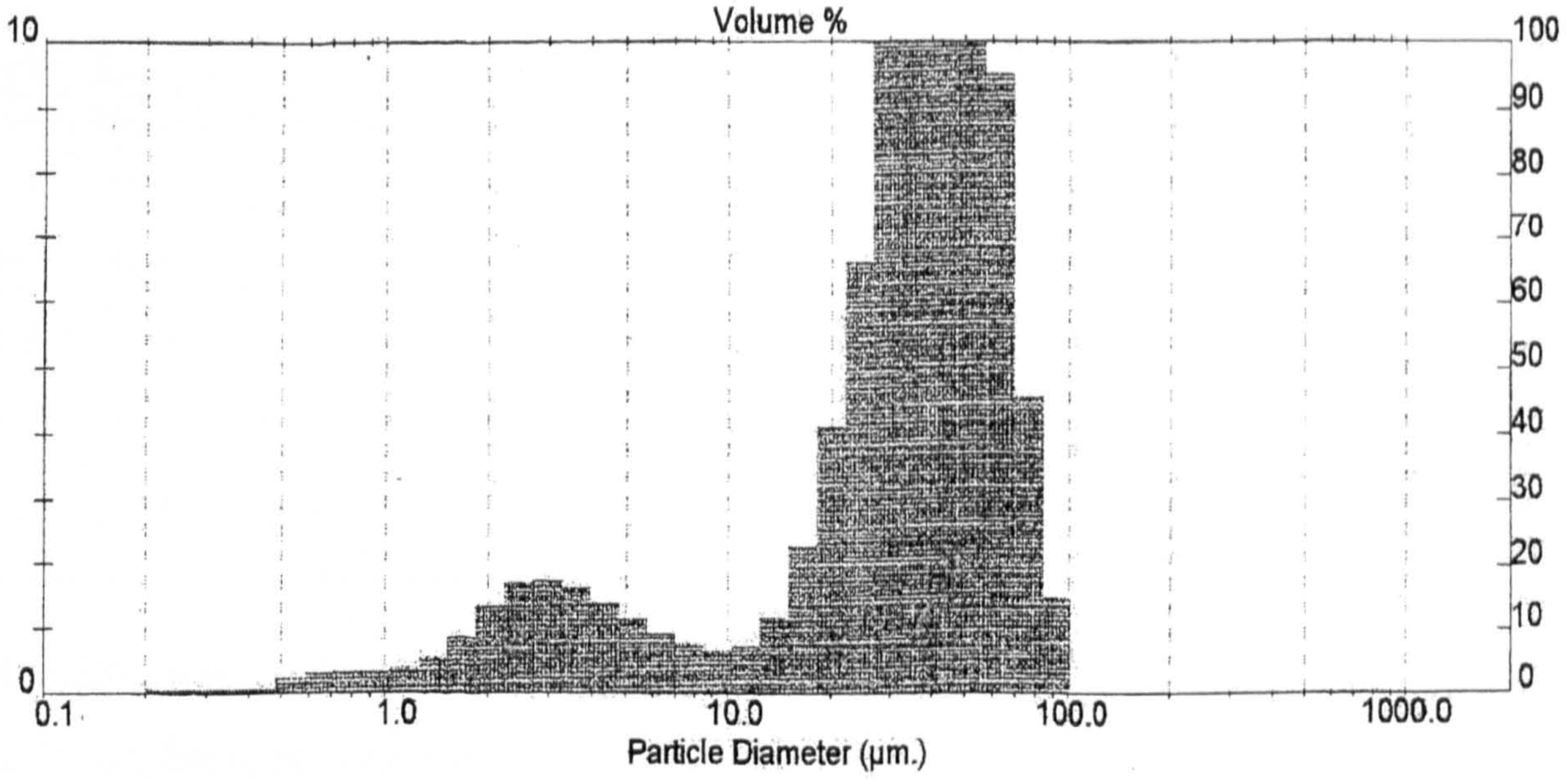


**Figure 5.1** Particle Size Distribution for milled P201 HA

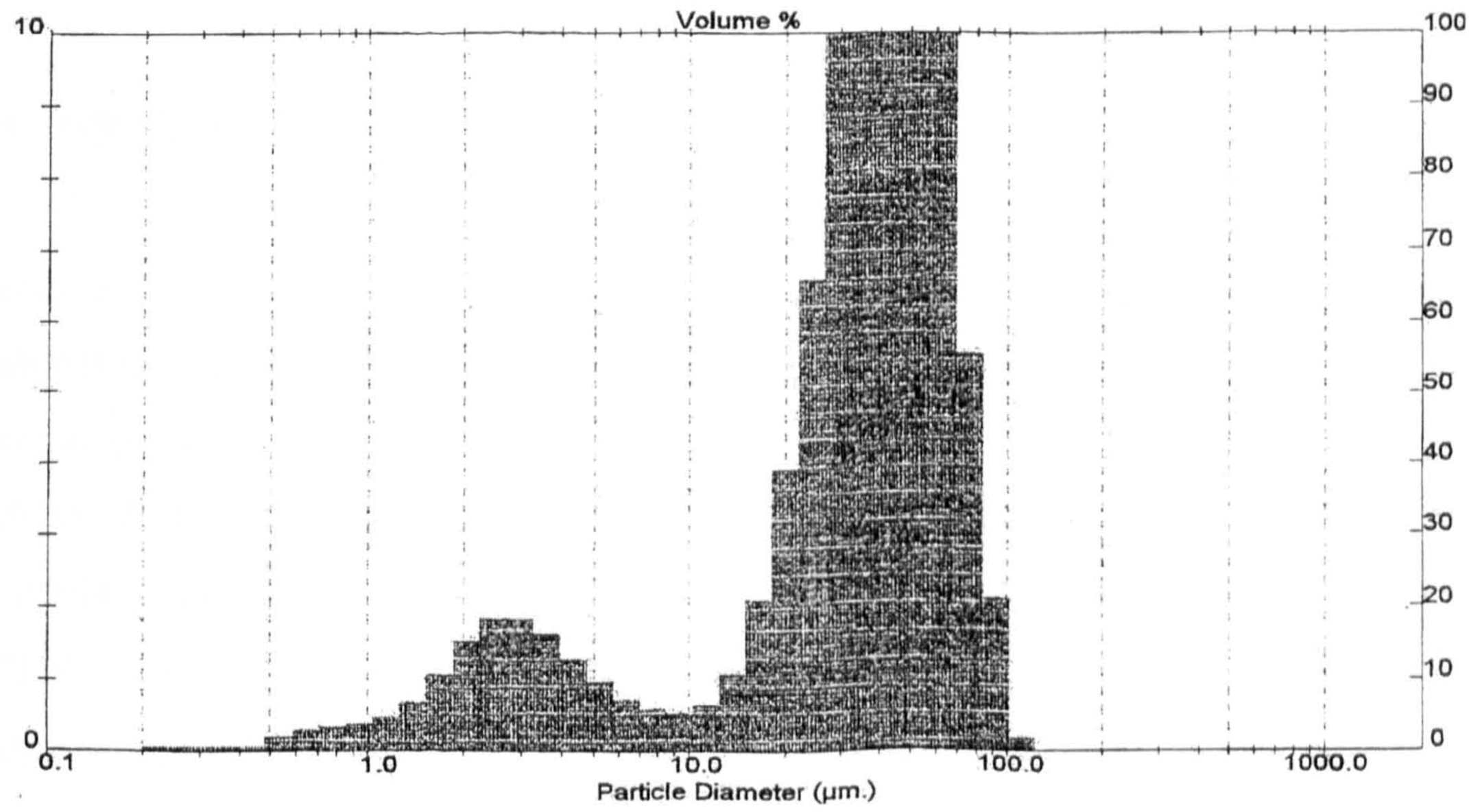


**Figure 5.2** Particle Size Distribution for unmilled P201 HA

## 5.2 X-RAY FLUORESCENCE (XRF)

XRF was performed on as-sintered P201 HA, after having been crushed with a pestle and mortar in order to return to powder form for the specimen preparation. The results from this analysis can be seen in Table 5.2.

**Table 5.2** Ca:P ratio for P201 HA sintered over a range of temperatures

| Sintering Temperature (°C) | % CaO | $\%P_2O_5$ | Ca/P Ratio |
|---|---|---|---|
| 1000 | 55.21 | 41.37 | 1.69 |
| 1100 | 56.07 | 41.17 | 1.72 |
| 1200 | 56.03 | 41.19 | 1.72 |
| 1250 | 56.56 | 42.58 | 1.68 |
| 1300 | 55.93 | 40.85 | 1.73 |

The Ca/P ratio for the P201 did not appear to vary with increasing temperature, but rather fluctuated between 1.68 and 1.73. The theoretical Ca/P ratio for stoichiometric HA is 1.67 (PDF card no. 9-432). The mean value of the Ca/P ratio for the P201 (~1.71±0.02) was found to be significantly greater, such that one would expect ~5wt% CaO phase impurity to exist, assuming both phases to be stoichiometric.

## 5.3 X-RAY DIFFRACTION

X-Ray diffraction was carried out on one specimen from each batch of HA sintered at each temperature. The most important feature on the traces relevant to the load bearing applications of the HA would have been tricalcium phosphate(TCP), a resorbable Ca-$PO_4$ material discussed previously in Chapter 2. From each trace, the highest intensity of TCP was recorded as a percentage of the total composition and noted as either α-TCP or β-TCP. The results from this analysis showed that none of the P201 HA batches decomposed to TCP, even at high temperature, however some CaO was noted at most temperatures.

Examples of XRD traces of P201 HA are displayed in Figure 5.3.

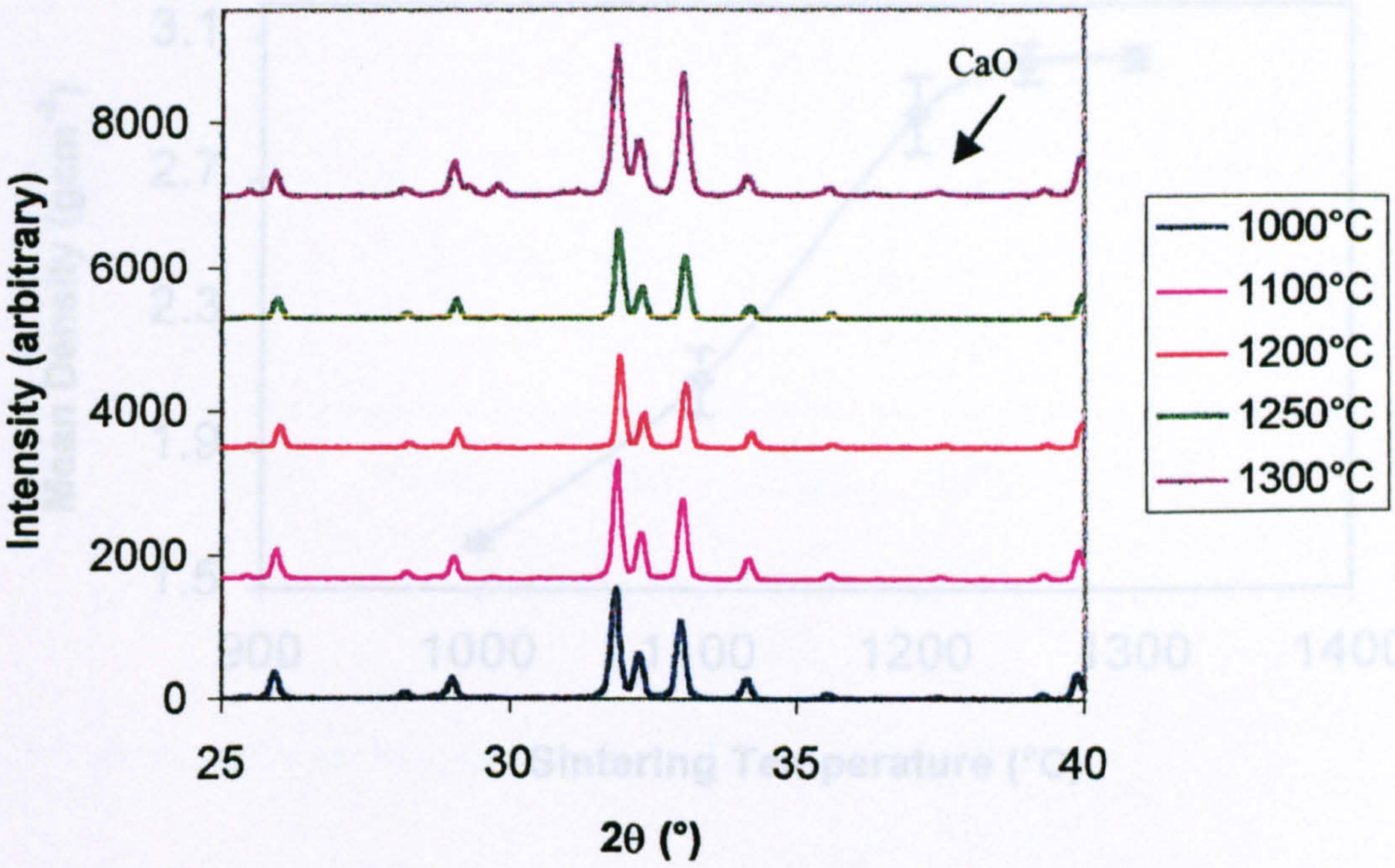


**Figure 5.3** XRD patterns for P201 HA at varying temperatures

## 5.4 MECHANICAL TESTING

The results of the density measurements, mechanical testing, and Weibull Modulus calculations are shown in Table 5.3.

**Table 5.3** Mean values for the mechanical properties of P201 HA sintered at different temperatures

| Sintering Temperature (°C) | Mean Density ($g.cm^{-3}$) | Mean Biaxial Flexural Strength (MPa) | Weibull Modulus (on 20 specimens) |
|---|---|---|---|
| 1000 | 1.64 ± 0.01 | 22.14 ± 6.78 | 0.94 |
| 1100 | 2.11 ± 0.09 | 28.04 ± 7.65 | 3.78 |
| 1200 | 2.88 ± 0.11 | 60.01 ± 14.70 | 3.86 |
| 1250 | 3.02 ± 0.05 | 20.53 ± 10.63 | 3.07 |
| 1300 | 3.04 ± 0.03 | 11.42 ± 2.36 | 6.16 |

Figures 5.4, 5.5, and 5.6 demonstrate the relationships between temperature and density, mechanical properties, and Weibull Modulus, respectively:

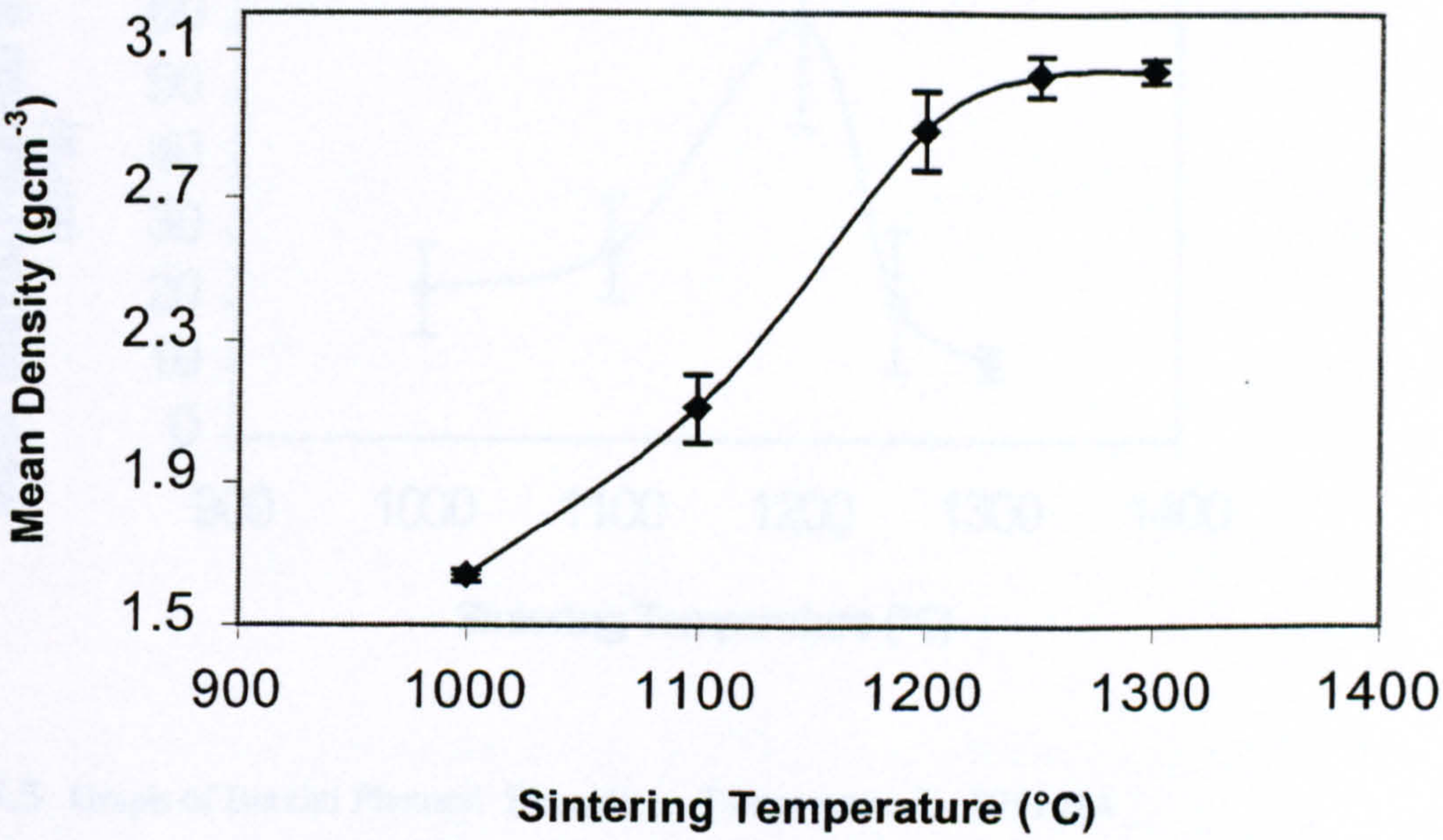


**Figure 5.4** Graph of Density vs Temperature for P201 HA

Referring back to Table 5.3, which shows the mean values for the densities at different temperatures, the following table shows the densities as a percentage of the theoretical density of HA (3.156 $g.cm^{-3}$) at the various temperatures.

**Table 5.4** Percentage of the theoretical density of P201 HA sintered at different temperatures

| Sintering Temperature (°C) | Percentage of theoretical density |
|---|---|
| 1000 | 51.9 |
| 1100 | 66.7 |
| 1200 | 91.2 |
| 1250 | 95.7 |
| 1300 | 96.2 |

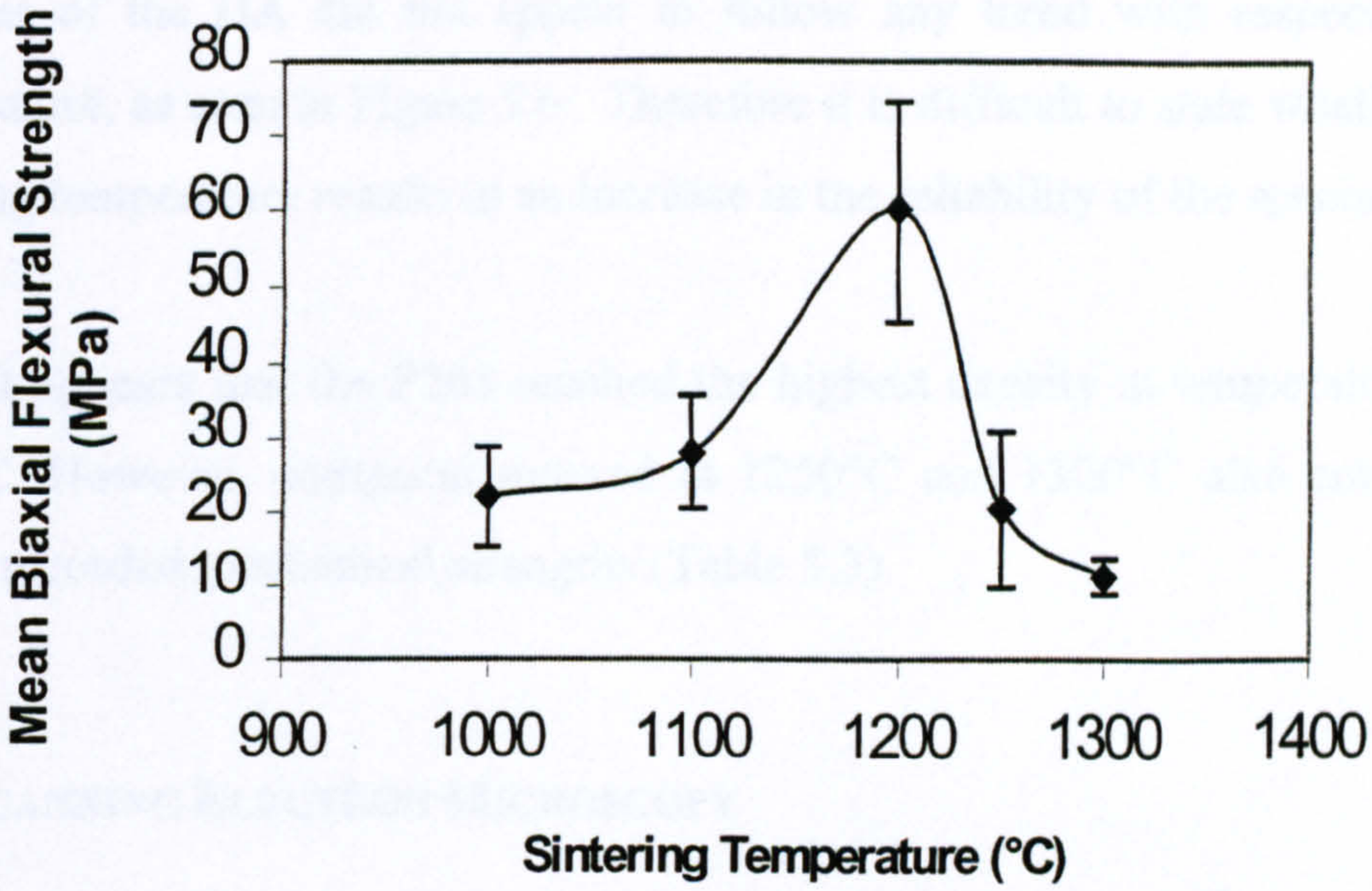


**Figure 5.5** Graph of Biaxial Flexural Strength vs Temperature for P201 HA

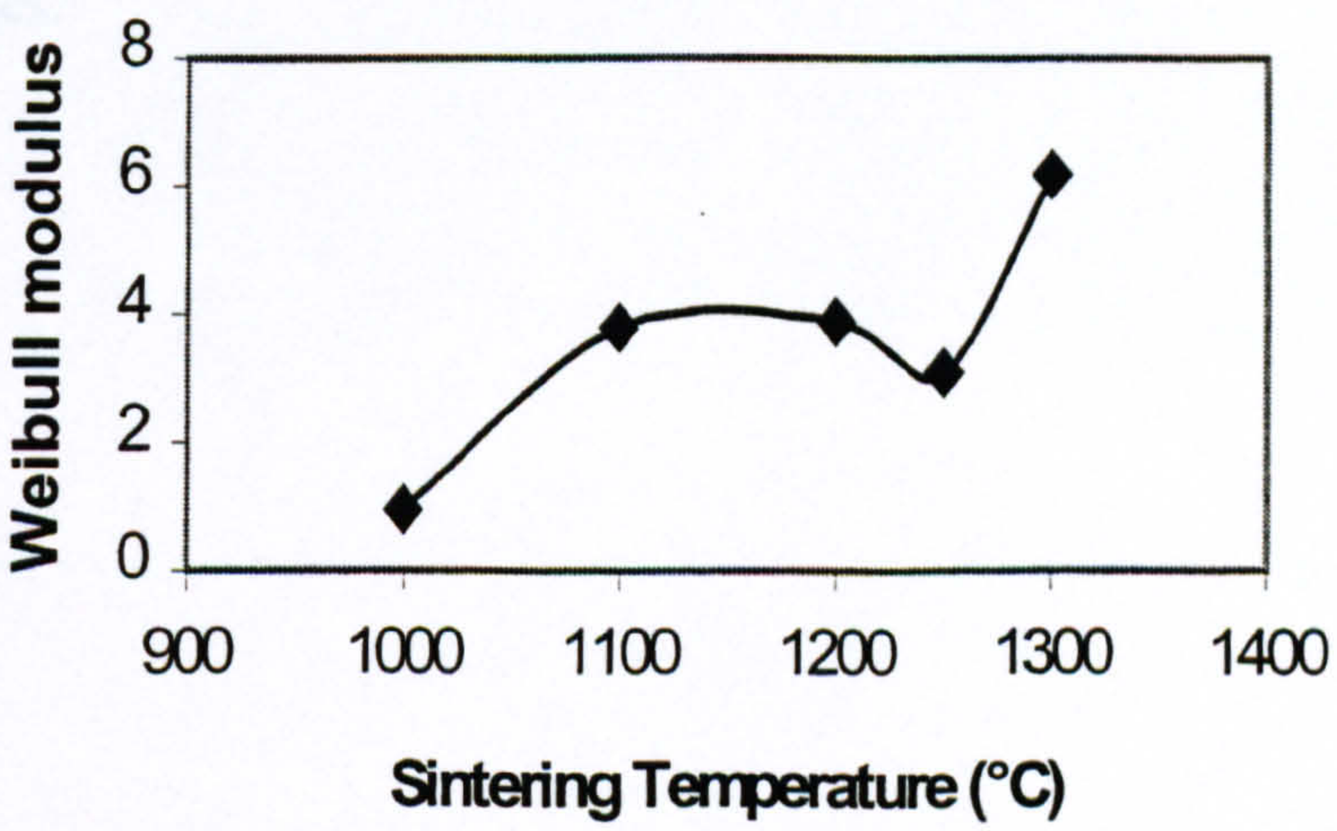


**Figure 5.6** Graph of Weibull Modulus vs Temperature for P201 HA

In Figure 5.4, the density of the HA increased steadily from 1000°C until around 1200°C, where it appeared to plateau. This was dissimilar to the mechanical behaviour of the HA,

in which the biaxial flexural strength (BFS) appeared to increase from 1000°C till 1200°C (Figure 5.5), yet decrease rapidly between 1200°C and 1250°C. The Weibull modulus of the HA did not appear to follow any trend with respect to the sintering temperature, as seen in Figure 5.6. Therefore it is difficult to state whether an increase in sintering temperature results in an increase in the reliability of the specimens.

Thus, it appears that the P201 reached the highest density at temperatures at and above 1200°C. However, compacts sintered at 1250°C and 1300°C also corresponded to the lowest recorded mechanical strengths (Table 5.3).

## 5.5 Scanning Electron Microscopy

Scanning electron micrographs were taken of the HA sintered at all temperatures, in order to determine the sintering behaviour of the ceramic and decipher the structures that resulted in high or low mechanical properties. In order to determine the grain structures, some of the specimens were etched (as described in section *4.4.9*). The images are on the following pages:

P201 HA sintered at 1000°C:

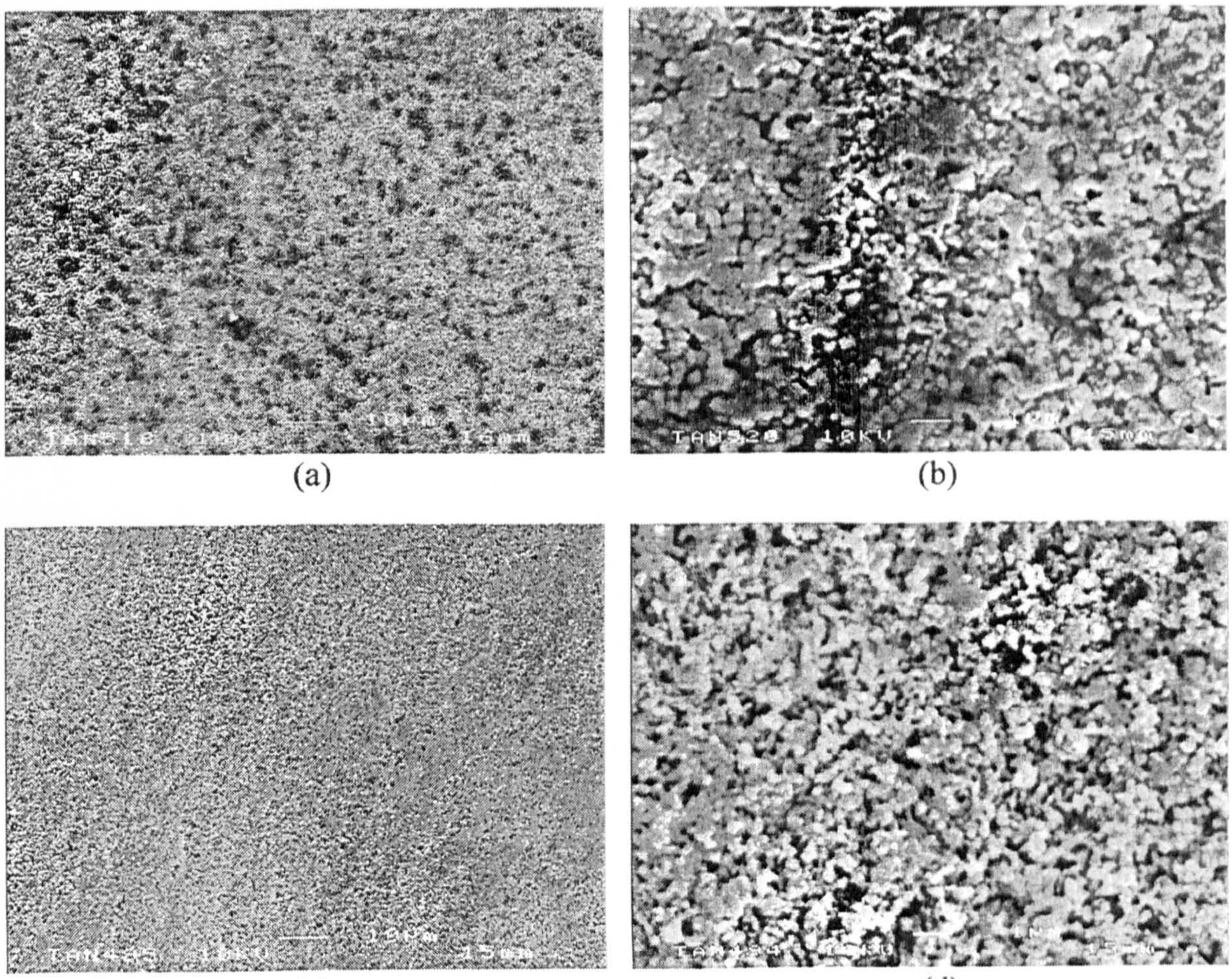

**Figure 5.7** P201 HA sintered at 1000°C. (a) + (b) Unetched HA, (c) + (d) Etched HA

Both the unetched and etched images indicate that at such a low temperature, little sintering has occurred. The particles have not coalesced, and there is a large amount of porosity. The particle sizes appear small, < 1μm, which contradicts the results from the particle size analysis, suggesting the existence of agglomerates as an explanation for the large sizes reported.

P201 HA sintered at 1100°C:

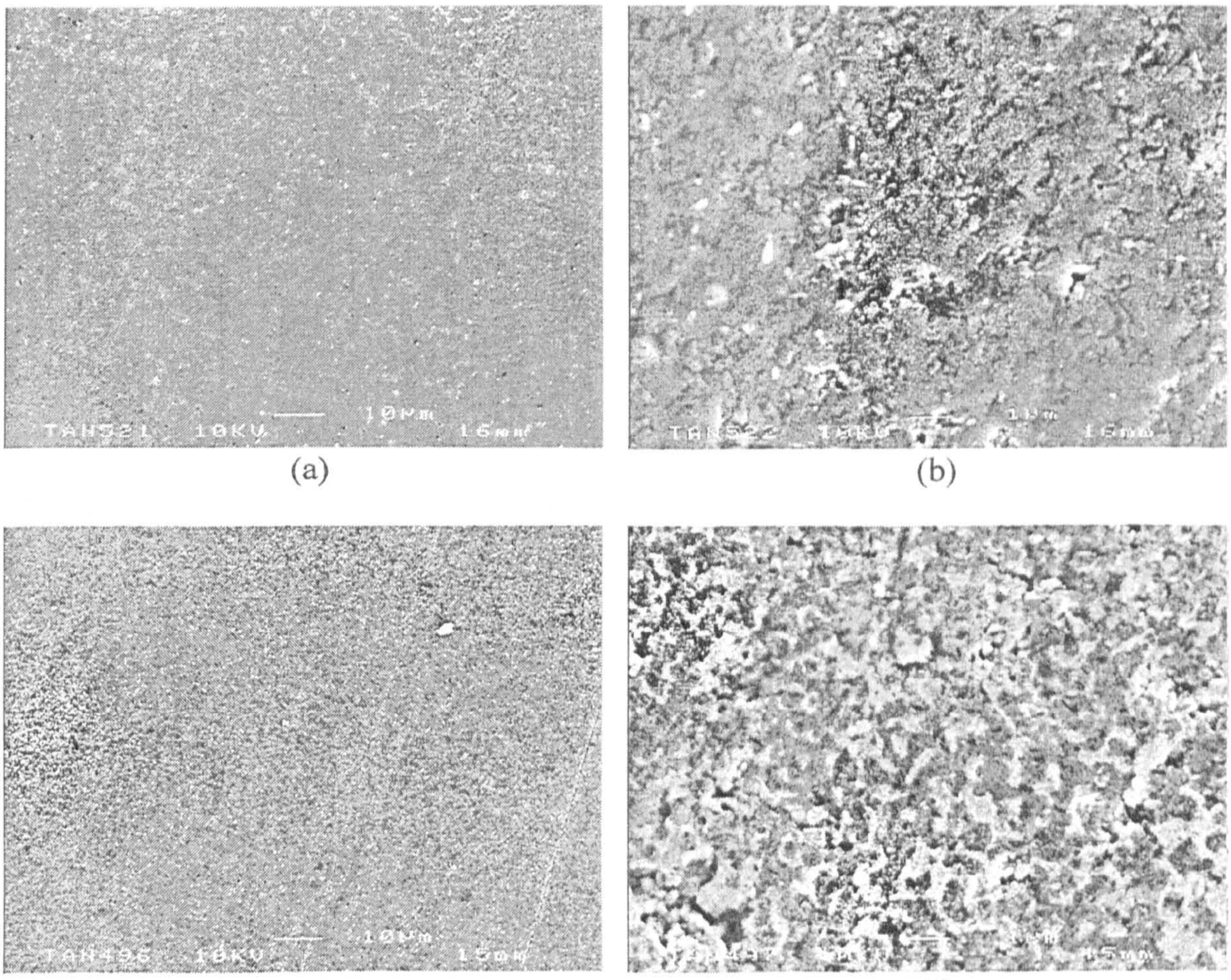

**Figure 5.8** P201 HA sintered at × 1100°C (a) + (b) Unetched HA, (c) + (d) Etched HA

Images (a) and (b) reveal porosity in the microstructure, represented by the white speckles, at low and high magnification. Images (c) and (d) show that the top surface of the polished specimen was very soluble in the etchant. A grain structure is barely visible underneath this layer. There is slightly less porosity than in the specimens sintered at 1000°C (Fig. 5.7), and the early signs of sintering are indicated by some particle coalescence underneath the top layer, seen in (d).

P201 HA sintered at 1200°C:

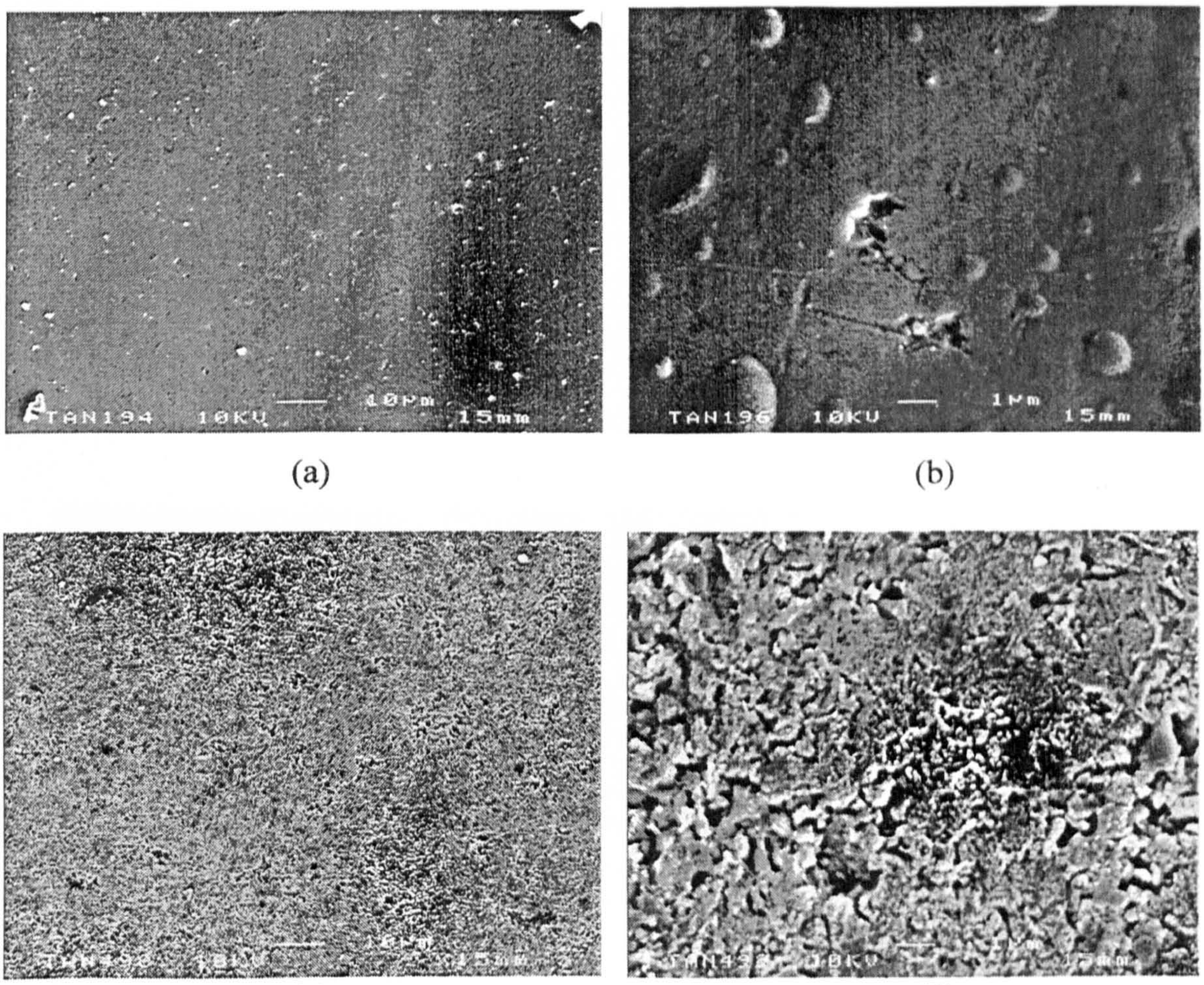


(a) (b)

(c) (d)

**Figure 5.9** P201 HA sintered at × 1200°C (a)+(b) Unetched HA, (c)+(d) Etched HA

Image (a) revealed a smaller number of white speckles than the specimen sintered at 1100°C, which at high magnification (b), appeared to be pores; however the individual pores at 1200°C are larger than those at 1100°C. Image (c) showed surface porosity and at high magnification (b), a grain structure was almost visible. A greater amount of sintering appeared to occur at this temperature. The grain sizes appeared to be <1 μm.

P201 HA sintered at 1250°C:

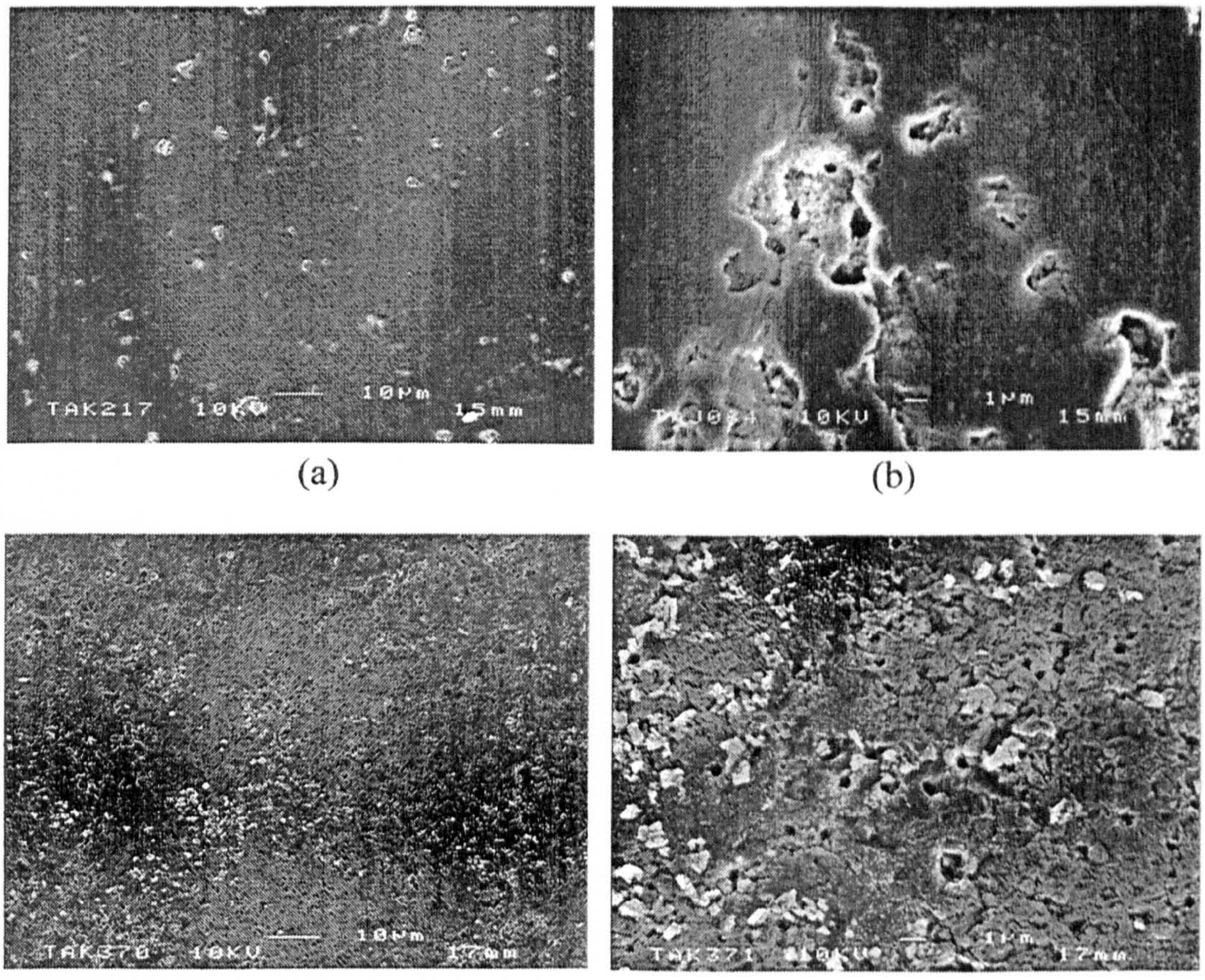


(a) (b)

(c) (d)

**Figure 5.10** P201 HA sintered at × 1250°C (a) + (b) Unetched HA, (c) + (d) Etched HA

At low magnification(a), the unetched HA showed a marginally smaller amount of porosity, i.e. less porosity than the specimen sintered at 1200°C, yet the individual pores appear to be slightly larger. The etched images (c)(d) indicate that the HA has reached a further stage of sintering than at 1200°C, i.e. the particles have not only coalesced but also experienced growth (the grain sizes appear to range between 0.5µm-1.5µm.

P201 HA sintered at 1300°C:

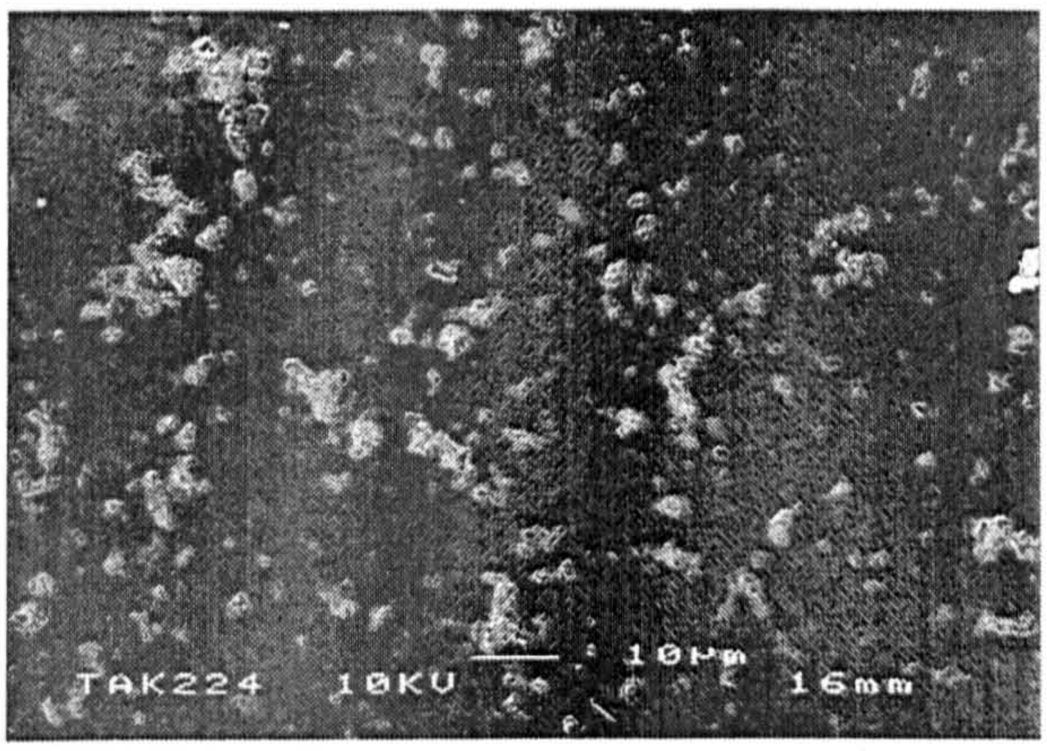


(a)

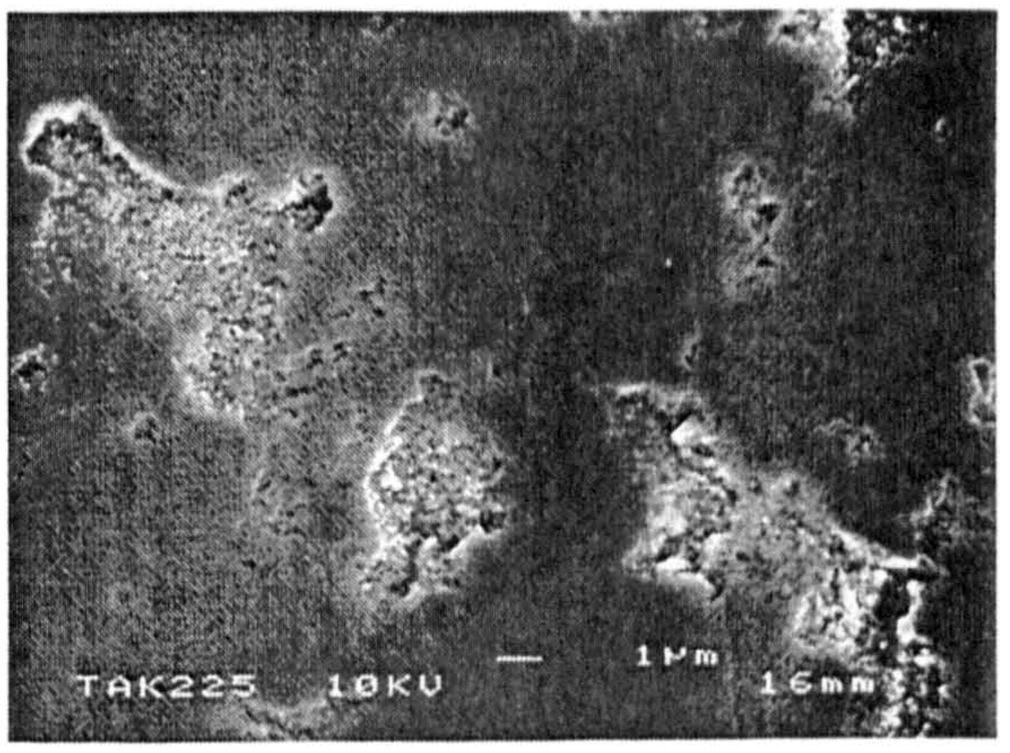


(b)

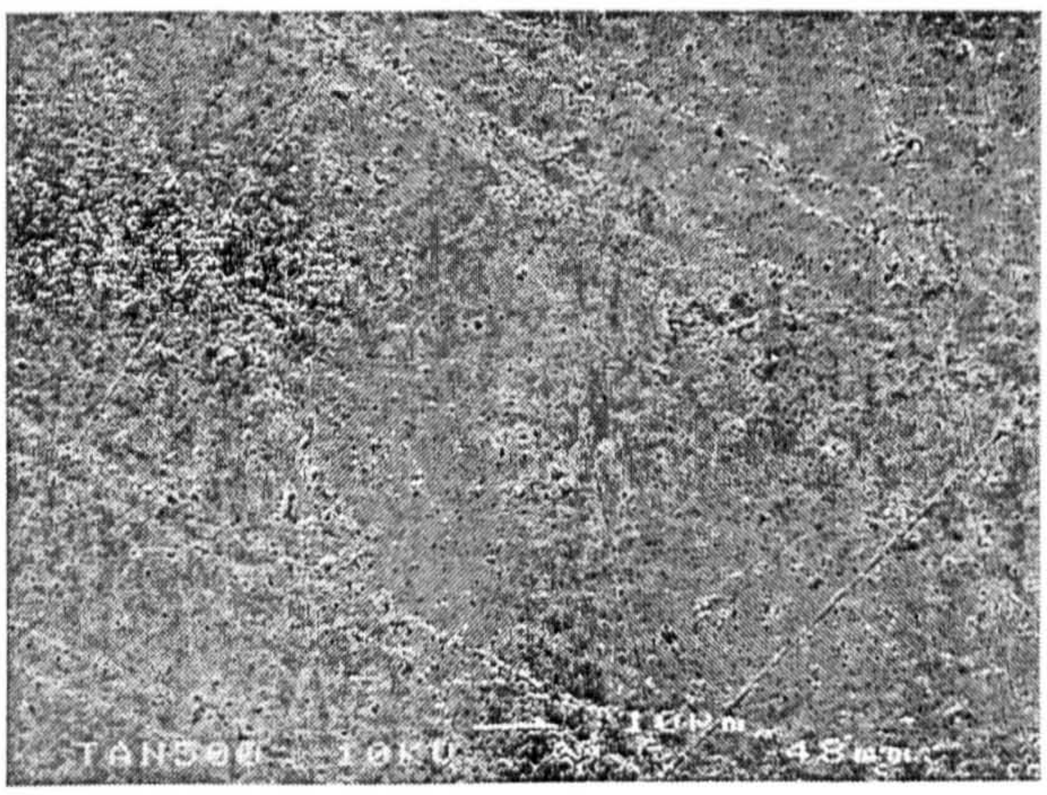

(c)

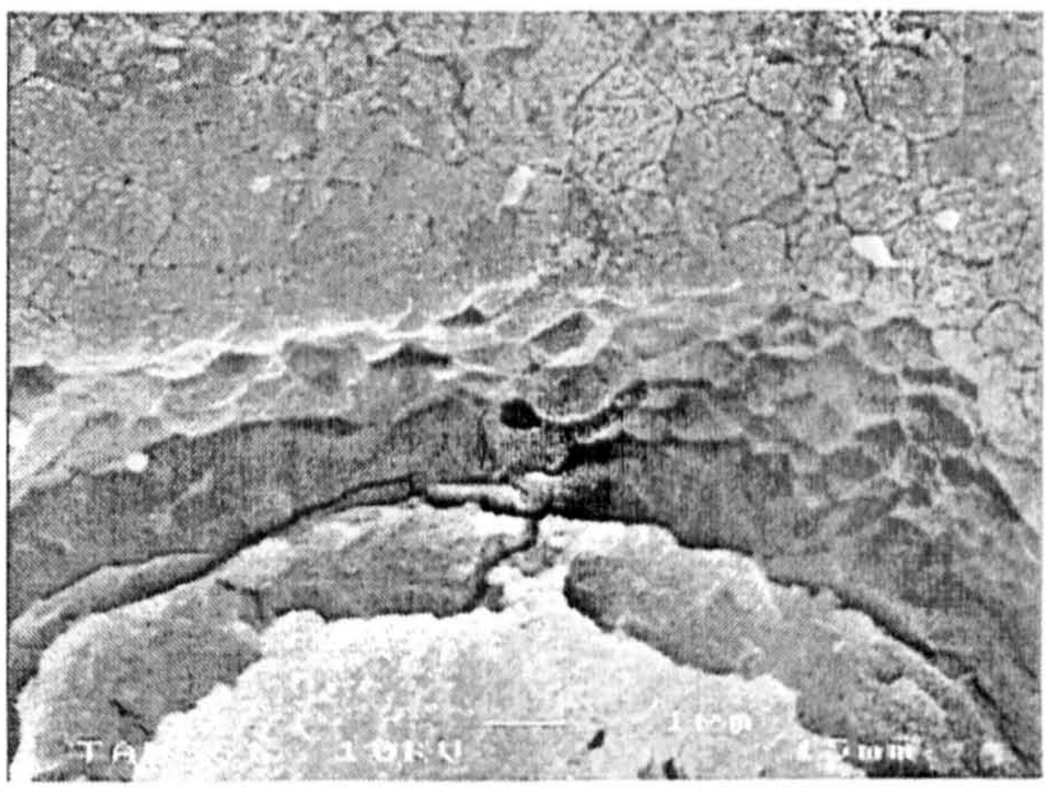

(d)

**Figure 5.11.** P201 HA sintered at 1300°C (a)+(b) Uetched HA, (c)+(d) Etched HA

The unetched HA appeared to show more porosity at low magnification (a) than the specimen sintered at 1250°C combined with a further increase in individual pore size. Examination of the etched HA demonstrated a significant increase in grain sizes, which indicated grain growth in between 1250°C and 1300°C, in addition to the continued coalescence of porosity .

## 5.6 DISCUSSION

Commercial P201 HA (Plasma Biotal Ltd.) was quoted by the manufacturer to have a median ($d_{0.5}$) particle size of 4μm. The median particle sizes of the unmilled/milled powders (~37μm) were much larger than this value. The detection of particles in excess of 10μm would seem to demonstrate the presence of powder agglomerates, which are not representative of the actual particle size. The histograms in Figure 5.1 and 5.2 therefore show bimodal distributions due to the detection of the particle size (~4μm) and the agglomerate size (~43μm). One must expect that due to the use of different machinery and general laboratory conditions, such an analysis cannot be repeated in another environment to produce identical results. However, a discrepancy of 33μm was too large to be justified by these conditions. Furthermore, there was very little difference between the unmilled and milled particle sizes (refer to Table 5.1). Therefore, the large particle sizes of both sets of powder combined with the large discrepancy in comparison to the commercial data indicated the presence of agglomerates in the HA analysed in the investigation.

The Ca/P ratios of the HA were calculated after sintering at 1000°C, 1100°C, 1200°C, 1250°C, and 1300°C. The XRF analysis revealed that there was no relationship between the sintering temperature and the Ca/P ratio of the HA. However, the mean value was significantly higher than the theoretical Ca/P ratio of stoichiometric HA (1.67(PDF card no.9-432)). This indicated that there was more Ca in the commercial P201 HA, relative to stoichiometric HA, which was corroborated by the presence of CaO in the XRD patterns (Figure 5.3).

This was in agreement with the literature where LeGeros (1993) stated that HA with Ca/P ratios of 1.67 and above in HA partially decompose to CaO on sintering, with no TCP. Similarly, ratios lower than 1.67 result in the decomposition of HA to TCP, a highly resorbable material described in Chapter 2. Therefore due to the high Ca/P ratios, it woul be expected that the P201 would not decompose to TCP, but perhaps other phases such as

CaO may exist after sintering at high temperature. Indeed the XRD analysis revealed that none of the HA batches decomposed to TCP, even at1300°C.

The results of the mechanical testing (Table 5.3) showed that the HA increased in biaxial flexural strength (BFS) from 1000°C up to 1200°C (where it peaked in strength), followed by a sharp decrease in strength up to 1300°C. The Weibull moduli (WM) did not increase/decrease as a function of sintering temperature, but rather fluctuate between 3.78 and 3.07 until 1250°C, followed by a sharp increase to 6.16 at 1300°C. The weakest specimen (1300°C) displayed the highest WM, which was twice that of the strongest specimen (1200°C)(refer to Table 5.3), which implies that the mechanical data retrieved from the weakest batch of HA was more statistically reliable than that of the strongest batch.

Despite the initial increase in strength up to 1200°C, followed by a decrease, the densities appeared to increase continuously from 1000°C to 1300°C. The weakest specimen was the most dense. When density is nearly maximised due to sintering, grain growth occurs as it becomes energetically more favourable for grain boundary reduction, as opposed to pore boundary reduction, to occur. As a result, the grains become larger, and the microstructure coarsens, therefore the density may be similar, but strength will decrease. According to Griffith's flaw theory (1920), described in section *2.3.2*, coarse grain structures (large grains) are poorer in strength than fine microstructures (small grains), which explained why the HA with coarser microstructures (sintered at 1250°C-1300°C) displayed lower BFS's in comparison to those sintered at and below 1200°C. Furthermore, the coalescence of microporosity will have contributed to the loss in strength above 1200°C, where micropore size begins to approach grain size.

The SEM micrographs (Figures 5.7-5.11) verified the grain growth occurring between 1200°C, and 1300°C, in which the grain sizes appeared to increase from <1μm at 1200°C to ≥1μm at 1300°C. (These results also verified the possibility of powder agglomeration in the particle size analysis, because the Malvern Mastersizer reported an average $d_{0.1}$ of 4μm, which is still much larger than the grains appeared in the micrographs.) At

temperatures below 1200°C, a definite grain structure was not present as the particles were just beginning to coalesce at 1000°C and 1100°C. The majority of the densification appeared to take place between 1100°C and 1200°C, as indicated by the SEM and the sharp increase in BFS (28.04±7.65 to 60.01±14.70 MPa) and density (2.11±0.09 to 2.88±0.11 $g.cm^{-3}$).

The highest strength reported for the P201 HA, 60.01±14.70 MPa, was very low in comparison to the values found in the literature. Lu et al (1998), Tampieri et al (1997), Willman (1996), and Aoki (1991) reported flexural strength values for HA of up to 110MPa, 130MPa, 100MPa, and 113MPa, respectively. The authors also reported much higher densities than the P201 in this investigation, which would explain the strength differences. At best, the densities of the P201 achieved 96.2% of the theoretical. These low densities may have been due to presence of the large agglomerates (~37mm) found, which would cause problems in achieving full packing density during the uniaxial pressing of the powder to produce a green compact. Additionally, these authors may have polished their specimens, which eliminates surface asperities (hence stress concentrations), and ultimately improves strength in testing situations. Furthermore, they may have performed 4 point bending tests, which generally yield higher flexural strengths than ring-on-ring biaxial flexure tests.

In this investigation, the decision was made not to polish specimens prior to mechanical testing, just for the sake of reporting high strengths, because HA implants are not generally placed in-vivo after polishing. Such low surface areas would not be condusive to instigating biological reactions and ultimately bone ingrowth. Therefore it was decided to test materials with the type of surface that would be implanted in-vivo. In addition, it was decided to consider the HA as a control that would be compared to the reinforced HA in the subsequent investigation. Therefore the mechanical properties of the HA in this investigation were considered to be relative values, as opposed to absolute values.

This investigation revealed that between the temperatures of 1000°C and 1300°C, P201 HA diplayed poor mechanical properties, with no decomposition to TCP. However it contained some CaO, which is also resorbable, an undesirable characteristic for an implant whose goal is to avoid rapid resorption. Furthermore, the presence of CaO has been reported to have an adverse effect on biological response (Hing, 2000). The poor mechanical properties were attributed to the low packing densities (due to the presence of large, hard agglomerates), which resulted in low as-sintered densities. Furthermore, at high sintering temperatures, the microstructure of the P201 coarsened, which resulted in decreased mechanical strength at and above 1250°C.

These results indicated that P201 HA from Plasma Biotal Ltd. contained agglomerates, which inhibited sufficient pressing, resulting in low densities and poor strength. Thus this material would appear to be an ideal candidate for testing the hypothesis of reinforcement via a second phase addition to promote liquid-phase-assisted sintering.

# CHAPTER 6

# PRODUCTION AND CHARACTERIZATION OF MATERIALS FOR REINFORCING HA AND THEIR ASSOCIATED COMPOSITES

## 6.1 PRODUCTION AND CHARACTERIZATION OF MATERIALS FOR REINFORCING HA

Two Ca/P-based glass additives for reinforcing P201 HA were produced as described in section *4.3.2*. The additives with pre-calculated Ca/P ratios of 0.5 and 0.835 were termed CAP1 and CAP2 respectively. The as-produced additives were hand-ground into powder form.

### 6.1.1 PARTICLE SIZE ANALYSIS

The results of the particle size analysis are displayed in Table 6.1:

**Table 6.1** Results from particle size analysis on CAP1 and CAP2

| Sample | $d_{0.1}$ (μm) | $d_{0.5}$ (μm) | $d_{0.9}$ (μm) | mode (μm) |
|---|---|---|---|---|
| CAP1/ Run 1 | 1.17 | 10.36 | 62.94 | 11.46 |
| CAP1/ Run 2 | 1.53 | 9.97 | 60.55 | 8.40 |
| CAP2/ Run 1 | 9.04 | 115.70 | 171.05 | 46.65 |
| CAP2/ Run 2 | 8.95 | 112.79 | 170.68 | 47.58 |

The particle size analysis revealed that CAP1 was much smaller than CAP2. Figures 6.1 and 6.2 display the particle size distribution for CAP1 and CAP2 respectively. The

histogram in Figure 6.2 revealed a bimodal distribution for CAP2, with modes at ~47μm and ~110μm.

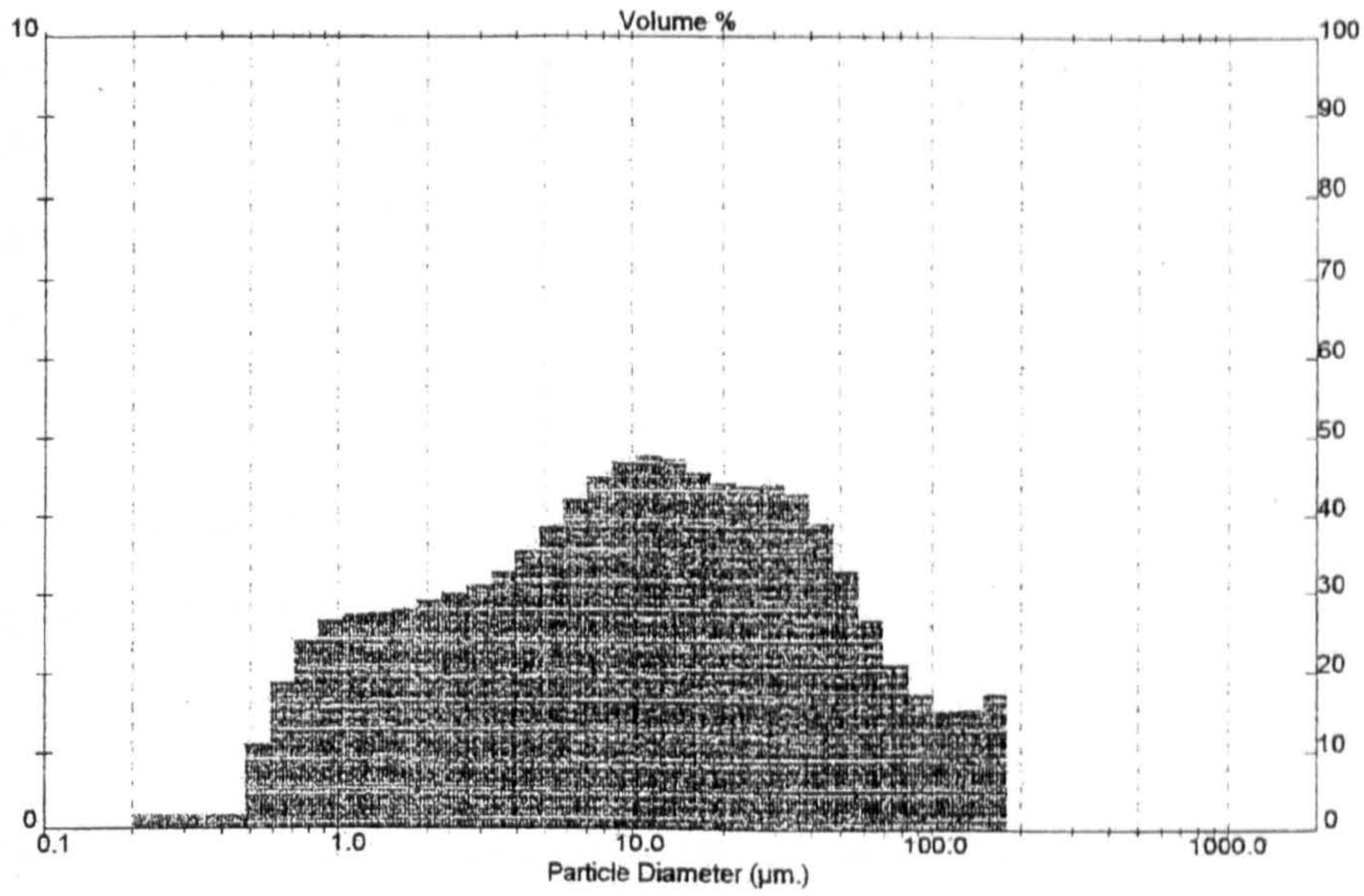


**Figure 6.1** Particle size distribution for CAP1

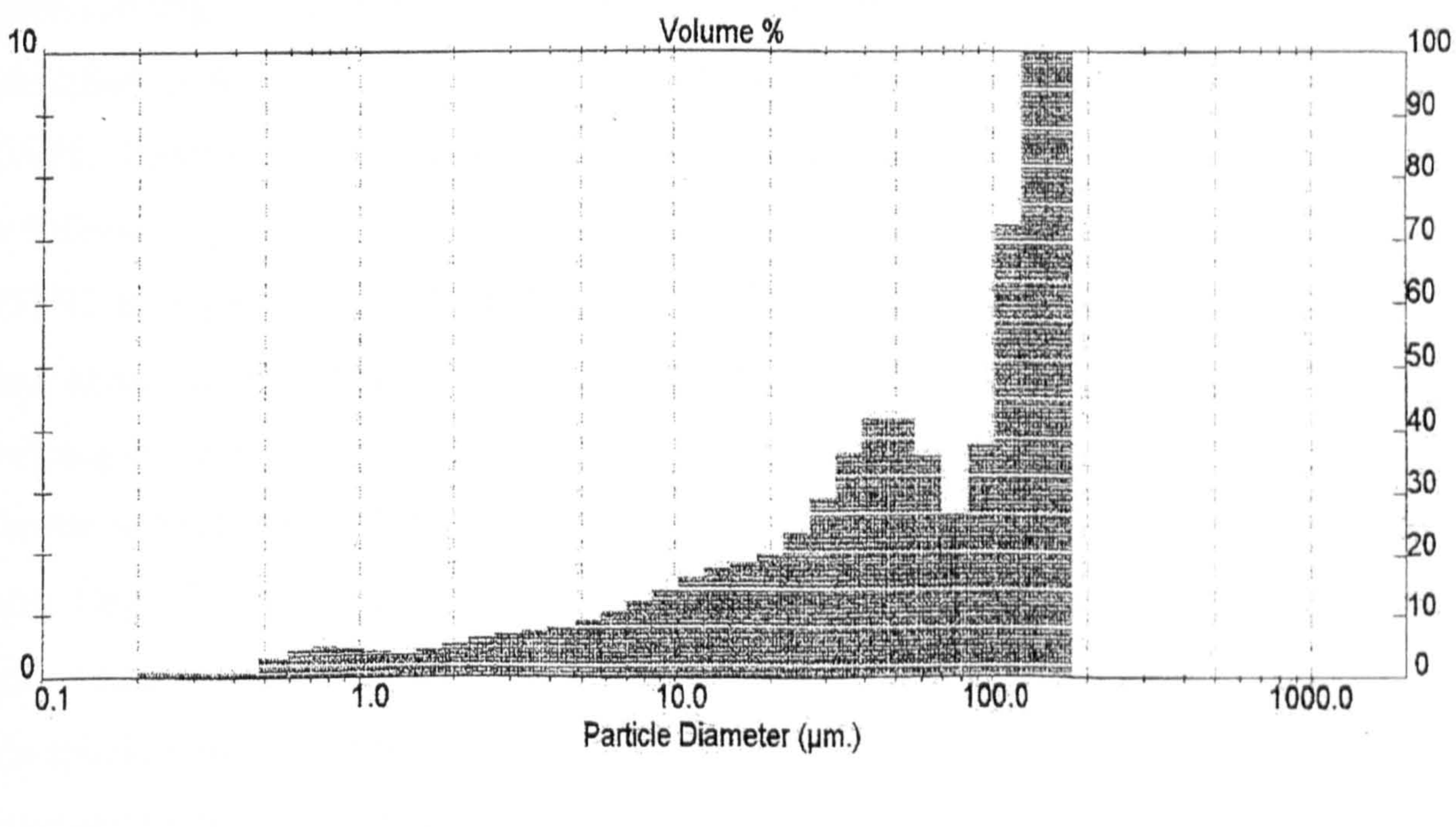


**Figure 6.2** Particle size distribution for CAP2

### 6.1.2 X-RAY FLUORESCENCE (XRF)

The results from the XRF analysis are shown in Table 6.2:

**Table 6.2** XRF results for CAP1 and CAP2

| Sample | wt% CaO | wt% $P_2O_5$ | Ca/P Ratio |
|---|---|---|---|
| CAP1 | 20.26 | 53.89 | 0.47 |
| CAP2 | 36.7 | 55.2 | 0.84 |

The Ca/P ratios calculated from the XRF data were very close to the ratios calculated from the pre-cursors; 0.5 and 0.835 for CAP1 and CAP2 respectively.

### 6.1.3 DIFFERENTIAL THERMAL ANALYSIS (DTA) AND X-RAY DIFFRACTION (XRD)

The main physical difference between CAP1 and CAP2 on processing was that CAP1 remained glassy when quenched, in contrast to CAP2, which crystallised spontaneously upon cooling. DTA of the two materials is shown in Figure 6.3. Regions of interest are identified as A, B, C, and D. Point A, at 467°C, shows the onset of the glass transition in CAP1. Point B, at 557.4°C shows the subsequent peak crystallisation temperature. This is followed by the melting of the crystalline phase, the onset of which is marked by C at 971°C, as expected for a glass. XRD of CAP1 as prepared, shown in Figure 6.4, reveals a lack of any significant crystalline organisation. In CAP2, the crystalline material shows a melting endotherm whose onset is marked by D at 1197°C; XRD of CAP2 as prepared, shown in Figure 6.5, demonstrated the majority of the crystalline phase to be $Ca_2P_2O_7$ (the $Ca_2P_2O_7$ peaks are marked with ⊗), with a Ca/P ratio of 1.0. The starting composition of CAP2 (Ca/P ratio of 0.835) would suggest the presence of some residual phosphate-based glass within CAP2, which is corroborated by the inflection point at E, followed by the crystallization at point F.

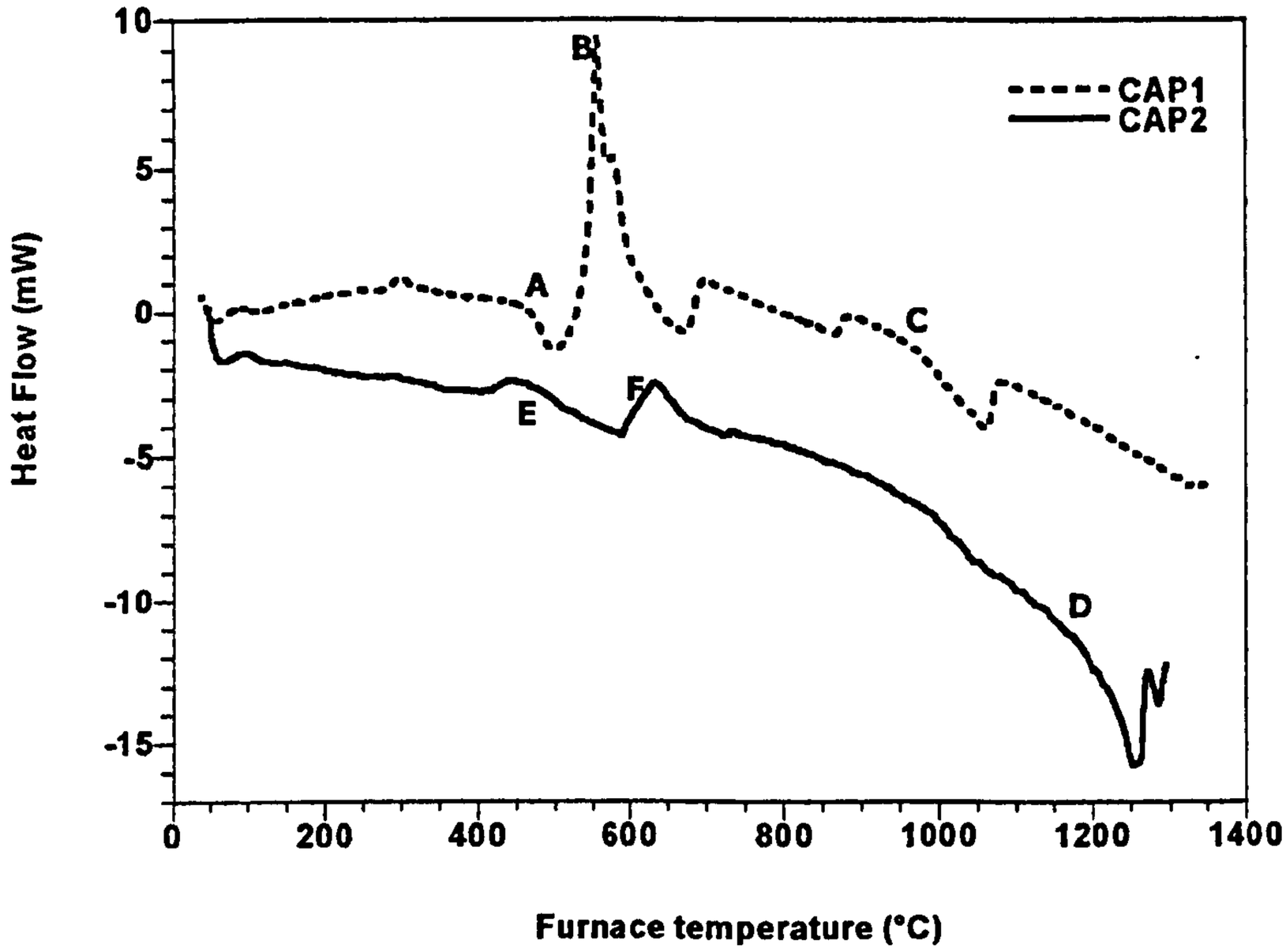


**Figure 6.3** DTA traces for CAP1 and CAP2

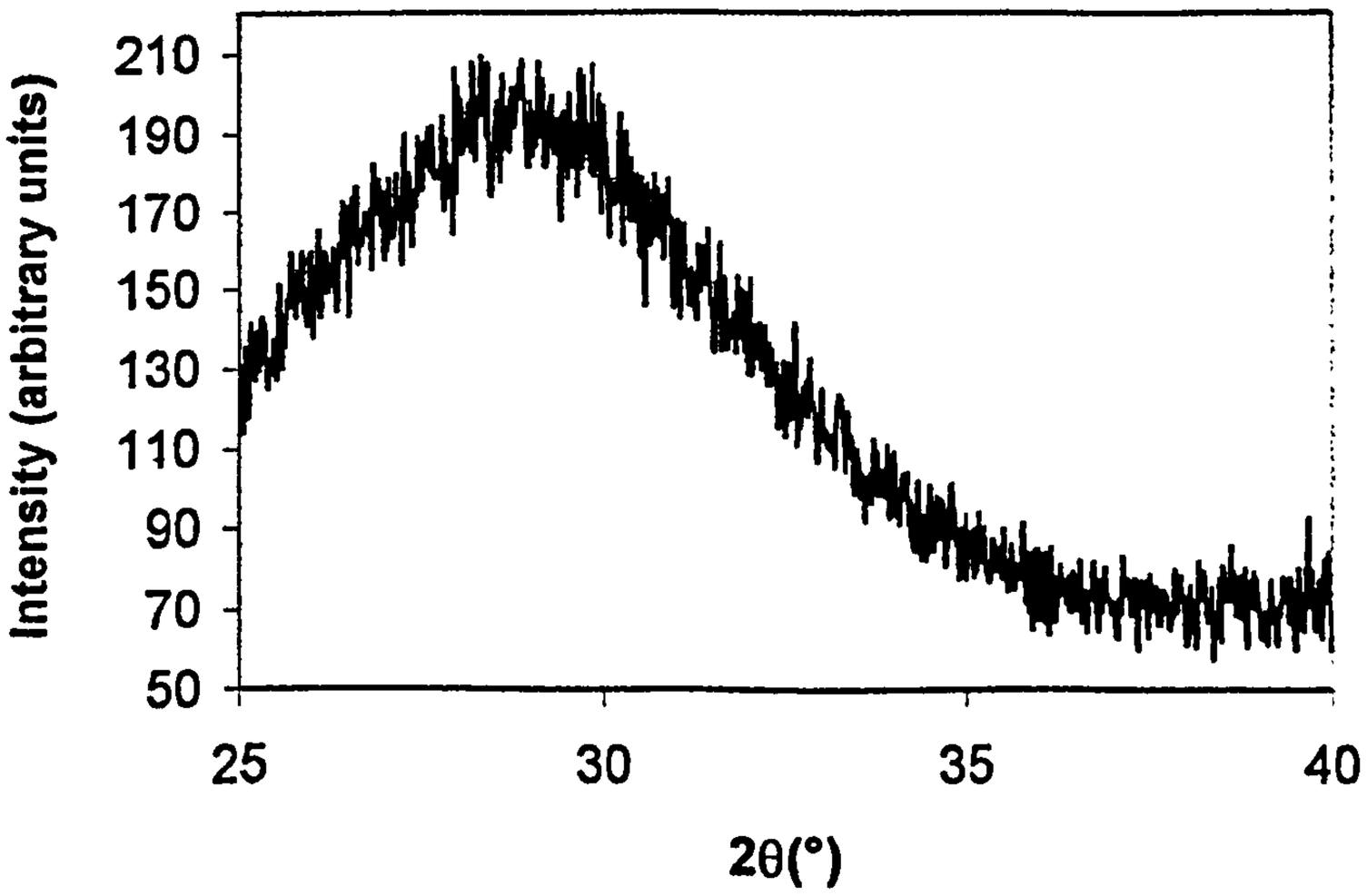


**Figure 6.4** XRD pattern for CAP1

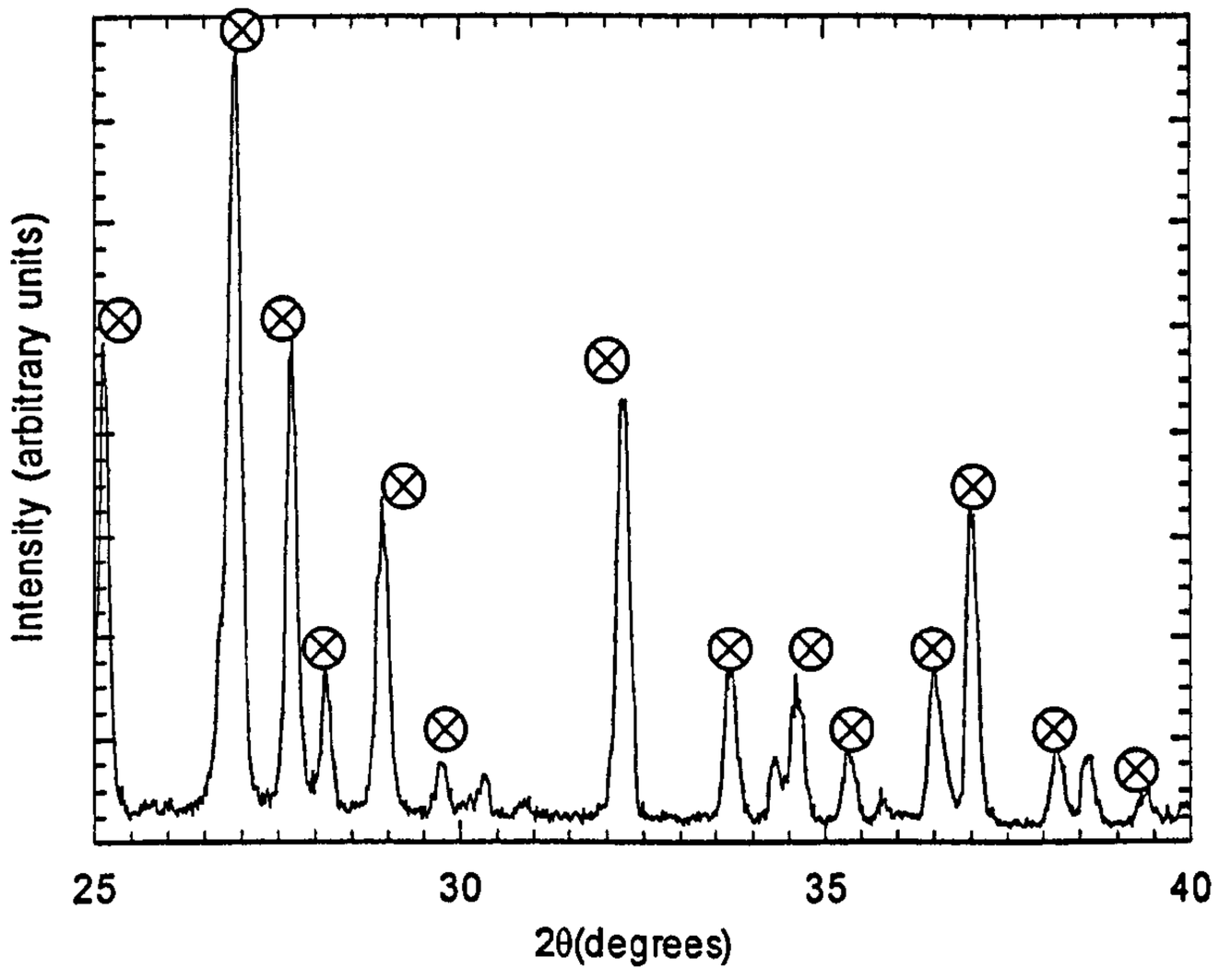


**Figure 6.5** XRD pattern for CAP2

## 6.2 PRODUCTION AND CHARACTERIZATION OF HA REINFORCED WITH CAP1

The objective of this investigation was to identify the optimal temperature for sintering HA containing 2.5 wt% additive. Following DTA, temperatures from 1000°C to 1300°C in increments of 50°C were investigated. Optimal sintering was considered in terms of optimising/maximizing the mechanical properties whilst maintaining minimal decomposition to TCP. The P201 reinforced with CAP1 was termed CAP1-HA. In order to maximise time efficiency, each batch contained only two pressed and sintered samples.

### 6.2.1 PARTICLE SIZE ANALYSIS

The CAP1-HA batches were prepared by wet milling (as described in section *4.3.3*). The specimens sintered from 1000°C to 1150°C were made from Batch 1, and the specimens

sintered from 1200°C to 1300° were made from Batch 2. The results from the particle size analysis are shown in Table 6.3.

**Table 6.3** Particle size analysis of CAP1-HA

| Batch | $d_{0.1}$ (μm) | $d_{0.5}$ (μm) | $d_{0.9}$ (μm) | mode (μm) |
|---|---|---|---|---|
| 1 | 11.49 | 39.71 | 152.68 | 36.44 |
| 2 | 1.27 | 21.39 | 82.26 | 42.59 |

Batch 2 appeared to have a smaller particle size distribution than Batch 1, yet it displayed a slightly larger mode. The particle size distributions for Batch 1and Batch 2 are illustrated in Figure 6.6 and Figure 6.7, respectively. Both histograms show the distributions to be bimodal, and Figure 6.6 shows the CAP1-HA to be almost tri-modal due to the detection of a few large agglomerates. In Figure 6.7, the bimodal nature of the CAP1-HA was due to the presence of HA agglomerates (displaying the higher mode of ~42μm) and the smaller CAP1-HA/HA particles (displaying a smaller mode of ~4μm).

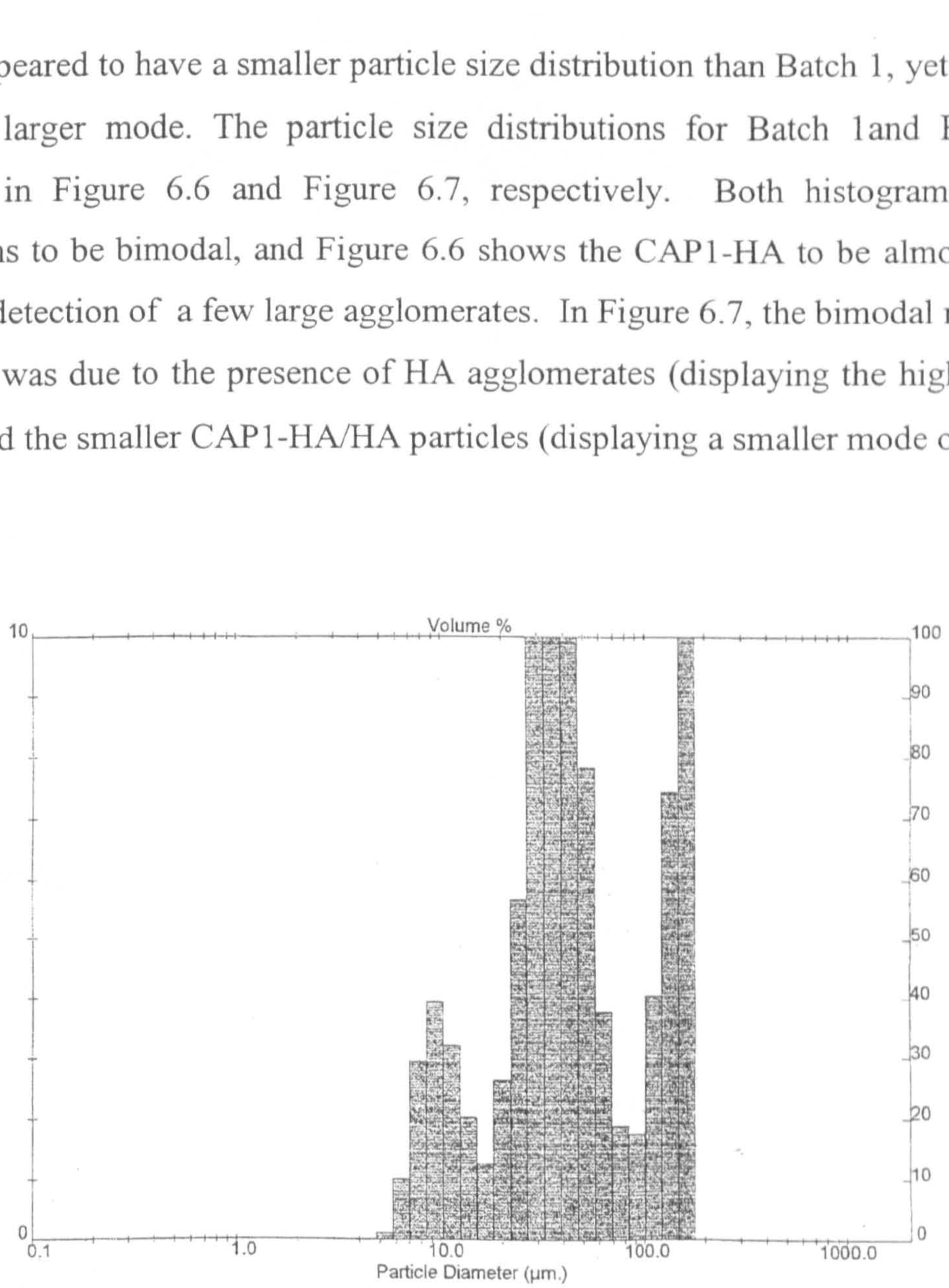


**Figure 6.6** Particle size distribution of CAP1-HA (Batch One)

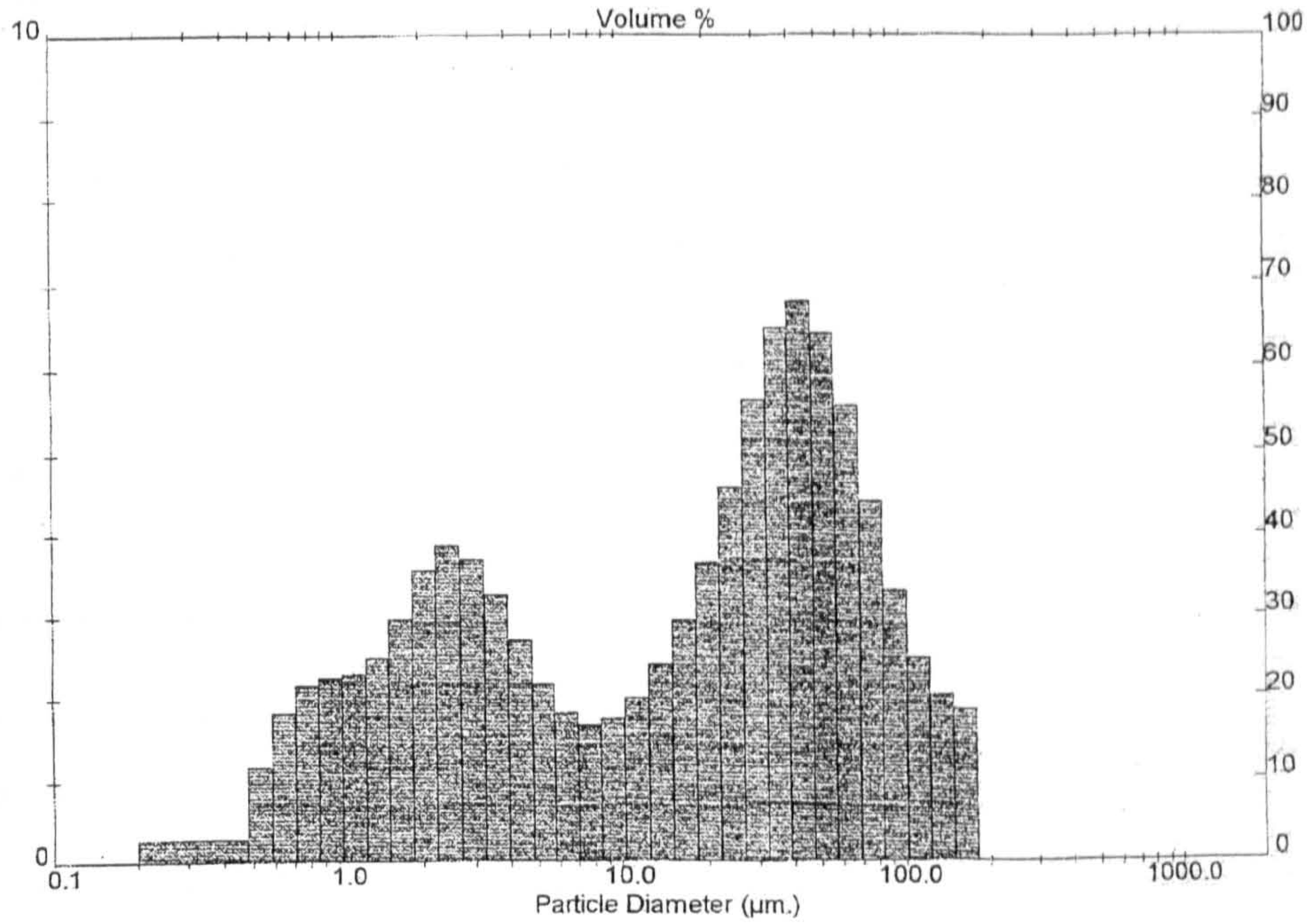


**Figure 6.7** Particle size distribution of CAP1-HA (Batch Two)

## 6.2.2 X-RAY FLUORESCENCE (XRF)

XRF analysis was performed on as-sintered specimens; the results are shown in Table 5.9.

**Table 6.4** XRF results for CAP1-HA sintered at a range of temperatures

| Sintering Temperature (°C) | wt% CaO | wt% $P_2O_5$ | Ca/P Ratio |
|---|---|---|---|
| 1000 | 50.55 | 38.53 | 1.66 |
| 1050 | 49.90 | 38.04 | 1.66 |
| 1100 | 50.55 | 38.54 | 1.65 |
| 1150 | 49.93 | 38.09 | 1.65 |
| 1200 | 50.30 | 38.33 | 1.66 |
| 1250 | 50.79 | 38.60 | 1.66 |
| 1300 | 51.25 | 38.93 | 1.66 |

The Ca/P ratio of the CAP1-HA did not vary with temperature, instead it randomly varied from 1.65 to 1.66, which is close to the theoretical Ca/P ratio of stoichiometric HA. However, relative to the Ca/P ratios of commercial P201 HA, which averaged at 1.71±0.02, the CAP1-HA was calcium deficient.

### 6.2.3 X-RAY DIFFRACTION (XRD)

X-Ray diffraction was carried out on one specimen from each batch, except for those sintered at 1050°C and 1150°C in order to maximise time efficiency. From each trace, the highest intensity of TCP was recorded and the intensity of TCP relative to HA (RI-TCP) was calculated as described in section *4.4.4*. The results of the phase composition analysis are shown in Table 6.5, Figure 6.8 (β-TCP is marked by ⊗;α-TCP is marked by ⊕), and Figure 6.9.

**Table 6.5** % of TCP in CAP1-HA at different temperatures

| Sintering Temperature (°C) | RI-TCP (%) |
|---|---|
| 1000 | 14 (β) |
| 1100 | 44 (β) |
| 1200 | 63 (β) |
| 1250 | 69 (β) |
| 1300 | 60 (β) / 13 (α) |

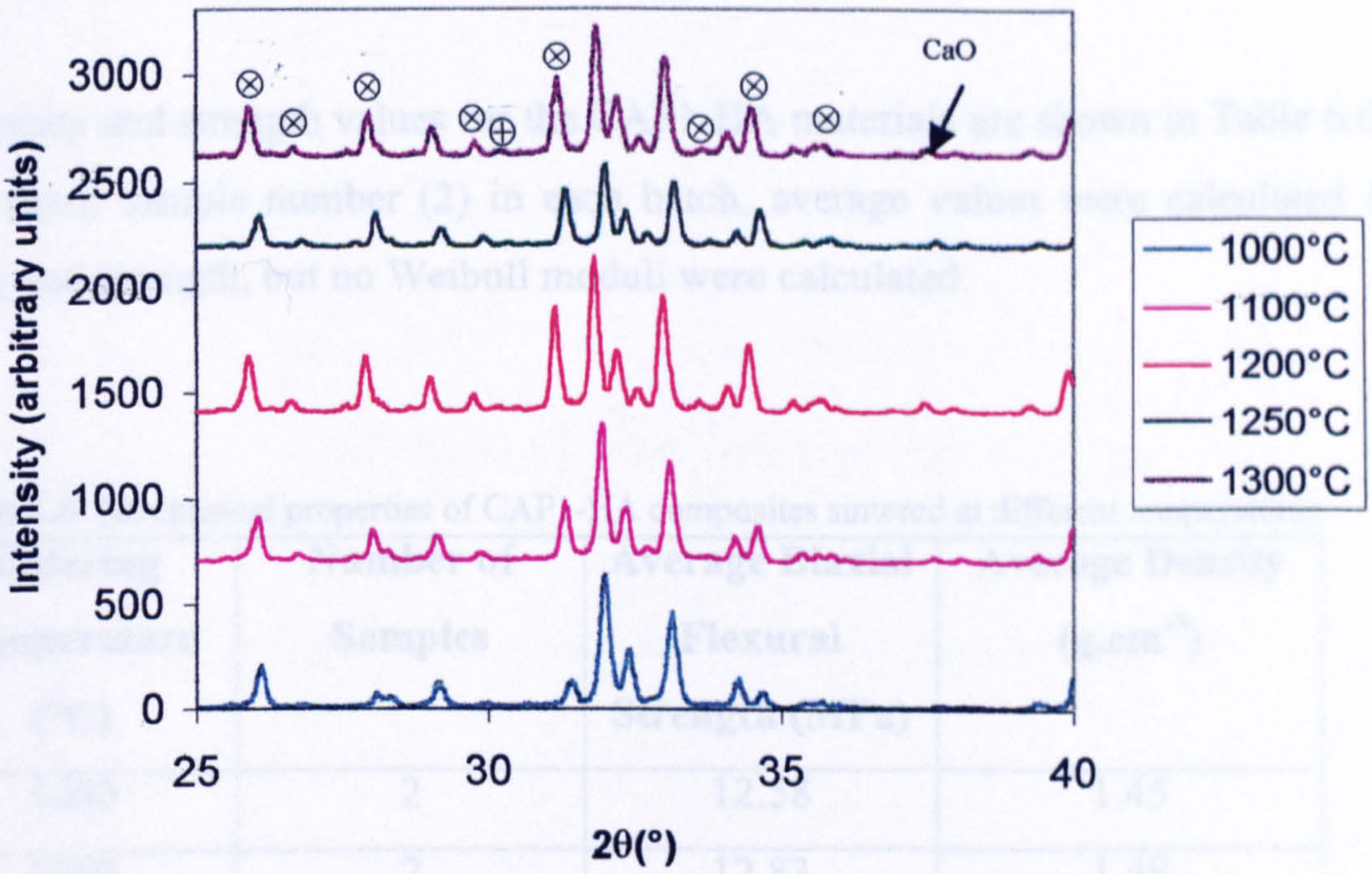


**Figure 6.8** XRD Traces for CAP-1HA at different temperatures

A graph of RI-TCP versus temperature can be seen in Figure 6.9. (The sum of α-TCP and β-TCP was used as the total amount of TCP for the specimens sintered at 1300°C)

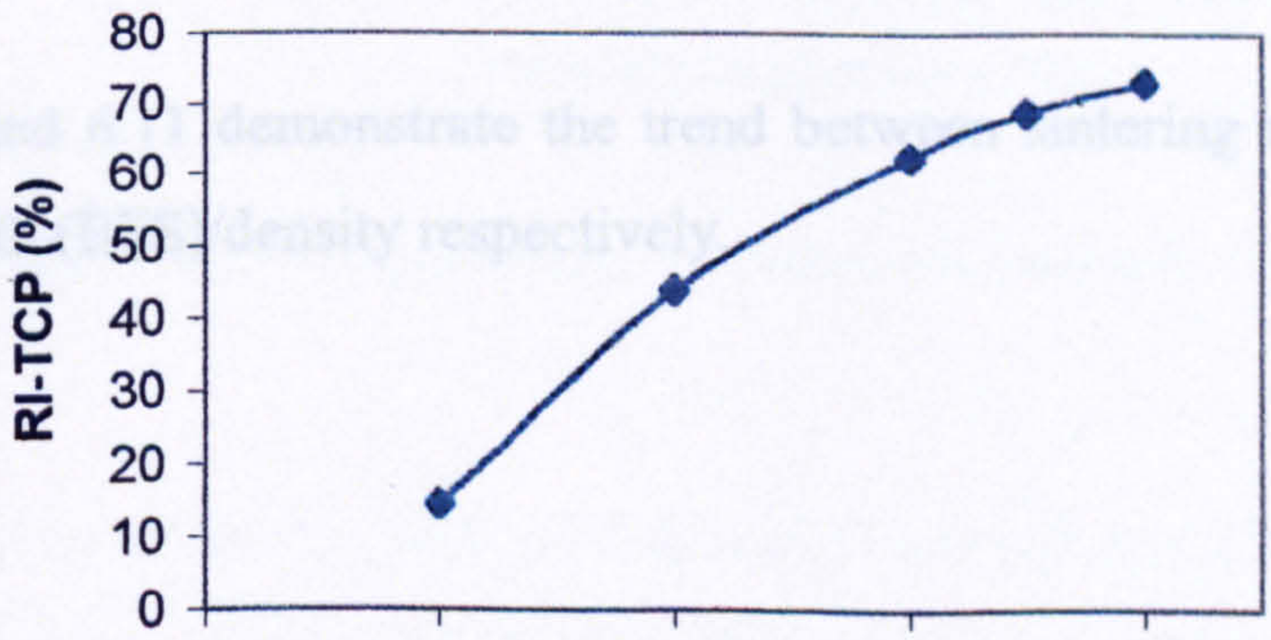


**Figure 6.9** Graph of RI-TCP vs sintering temperature for CAP1-HA

The RI-TCP appeared to increase steeply until 1200°C, where it continued to increase at a more gradual rate until 1300°C.

### 6.2.4 MECHANICAL PROPERTIES

The density and strength values for the CAP1-HA materials are shown in Table 6.6. Due to the small sample number (2) in each batch, average values were calculated for the density and strength, but no Weibull moduli were calculated.

**Table 6.6** Mechanical properties of CAP1-HA composites sintered at different temperatures

| Sintering Temperature (°C) | Number of Samples | Average Biaxial Flexural Strength (MPa) | Average Density ($g.cm^{-3}$) |
|---|---|---|---|
| 1000 | 2 | 12.58 | 1.45 |
| 1050 | 2 | 12.83 | 1.48 |
| 1100 | 2 | 11.33 | 1.52 |
| 1150 | 2 | 11.96 | 1.56 |
| 1200 | 2 | 12.43 | 1.68 |
| 1250 | 2 | 14.75 | 1.84 |
| 1300 | 2 | 26.59 | 2.18 |

Figures 6.10 and 6.11 demonstrate the trend between sintering temperature and biaxial flexural strength (BFS)/density respectively.

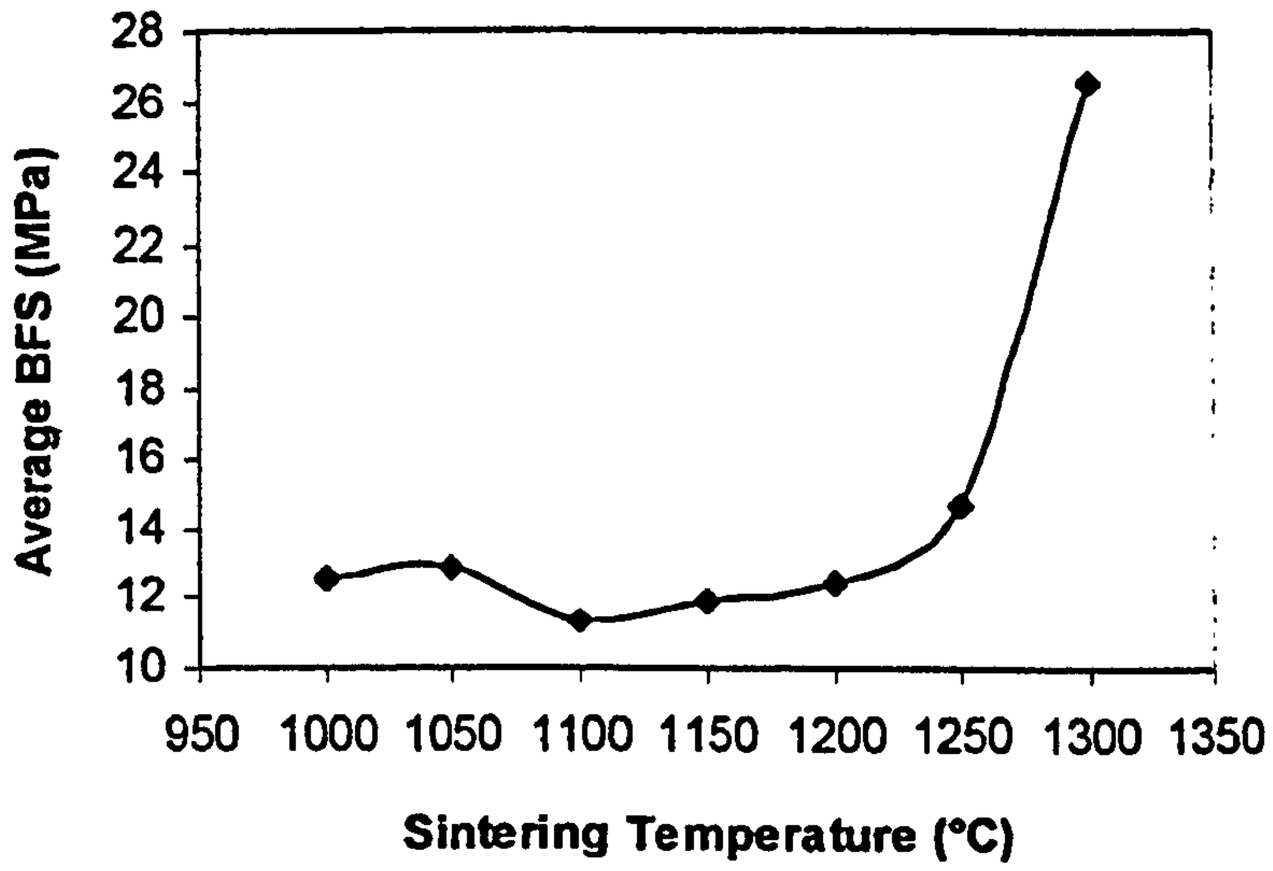


**Figure 6.10** Average BFS vs temperature for CAP1-HA

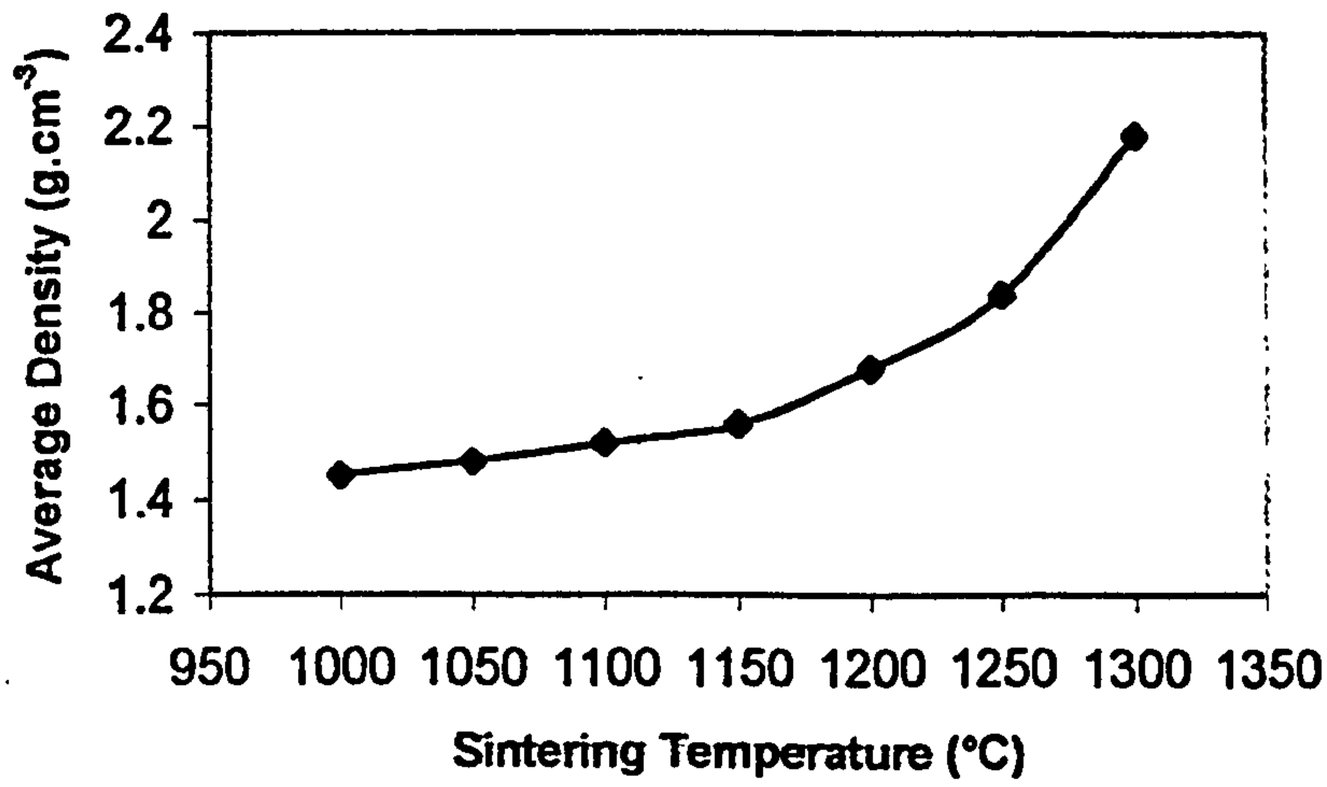


**Figure 6.11** Average density vs sintering temperature for CAP1-HA

The steepest increase in the BFS of CAP1-HA was observed between 1250°C and 1300°C. This also corresponds to the most significant increase in density, which occurred in the same temperature range; furthermore, the maximum values of density and strength both occurred at 1300°C. These maximum values differ from that of pure HA, whose greatest strength occurred at 1200°C, and greatest density at 1300°C.

With regards to the density, because CAP1-HA is a composite and contains a Ca/P-based glass additive with HA, it should be compared to a theoretical density for the actual composite. Nevertheless, due to the very small amount (2.5 wt %) of the reinforcing glass, it is acceptable to compare the composite's density to the theoretical value of HA's density (3.16 $g.cm^{-3}$). Referring back to Table 6.6, which shows the averages for the densities at different temperatures, the following table shows the percentage of the theoretical density of CAP1-HA at the various temperatures:

**Table 6.7** Percentage of the theoretical density of CAP1-HA sintered at different temperatures

| Sintering Temperature (°C) | Percentage of theoretical density |
|---|---|
| 1000 | 45.8 |
| 1050 | 46.8 |
| 1100 | 48.1 |
| 1150 | 49.4 |
| 1200 | 53.2 |
| 1250 | 58.2 |
| 1300 | 68.9 |

The density of CAP1-HA is far from that of its theoretical value even at high temperatures. This may well indicate that even higher temperatures are needed to achieve theoretical density, yet at the expense of the phase composition.

### 6.2.5 SCANNING ELECTRON MICROSCOPY

Scanning electron micrographs were taken of CAP1-HA at the given sintering temperatures:

CAP1-HA sintered at 1000°C:

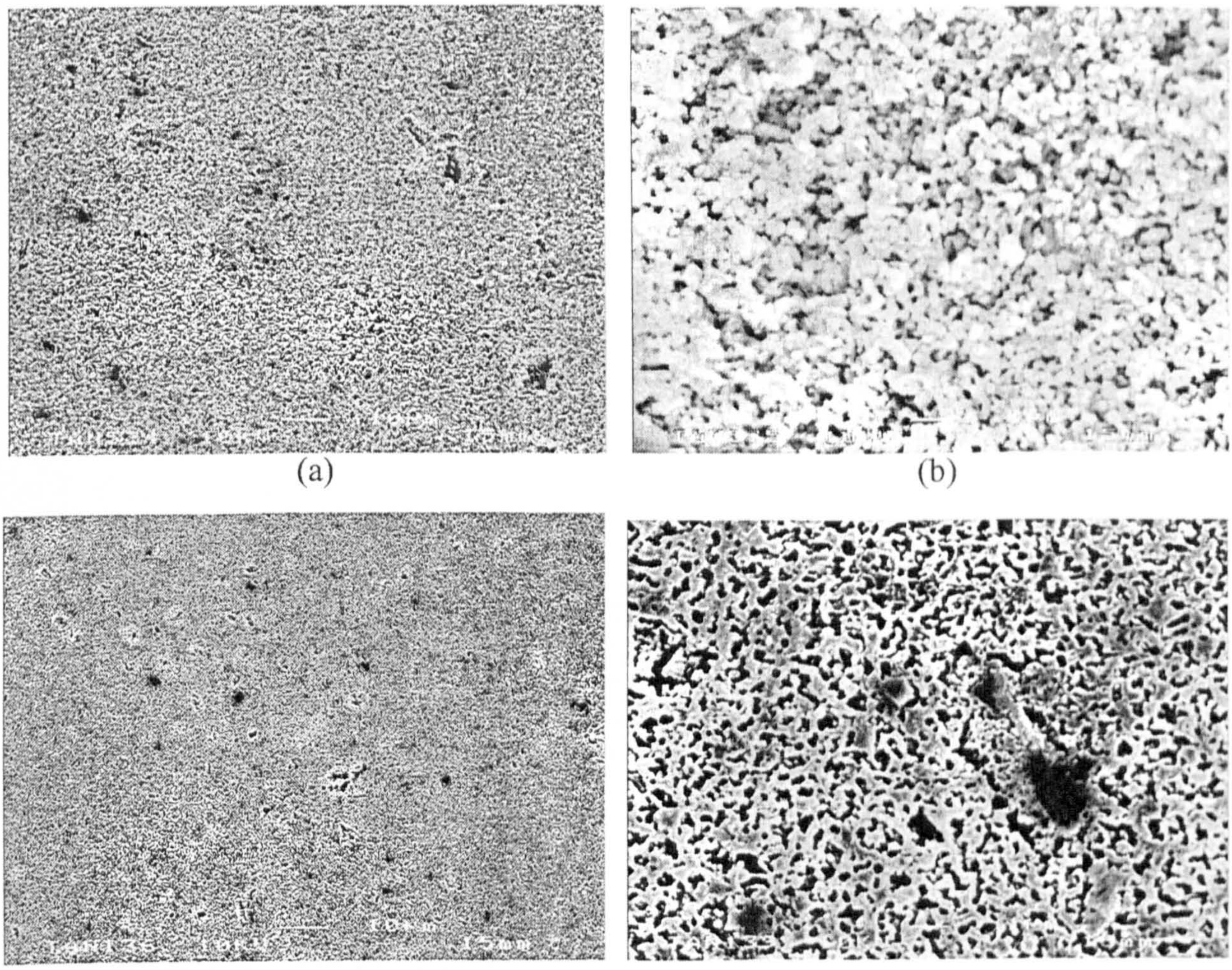

(a) (b)

(c) (d)

**Figure 6.12** CAP1-HA sintered at 1000°C (a)+(b)Unetched CAP1-HA, (c)+(d) Etched CAP1-HA

The unetched images (a)(b) at high and low magnification are similar to that of P201 HA sintered at 1000°C, (Figure 5.7) in that the particles are just beginning to coalesce in the early stages of sintering. The etched images (c)(d) display a great deal of porosity, which may be due to not only the insufficient sintering, but also the fact that there is a highly resorbable constituent which dissolved in the etching process.

CAP1-HA sintered at 1100°C:

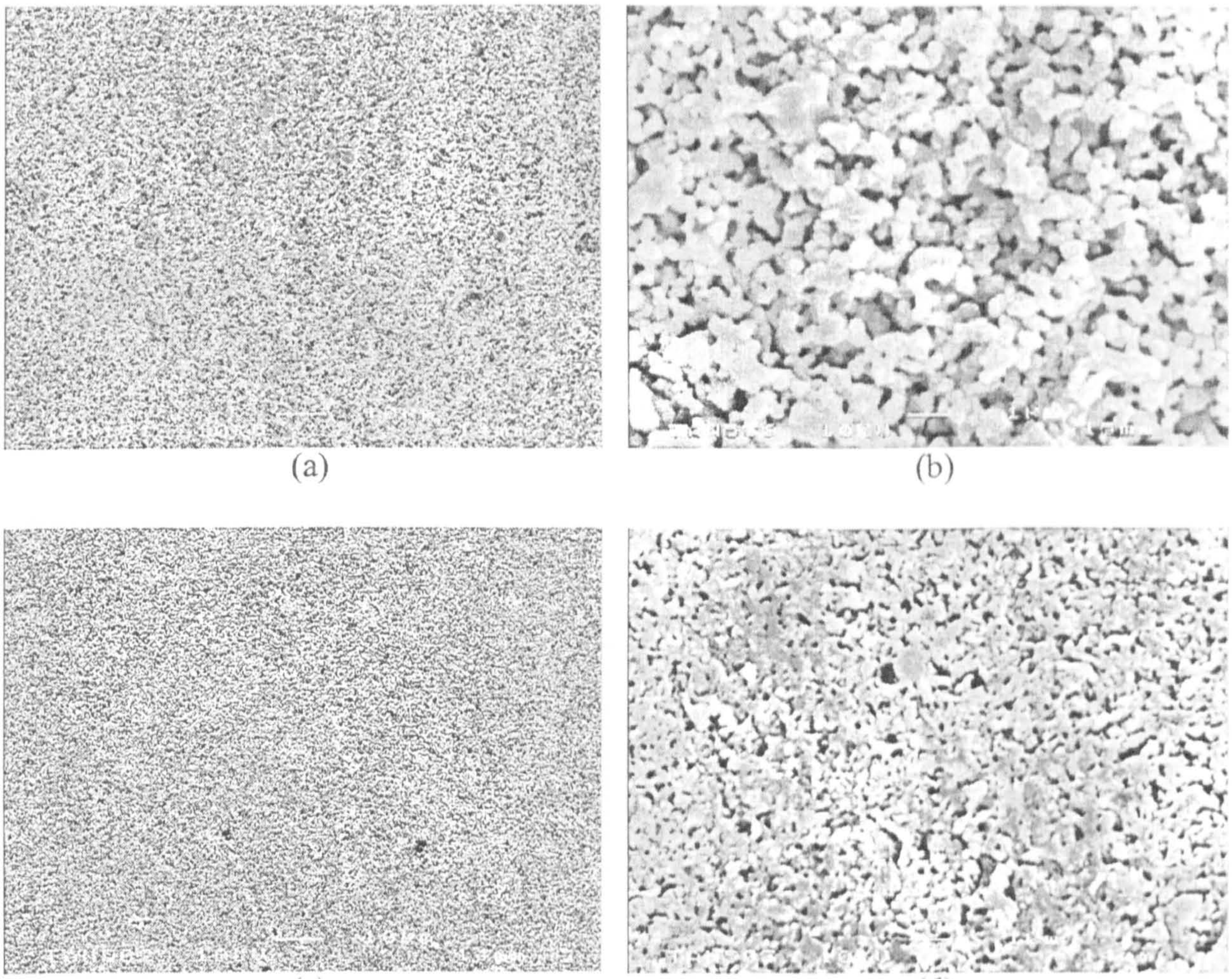


**Figure 6.13** CAP1-HA sintered at × 1100°C (a)+(b) Unetched CAP1-HA, (c)+(d) Etched CAP1-HA

The unetched images show that sintering has progressed from the specimens sintered at 1000°C, in that the particles have experienced slightly more coalescence, however, the specimen is still very porous. The etched images (c)(d) revealed more of the grain structure and reinforce the fact that there was an increase in coalescence that occurred between 1000°C and 1100°C.

CAP1-HA sintered at 1200°C:

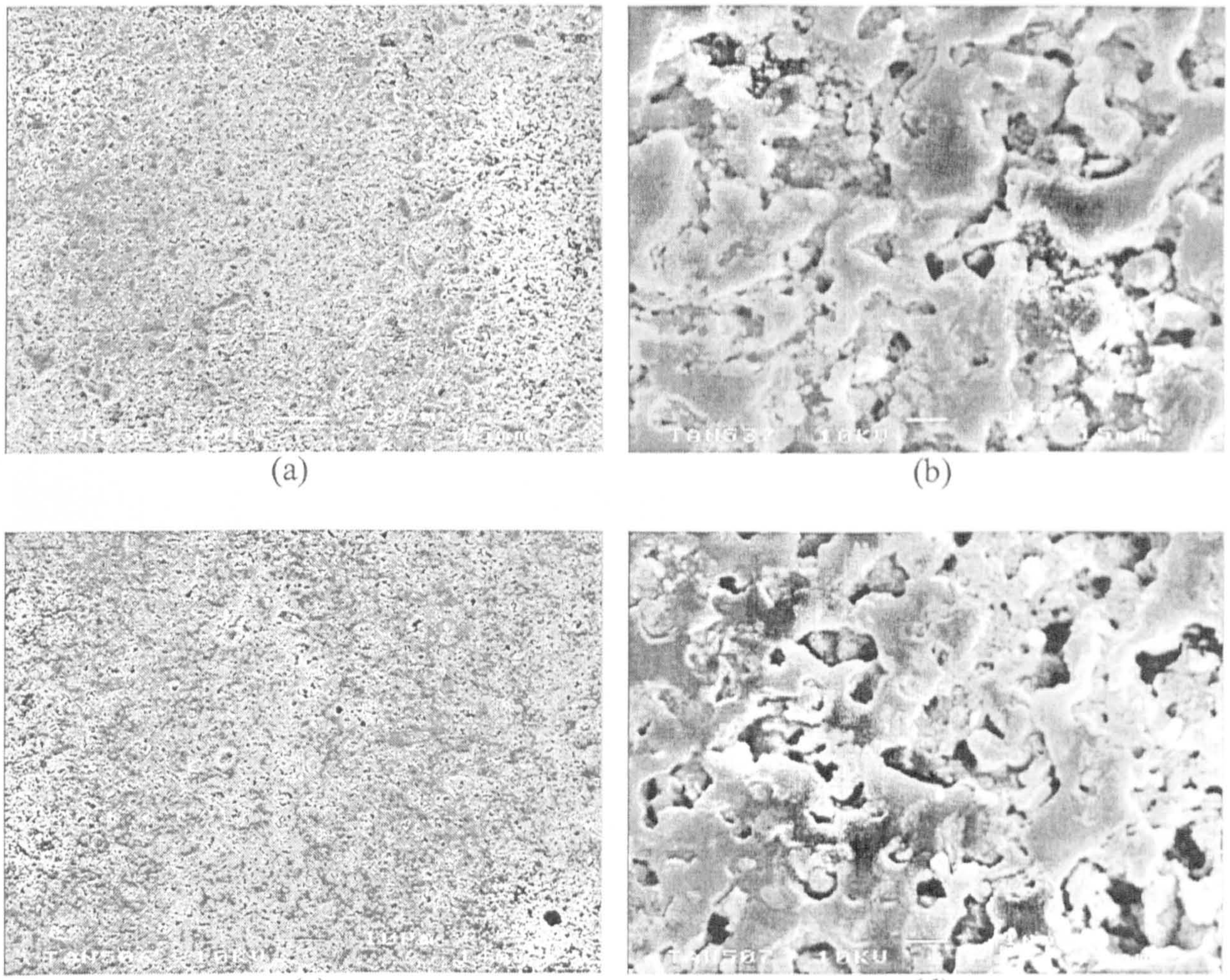


**Figure 6.14** CAP1-HA sintered at 1200°C (a)+(b) Unetched CAP1-HA, (c)+(d) Etched CAP1-HA

The unetched images (a)(b) reveal that this specimen has undergone more sintering than that at 1100°C, due to the early signs of porosity elimination. A portion of the microstructure appears to have dissolved in the etching process, referring to images (c) and (d), leaving a highly porous surface; this may be due to the presence of a highly soluble secondary phase, i.e.TCP.

## CAP1-HA sintered at 1250°C:

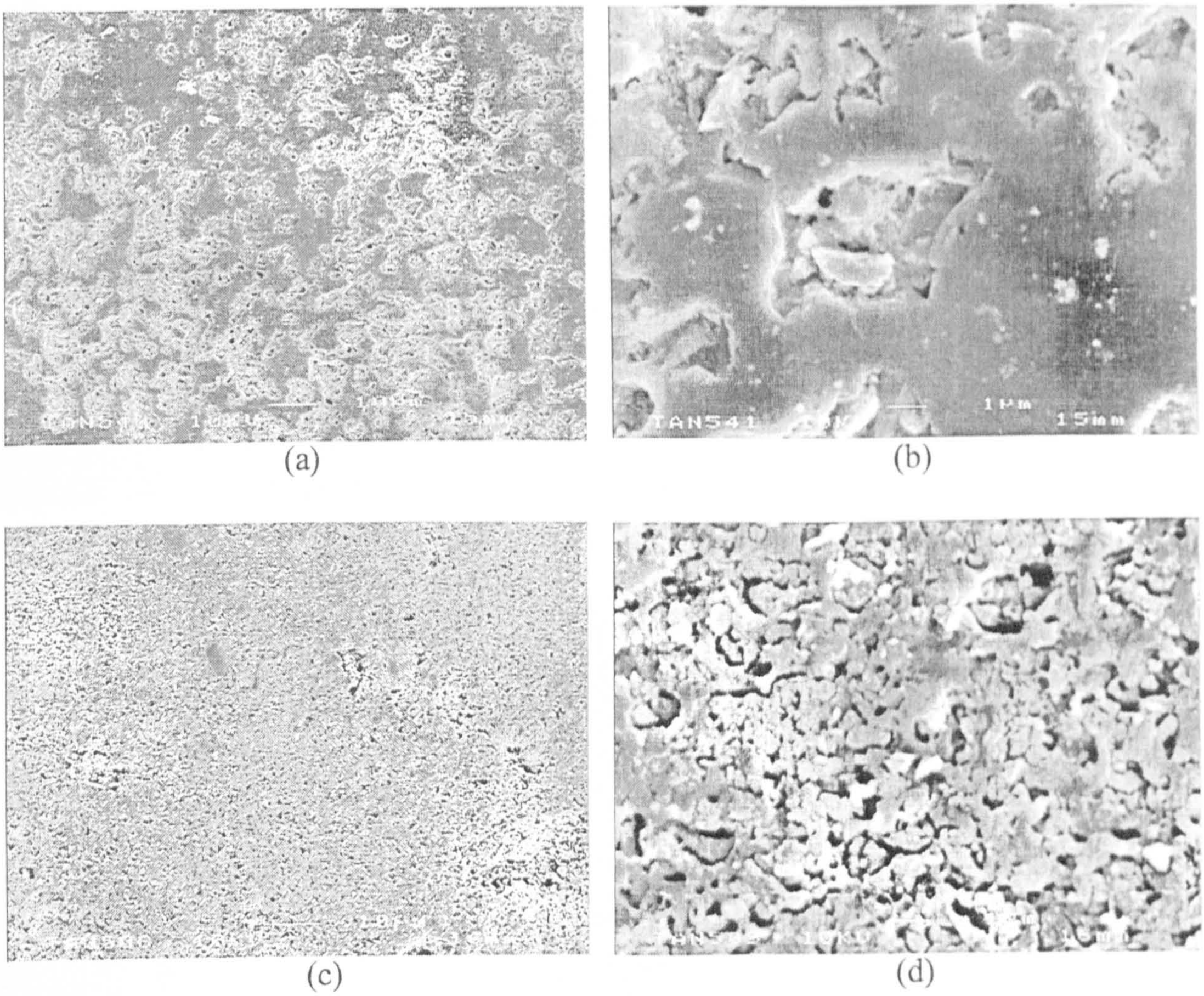


(a) (b)

(c) (d)

**Figure 6.15** CAP1-HA sintered at 1250°C (a)+(b) Unetched CAP1-HA, (c)+(d) Etched CAP1-HA

Image (a) reveals a highly microporous surface, as indicated by the lighter, concave regions. However, at higher magnification (b), the areas in between the pores are smooth and indicate that the specimen has undergone far more sintering than its counterpart at 1200°C. Image (c) shows that the etchant removed a great deal of the surface, in which the larger concave areas match with the larger light regions in image (a). These etched images indicate the presence of a highly resorbable secondary phase, which corroborate with the XRD analysis, in which the batch contained a RI-TCP of 69 %.

CAP1-HA sintered at 1300°C:

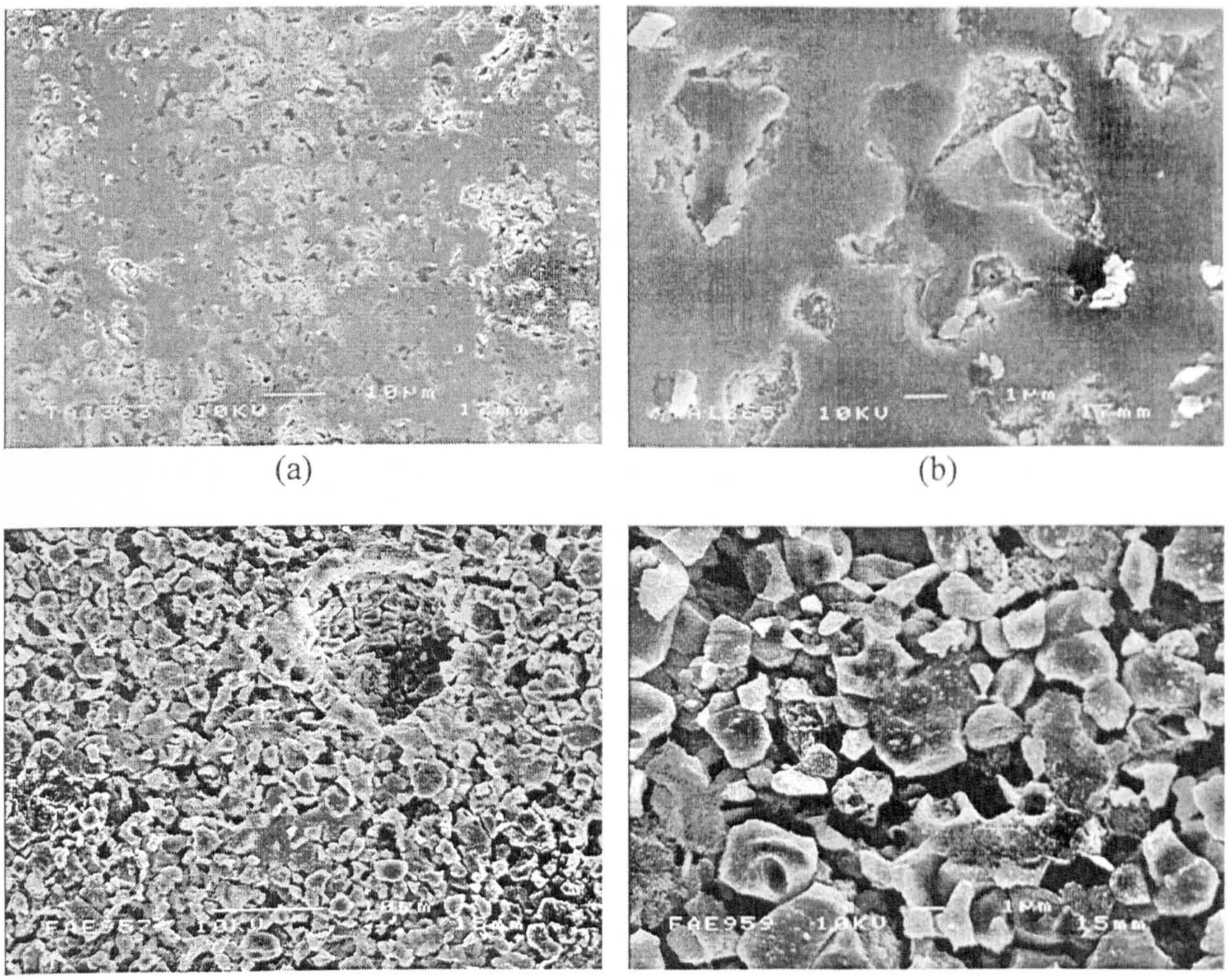


(a) (b)

(c) (d)

**Figure 6.16** CAP1-HA sintered at 1300°C (a)+(b) Unetched CAP1-HA, (c)+(d) Etched CAP1-HA

Image (a) revealed a decrease in the size and number of micropores in comparison to that of 1250°C; furthermore, the individual speckles were also smaller. The etching process revealed a definite grain structure in (c) and (d), with an average grain size of ≤1μm. The concave area in (c) may be a result of over-etching in a region consisting of soluble material, i.e.TCP.

## 6.3 PRODUCTION AND CHARACTERIZATION OF P201 HA REINFORCED WITH CAP2

As a result of the decomposition to TCP, experienced by the HA whence being reinforced with CAP1, the objective of this investigation was to firstly produce a Ca/P-based glass additive with a Ca:P ratio of 0.835 (CAP2), the process of which was described in section *4.3.2.* Then, 1/2.5/3.25/4/5 wt % of CAP2 was added to the P201 HA (as described in section *4.3.2*), and the composites were named CAP2-HA. All samples were sintered at 1300°C on the basis that the DTA trace (Figure 6.3) showed the CAP2 to have a melting endotherm at 1197°C (therefore by 1300°C, the viscosity would be adequate enough for liquid-assisted sintering). Below 1300°C, the effect of reinforcing with CAP2 was assumed to be negligible. As for the unfortunate amount of TCP present in CAP1-HA at 1300°C, the CAP2 was not as Ca-deficient as CAP1, and it was assumed that therefore it would not initiate decomposition of the HA in the composite to TCP to such a degree.

### 6.3.1 PARTICLE SIZE ANALYSIS

Particle size analysis was carried out on the 2.5/4/5 wt % composites on the basis that they were the most widely investigated weight percents in the glass-reinforced HA literature. The results of the particle size analysis are shown in Table 6.8.

**Table 6.8** Particle size analysis on CAP2-HA with different wt %'s

| Sample | $d_{0.1}$ (μm) | $d_{0.5}$ (μm) | $d_{0.9}$ (μm) | mode (μm) |
|---|---|---|---|---|
| 2.5 wt %/Run 1 | 1.84 | 32.49 | 134.86 | 94.52 |
| 2.5 wt %/Run 2 | 1.87 | 33.23 | 133.52 | 83.92 |
| 4 wt %/ Run 1 | 1.74 | 18.89 | 122.29 | 2.59 |
| 4 wt %/ Run2 | 1.75 | 19.99 | 128.87 | 2.58 |
| 5 wt %/ Run 1 | 1.84 | 40.36 | 147.31 | 2.56 |
| 5 wt %/ Run 2 | 1.91 | 43.83 | 148.96 | 2.57 |

There did not appear to be a trend between wt % of CAP2 and particle size. The 5 wt % CAP2-HA appeared to have the largest particle size, then 2.5 wt % CAP2-HA came second, with 4 wt % CAP2-HA in last. The modes of the 4 and 5 wt % CAP2-HA were small due to the biomodal nature of their distributions, causing the mode to be calculated as the first peak in the histogram (~2μm), as opposed to the second peak in the case of the 2.5 wt% CAP2-HA (~80-90μm). The histograms representing the particle size distributions of Run 1 from each weight percent category are shown in Figures 6.17, 6.18, and 6.19.

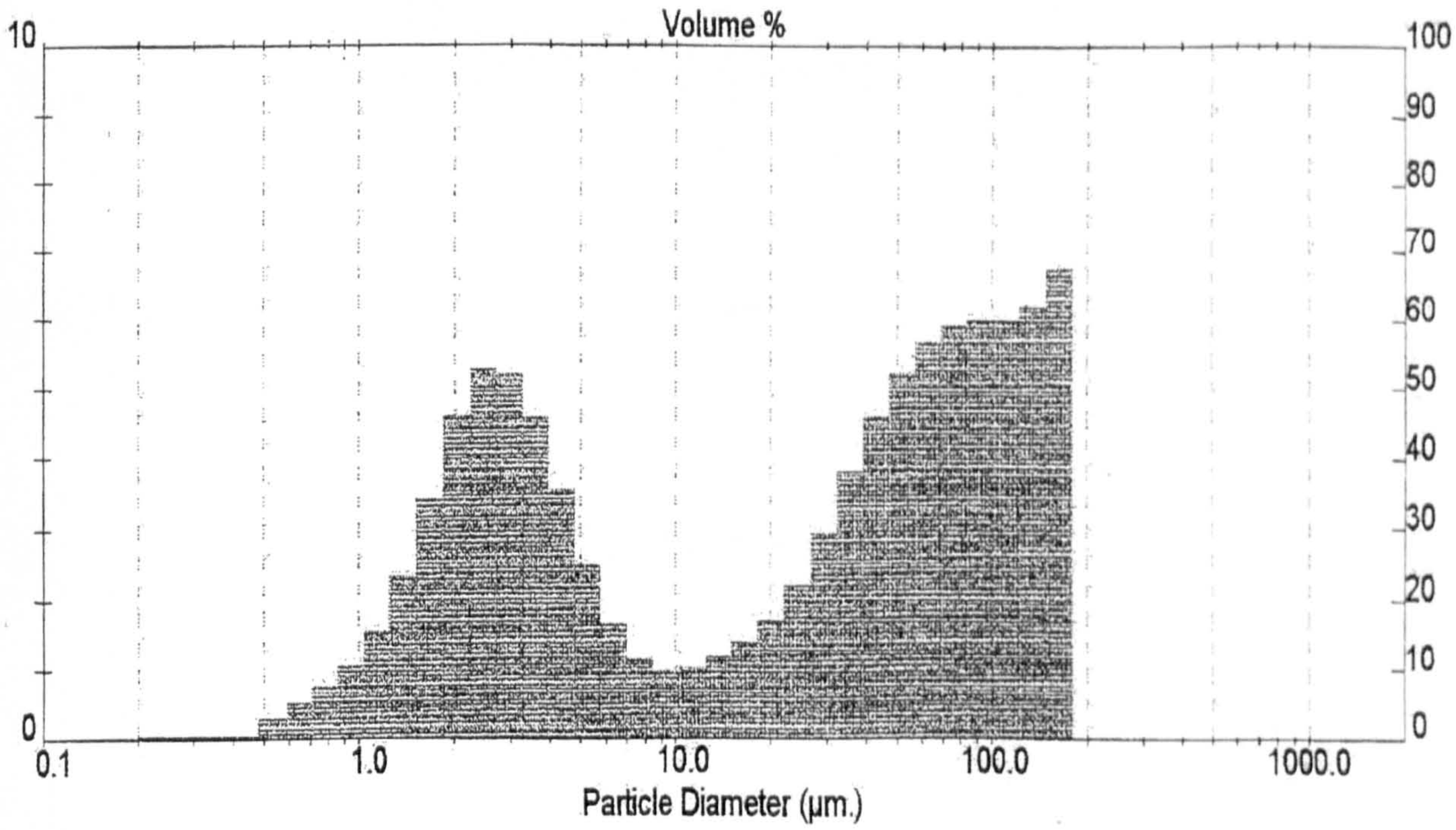


**Figure 6.17** Particle size distribution of 2.5 wt % CAP2-HA

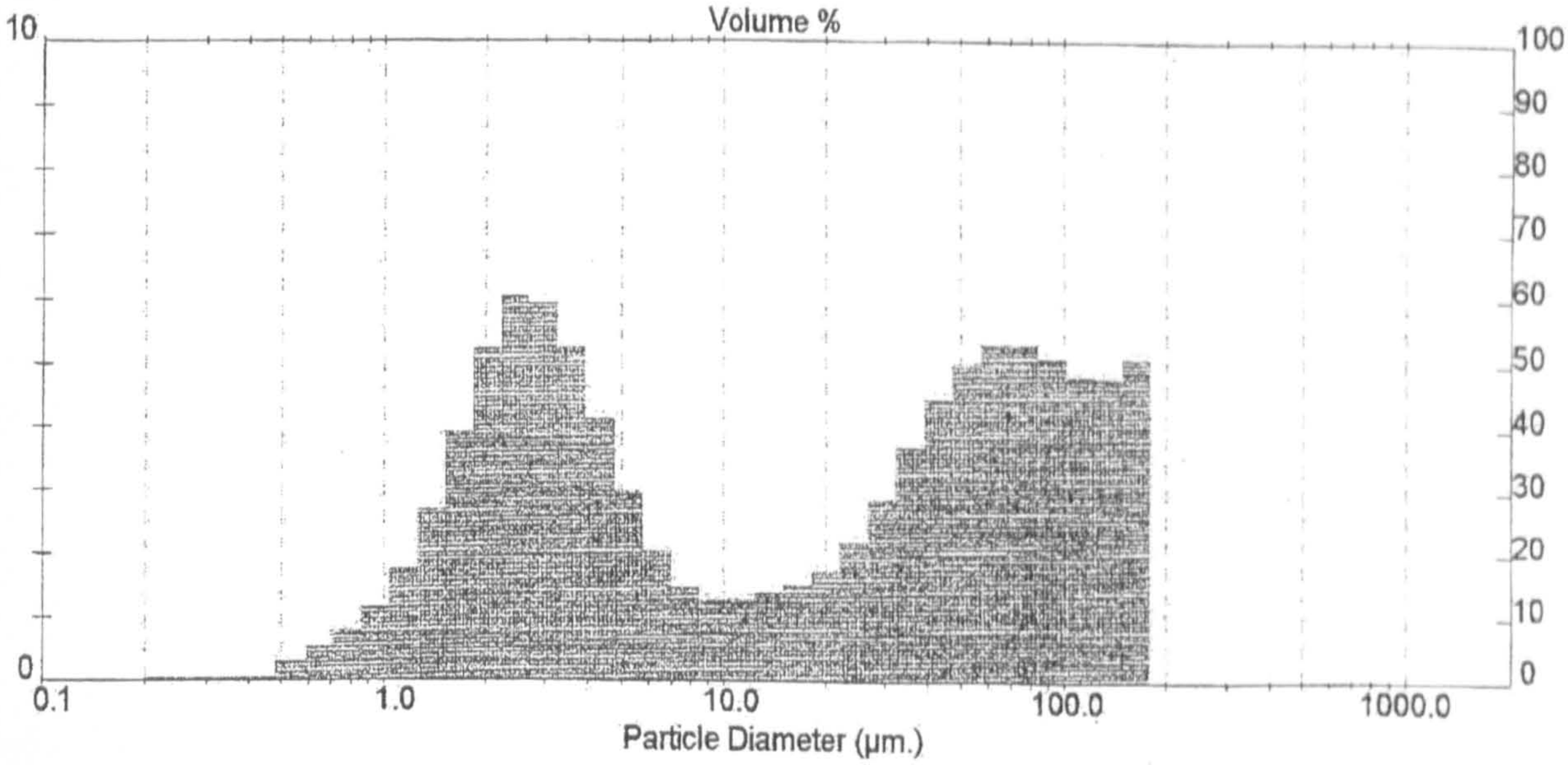


**Figure 6.18** Particle size distribution of 4 wt % CAP2-HA

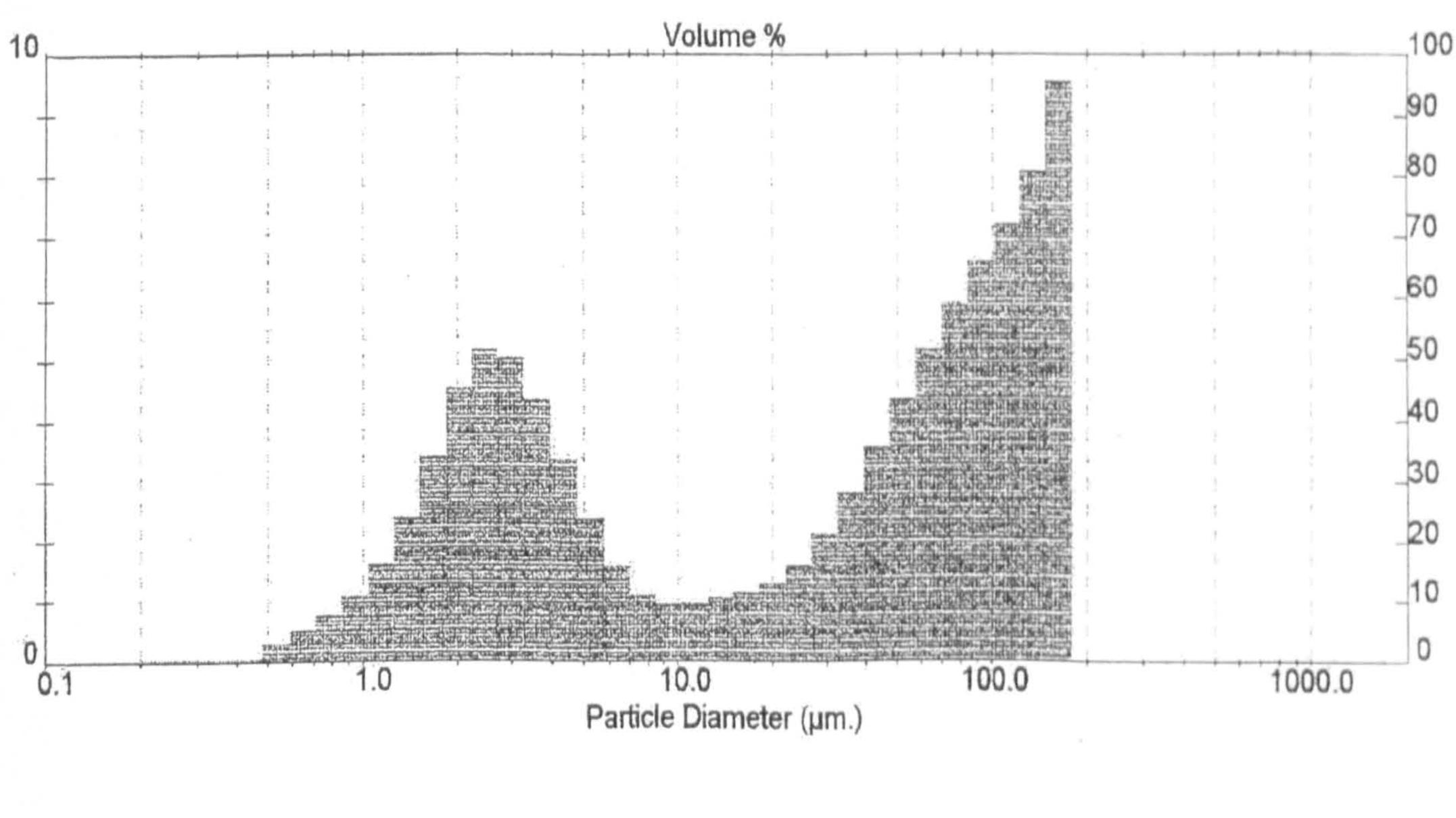


**Figure 6.19** Particle size distribution of 5 wt % CAP2-HA

### 6.3.2 X-RAY FLOURESCENCE (XRF)

XRF was performed on as-sintered specimens; the results are shown in Table 6.9:

**Table 6.9** XRF results for CAP2-HA with different wt% additive

| Wt% CAP2 | wt% CaO | wt% $P_2O_5$ | Ca/P ratio |
|---|---|---|---|
| 1 | 49.14 | 36.78 | 1.69 |
| 2.5 | 55.20 | 41.15 | 1.69 |
| 3.25 | 52.97 | 41.28 | 1.62 |
| 4 | 55.02 | 41.56 | 1.68 |
| 5 | 54.84 | 41.68 | 1.67 |

The ratios were much closer to the Ca/P ratios of the P201 HA (1.68-1.73) than the CAP1-HA (1.65-1.66). The Ca/P ratios of the CAP2-HA appeared to decrease with increasing wt% CAP2, disregarding the presumed anomalous result of the 3.25 wt% CAP2-HA. This was expected as, theoretically, increasing the amount of CAP2 (which has a Ca/P ratio of 0.835) which is added to the HA, from 1-5 wt%, should bring down the overall Ca/P ratio of the CAP2-HA composite.

### 6.3.3 X-RAY DIFFRACTION (XRD)

The XRD analysis revealed that only α-TCP was present in the as-sintered composites, with no β-TCP, as shown in Figure 6.20 (the TCP peaks are marked with an X). The results of the XRD analysis, i.e. RI-TCP found, on CAP2-HA of all batches in each wt % are displayed in Table A.2.1 in Appendix A.2. The average values of TCP for each wt % category are shown in Table 6.10. The amount of α-TCP increased with increasing wt % CAP2 additive within the composites, with the steepest rise in TCP from 2.5-4 wt% CAP2; the trend is shown in Figure 6.21.

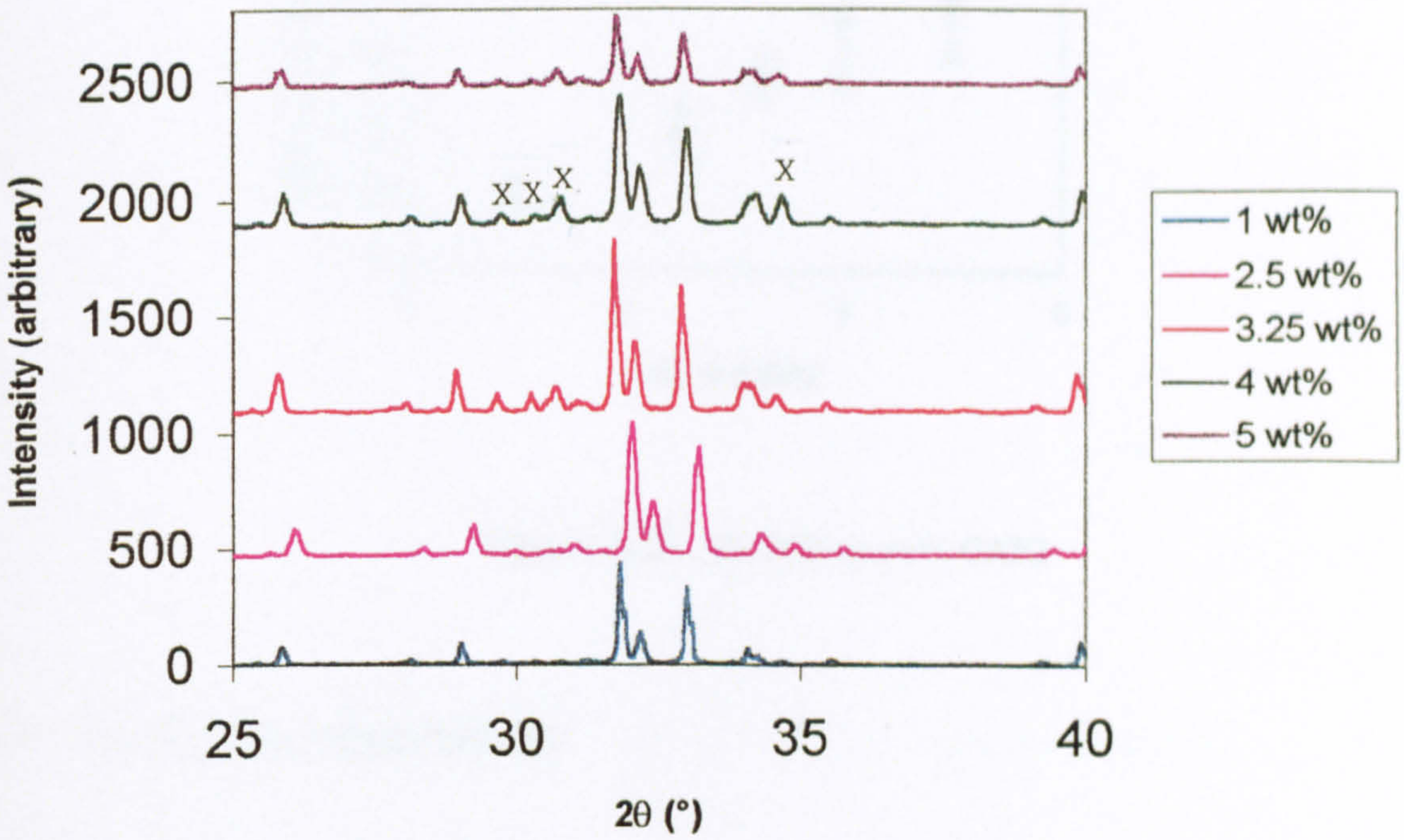


**Figure 6.20** XRD Pattern for CAP2-HA at all wt%'s

**Table 6.10** Mean RI-TCP in CAP2-HA with different wt % additive

| Wt % | Mean RI-TCP (%) |
|---|---|
| 1 | 5.3±1.3 |
| 2.5 | 9.9±2.0 |
| 3.25 | 13.4±1.3 |
| 4 | 18.2±5.2 |
| 5 | 19.8±4.5 |

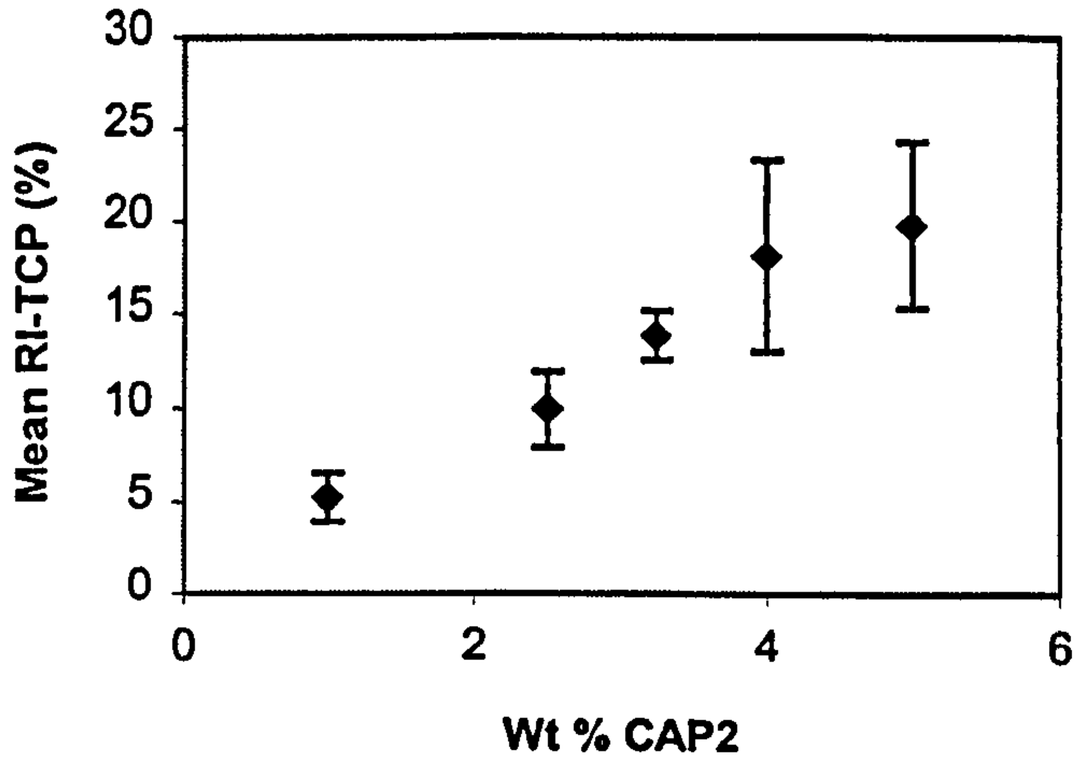


**Figure 6.21** RI-TCP vs wt % CAP2

### 6.3.4 MECHANICAL PROPERTIES

The biaxial flexural strength (BFS), density, and Weibull moduli were calculated for each of the batches within the wt % categories of the CAP2-HA and the mean values are shown in Tables 6.11(strength)/6.12 (density)/6.14 (Weibull modulus of the BFS's).

**Table 6.11** Mean values for the BFS of CAP2-HA materials with varying amounts of CAP2

| Wt % | Mean BFS (MPa) |
|---|---|
| 1 | 74.34 ± 8.59 |
| 2.5 | 91.77 ± 17.29 |
| 3.25 | 92.68 ± 13.72 |
| 4 | 105.26 ± 19.74 |
| 5 | 89.73 ± 11.73 |

The following graph, Figure 6.22, demonstrates the relationship between wt % of CAP2 and mean biaxial flexural strength (BFS):

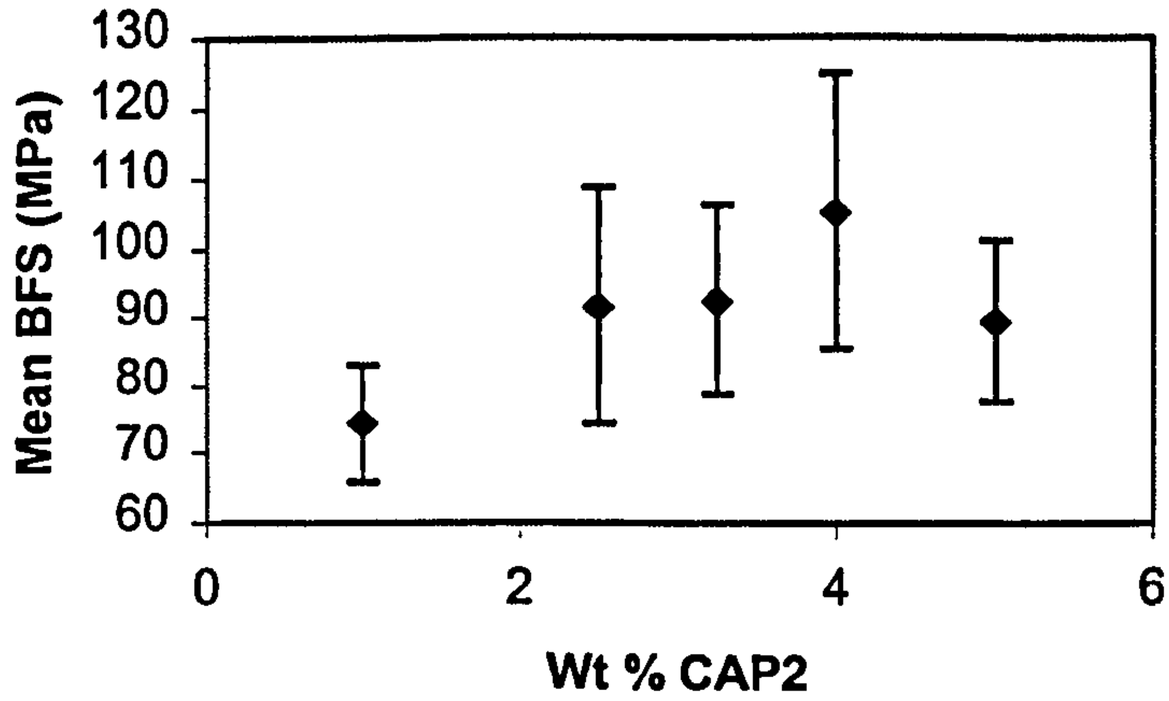


**Figure 6.22** Graph of BFS vs wt % CAP2 for CAP2-HA

The BFS of the CAP2-HA appeared to increase with increasing wt % of CAP2 and peak at 4 wt %, but then decreased steeply at 5 wt %. This may indicate that CAP2 is a sintering aid, therefore as the wt % increases, the degree of sintering increases (hence grain shrinkage), but at 5 wt %, perhaps there is excessive grain growth, which lowers the mechanical properties. The results of the density (D) measurements may be seen in Table 6.12.

**Table 6.12** Mean density of CAP2-HA materials with varying amounts of CAP2

| Wt % | Mean Density ($g.cm^{-3}$) |
|---|---|
| 1 | 2.83 ± 0.12 |
| 2.5 | 3.08 ± 0.03 |
| 3.25 | 2.96 ± 0.04 |
| 4 | 2.96 ± 0.03 |
| 5 | 3.03 ± 0.17 |

The following graph, Figure 6.23, demonstrates the relationship between wt % of CAP2 and density:

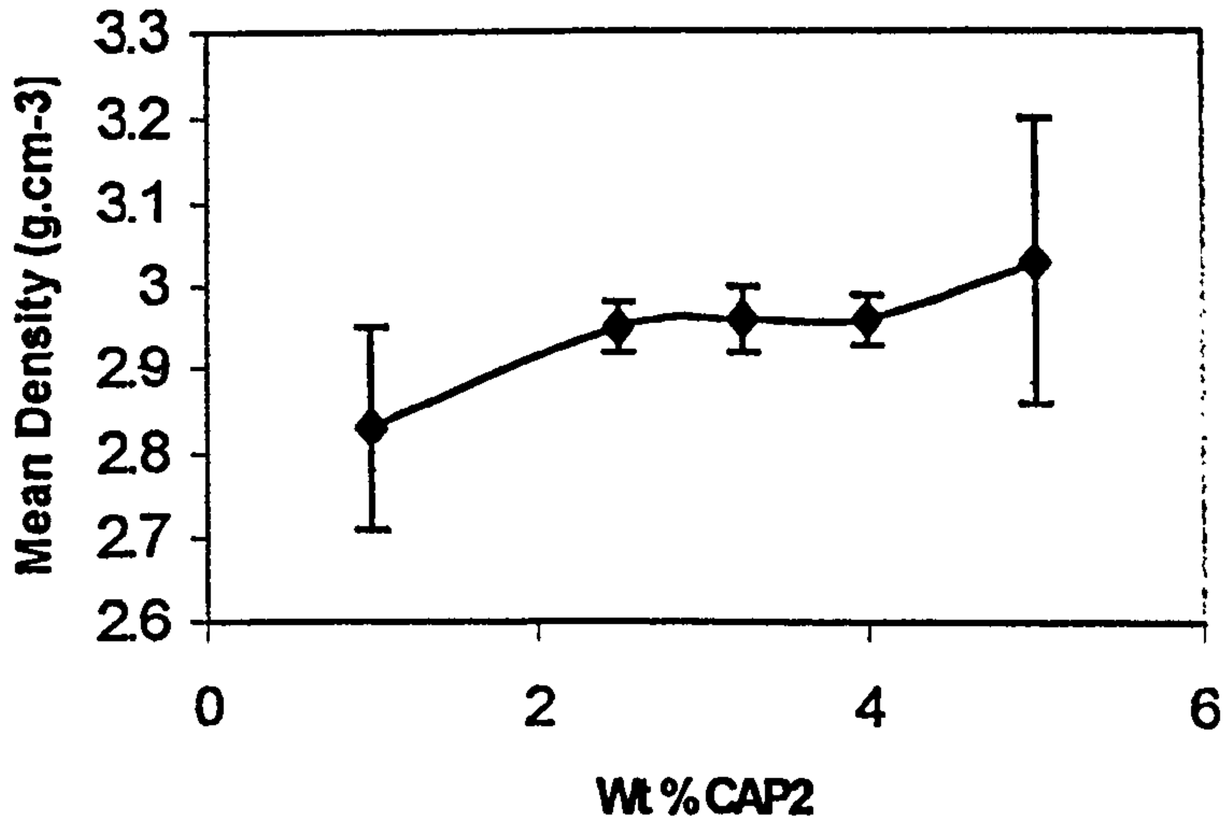


**Figure 6.23** Graph of density vs wt % CAP2 for CAP2-HA

The density appeared to increase between 1 and 2.5 wt % CAP2. Between 2.5 wt % and 4 wt % CAP2, the density settled, followed by another increase up to 5 wt % CAP2. The densities of the 1 and 5 wt % CAP2-HA both varied widely, as indicated by their large standard deviations.

The percentages of theoretical density achieved are stated below in Table 6.13:

**Table 6.13** Percentages of the theoretical density of CAP2-HA with varying amounts of CAP2

| Wt % of CAP2 | Percentage of theoretical density |
|---|---|
| 1 | 89.6 |
| 2.5 | 93.4 |
| 3.25 | 93.7 |
| 4 | 93.7 |
| 5 | 95.9 |

The results from this table are confusing because the 5 wt % samples have a larger median ($d_{0.5}$) particle size then the 4 wt % samples, yet they are closer to reaching theoretical density.

The Weibull moduli of all specimens from each wt % category are shown in Table 6.14:

**Table 6.14** Weibull moduli of all CAP-2HA

| Wt % CAP2 | WM (for all samples in each wt % category) |
|---|---|
| 1 | 9.8 |
| 2.5 | 6.2 |
| 3.25 | 7.8 |
| 4 | 6.9 |
| 5 | 8.7 |

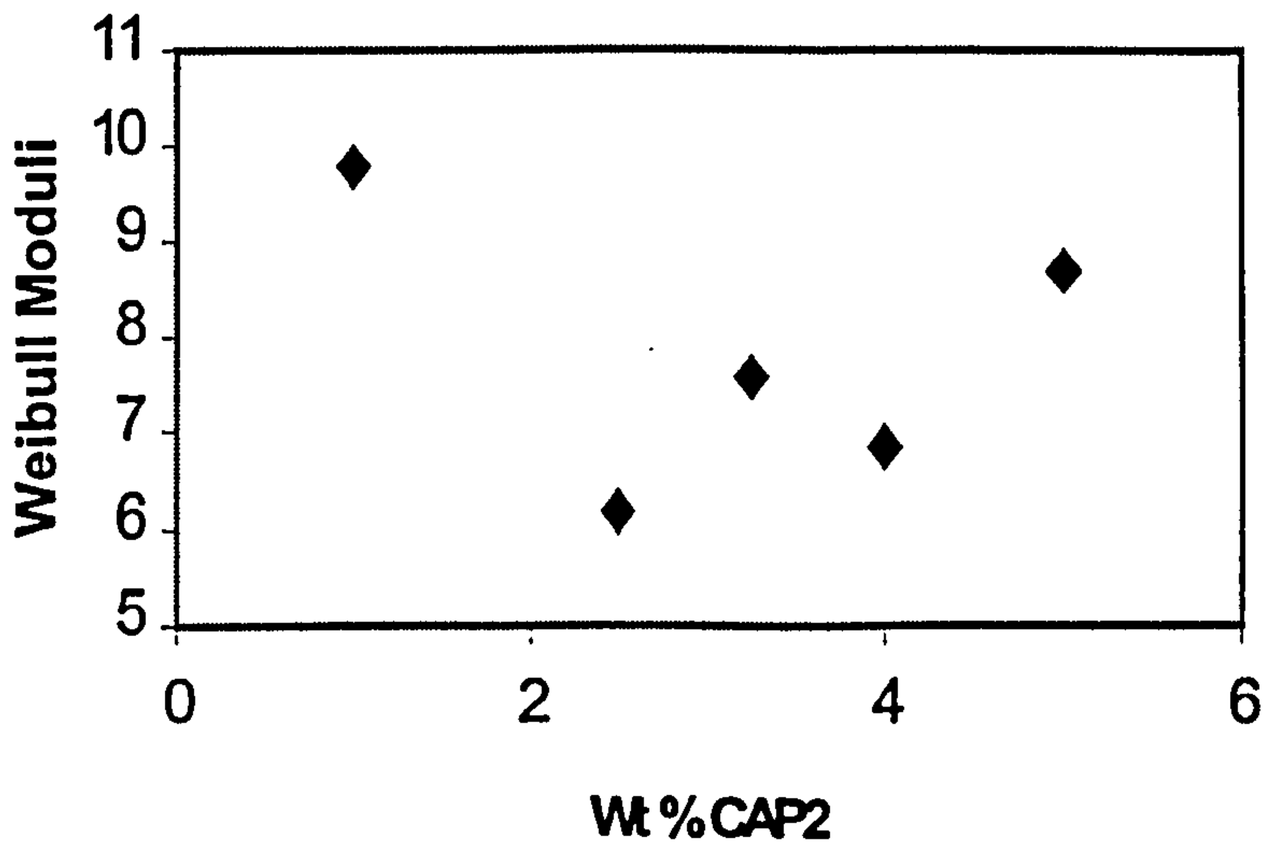


**Figure 6.24** Weibull moduli of all CAP2-HA

From Figure 6.24, there does not appear to be any particular trend between the wt % of CAP2 and the Weibull modulus of the batch; the values vary considerably. However, the Weibull moduli of the 1 wt % batches appeared to be the highest , and that of 2.5 wt % appeared to be the lowest.

### 6.3.4 SCANNING ELECTRON MICROSCOPY

Scanning electron micrographs were taken of 1/2.5/3.25/4/5 wt % CAP2-HA and are as follows:

1 wt % CAP2-HA:

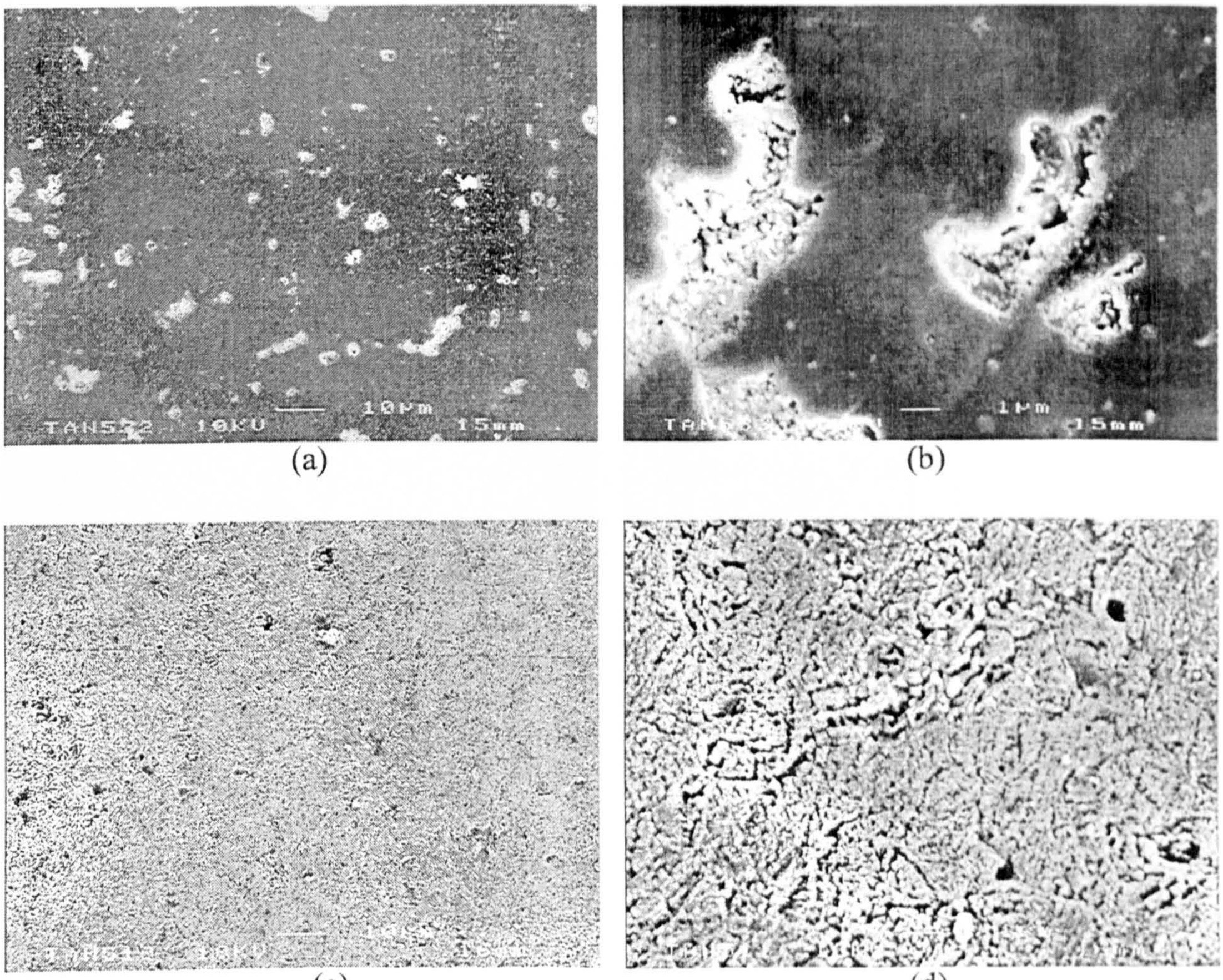


(a) (b)

(c) (d)

**Figure 6.25** 1 wt % CAP2-HA (a)+(b) Unetched, (c)+(d) Etched

Image (a) revealed white speckles on the polished surface, which at higher magnification in image (b), appeared to be concave areas/pores, similar to those found in CAP1-HA at 1250°C (Fig. 6.15) and 1300°C (Fig. 6.16). From image (c), it appeared that the etchant dissolved these pores, as indicated by the small darker holes. The microstructure from image (d) indicated that sintering was almost complete at this temperature and the grains, though difficult to decipher, appeared to be 1-2µm in size.

## 2.5 wt % CAP2-HA:

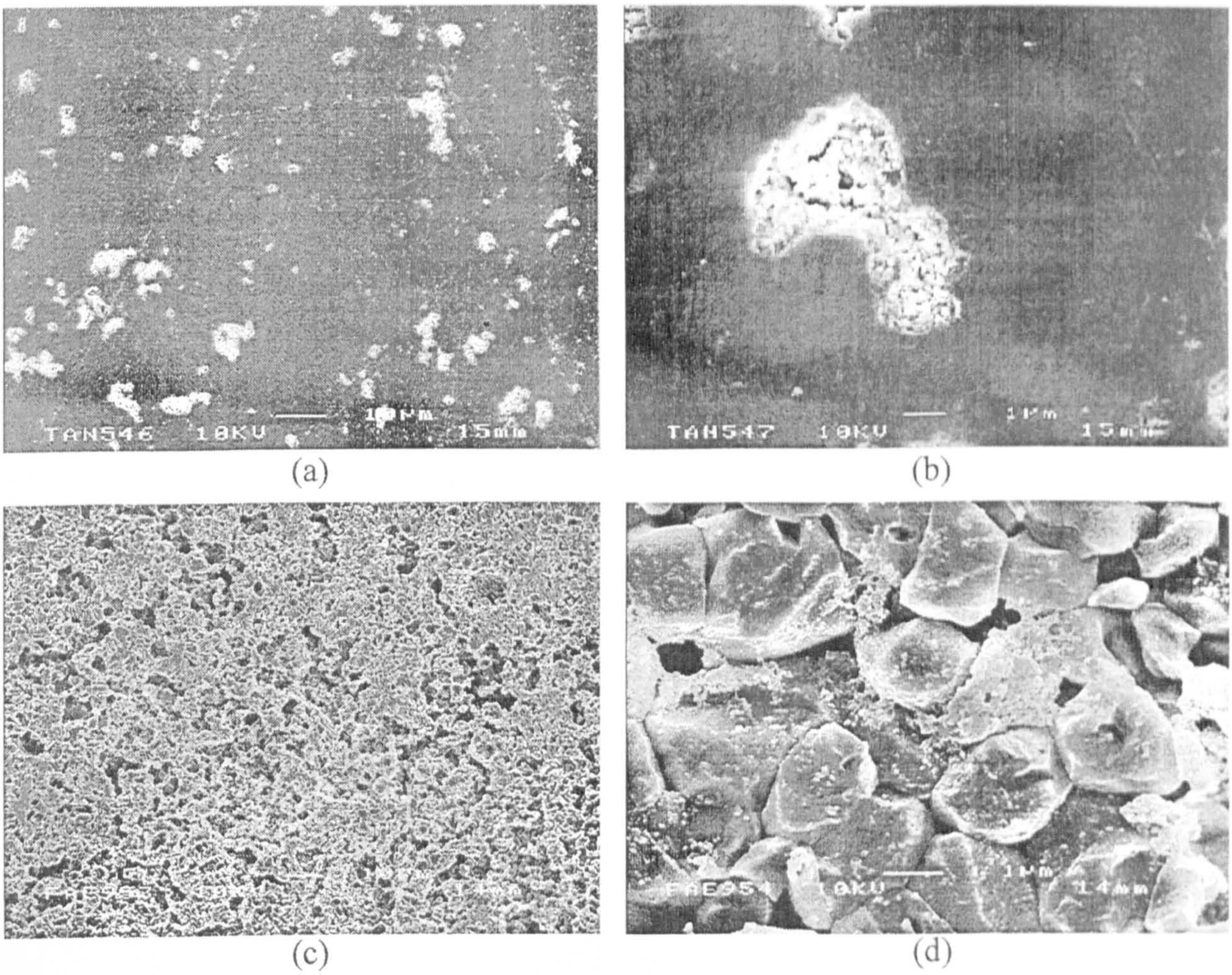


(a) (b) (c) (d)

**Figure 6.26** 2.5 wt % CAP2HA (a)+(b) Unetched, (c)+(d) Etched

The speckles in image (a) were similar in number, but larger in individual size, than the 1 wt% CAP2-HA. At higher magnification in image (b), these speckles/pores were similar in shape and texture to that of 1 wt % CAP2HA. The etchant appeared to have dissolved the contents of these pores, as seen in image (c), and higher magnification in image (d) revealed that residual material from the pores were still present in the form of a fine-layered net-like material. A definite grain structure was visible in image (d) and showed an average grain size of 1-2μm.

## 3.25 wt % CAP2-HA:

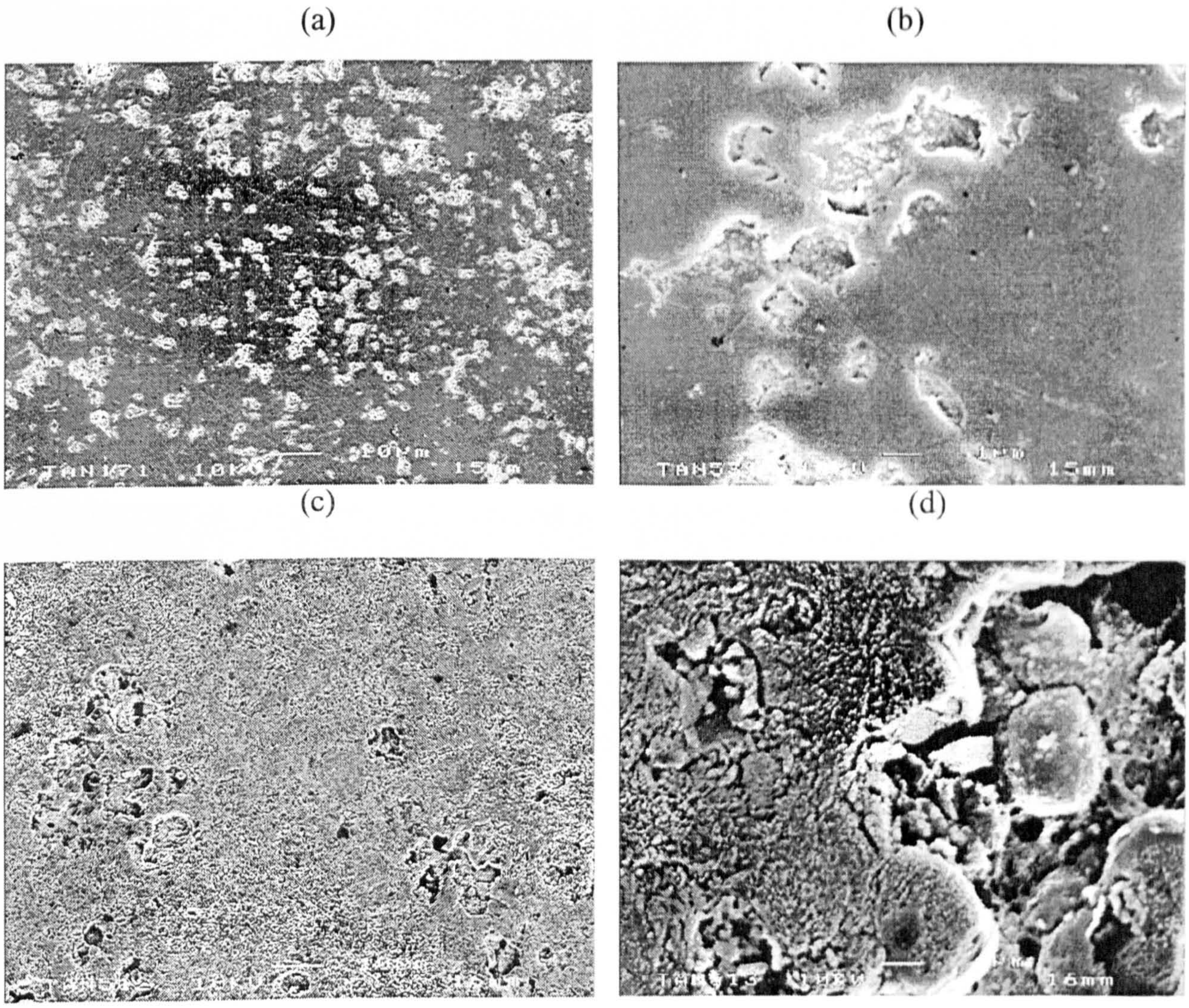


**Figure 6.27** 3.25 wt % CAP2-HA (a)+(b) Unetched, (c)+(d) Etched

There was a huge increase in the number of white speckles/pores as revealed by image (a) in comparison to 2.5 wt% CAP2-HA; some of the pores appeared to have merged. At higher magnification, the pores were similar to those found in the other CAP2-HA specimens. Image (c) showed that yet again, the etchant dissolved the contents of the pores, revealing many, small concave regions for the individual pores, and larger concave regions deriving from pore mergence. The grains appeared to be larger in size to that of 2.5 wt% CAP2-HA, i.e. 2-3μm.

## 4 wt % CAP2-HA:

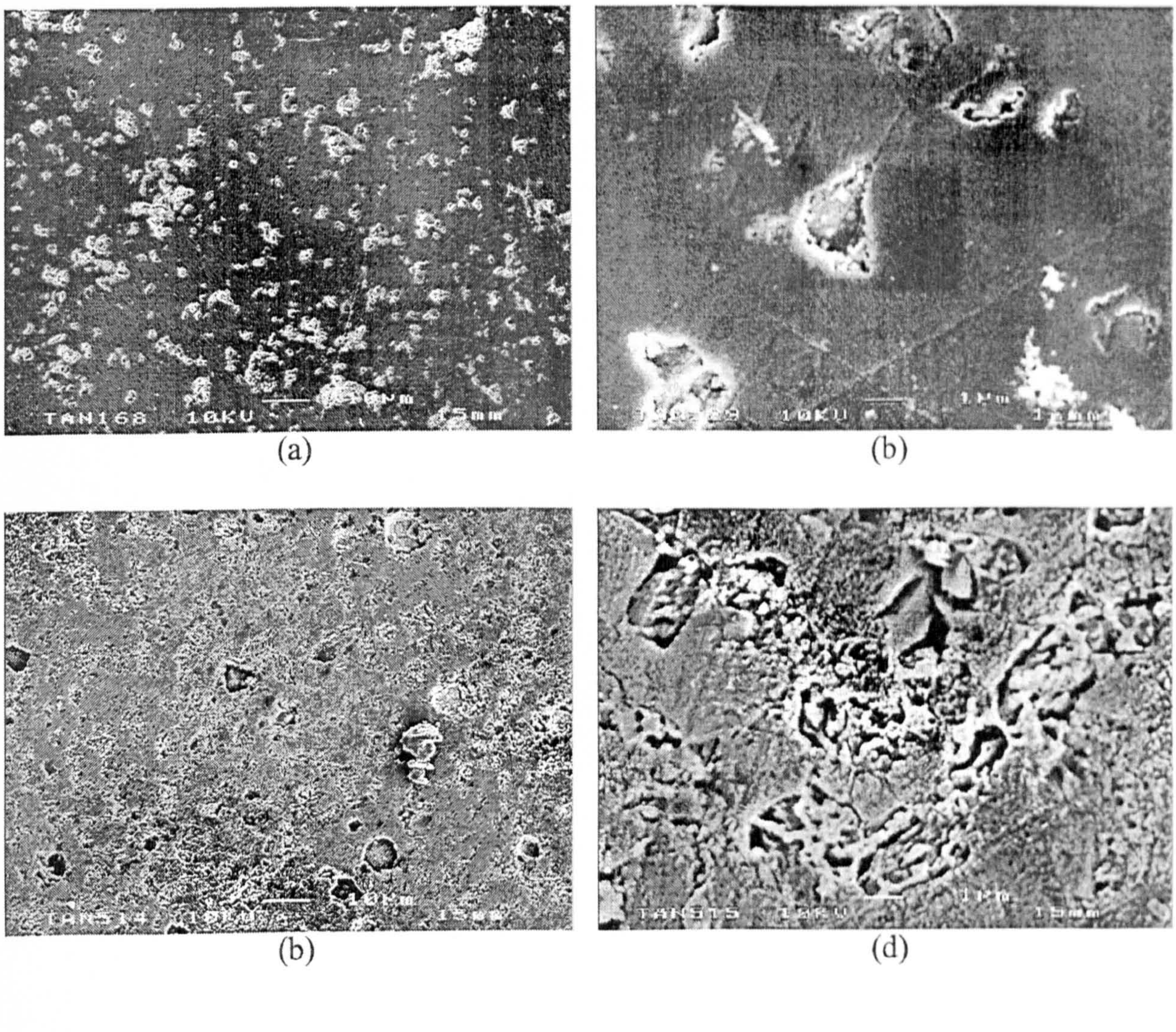


**Figure 6.28** 4 wt % CAP2-HA (a)+(b) Unetched, (c)+(d) Etched

Image (a) shows that this specimen contained a similar amount of speckles/pores as 3.25 wt % CAP2-HA, and at higher magnification, both of their pores looked similar in structure. The etched image (d) complemented image (a) in a similar manner as 3.25 wt% CAP2-HA did. Image (d) revealed that the grains were slightly larger than that of 3.25 wt % CAP2HA, averaging around 3μm..

5 wt % CAP2-HA:

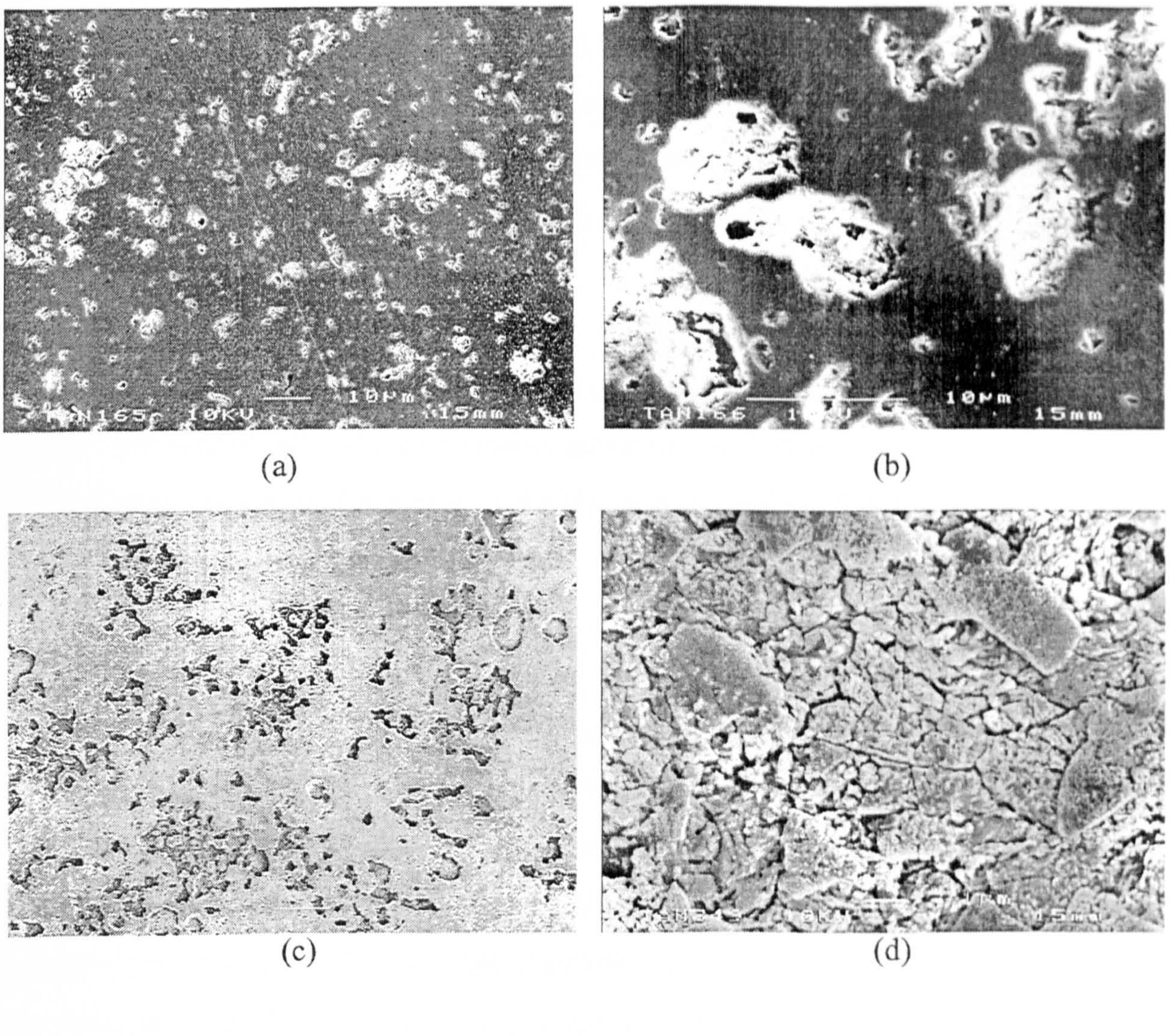


(a) (b)

(c) (d)

**Figure 6.29** 5 wt % CAP2-HA (a)+(b) Unetched, (c)+(d) Etched

Image (a) showed that there were a smaller number of speckles/pores, yet there appeared to be more pore mergence than in 4wt % CAP2-HA. At higher magnification, seen in image (b), the speckles are ~ 10 µm in diameter. The etching process revealed a lot of porosity in image (c) and at higher magnification, the grains appeared to be larger than the other CAP2-HA batches; ~5µm.

## 6.4 DISCUSSION

### 6.4.1 PRODUCTION AND CHARACTERIZATION OF MATERIALS FOR REINFORCING HA

The particle size analysis revealed that CAP1 had a much smaller median particle size (~9-10mm) than CAP2 (~112-115mm). The additives were not milled prior to particle size analyis; they were hand crushed until a fine consistency was reached , and the fact that the CAP2 was physically much harder to crush in the pestle and mortar justified this large discrepancy.

The XRF analysis revealed the CAP1 to be more Ca-deficient (Ca/P ratio=0.47) than the CAP2 (Ca/P ratio=0.84). Therefore it was assumed that in composite form, the CAP1 would slightly reduce the Ca/P ratio of the HA, and cause more HA to decompose to TCP (LeGeros, 1993) than CAP2 addition would.

The most important feature of the DTA trace was the onset of the melting endotherm for CAP1 (971°C) and CAP2 (1197°C). This meant that at temperatures higher than 971°C and at 1197°C, CAP1 and CAP2, respectively, experienced a reduction in viscosity sufficient enough to perform liquid-assisted sintering. CAP2 was a crystalline material, the majority of its' crystalline phases due to the presence of $Ca_2P_2O_5$ (as shown by XRD in Figure 6.4), whilst CAP1 lacked any crystalline organization. CAP1 did vitrify upon quenching and was classified as a glass, as opposed to CAP2 which, due to its' crystalline nature, was regarded as synonymous to a glass-ceramic.

### 6.4.2 PRODUCTION AND CHARACTERIZATION OF CAP1-HA

The particle sizes of the CAP1-HA batch 1 were very different to batch 2 (refer to Table 6.3). The reasons for the general difference in particle size was attributed to batch variability. Batch 1 displayed a larger $d_{0.1}$, $d_{0.5}$, and $d_{0..9}$ than batch 2, yet displayed a smaller mode. The greatest difference could be seen between the $d_{0.9}$ of batch 1 and 2, which was 152.7μm and 82.3μm, respectively. From the histogram of batch 1, it is apparent that there were only a few particles lying in the upper end of the distribution, which caused this huge difference. Regardless of this anomaly, the modes of the two

batches were similar (36.4-42.6μm) and were slightly smaller than the modes of the HA reported in Chapter 5 (43.4-43.7μm).

XRF analysis revealed the Ca/P ratios of all the CAP1-HA batches (1.65-1.66), sintered at the temperatures stated in Table 6.4, were lower than that of HA (1.68-1.73). The CAP1-HA, as predicted from the XRF analysis on CAP1 alone, was more Ca-deficient than HA alone, as a result of the CAP1 addition, which had a Ca/P ratio of 0.47. According to the literature, this signified that the HA in the composite would decompose to TCP during sintering. If the commercial HA had the correct stoichiometric Ca/P ratio of 1.67, then the CAP1-HA would display an even lower Ca/P ratio than the reported 1.65-1.66, which would be indicative of the amount of decomposition it would experience at high temperature.

After sintering at a range of temperatures, XRD analysis did indeed reveal a huge presence of TCP within the composite (Table 6.5), which was predicted from the XRF results. Despite the fact that the Ca/P ratio did not change with respect to the sintering temperatures, the amount of TCP increased with increasing sintering temperature. This could be due to an increase in activation energy within the system, resulting from an increase in temperature, which would enhance the re activity of the glassy phase (hence the decomposition process).

The HA within the composite only decomposed to β-TCP up until 1300°C, where it started to decompose to α-TCP. This is consistent with the literature, in which LeGeros (1993), Kuroyama et al (1991), and Tampieri et al (1997) stated that β-TCP is more stable at low temperature and α-TCP is more stable at higher sintering temperatures (~1300-1350°C). The huge amount of TCP present would have been detrimental to the in-vivo mechanical stability of the composites, whereby the TCP (i.e. the major phase in the composite) would have resorbed, leaving little scaffolding material for structural support. Already the possibility of using this composite in clinical applications seemed limited, due to the disappointing results of the phase composition analysis.

The mechanical properties of the CAP1-HA composites sintered at all temperatures were extremely poor in comparison to the mechanical properties of the HA in Chapter 5. The highest BFS's for CAP1-HA and HA were 26.6MPa (1300°C) and 60.01±14.70MPa (1200°C), respectively. It appeared that mixing the HA with CAP1 caused the HA to experience a reduction in strength, which was far from expected, seeing as the authors stated in Table 3.13 reported an increase in strength when reinforcing HA with an additive that was very similar to CAP1. Biaxial flexural strengths of up to 100 MPa were reported for $CaO-P_2O_5$ glass-reinforced HA systems, which was considerably higher than those reported in this investigation. Furthermore, Knowles et al (1994) reported that it was the presence of β-TCP, which enhanced the mechanical strength of HA.

However in this investigation, the large amount of β-TCP present in the composites did not appear to increase the strength of the HA after being reinforced with CAP1. The melting endotherm of CAP1 experienced an onset at 971°C, which meant that at sintering temperatures of greater than 1200°C, its viscosity would be very low, and it would be aggressive and reactive, causing the corrosive degradation of HA to TCP with accompanying high porosity. At temperatures below 1200°C, a progressive decrease in temperature and hence increase in the CAP1 viscosity combined with the presence of large agglomerates (~152μm), which would inhibit full packing potential in the green state, may have resulted in a minimal driving force for liquid-assisted sintering and therefore minimal densification at these temperatures.

The densities of the composites increased with increasing sintering temperature and were also extremely low, which explained the poor mechanical properties. The highest density value, 2.18 $g.cm^{-3}$ (69% of theoretical), occurred at a sintering temperature of 1300°C; HA also achieved its highest density at this temperature (3.04±0.03) (96%theoretical), which was significantly larger. Obviously, very little densification occurred within the composite, even at high temperature. This is unusual, seeing as glass additives were reported by the authors in Table 3.13 to be fundamental to liquid-assisted sintering, a process in which the glass (which, at sintering temperature, is a liquid) is a sintering aid, improving the sinterability of the starting material. The CAP1-HA composites

experienced much less densification than they what was originally predicted. As mentioned previously, this corroborates with the results of the particle size analysis, which detected agglomerates as large as 152μm, which prevented full packing density in the green state, and therefore affected the as-sintered densities.

Scanning electron microscopy identified the reason as to why the CAP1-HA densities were so low. At first, the micrographs of the CAP1-HA look very similar to that of HA in Chapter 5, in terms of particle coalescence at 1000-1100°C. However, there was a great deal of porosity in the composites at low and at high temperatures. As the sintering temperature increased and the composite started to sinter properly (Figure 6.14-6.16), the material in proximity to the pores (indicated by the white speckles in the micrographs) appeared to dissolve the most in the etchant. This implied that the material surrounding the pores was more resorbable than the rest of the specimen surface, and therefore mostly consisted of TCP, which would be very vulnerable during the etching process. It could therefore be hypothesized that the pores originally contained CAP1 particles, which had melted and reacted with the surrounding HA. TCP has previously been reported to have superior mechanical properties to that of HA (Raynaud et al, 1998) (Akao et al, 1982). However, in this investigation, any increase in strength resulting from β-TCP content was nullified by the increased porosity of the CAP1-HA compared to the HA.

The micrographs also verified the existence of powder agglomerates in the particle size analysis, which reported median particle sizes of 21.4-39.71μm, whilst the grain sizes in Figure 6.16, indicate an average grain size ≤1μm. Unfortunately, the etched micrograph of the composite sintered at 1300°C was the only one displaying a definite grain structure for two reasons. Firstly, in general, the presence of a highly resorbable second phase resulted in difficulties with one phase being continuously over-etched, and secondly, the composite sintered at 1300°C was deliberately etched with a stronger etchant (2.5 %orthophosphoric acid, as opposed to 0.5%) in order to identify an approximate grain size in the HA.

### 6.4.3 PRODUCTION AND CHARACTERIZATION OF CAP2-HA

The particle size analysis revealed bimodal distributions for CAP2-HA, as with the HA in Chapter 5. The two modes for the CAP2-HA and HA were ~2.5μm/~100μm and ~3.5μm/~40μm, respectively. The smaller particle fraction decreased in mode from ~3.5μm to ~2.5μm, which implies that some of the CAP2-HA milled effectively and therefore the particle size reduced and did not agglomerate. The larger particle fraction increased in mode from ~40mm to ~100mm, which implies that the large particles seen in the histograms (Figures 6.17-6.19) had reduced slightly from > 100μm, but had not finished milling in the CAP2-HA powder.

The Ca/P ratios of CAP2-HA, determined by XRF, ranged between 1.66-1.69 for all wt % categories, apart from an unusually low ratio of 1.62 for the 3.25 wt% CAP2-HA. Apart from the anomaly at 3.25 wt%, the ratios were generally higher than the CAP1-HA composites (ratios of 1.65-1.66) and lower than the HA investigated in Chapter 5 (ratios of 1.68-1.73). This was expected because the Ca/P ratios of the CAP1 and CAP2 were 0.47 and 0.84 respectively, therefore CAP2 did not lower the Ca/P ratio of the HA to the extent that CAP1 did. Therefore, less decomposition of the HA to TCP within this composite was predicted, in comparison to CAP1-HA. As regards to the effect of increasing CAP2 addition, the Ca/P ratio appeared to decrease slightly with increasing wt % CAP2 (despite the anomaly at 3.25 wt % ). This was expected because the Ca/P ratio of CAP2 was lower than that of HA, therefore the larger the amount of CAP2 added, the more the Ca/P ratio of the composite would decrease.

XRD was used to assess the relative intensity of TCP (RI-TCP). As expected, referring to Table 6.10, the CAP2-HA experienced much less decomposition during sintering than the CAP1-HA. In addition, the amount of decomposition to TCP increased with increased wt% CAP2 (Figure 6.21), because the CAP2 additive decreased the Ca/P ratio of the HA; therefore, the higher the addition, the lower the ratio of the HA, and the increased likelihood of decomposition at high sintering temperatures. It was interesting to note that the 2.5 wt % CAP2-HA (which had the same wt % additive as all the CAP1-

HA) and the CAP1-HA, both sintered at 1300°C, contained 10% α-TCP and 60% β-TCP/13% α-TCP, respectively. Even at higher additions of CAP2, such as 5 wt %CAP2-HA, the amount of decomposition was was still significantly smaller( 20% α-TCP). In terms of phase composition, the CAP2-HA had superior properties to CAP1-HA because it contained less TCP, hence a smaller potential in-vivo solubility. The counter-argument may be that the CAP1-HA contained mostly β-TCP, which according to Kuroyama et al (1991) is less soluble than α-TCP, where CAP2-HA contained only α-TCP. While CAP1-HA contained mostly β-TCP, the difference in %TCP between the two composites was large enough to disregard solubility differences between the TCP polymorphs.

Knowles et al (1994) found that the β- to α-TCP transformation involved a larger volume change than the HA to β-TCP transformation and resulted in a disruption of the overall structure of the material, hence a decrease in mechanical strength. Extrapolating upon these comments, CAP2-HA (which contained only α-TCP) could be expected to be mechanically inferior to CAP1-HA (which contained a large proportion of β-TCP). However, the results of the mechanical testing of CAP2-HA showed otherwise, which may be related to the density variation between the two.

Referring to Table 6.11, the BFS's of CAP2-HA were high, ranging between 74.34±8.59 MPa (1wt%) and 105.26±19.74 MPa (5wt%), as opposed to CAP1-HA, whose strength at 1300°C was 26.59 MPa. To compare consistently, the BFS's of the 2.5 wt% CAP2-HA and the CAP1-HA (2.5wt% CAP1 throughout) were 91.77±17.29 MPa and 26.59 MPa respectively. The addition of CAP2 to HA increased the BFS of P201 HA (1200°C) from 60.01±14.70 MPa to 91.77±17.29 MPa, with an improvement of ~31 MPa, as opposed to the addition of CAP1 which weakened P201 HA by ~34 MPa. The CAP1 and CAP2 appeared to affect the strength of HA in equal magnitude, but opposite direction. The melting endotherm of CAP2 (determined by DTA in section 6.1.3) was shown to be 1197°C, which was very close to the sintering temperature of the composites (1300°C). Therefore, the CAP2 was in liquid form at the temperature necessary to enhance densification, i.e. near the sintering temperature. CAP1, on the other hand, whose

melting endotherm was shown to be 971°C, was in liquid form at perhaps too low a temperature and affected the microstructure in a manner detrimental to the subsequent sintering process.

Increasing the amount of CAP2 additive increased the BFS of the composite, until the addition reached 5wt%, upon which the strength decreased to 89.73±11.73 MPa, a figure between the BFS of 1 wt% CAP2-HA (74.34±8.59 MPa) and 2.5 wt% CAP2-HA (91.77±17.29 MPa). From 1-4 wt %, the CAP2 appeared to behave as a reinforcing additive and performed liquid-assisted sintering, as it gradually increased the BFS of the composites. However, the decrease in BFS at 5 wt % indicated that the reason for such behaviour lay in the microstructure of the composite, i.e. was perhaps due to the presence of coarse grains. The Weibull moduli (WM) of the CAP2-HA composites did not appear to have a relationship with the wt % of CAP2, but the values merely ranged between 6.2-9.8, which were higher than the WM (6.16) of the HA in Chapter 5, sintered at 1300°C. Therefore the addition of CAP2 not only increased the strength of the HA but also increased the reliability of the mechanical data.

The densities of the composites increased with increasing wt % CAP2, which verified the reinforcing capability of the CAP2 material. Furthermore, the densities ranged from 2.83±0.12 $g.cm^{-3}$ at 1 wt % (89.6 % theoretical) to 3.03±0.17 $g.cm^{-3}$ at 5 wt % (95.9 % theoretical), which were much closer to the density of HA at 1300°C (3.04±0.03 $g.cm^{-3}$, 96% theoretical)) than CAP1-HA at 1300°C (2.18 $g.cm^{-3}$, 68.9 % theoretical).

The micrographs revealed information which explained the mechanical properties of the CAP2-HA composites between wt % categories, as well as the strength difference between CAP1-HA and CAP2-HA. Firstly, there was a similar degree of porosity and similar grain structure in the 1 and 2.5 wt % CAP2-HA, followed by an increase in both at 3.25 wt %, which was similar at 4 wt %. However, at 5 wt %, there was significant coarsening of the microstructure. As 5 wt% CAP2-HA displayed the highest density, the reason for the decrease in strength is possibly due to the presence of these large

micropores, which would act as stress-raisers, thereby decreasing the BFS of the composite.

Secondly, comparing the 2.5 wt% CAP2-HA and the CAP1-HA sintered at 1300°C (which also contained 2.5 wt%), the grains of the former were slightly larger than the grains of the latter, from which one would assume that the CAP1-HA would exhibit better mechanical properties. However, the CAP2-HA was much stronger due to the significantly smaller degree of porosity displayed in the microstructure. Furthermore, CAP1-HA contained micropores that were 2-3mm in diameter, whilst the micropores in CAP2-HA were <1μm in diameter.

At 1300°C, CAP2-HA experienced much less decomposition than CAP1-HA, and also displayed better mechanical properties. The better sinterability of CAP2-HA was due to the compatibility of the viscosity of CAP2 and the HA at the sintering temperature, as well as the higher densities achieved in the green and as-sintered state. As for the ideal wt% CAP2 for promoting minimal decomposition and maximum strength, the 2.5 wt % CAP2-HA was chosen because it had a RI-TCP of ~10% (2$^{nd}$ lowest) and a middle range strength (~92 MPa). On either side of this composite, the strength was too low or the RI-TCP was too high.

# CHAPTER 7

# INVESTIGATION INTO THE EFFECT OF PHYSIOLOGICAL SOLUTION ON HYDROXYAPATITE AND ITS' REINFORCED COMPOSITES

The investigations from the previous chapter revealed that reinforcing P201 HA with CAP1 decreases the strength and increases phase decomposition, yet reinforcement with CAP2 increased the strength, with minimal phase decomposition. Therefore it was decided to exclude CAP1-HA from further investigation. Furthermore, the CAP2-HA appeared to be the strongest, with minimal phase decomposition at a sintering temperature of 1300°C and 2.5 wt % CAP2, therefore all CAP2HA specimens were prepared in this manner for this study. In order to maintain consistency in density and surface porosity, the P201 HA samples were also sintered at this temperature (despite the optimum strength being at 1200°C), previous XRD analysis having demonstrated that P201 did not experience phase decomposition to TCP at these temperatures.

## 7.1 PRE-SOAK PROPERTIES

Prior to soaking the dense P201 and CAP2-HA in Ringer's solution, all samples were labelled according to which day in the 30 day cycle they would be analysed. There were 30 samples in each category (eg.P201) and 5 samples in each batch, related to the day for analysis, labelled "MD1" for mechanical degradation after day 1, and "MD2" for mechanical degradation after day 2, etc. All samples were sintered at 1300°C.

### 7.1.1 X-RAY DIFFRACTOMETRY

There was no β-TCP present in the batches, hence only the RI-TCP of α-TCP are shown in Table 7.1; P201 contained no α-TCP, which is consistent with the phase composition of P201 in the previous investigation.

**Table 7.1** Percentages of RI-TCP for P201 HA and CAP2-HA in the mechanical degradation study

| Batch | RI-TCP (%) | |
|---|---|---|
| | P201 | CAP2-HA |
| MDO (dry control) | 0 | 14 |
| MD1 | 0 | 13 |
| MD2 | 0 | 13 |
| MD4 | 0 | 17 |
| MD8 | 0 | 17 |
| MD30 | 0 | 6 |

All of the dry CAP2-HA batches in Table 7.1 contained marginally larger amounts of α-TCP than its' 2.5 wt % counterpart in the previous investigation. Nevertheless, the purpose of analysing the phase composition in this particular investigation was to decipher any changes between pre- and post-soaking values, as opposed to simply pre-soaking values.

### 7.1.2 DENSITY MEASUREMENTS

The densities of the P201 appeared to be higher than that of the CAP2-HA. The results may be seen in Table 7.2.

**Table 7.2** Mean density values for P201 HA and CAP2-HA in the mechanical degradation study

| Batch | Mean Density ($g.cm^{-3}$) | |
|---|---|---|
| | P201 | CAP2-HA |
| MDO (dry control) | 3.03 ± 0.03 | 3.01 ± 0.01 |
| MD1 | 3.08 ± 0.03 | 2.92 ± 0.06 |
| MD2 | 3.06 ± 0.02 | 3.01 ± 0.05 |
| MD4 | 3.09 ± 0.003 | 2.99 ± 0.01 |
| MD8 | 3.07 ± 0.01 | 3.01 ± 0.01 |
| MD30 | 3.02 ± 0.09 | 2.96 ± 0.02 |

## 7.2 POST-SOAK PROPERTIES

### 7.2.1 X-RAY DIFFRACTOMETRY

The results from the XRD analysis are shown in Table 7.3. The P201 appeared to contain no α-TCP, apart from day 2, whilst the RI-TCP present in CAP2-HA fluctuated. With respect to the corresponding pre-soaked values, the RI-TCP in CAP2-HA, decreased after 1, increased after day 2, and then decreased up until day 30, where it appeared to equate its respective pre-soaked value. Figure 7.1 displays the trends observed in the phase composition pre- and post-soaking for CAP2-HA only (the results for P201 HA are not illustrated due to the fact that most samples displayed 0 % α-TCP pre- and post-soaking).

**Table 7.3** The effect of Ringer's solution on the phase composition of CAP2-HA

| Batch | RI-TCP (%) | |
|---|---|---|
| | P201 | CAP2-HA |
| MDO (dry control) | 0 | 14 |
| MD1 | 0 | 10 |
| MD2 | 2 | 15 |
| MD4 | 0 | 16 |
| MD8 | 0 | 13 |
| MD30 | 0 | 6 |

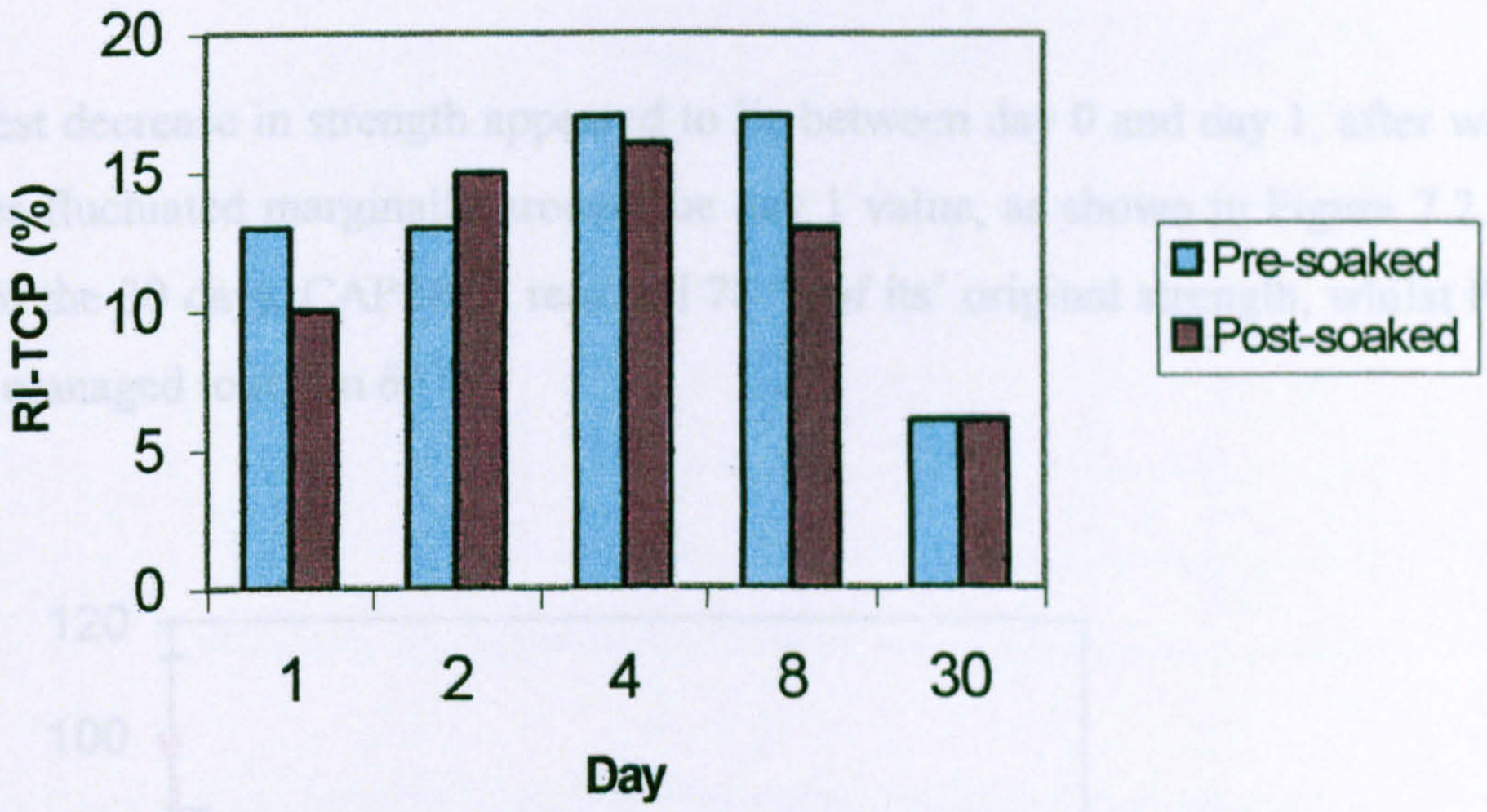


**Figure 7.1** The effect of Ringer's solution of the RI-TCP of CAP2-HA

### 7.2.2 MECHANICAL PROPERTIES

The results of the biaxial flexural tests performed under environmental conditions on all batches are shown in Table 7.4.

**Table 7.4** Mean Biaxial Flexural Strengths for P201 HA and CAP2-HA in the mechanical degradation study

| Batch | Mean Biaxial Flexural Strength (MPa) | | | |
|---|---|---|---|---|
| | P201 | % Original Strength | CAP2-HA | % Original Strength |
| MDO (dry control) | 10.93 ± 1.06 | 100 | 98.01 ± 15.99 | 100 |
| MD1 | 7.89 ± 2.09 | 72 | 68.74 ± 17.99 | 70 |
| MD2 | 7.39 ± 0.96 | 68 | 65.27 ± 16.55 | 66 |
| MD4 | 10.33 ± 2.46 | 95 | 63.79 ± 11.91 | 65 |
| MD8 | 8.76 ± 1.56 | 80 | 68.07 ± 11.54 | 69 |
| MD30 | 6.54 ± 1.68 | 60 | 76.23 ± 7.62 | 78 |

The largest decrease in strength appeared to lie between day 0 and day 1, after which the values fluctuated marginally around the day 1 value, as shown in Figure 7.2. At the end of the 30 days, CAP2-HA retained 78 % of its' original strength, whilst P201 HA only managed to retain 60 %.

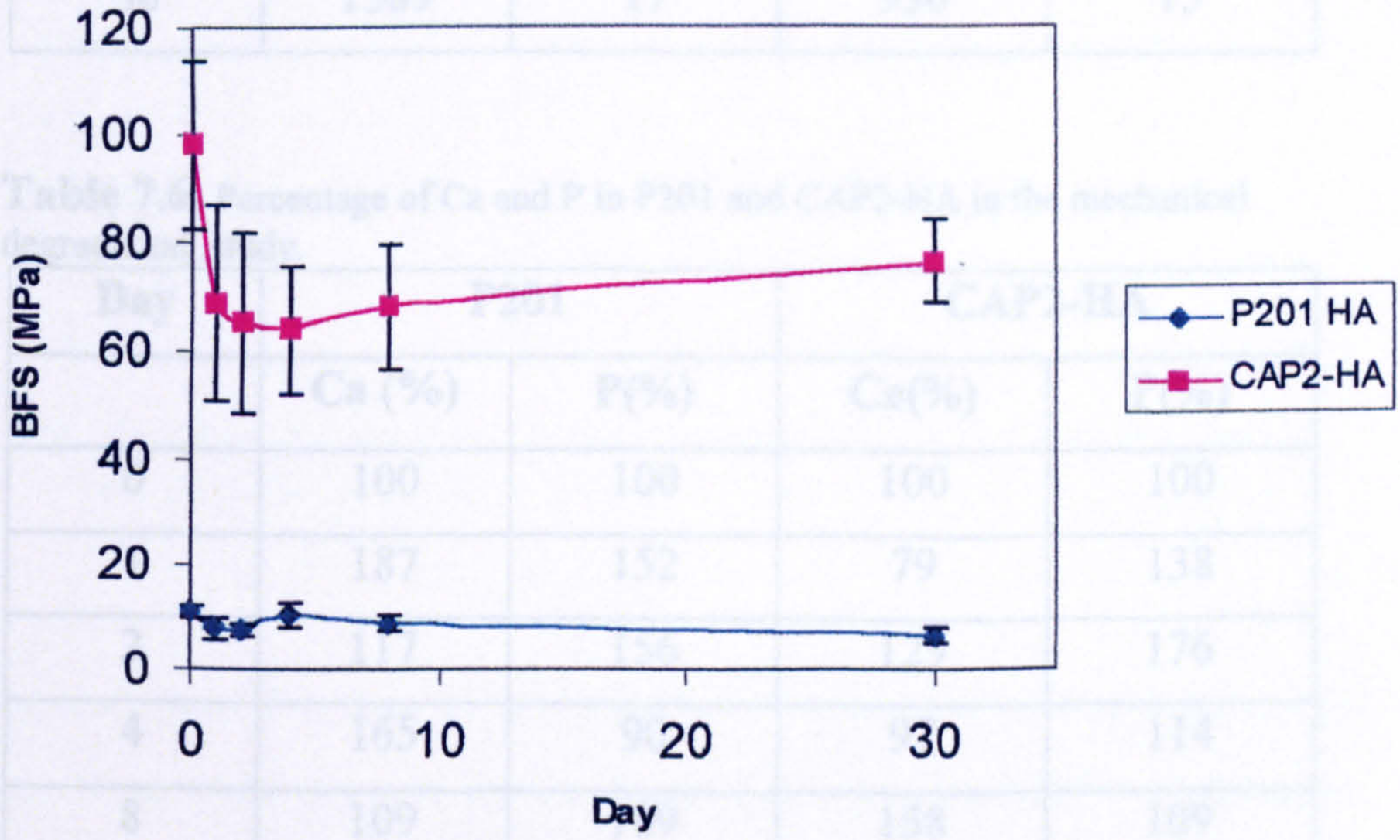


**Figure 7.2** The effect of Ringer's solution on the BFS of P201 HA and CAP-2HA.

### 7.2.3 ICPMS RESULTS

ICPMS was used to analyse the ionic content of Ringer's solution, pre- and post-soaking, as described in section 4.4.8. For the purpose of this investigation, the most relevant ions for consideration were the calcium (Ca) and phosphorus (P) ions because resorption and re-precipitation processes in Ca/P based ceramics involve the loss of Ca and P followed by the formation of a Ca/P-rich layer on the sample surface. The results (semi-quantitative) are shown in Table 7.5 and the percentages are shown in Table 7.6:

**Table 7.5** Concentration of Ca and P in P201 and CAP2-HA in the mechanical degradation study

| Day | P201 | | CAP2-HA | |
|---|---|---|---|---|
| | Ca ($\mu gl^{-1}$) | P($\mu gl^{-1}$) | Ca($\mu gl^{-1}$) | P($\mu gl^{-1}$) |
| 0 | 927 | 21 | 927 | 21 |
| 1 | 1737 | 32 | 740 | 29 |
| 2 | 1090 | 33 | 1195 | 37 |
| 4 | 1537 | 19 | 895 | 24 |
| 8 | 1018 | 23 | 1468 | 23 |
| 30 | 1589 | 17 | 930 | 15 |

**Table 7.6** Percentage of Ca and P in P201 and CAP2-HA in the mechanical degradation study.

| Day | P201 | | CAP2-HA | |
|---|---|---|---|---|
| | Ca (%) | P(%) | Ca(%) | P(%) |
| 0 | 100 | 100 | 100 | 100 |
| 1 | 187 | 152 | 79 | 138 |
| 2 | 117 | 156 | 129 | 176 |
| 4 | 165 | 90 | 97 | 114 |
| 8 | 109 | 109 | 158 | 109 |
| 30 | 171 | 81 | 100 | 71 |

The results of the ICPMS analysis are illustrated in Figures 7.3 and 7.4.

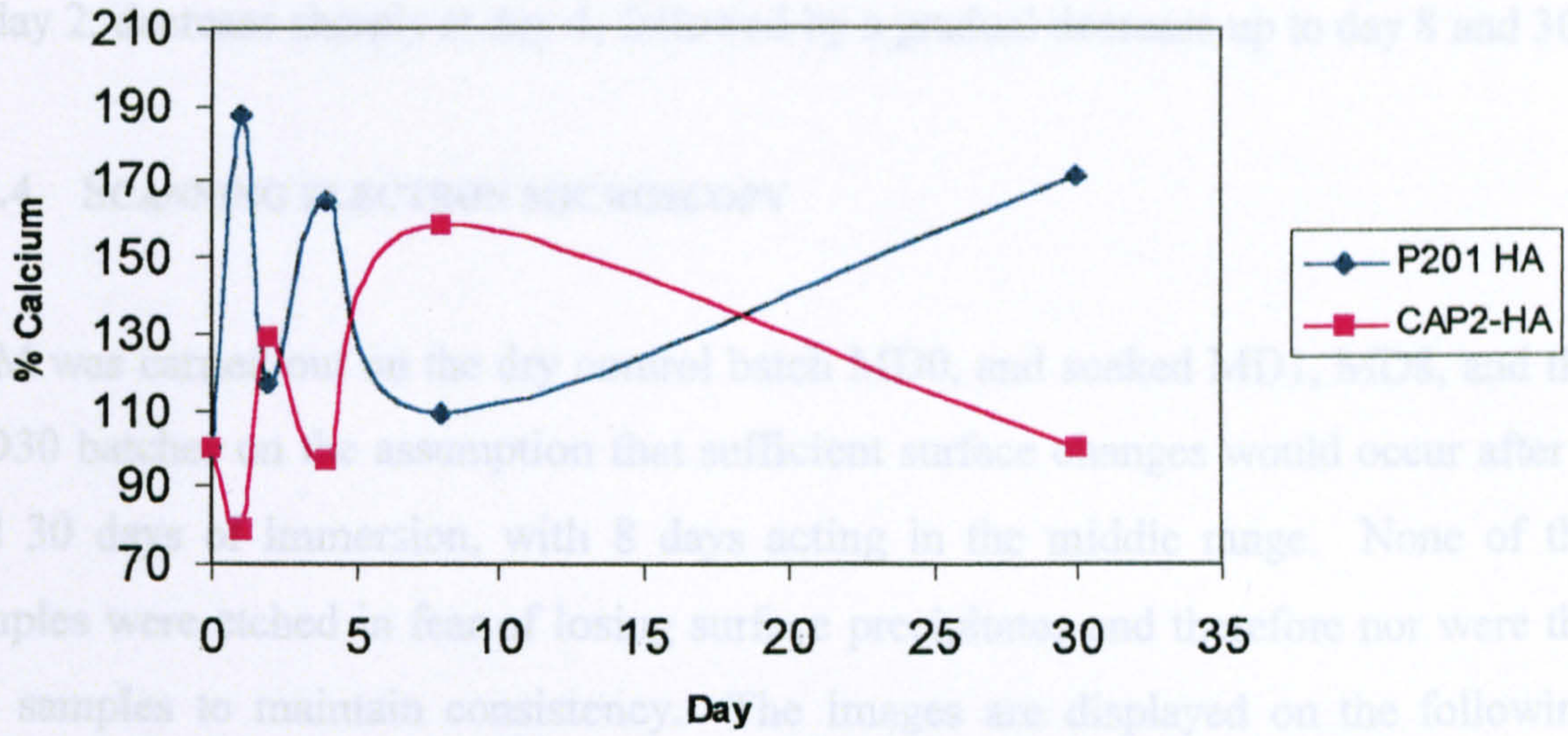


**Figure 7.3** The effect of soaking time on the Ca concentration in solution for P201 and CAP2-HA.

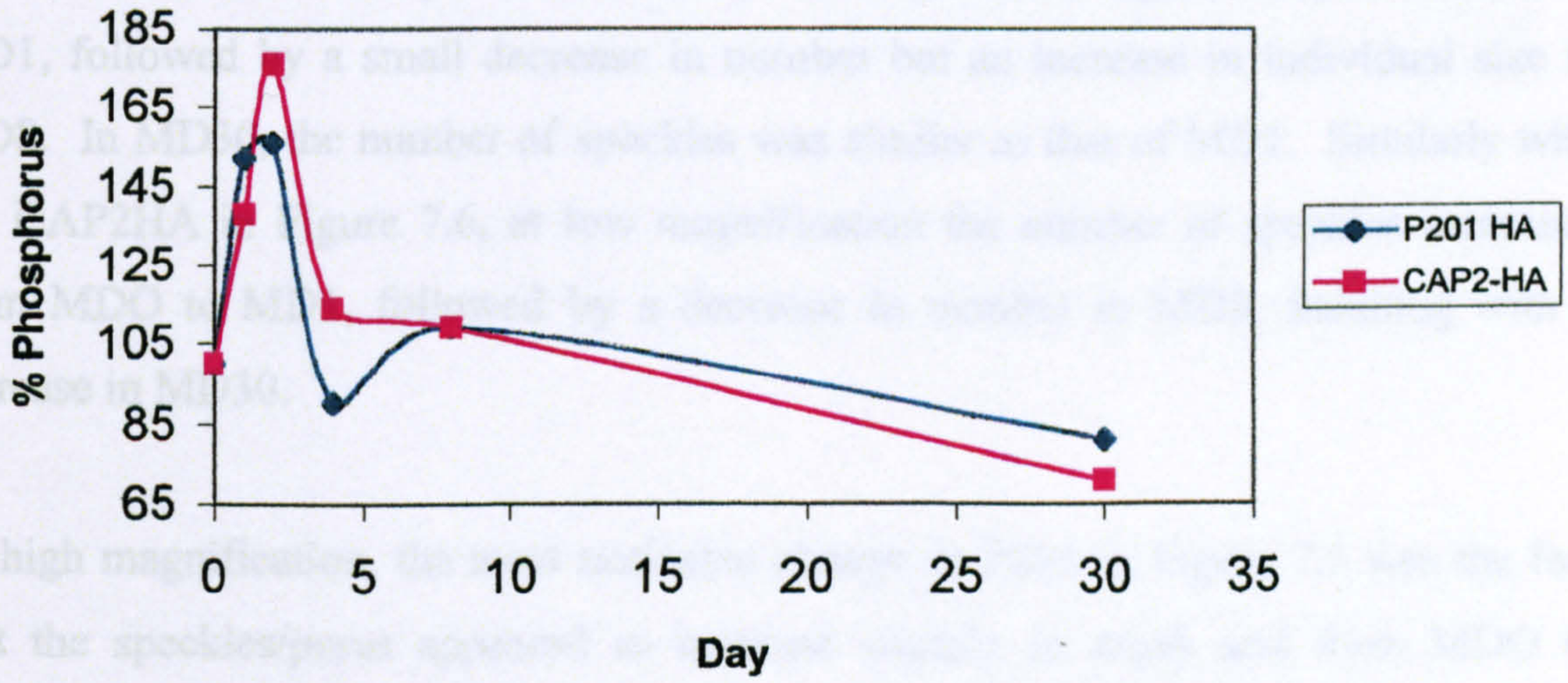


**Figure 7.4** The effect of soaking time on the P concentration in solution for P201 HA and CAP2HA.

Referring to Figure 7.3, the HA and CAP2-HA appeared to mirror-image each other almost perfectly with respect to the amount of calcium ($Ca^{2+}$) in solution. As the amount of Ca increased with regards to the HA, it decreased with regards to the CAP2-HA and vice-versa. At the end of the testing period, the release of $Ca^{2+}$ ions in solution was greatest from the HA in comparison to the CAP2-HA. The amount of phosphorus (P) in solution with regards to HA appeared to fluctuate in a similar

manner to that of CAP2-HA. Both species caused the amount of P in solution to peak at day 2, decrease sharply at day 4, followed by a gradual decrease up to day 8 and 30.

### 7.2.4 SCANNING ELECTRON MICROSCOPY

SEM was carried out on the dry control batch MD0, and soaked MD1, MD8, and the MD30 batches on the assumption that sufficient surface changes would occur after 1 and 30 days of immersion, with 8 days acting in the middle range. None of the samples were etched in fear of losing surface precipitates and therefore nor were the dry samples to maintain consistency. The images are displayed on the following pages.

The most significant structures were the white speckles/pores on the specimen surfaces. With reference to the P201 HA in Figure 7.5, at low magnification there was a small amount of speckles at MDO, which increased significantly in number at MD1, followed by a small decrease in number but an increase in individual size in MD8. In MD30, the number of speckles was similar to that of MD1. Similarly with the CAP2HA in Figure 7.6, at low magnification the number of speckles increased from MDO to MD1, followed by a decrease in number in MD8, finishing with a increase in MD30.

At high magnification, the most noticable change in P201 in Figure 7.5 was the fact that the speckles/pores appeared to increase slightly in depth and from MDO to MD30. CAP2HA in Figure 7.6 did not appear to experience these changes.

These speckles were identified in the previous investigation as areas of resorption/soluble material, i.e. α-TCP and CaO. The fluctuations seen in the amount of α-TCP present may be due to resorption/reprecipitation processes, and therefore these results must be cross-referenced with the phase composition analysis and ICPMS analysis in order to very this hypothesis.

LOW MAGNIFICATION HIGH MAGNIFICATION

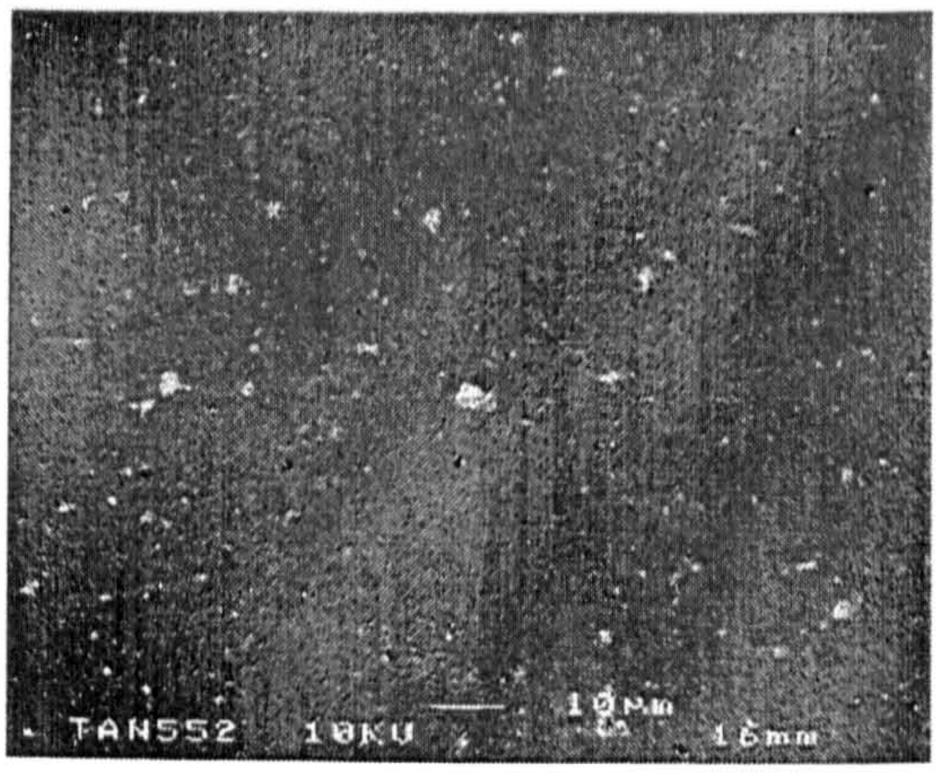


(a1)

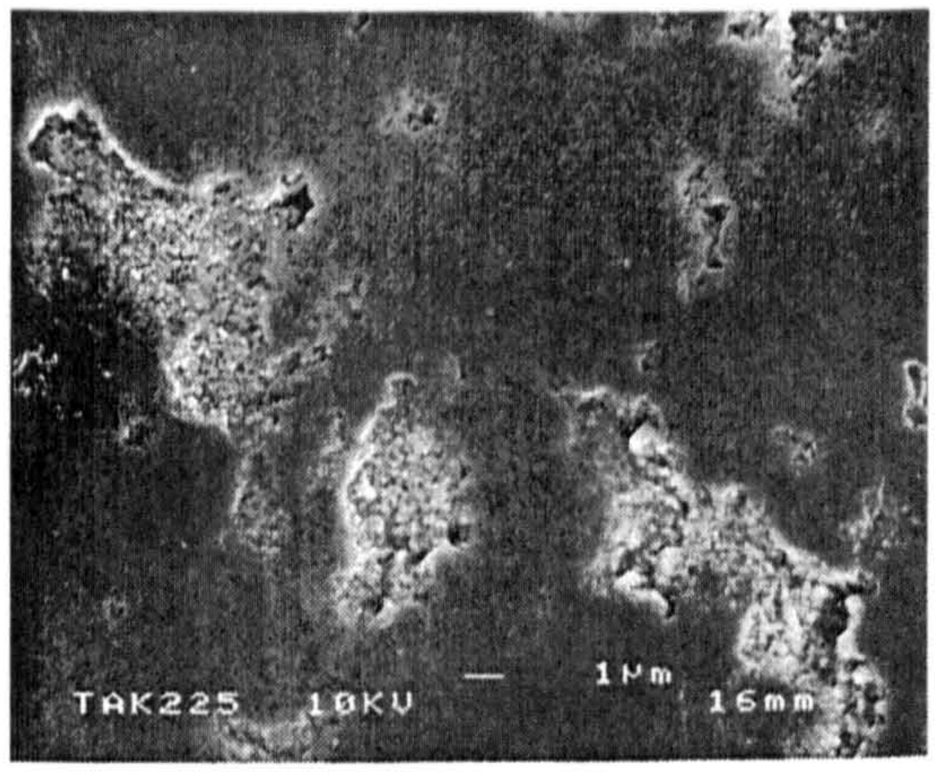


(a2)

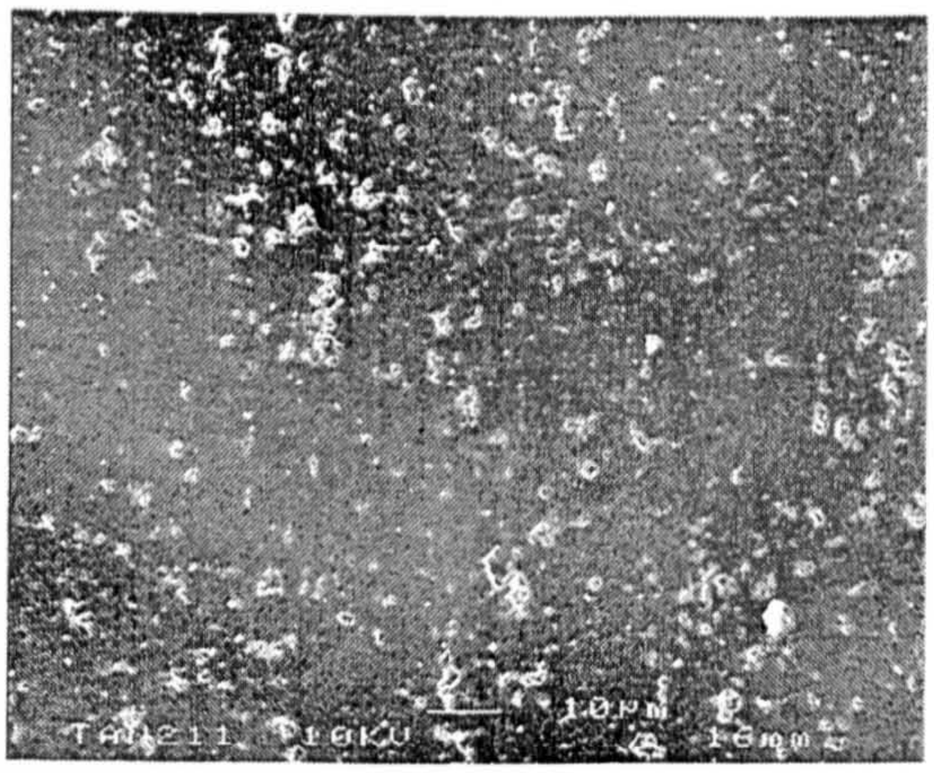


(b1)

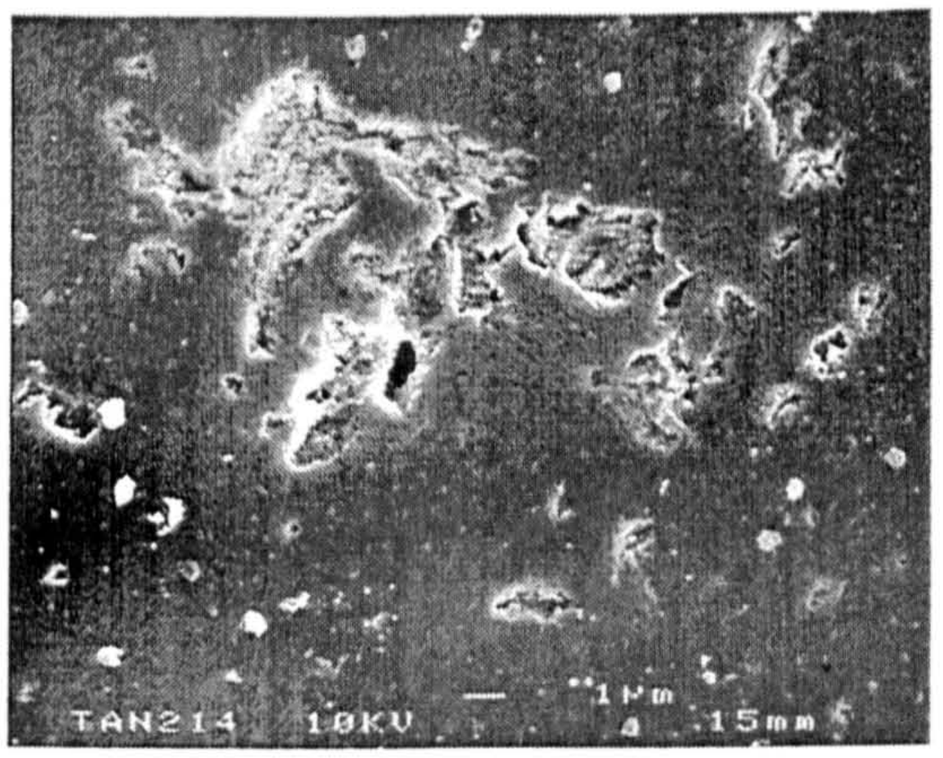


(b2)

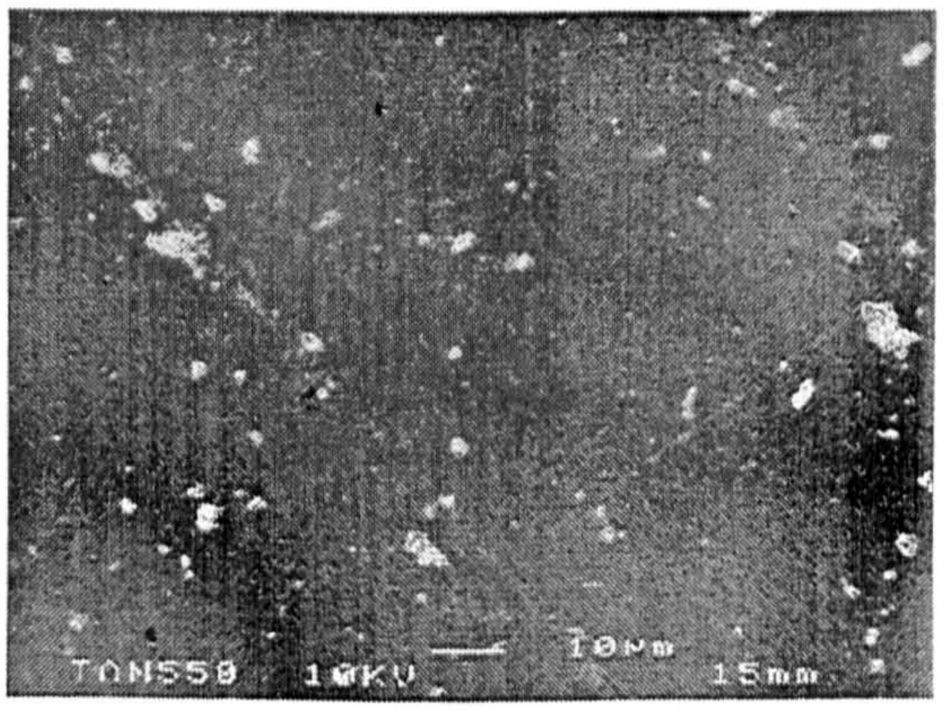


(c1)

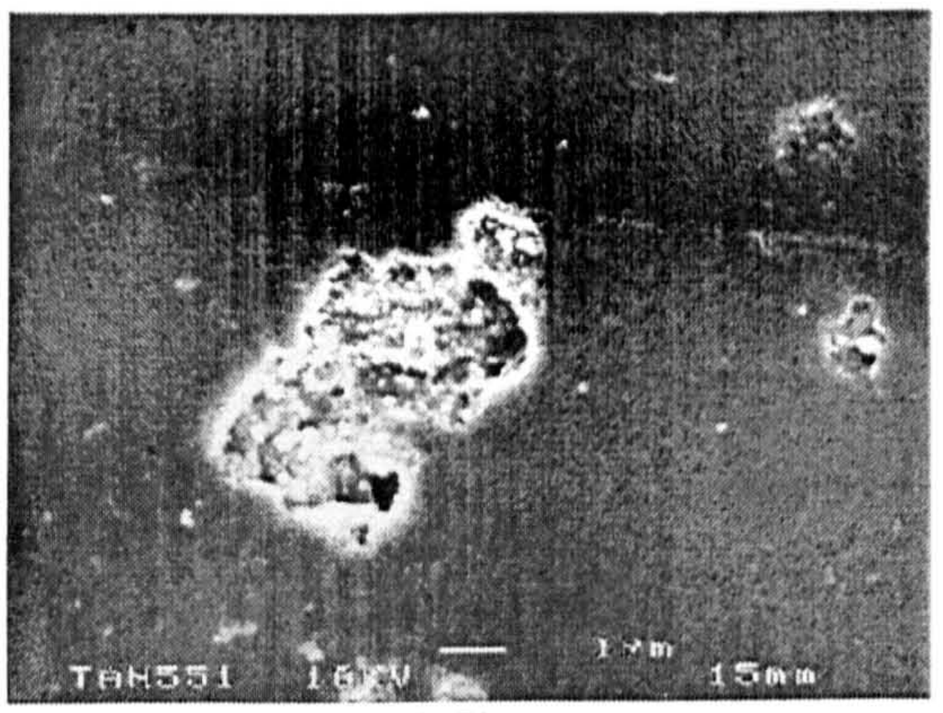


(c2)

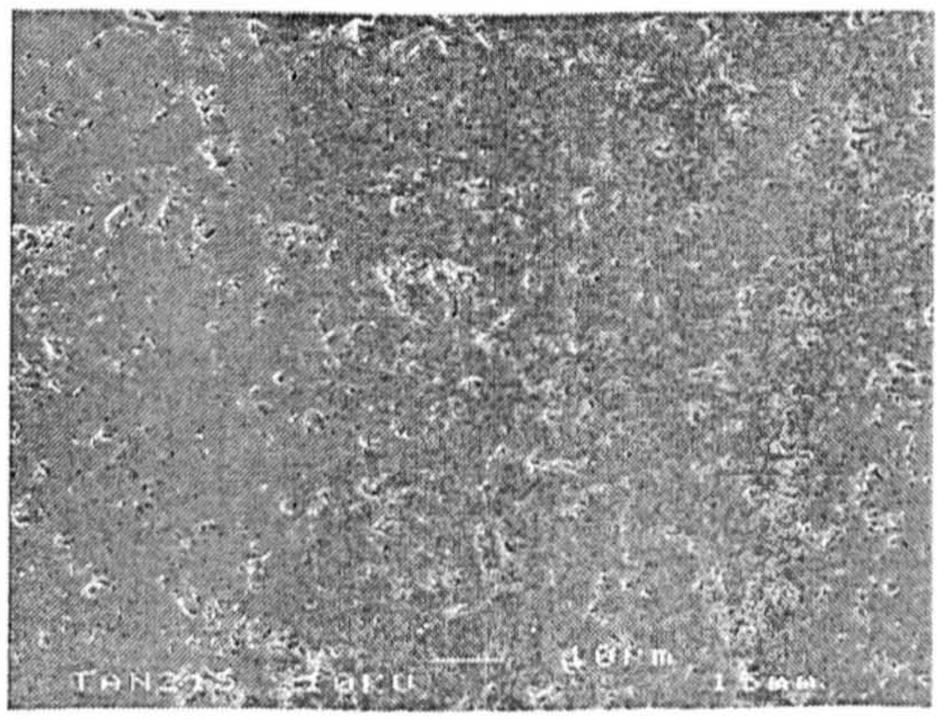


(d1)

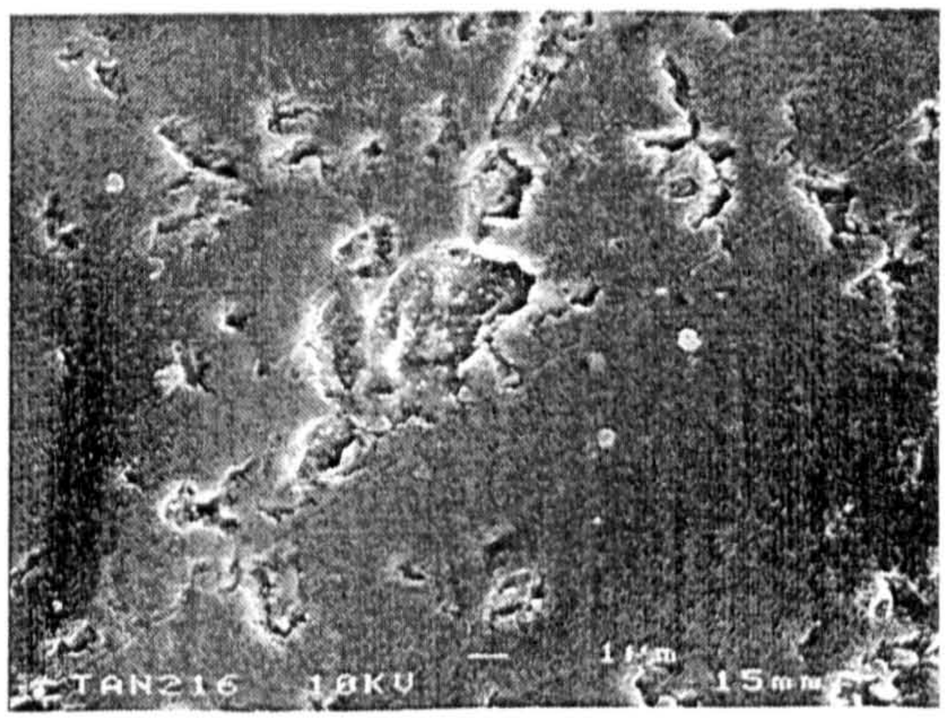


(d2)

**Figure 7.5** P201 HA in the mechanical degradation study (a) MDO (b) MD1 (c) MD8 (d) MD30

LOW MAGNIFICATION

HIGH MAGNFICATION

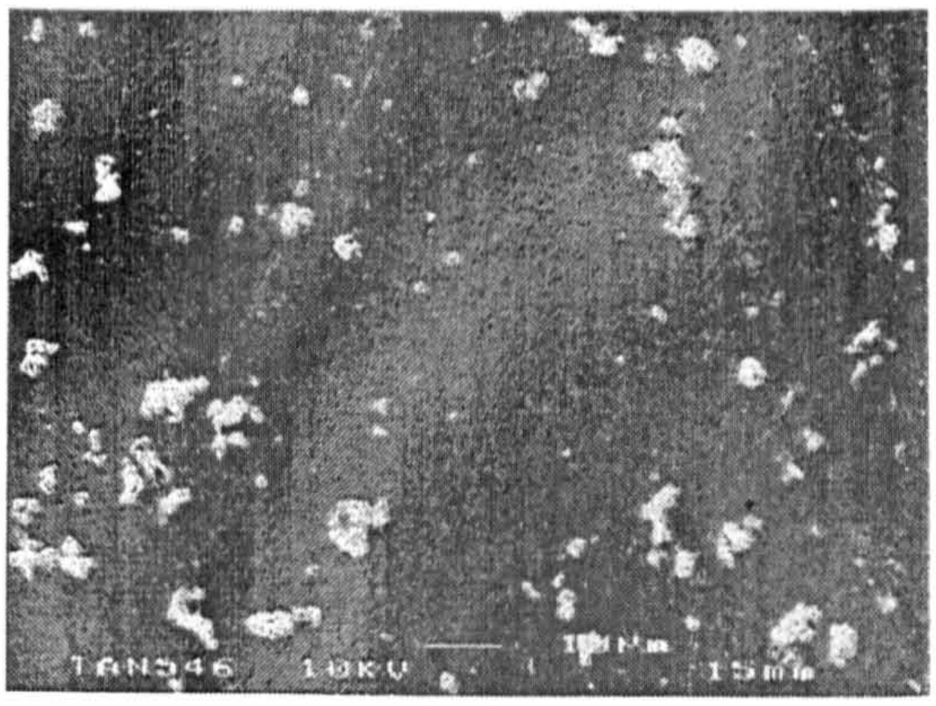


(a1)

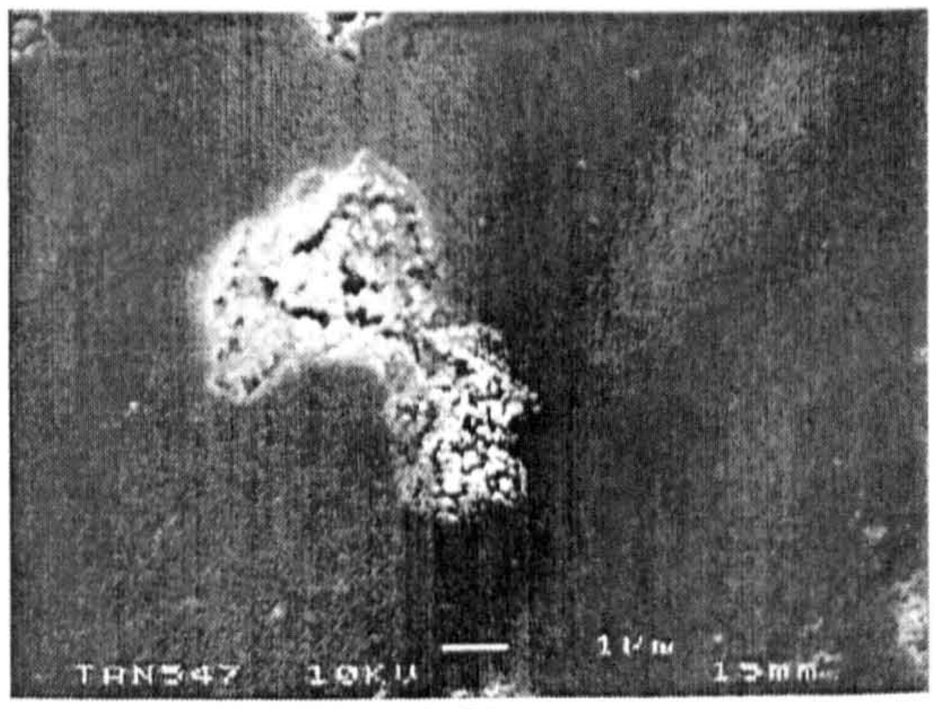


(a2)

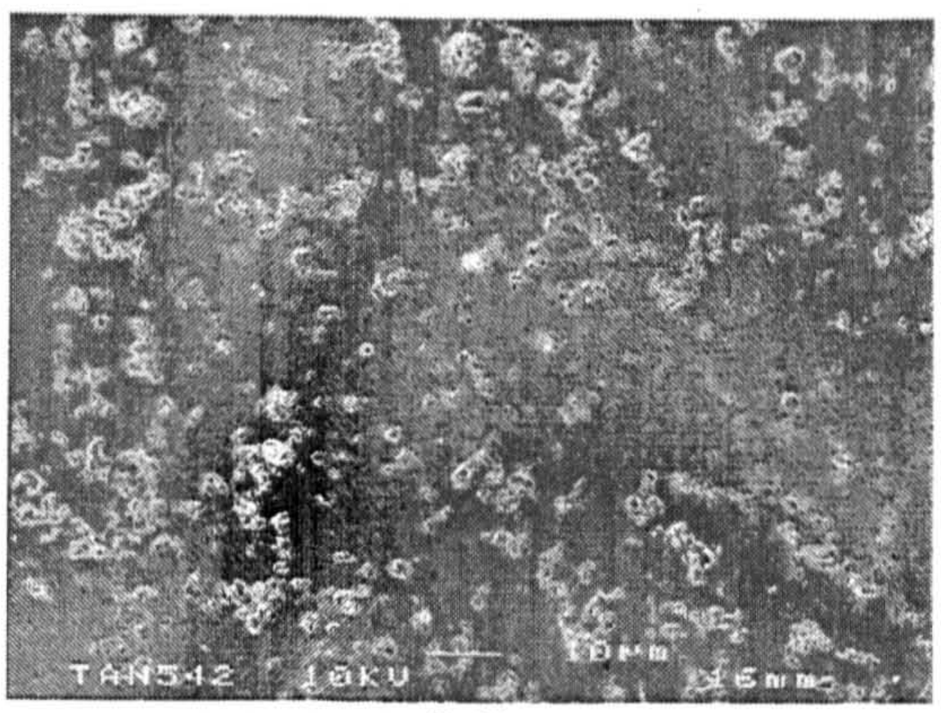


(b1)

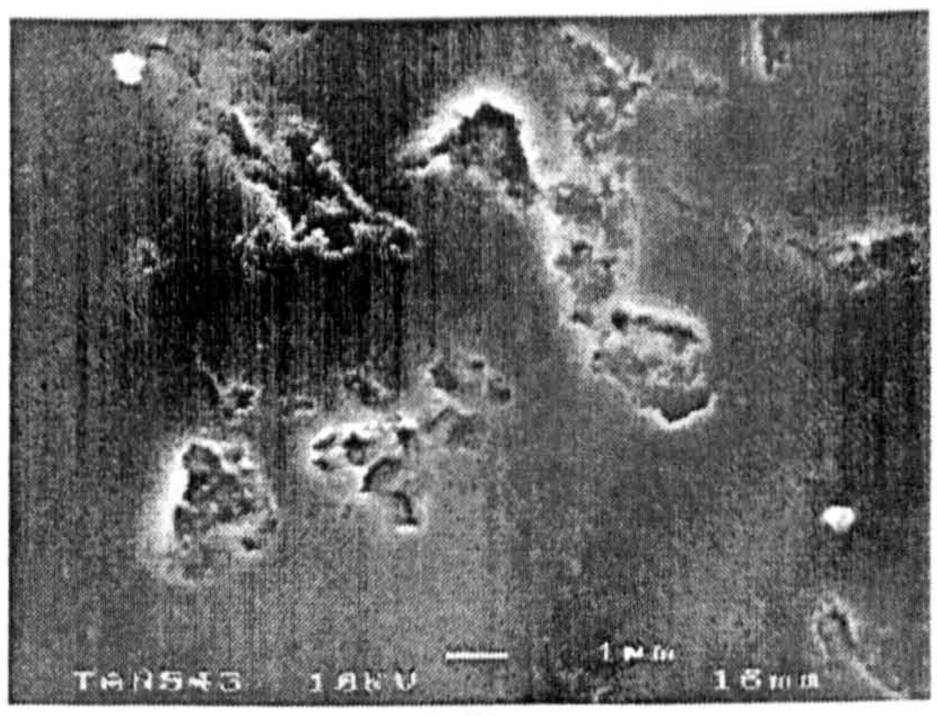


(b2)

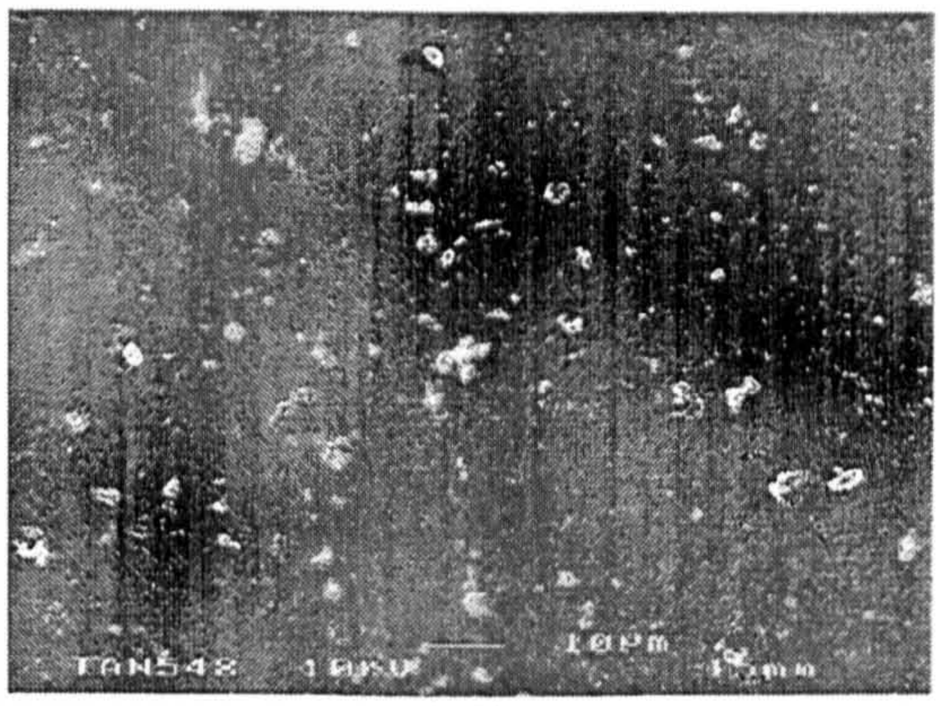


(c1)

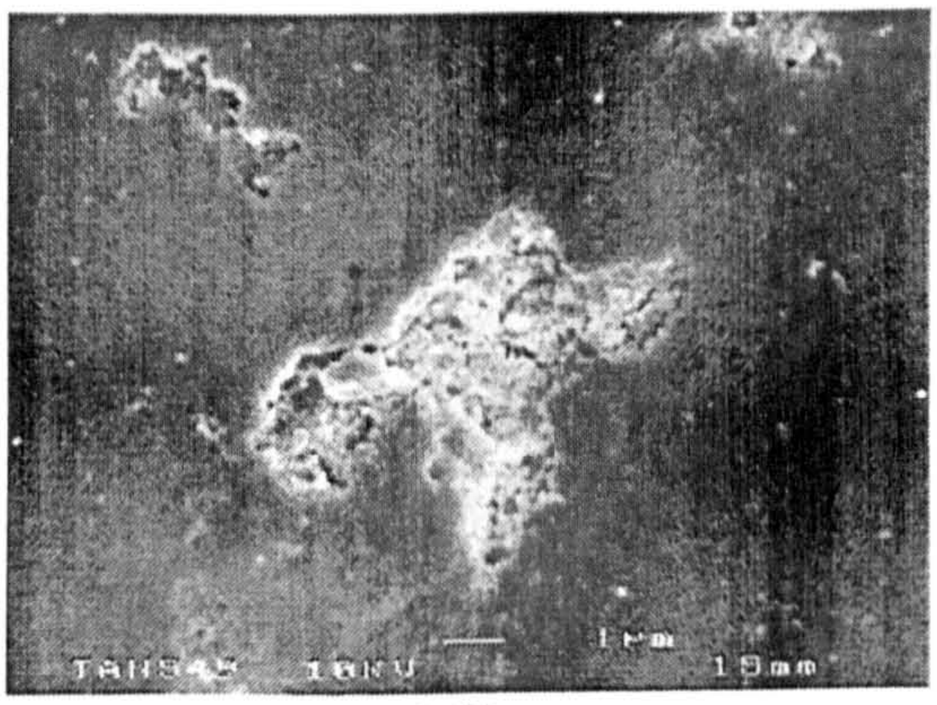


(c2)

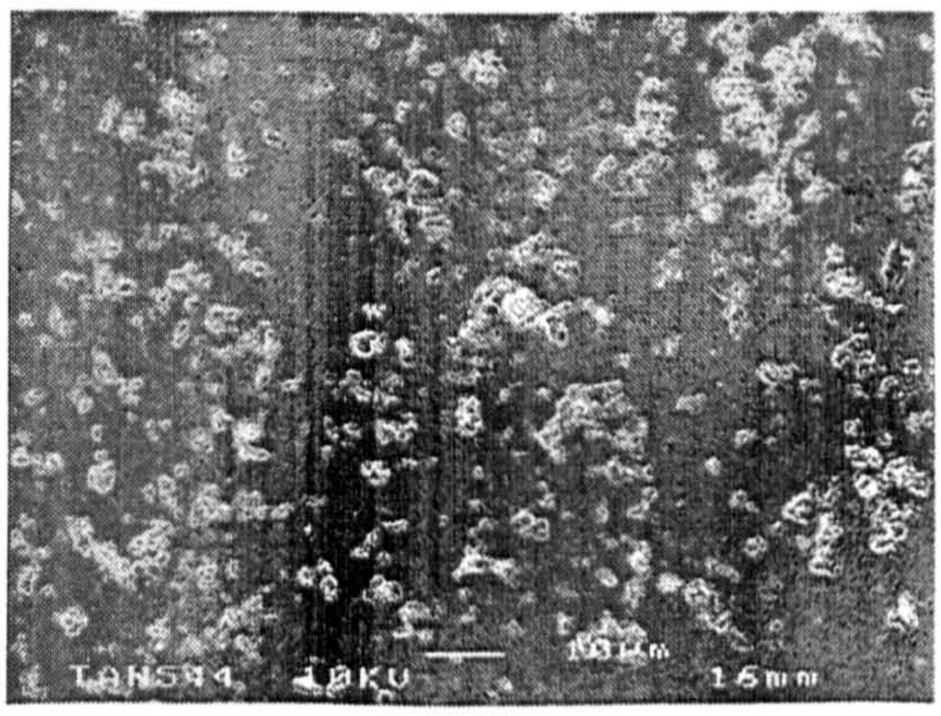


(d1)

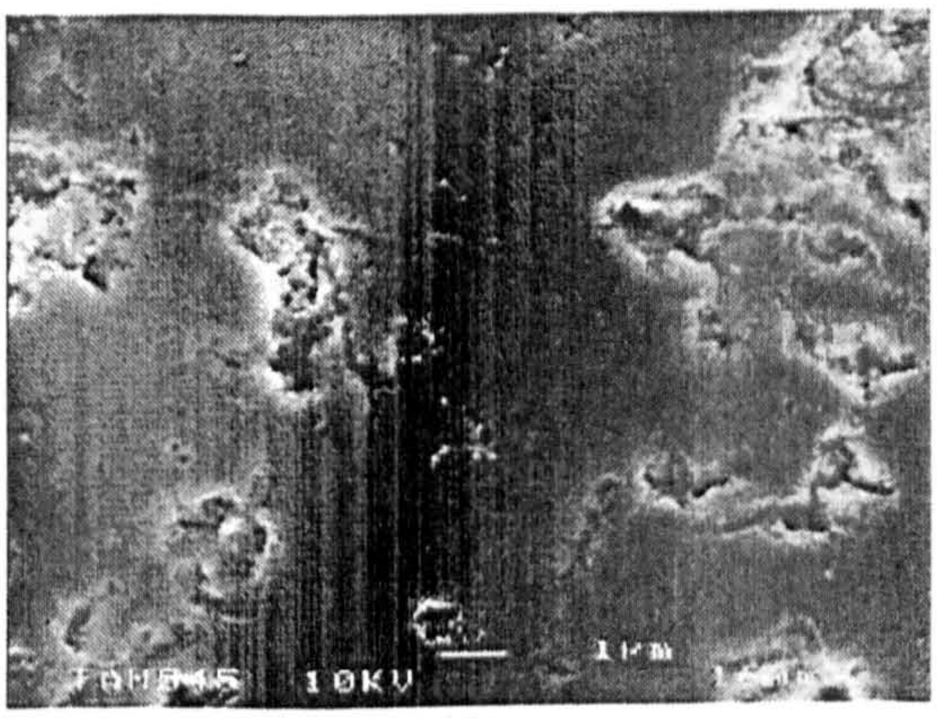


(d2)

**Figure 7.6** CAP2-HA in the mechanical degradation study (a) MDO (b) MD1 (c) MD8 (d) MD30

## 7.3 DISCUSSION

Immersing the HA and CAP2-HA in Ringer's solution (RS) over the 30 day period affected their physical and mechanical properties. The activity of the two materials in solution, in terms of loss/gain of ions, affected the mechanical properties, the effect of which was verified by microscopical analysis. Therefore, in order for the results to be explained in context, this discussion will focus on the fluctuations in the mechanical properties of the two materials, in terms of phase composition, concentration of ions in solution, and microstructure.

In the previous investigation, it was stated that there was a possible relationship between the amount of TCP present in CAP2HA and its' BFS, in that the higher the TCP content, the lower the BFS. On day 2, the CAP2-HA experienced a decrease in strength with an increase in %TCP, and on day 8, the CAP2-HA experienced an increase in strength with decreased %TCP. Furthermore, between day 8 and day 30, CAP2-HA experienced the largest increase in BFS and the largest decrease in %TCP. Therefore, one can assume that the trend between strength and %TCP has occurred again. However, on days 1 and 4, the CAP2-HA experienced decreases in strength with decreased %TCP. Furthermore, the HA also experienced a constant reduction in BFS (with an exception of day 4), despite containing no TCP (apart from day 2). The BFS strength of the HA and CAP2-HA was obviously being affected by a further factor, possibly surface dissolution/re-precipitation processes, as characterized by the results of the ICPMS and SEM.

At day 0, both the HA and CAP2-HA contained a few white speckles on their surfaces, which were confirmed, by higher magnification, to be slightly concave areas, i.e. surface pores. At day 1, there was a huge increase in the number of pores in both the HA and CAP2-HA, which meant that something from their surfaces was dissolving in solution. The ICPMS data revealed that at day 1, the P201 released both Ca and P into solution, whereas the CAP2-HA only released P into solution, and gained Ca. This should not be interpreted as HA being more resorbable than CAP2-HA, but rather because the CAP2-HA contained more TCP to begin with, after being soaked in solution, the TCP in CAP2-HA immediately was released into solution and re-precipitated back onto the CAP2-HA as a relatively Ca-rich apatitic layer, as

indicated by the loss of Ca from solution. This is consistent with the findings of Knabe et al (1997) and Zyman et al (1998), who found that some bioactive ceramics form Ca-rich surfaces following implantation, which provide a bonding interface with tissues, and may further facilitate osteoblastic growth. In terms of the mechanical properties, the increase in the number of pores explain the loss of strength, because they acted as stress-raisers, thereby decreasing the stress required to propogate cracks through the specimens.

Unfortunately, micrographs were not taken of the MD2 and MD4 specimens for reasons explained in section *7.2.3*. However, with regards to the HA, because the BFS decreased at day 2 and increased at day 4, one can assume that the amount of surface pores increased at day 2 and decreased at day 4. Similarly with CAP2-HA, the BFS decreased at day 2 and continued to decrease at day 4, which indicates a gradual increase in surface porosity from day 1 to day 4.

Porosity was explained previously as a function of ion release. At day 2, the P201 released more P, but gained Ca. This dissolution behaviour was reminiscent of CAP2-HA at day 1, which indicated that the HA was not dissolving at the same rate as CAP2-HA, and was in fact one day behind in terms of the dissolution/re-precipitation which CAP2-HA experienced at day 1. In fact, the delayed dissolution behaviour of Ca with regards to the HA explained the mirror image seen in Figure 7.3, whereby on the days that CAP2-HA gained Ca, the HA released Ca in solution. This behaviour highlighted the difference in dissolution between bioceramics that contain resorbable Ca-P materials, such as TCP, in comparison to bioceramics that are much less soluble, such as HA.

At day 8, the microstructure of the HA revealed a slightly larger amount of surface porosity to that of the HA at day 0 (control); accordingly, the BFS (8.761.56 MPa) was slightly lower than that at day 0 (10.93±1.06 MPa). The CAP2-HA displayed a similar amount of surface porosity to that of day 1, the difference being the size of the pores at day 8 were smaller than that of day 1; accordingly, the BFS of day 1 and day 8 were very similar; 68.74±17.99 MPa and 69.07±11.54 MPa, respectively. The HA

released P into solution and gained Ca at this point, whilst CAP2-HA released both ions into solution.

At day 30, the HA displayed its' weakest BFS (6.54±1.68 MPa) throughout the testing period as well as the most surface porosity. There appeared to be inverse relationship between strength and porosity, in that the strength decreased when the specimens displayed more surface porosity. However, the same assumption could not be applied to CAP2-HA, because at day 30, a BFS of 76.2±37.62 MPa was obtained, despite the specimen surface containing a similar amount of porosity to the specimen at day 1, which had a BFS of 68.74±17.99 MPa. However, the CAP2-HA contained some TCP throughout the 30 day period, regardless of fluctuations, and because the changes in strength did not always correspond with the surface porosity, it is possible that the CAP2-HA maintained mechanical integrity due to the presence of TCP.

In Chapter 6, CAP1-HA experienced far more decomposition during sintering, and displayed weaker mechanical properties to the CAP2-HA, which displayed much less decomposition. However, the CAP1-HA was much more porous than the CAP2-HA, which attributed to its' poor mechanical properties. It is possible that the presence of TCP, combined with the effects of the liquid-assisted sintering process instigated by the addition of CAP2, enhanced the mechanical properties of HA. Calcium-deficient ceramics like TCP have been previously reported (Akao et al, 1982) (Raynaud et al, 1998) (Furakawa et al, 2000) to display superior mechanical properties to Ca/P ceramics with a Ca/P ratio of 1.67 (such as HA).

Regardless of the reported mechanical properties of TCP, it is not ideal to create a bone substitute material which solely consists of TCP, because TCP is extremely resorbable, as pointed out in the literature, and as proven by the dissolution rate of CAP2-HA during its' first day in solution. If the substitute material dissolves too quickly in the first 24 hours of implantation, any form of mechanical stress, be it large or small, will be detrimental to the mechanical integrity of the system because there will be less material to absorb the stress.

Thus, the presence of TCP caused the CAP2-HA to be more resorbable in physiological solution than P201 HA, however it was still the stronger species, pre- and post-soaking. The commercial HA also experienced some resorption; however this behaviour was believed to be primarily due the presence of CaO as detected in the investigation in Chapter 5. The CAP2-HA proved to be more ideal for bone substitution than the HA (even though the RI-TCP in the CAP2-HA was initially < 20%), because at the end of the 30 day period, not only was it much stronger than the HA, but it retained more strength.

# CHAPTER 8

# INVESTIGATION INTO THE PRODUCTION OF POROUS HA AND POROUS CAP2-HA

## 8.1 CHARACTERIZATION OF POROUS P201 HA

This investigation was divided into two sections. First, a pilot study was carried out in order to find the optimum sintering conditions of porous P201 HA (pHA) in terms of physical/mechanical properties. Once the optimum sintering conditions were established, another study was carried out in order to repeat production/characterization at this temperature. For both studies, each batch contained 5 samples.

### 8.1.1 PILOT STUDY

Porous P201 HA was initially produced via the burn-out method YU foam (IRC in Biomedical Materials, UK), as detailed in section *4.3.4*. In order to determine the sintering temperature that resulted in optimum mechanical properties, the foams were sintered at a range of temperatures,i.e. 1200°C, 1250°C, and 1300°C.

#### 8.1.1.1 X-Ray Diffractometry

As with the dense P201, the results of the X-ray diffractometry showed no evidence of α– or β-TCP at 1200°C, 1250°C, or 1300°C.

### 8.1.1.2 Mechanical Properties

The results of the mean density, porosity, and ultimate compressive strength (UCS) measurements are displayed in Table 8.1, and Figures 8.1-8.3 (mean values) and Figure 8.4 (all values).

**Table 8.1** Porosity, density, and strength measurements for pHA sintered at different temperatures

| Materials | Sintering Temperature (°C) | Mean Total Porosity (%) | Mean Closed Porosity (%) | Mean Apparent Density ($g.cm^{-3}$) | Mean UCS (MPa) |
|---|---|---|---|---|---|
| HA slurry YU foam | 1200 | 72.13 ± 5.89 | 13.09 ± 1.02 | 0.88 ± 0.19 | 1.29 ± 0.18 |
| HA slurry YU foam | 1250 | 66.67 ± 1.79 | 10.09 ± 0.45 | 1.05 ± 0.06 | 1.76 ± 1.00 |
| HA slurry YU foam | 1300 | 64.24 ± 2.54 | 12.72 ± 0.42 | 1.13 ± 0.08 | 2.85 ± 0.51 |

Preliminary mechanical tests showed that the UCS of the pHA increased with increasing sintering temperature (Figure 8.1), yet the actual values were very low compared to that of the dense HA characterized in Chapter 5. This was expected due to the macroporous structure of the specimens. Similarly to the strength, the densities of the pHA appeared to increase with increasing temperature (Figure 8.2). The sintering temperature of pHA that corresponded to the highest UCS/apparent density was 1300°C.

The total porosity of the pHA decreased with increasing sintering temperature, whilst the closed porosity increased slightly from 1200°C to 1250°C, followed by a slight decrease from 1250°C to 1300°C, as seen in Figure 8.3. Figure 8.4 shows that as the total porosity of the pHA increased, the UCS decreased. The strongest batch (sintered at 1300°C) displayed the lowest porosity.

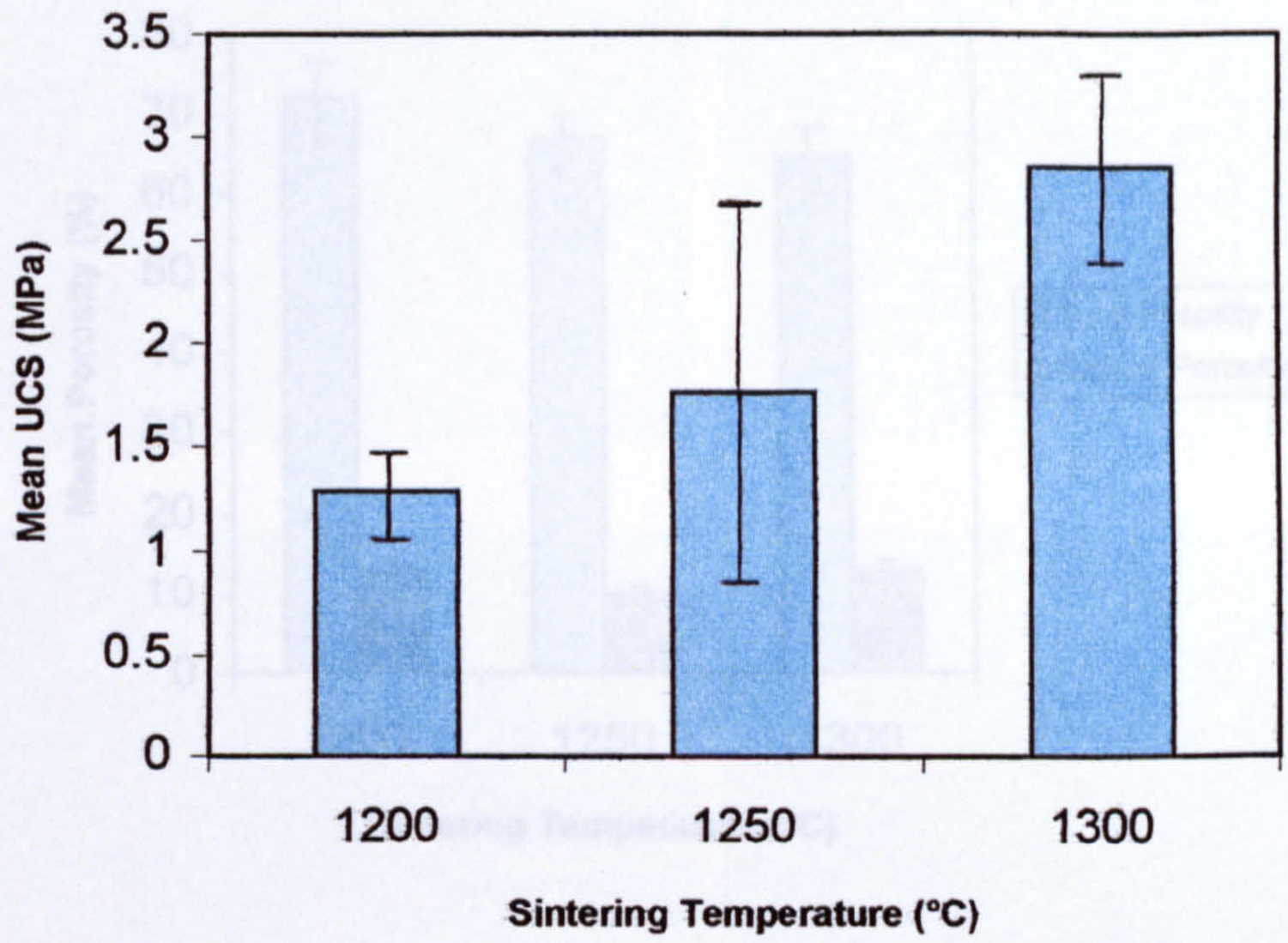


**Figure 8.1** The effect of sintering temperature on the UCS of pHA

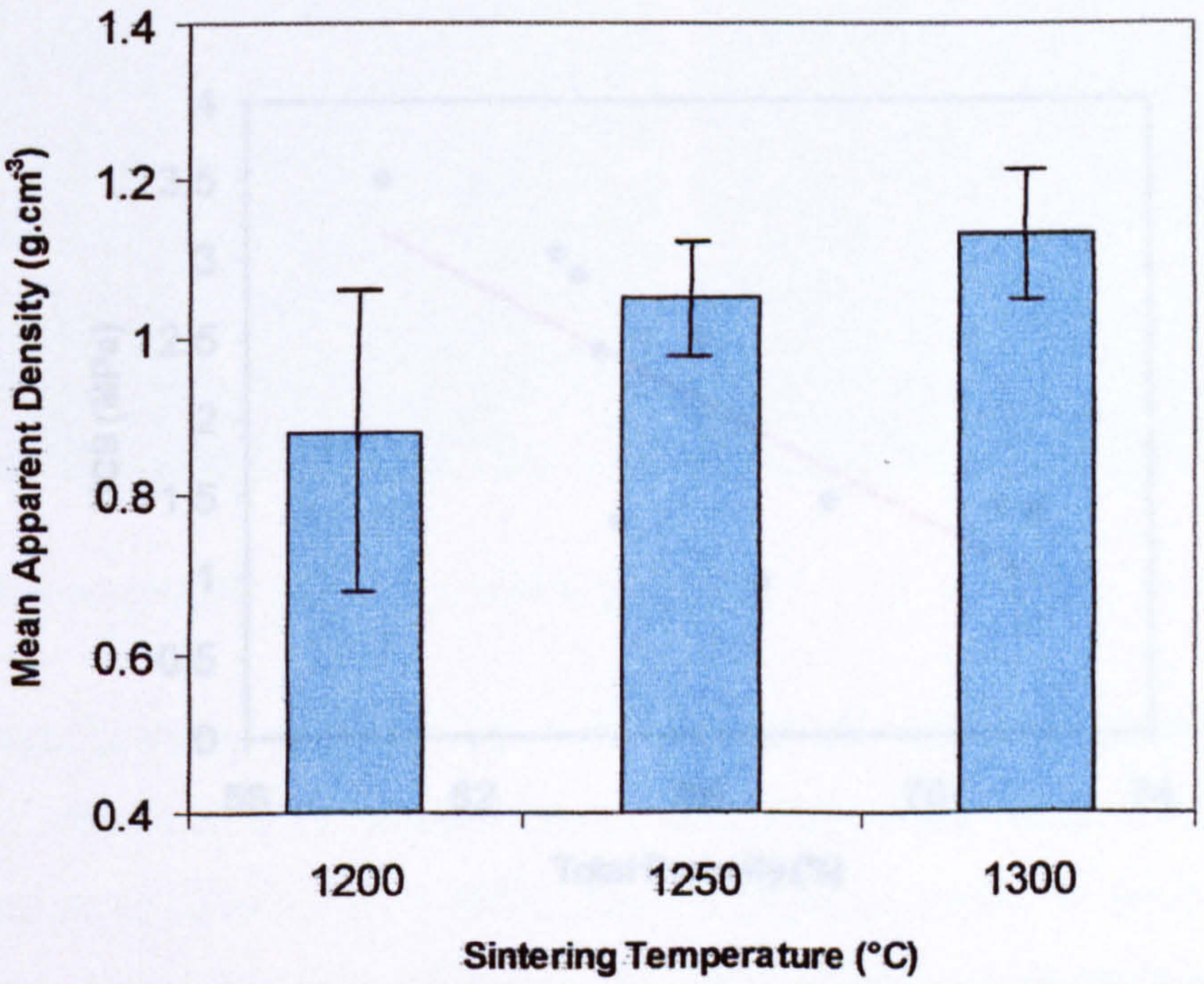


**Figure 8.2** The effect of sintering temperature on the apparent density of pHA

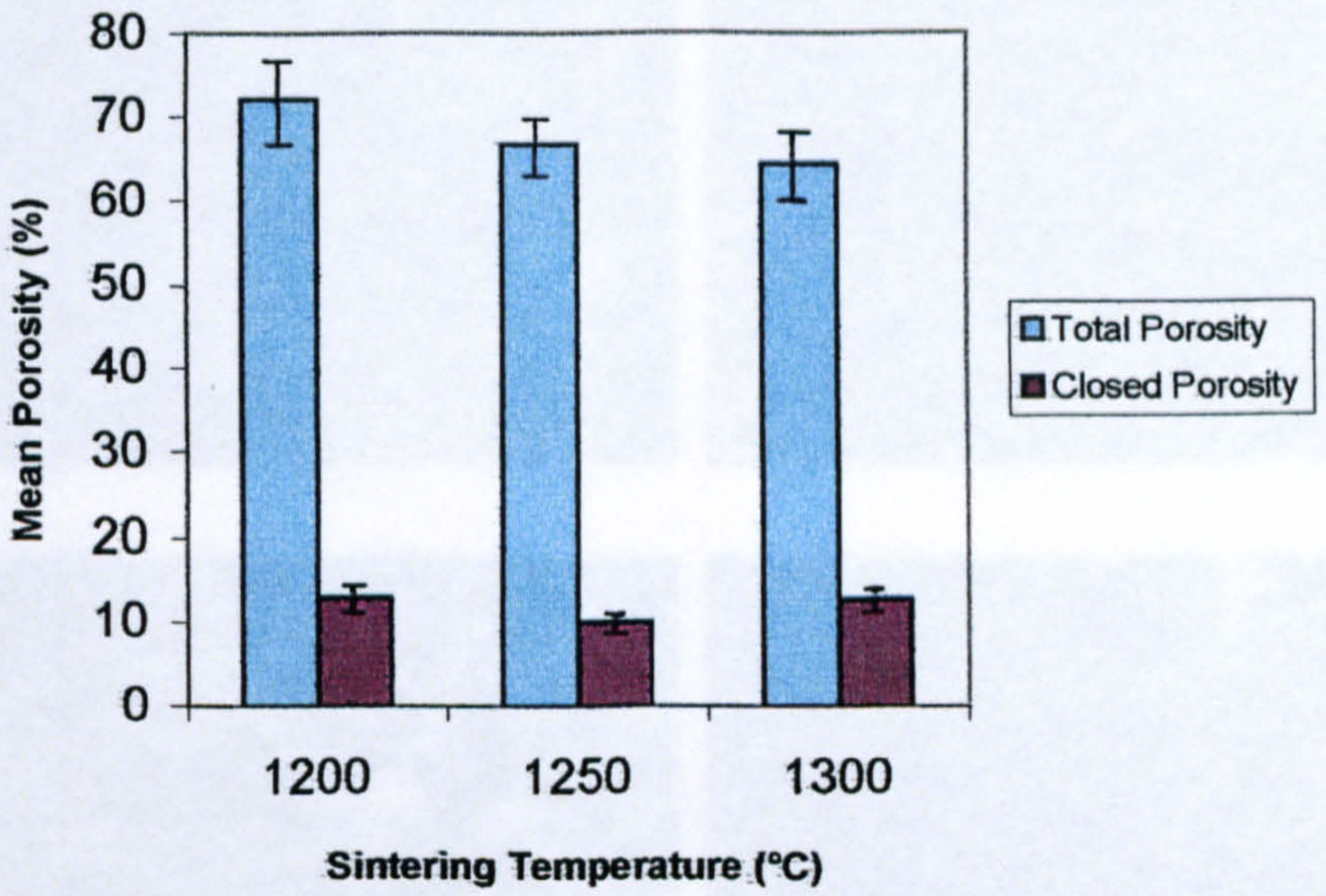


**Figure 8.3** The effect of sintering temperature on the porosity of pHA

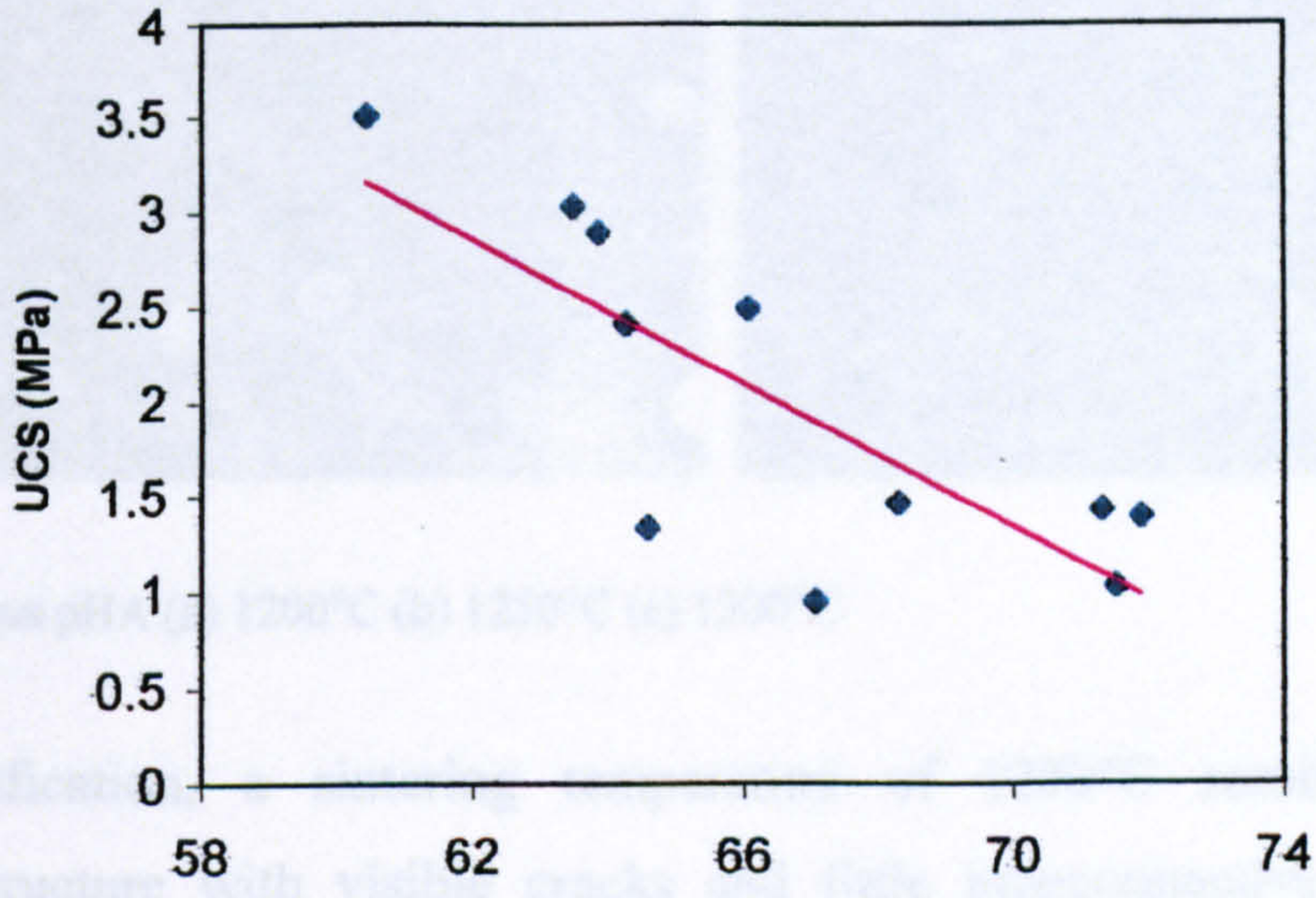


**Figure 8.4** The relationship between strength and total porosity for all pHA specimens

### 8.1.1.3 SCANNING ELECTRON MICROSCOPY

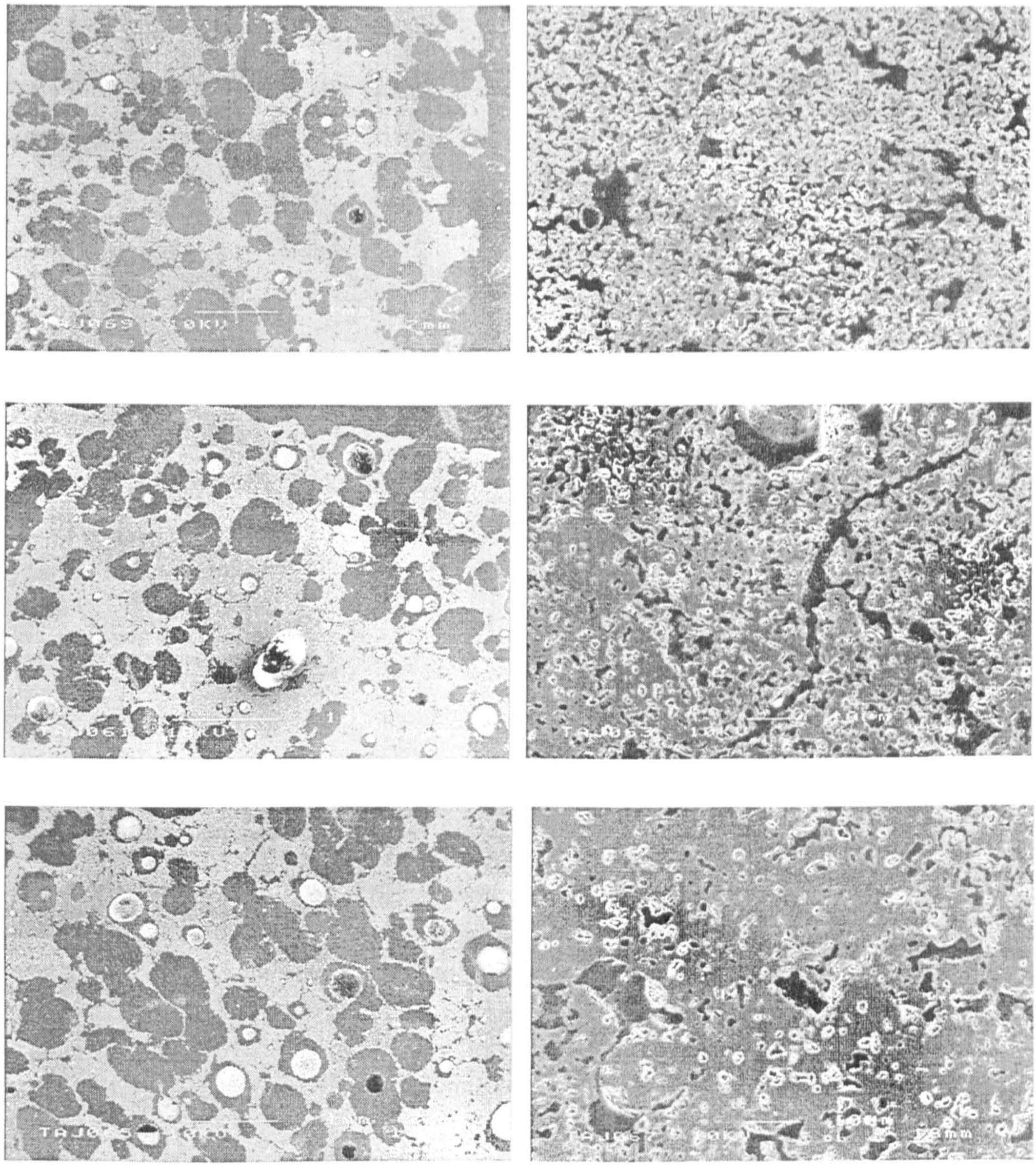


**Figure 8.5** Porous pHA (a) 1200°C (b) 1250°C (c) 1300°C

At low magnification, a sintering temperature of 1200°C resulted in a highly macroporous structure with visible cracks and little interconnective porosity, which remained similar at 1250°C. At 1300°C, the macropores appear to have a more uniform size and shape. At higher magnification, the pHA struts sintered at 1200°C and 1250°C both displayed large amounts of microporosity, yet there was an apparent reduction in microporosity at a sintering temperature of 1300°C.

### 8.1.2 STUDY AT OPTIMAL SINTERING CONDITIONS

From the pilot study, it was evident that the pHA sintered at 1300°C displayed optimal mechanical properties, therefore on this basis the following investigation was carried out at this sintering temperature.

#### 8.1.2.1 X-Ray Diffractometry

The results of the x-ray diffraction showed no evidence of α- or β-TCP in the porous pHA produced using the YU (IRC in Biomedical Materials) or the BU (Foam Engineers Ltd., UK) foam.

#### 8.1.2.2 MECHANICAL PROPERTIES

In this study, YU and BU foams were used in the burn-out technique at the optimal sintering temperature (1300°C). Two batches, containing 5 specimens each, were produced for each foam type. The results of the mean porosity, density, and strength measurements are displayed in Table 8.2, and illustrated in Figures 8.6 and 8.7.

**Table 8.2** Porosity, density, and strength measurements for pHA using YU and BU foam

| Materials | Sintering Temperature (°C) | Mean Total Porosity (%) | Mean Closed Porosity (%) | Mean Apparent Density ($g.cm^{-3}$) | Mean UCS (MPa) |
|---|---|---|---|---|---|
| HA slurry YU foam | 1300 | 68.99 ± 6.72 | 17.99 ± 5.63 | 0.98 ± 0.21 | 2.19 ± 1.20 |
| HA slurry BU foam | 1300 | 68.52 ± 2.11 | 11.06 ± 1.69 | 0.99 ± 0.06 | 1.29 ± 1.02 |

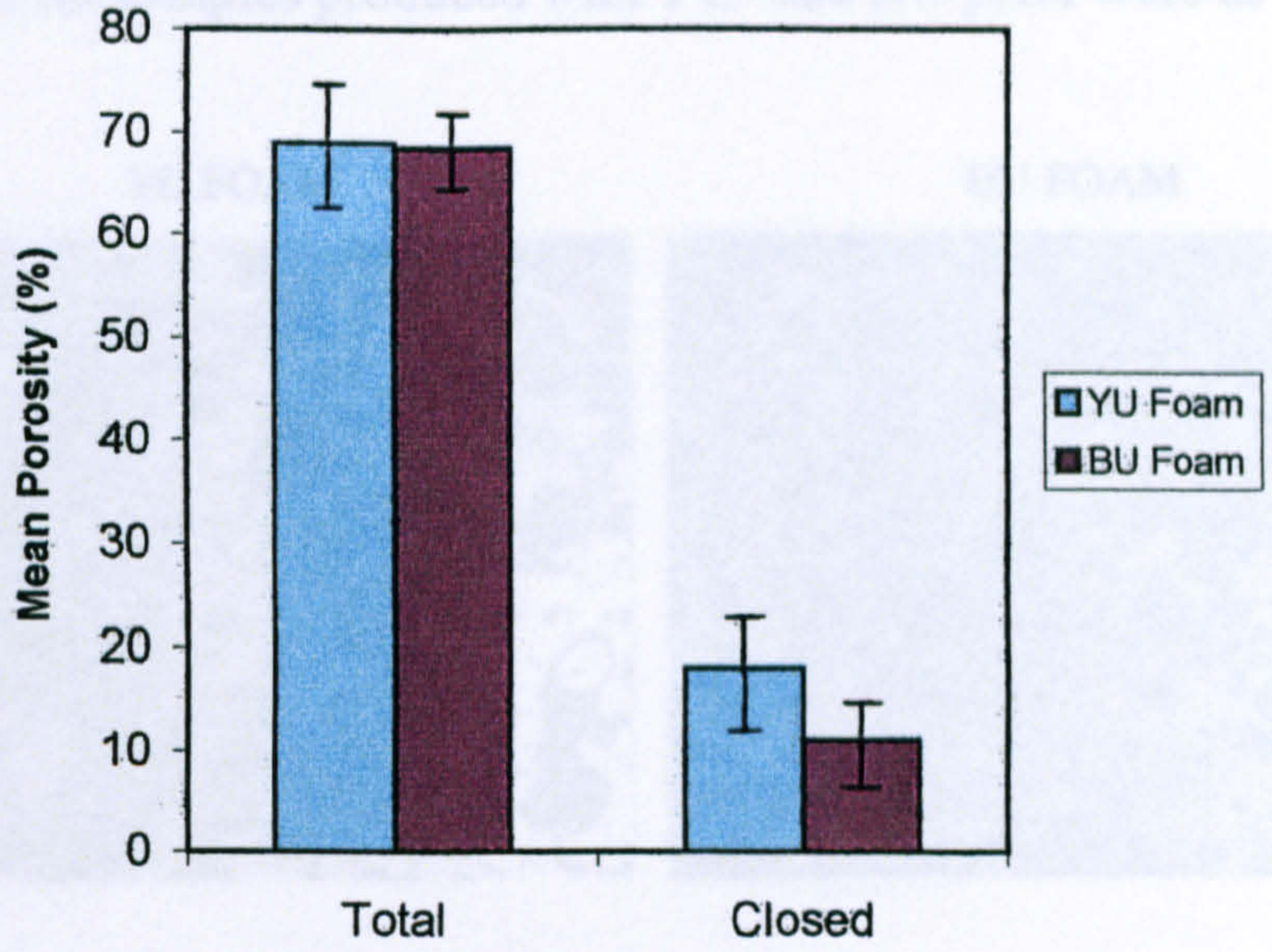


**Figure 8.6** A comparison of the total/closed porosity between pHA made with YU and BU foam.

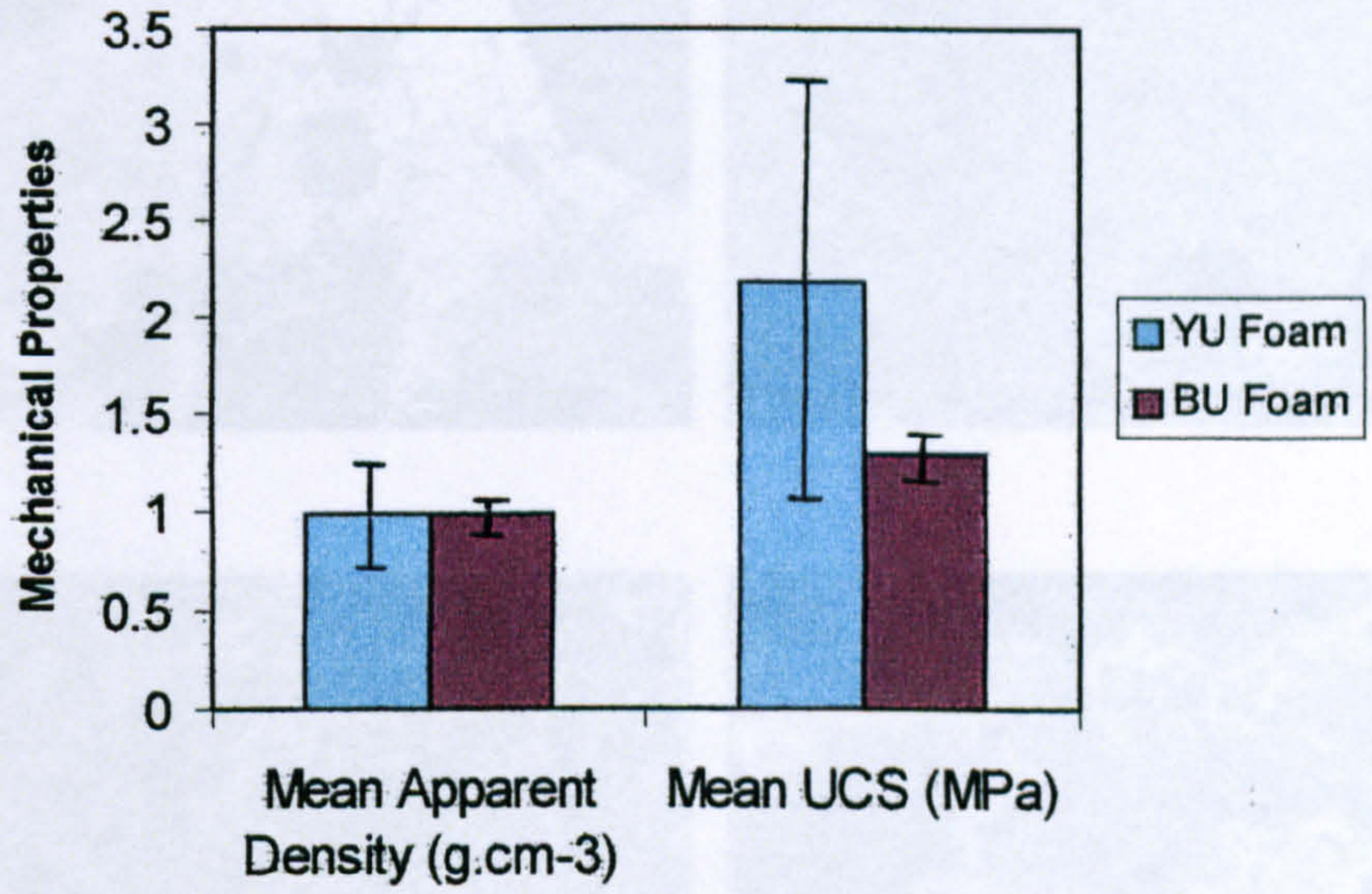


**Figure 8.7** A comparison of the density/strength of pHA made with YUand BU foam

Referring to Figure 8.6, the use of YU foam as a polymeric pre-cursor resulted in pHA having similar total porosity, higher closed porosity. The mechanical properties in Figure 8.7 show that despite having similar densities, the pHA produced with YU foam (YU-pHA) was stronger.

### 8.1.2.3 SCANNING ELECTRON MICROSCOPY

SEM analysis of the samples produced with YU- and BU-pHA were as follows:

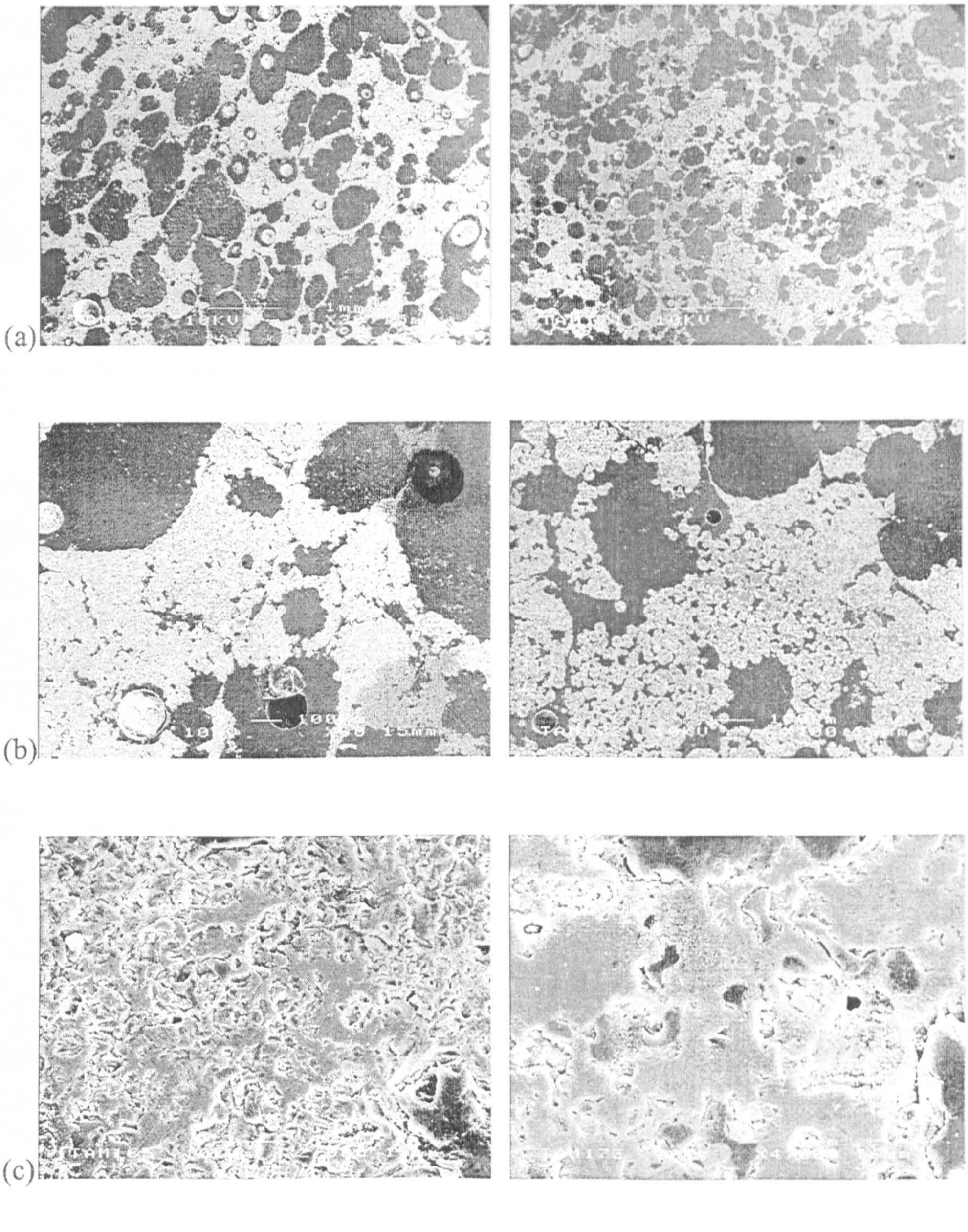


**Figure 8.8** YU-/BU-pHA sintered at 1300°C

In Figure 8.8, image (a) showed that YU-pHA macrostructurally contained pores of various sizes with some interconnectivity, whilst there appeared to be more macroporosity in the BU-pHA, and the BU foam pores were also slightly smaller, referring to the micron bar. At medium magnification in image (b), there appeared to be some porosity within the struts of YU-pHA, as well as some darker regions of interest in the bottom right of the micrograph. At this magnification, BU-pHA revealed more microporosity within the struts; there was much better densification in YU-pHA than in BU-pHA. Image (c) revealed that at high magnification, both YU-pHA and BU-pHA contained considerable porosity, as indicated by the concave regions, much like the dense HA reported in Chapter 5.

## 8.2 CHARACTERIZATION OF REINFORCED POROUS HA

After extensive analysis of the dense materials in Chapter6, the dense CAP2-HA appeared to have the strongest dry mechanical properties in comparison to the dense HA; hence, for the purpose of this study, porous CAP2-HA (pCAP2-HA) was also produced and characterized. Each batch reported in sections 8.2.1 and 8.2.2 contained five samples.

### 8.2.1 PILOT STUDY

As with the pHA, a preliminary study was carried out using YU foam (to produce YU-pCAP2-HA) in order to determine the sintering temperature which corresponded to the highest mechanical strength; the batches were sintered at 1250°C, 1300°C, and 1350°C. Unfortunately, no analysis was carried out on the batch sintered at 1250°C, because the samples disintegrated in the furnace, possibly due to lack of densification.

### 8.2.1.1 X-Ray Diffractometry

X-ray diffraction of the two batches (Table 8.3) showed that the RI-TCP (α) increased with increasing sintering temperature. This indicated that at 1350°C, the pCAP2-HA would be more resorbable than at 1300°C, which is undesirable for high load-bearing applications. However,these results must be balanced against the mechanical criteria in selection of the optimal sintering temperature.

**Table 8.3** Effect of sintering temperature of the RI-TCP of pCAP2-HA

| Sintering Temperature (°C) | RI-TCP (%) |
|---|---|
| 1300 | 21 |
| 1350 | 38 |

### 8.2.1.2 Mechanical Properties

The results of the mean porosity, density, and strength measurements are displayed in Table 8.4 and the mean values illustrated in Figures 8.9 to Figure 8.11, with all values used in Figure 8.12.

**Table 8.4** Porosity, density, and strength measurements for pCAP2-HA sintered at different temperatures

| Materials | Sintering Temperature (°C) | Mean Total Porosity (%) | Mean Closed Porosity (%) | Mean Apparent Density ($g.cm^{-3}$) | Mean UCS (MPa) |
|---|---|---|---|---|---|
| CAP2-HA YU foam | 1300 | 79.42 ± 1.54 | 3.09 ± 1.81 | 0.65 ± 0.05 | 0.33 ± 0.11 |
| CAP2-HA YU foam | 1350 | 73.51 ± 4.27 | 17.53 ± 11.71 | 0.84 ± 0.14 | 0.87 ± 0.34 |

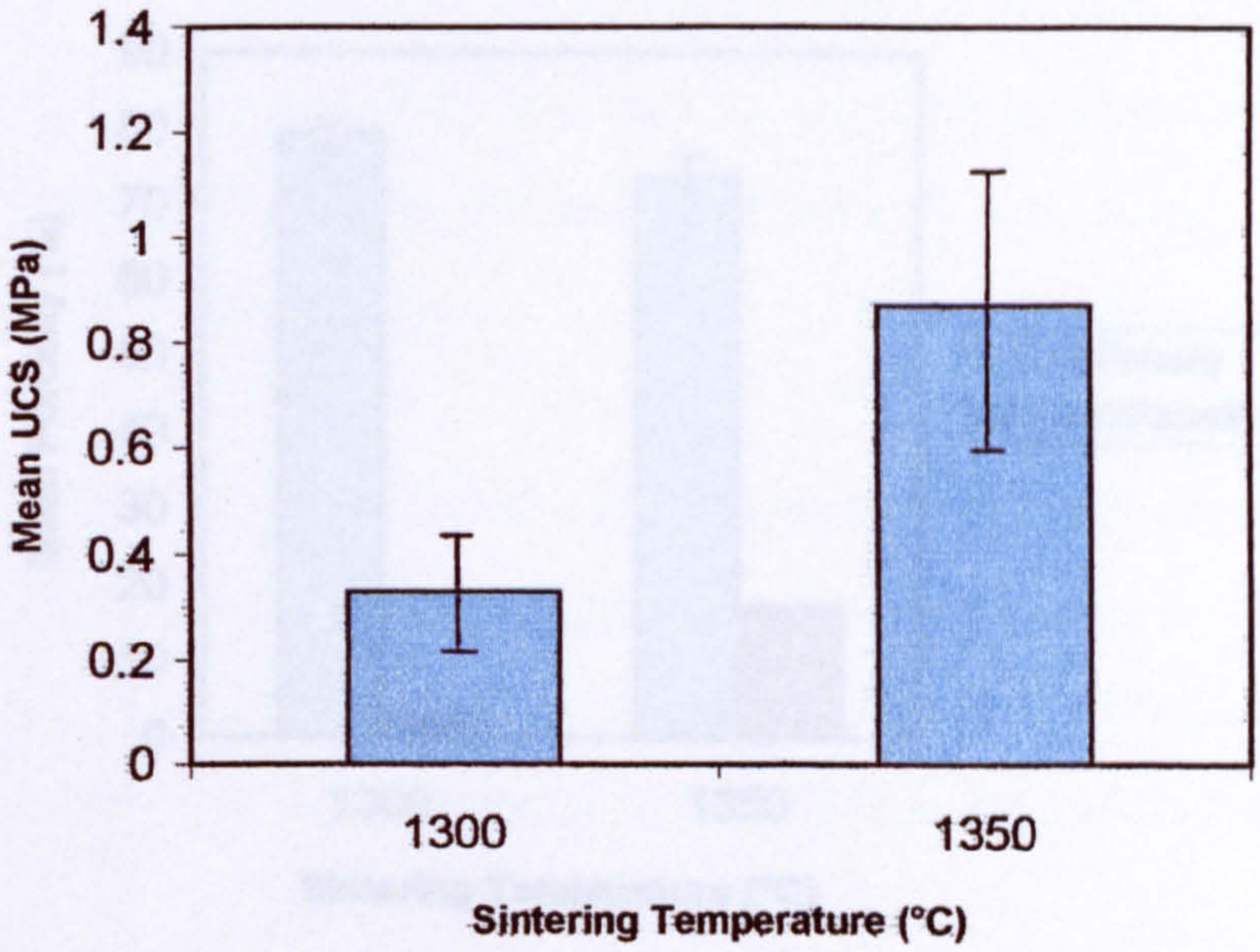


**Figure 8.9** The effect of sintering temperature on the UCS of pCAP2-HA

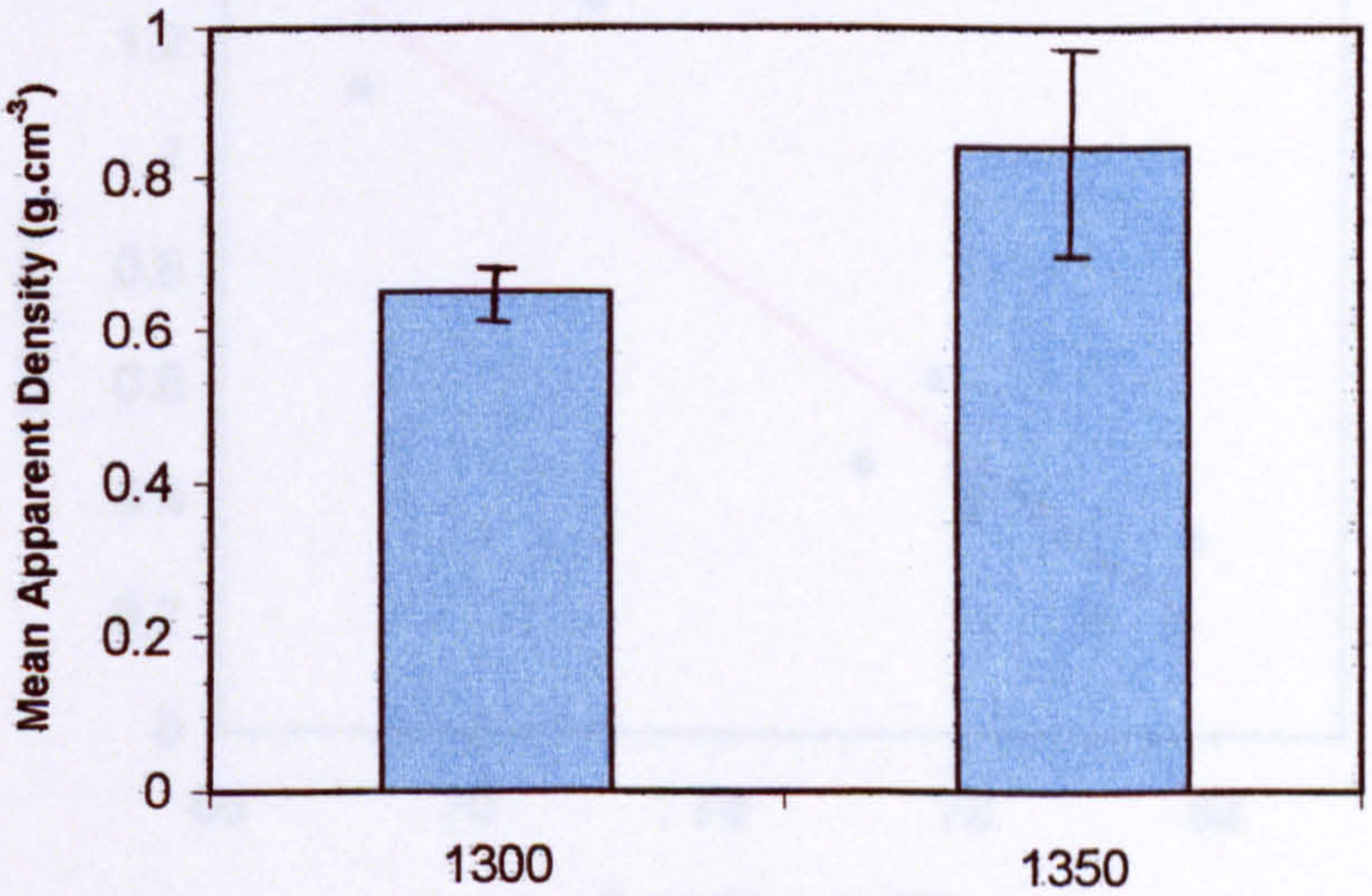


**Figure 8.10** The effect of sintering temperature on the apparent density of pCAP2-HA

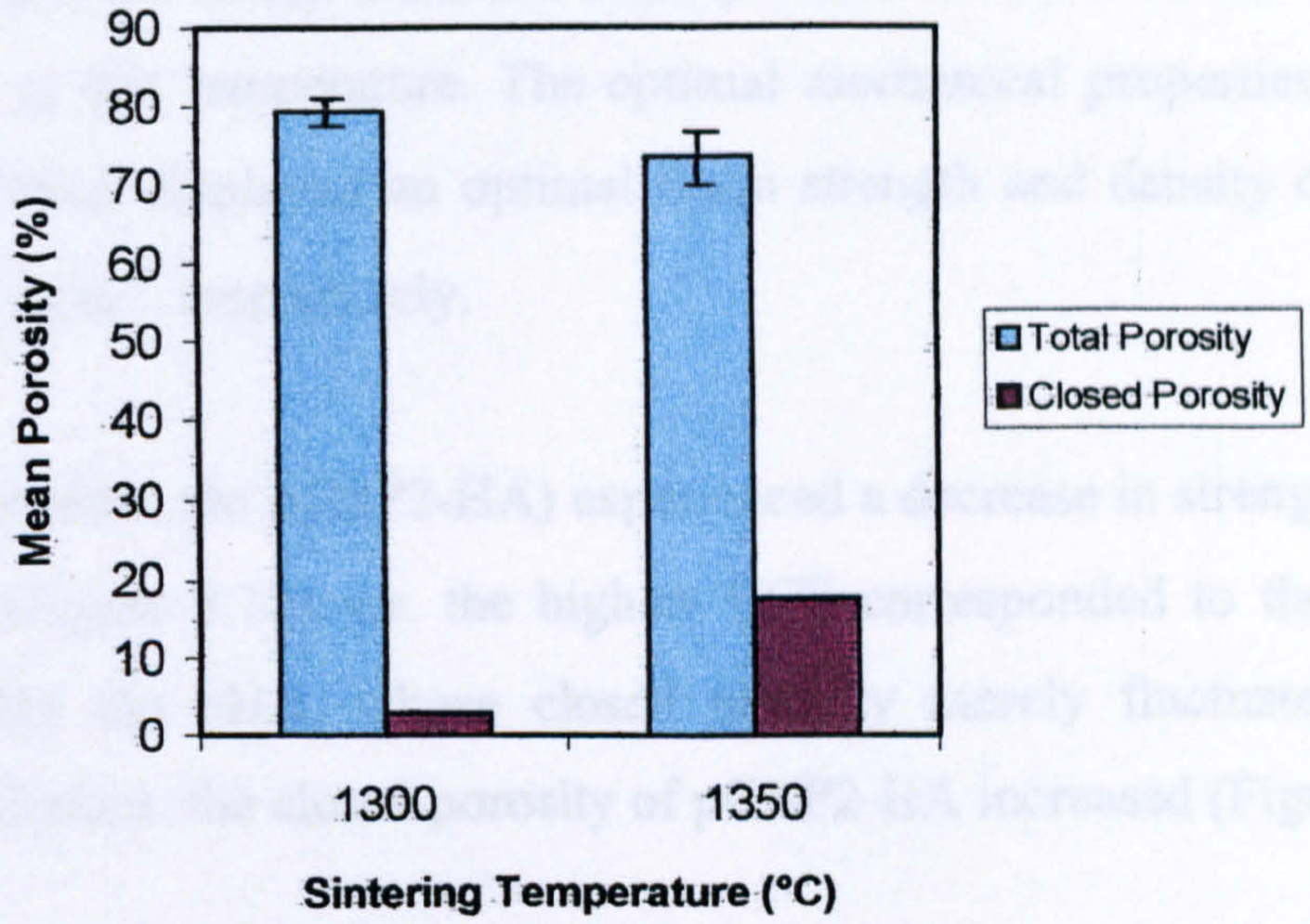


**Figure 8.11** The effect of sintering temperature on the porosity of pCAP2-HA

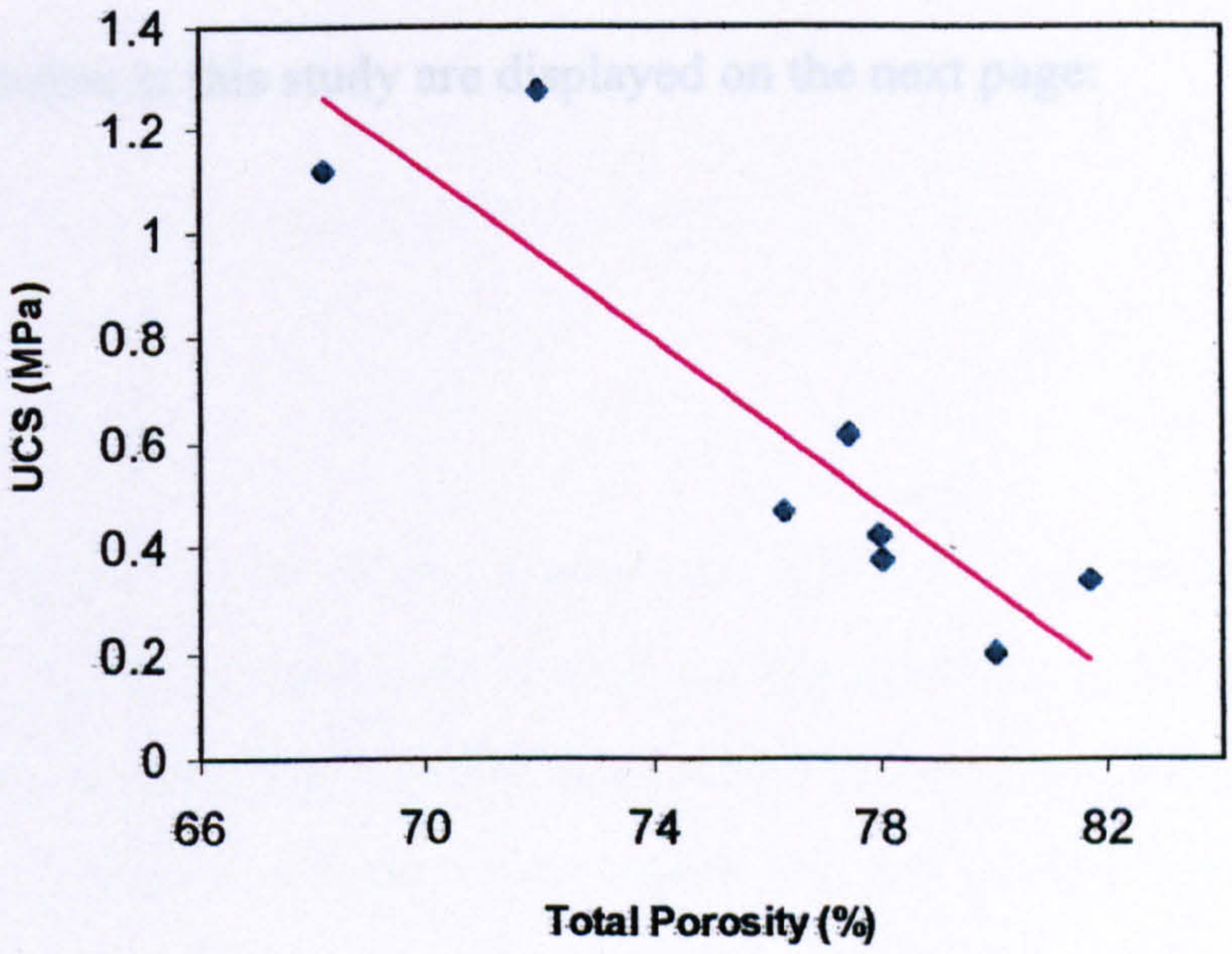


**Figure 8.12** The relationship between strength and total porosity for pCAP2-HA

As with the pHA, the pCAP2-HA experienced an increase in UCS and density with increased sintering temperature, shown in Figure 8.9 and Figure 8.10, respectively. A sintering temperature of 1350°C was therefore chosen as the optimum because the best mechanical properties (mean UCS and density of 0.87±0.34 MPa and 0.84±0.14 $g.cm^{-3}$) were obtained at this temperature. The optimal mechanical properties were lower than that of pHA, which displayed an optimal mean strength and density of 2.85±0.51 MPa and 1.19±0.08 $g.cm^{-3}$, respectively.

Similarly to the pHA, the pCAP2-HA) experienced a decrease in strength with increasing total porosity (Figure 8.12), i.e. the highest UCS corresponded to the lowest porosity. However, unlike the pHA, whose closed porosity merely fluctuated with increased sintering temperature, the closed porosity of pCAP2-HA increased (Figure 8.11).

### 8.2.1.3 Scanning Electron Microscopy

SEM of the batches in this study are displayed on the next page:

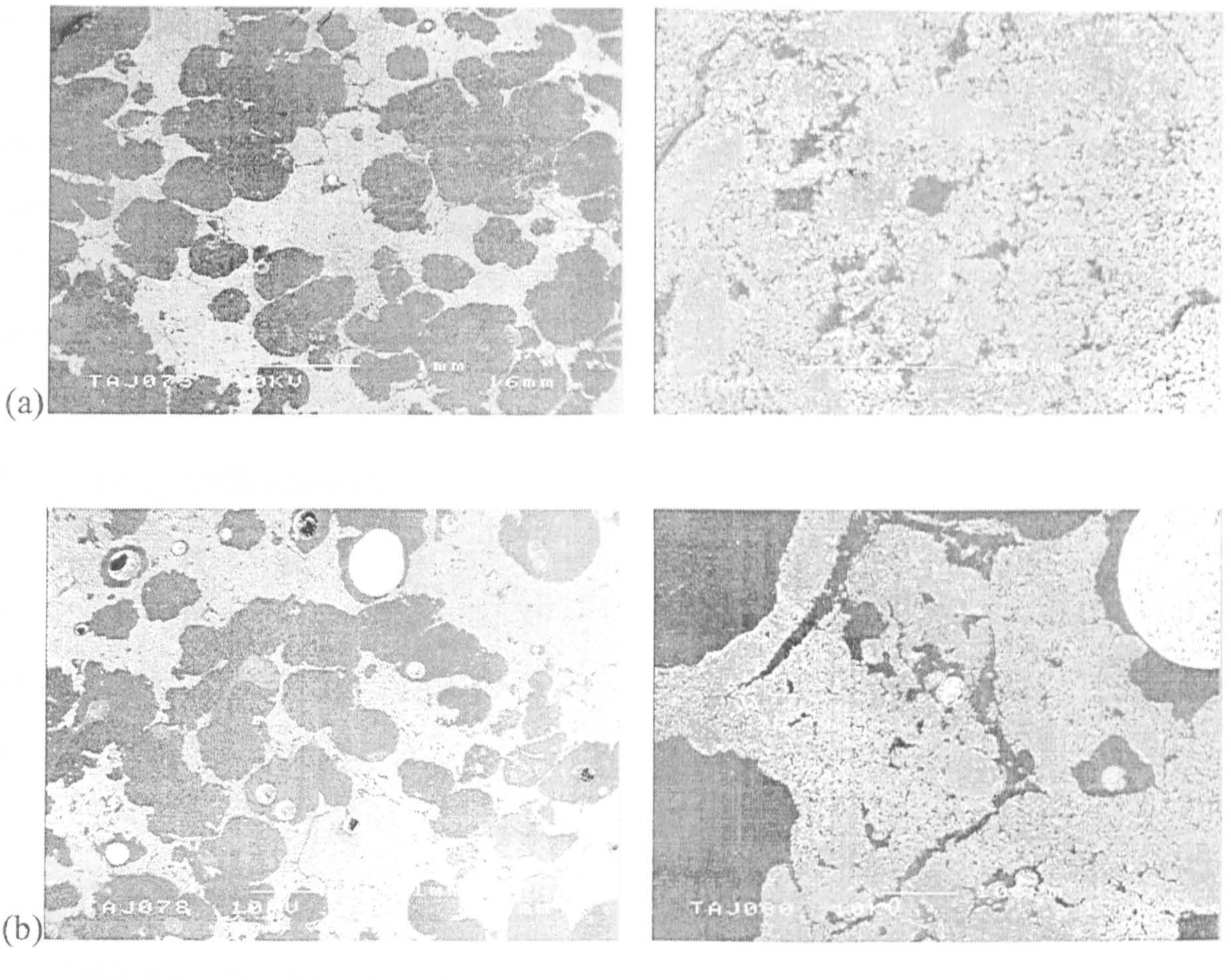


**Figure 8.13** YU-pCAP2-HA (a) 1300°C (b) 1350°C

The macrostructure of pCAP2-HA sintered at 1300°C (ai) at low magnification revealed a large amount of interconnectivity as well as the presence of thick struts, with some cracks. Higher magnification (aii) revealed a large amount of porosity and small cracks within the struts. At a higher sintering temperature (bi), the pCAP2-HA displayed a similar amount of interconnectivity than that sintered at 1300°C (a), slightly thicker struts, and slightly less cracks. At higher magnification (bii), the struts appear to have a similar amount of internal porosity/cracks to that of 1300°C.

### 8.2.2 STUDY AT OPTIMAL SINTERING CONDITIONS

The pilot study identified pCAP2-HA sintered at 1350°C as having optimal conditions, therefore, for the purpose of this investigation, YU-pCAP2-HA and BU-pCAP2-HA were produced and characterized at this optimal sintering temperature. Two batches were sintered at 1350°C and a further two batches at 1400°C; it was decided to experiment with increasing the sintering temperature in the hope of improving the mechanical properties at the risk of increasing phase decomposition.

#### 8.2.2.1 X-ray Diffractometry

The results of the x-ray diffraction on all batches (Table 8.5, Figure 8.14) only display the amount of RI-TCP of α-TCP detected, as no β-TCP was present in any of the samples. One representative sample was chosen from each batch for analysis.

**Table 8.5** The effect of sintering temperature and foam-type on the RI-TCP of pCAP2-HA

| Materials | Sintering Temperature (°C) | RI-TCP (%) |
|---|---|---|
| CAP2-HA YU foam | 1350 | 17 |
| CAP2-HA BU foam | 1350 | 19 |
| CAP2-HA YU foam | 1400 | 19 |
| CAP2-HA BU foam | 1400 | 23 |

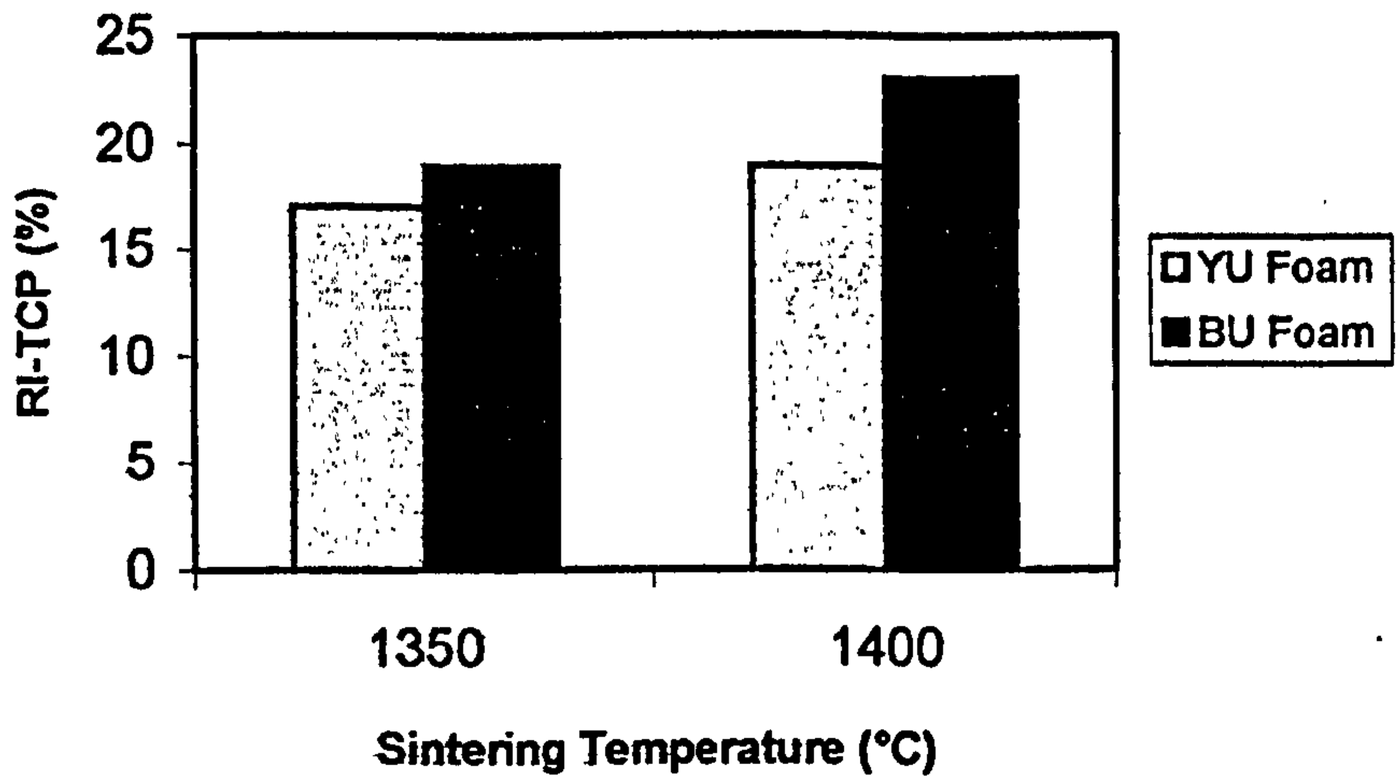


**Figure 8.14** The effect of sintering temperature on the RI-TCP of YU-/BU-pCAP2-HA

The batches deriving from the YU and BU foam showed an increase in the amount of phase decompositon to α-TCP with increasing sintering temperature. In comparing the foams, the BU-pCAP2-HA experienced more phase decomposition than the YU-pCAP2-HA at both temperatures.

### 8.2.2.2 Mechanical Properties

In this study, YU and BU polyurethane foam were used in the burn-out technique at the optimal sintering temperature (1350°C). The results of the mean porosity, density, and strength measurements are displayed in Table 8.6, and these mean values illustrated in Figures 8.15-8.18, all values displayed in Figure 8.19.

**Table 8.6** Porosity, density, and strength measurements for YU-/BU-pCAP2-HA sintered at different temperatures

| Materials | Sintering Temperature (°C) | Mean Total Porosity (%) | Mean Closed Porosity (%) | Mean Apparent Density ($g.cm^{-3}$) | Mean UCS (MPa) |
|---|---|---|---|---|---|
| CAP2-HA YU foam | 1350 | 75.20 ± 1.15 | 12.98 ± 1.51 | 0.78 ± 0.04 | 0.66 ± 0.23 |
| CAP2-HA BU foam | 1350 | 79.31 ± 0.83 | 12.86 ± 4.59 | 0.65 ± 0.03 | 0.46 ± 0.20 |
| CAP2-HA YU foam | 1400 | 71.91 ± 0.76 | 11.98 ± 1.21 | 0.89 ± 0.02 | 0.58 ± 0.29 |
| CAP2-HA BU foam | 1400 | 76.05 ± 1.63 | 12.29 ± 1.25 | 0.76 ± 0.05 | 0.76 ± 0.37 |

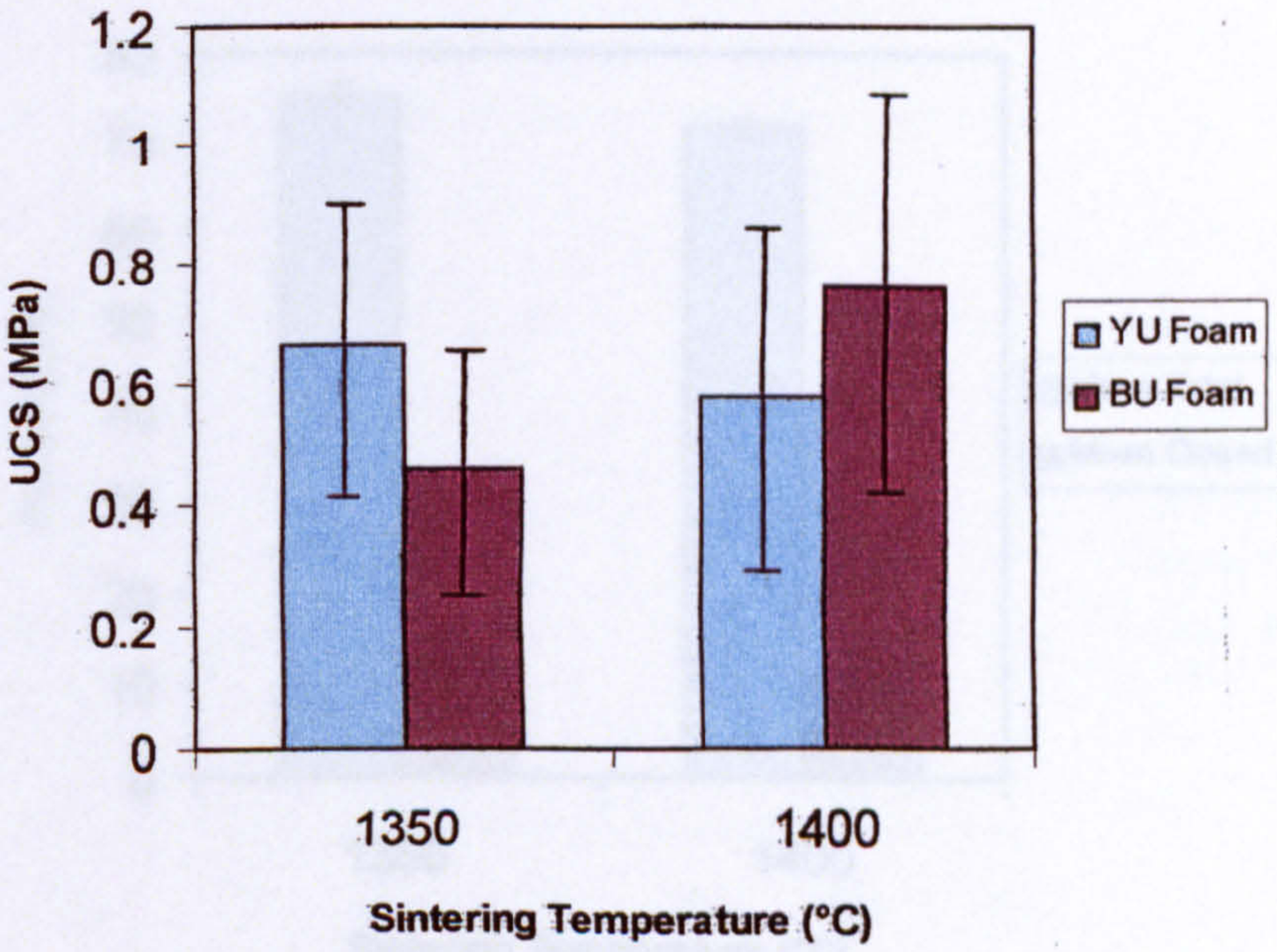


**Figure 8.15** The effect of sintering temperature on the UCS of pCAP2-HA made with YU/BU Foam

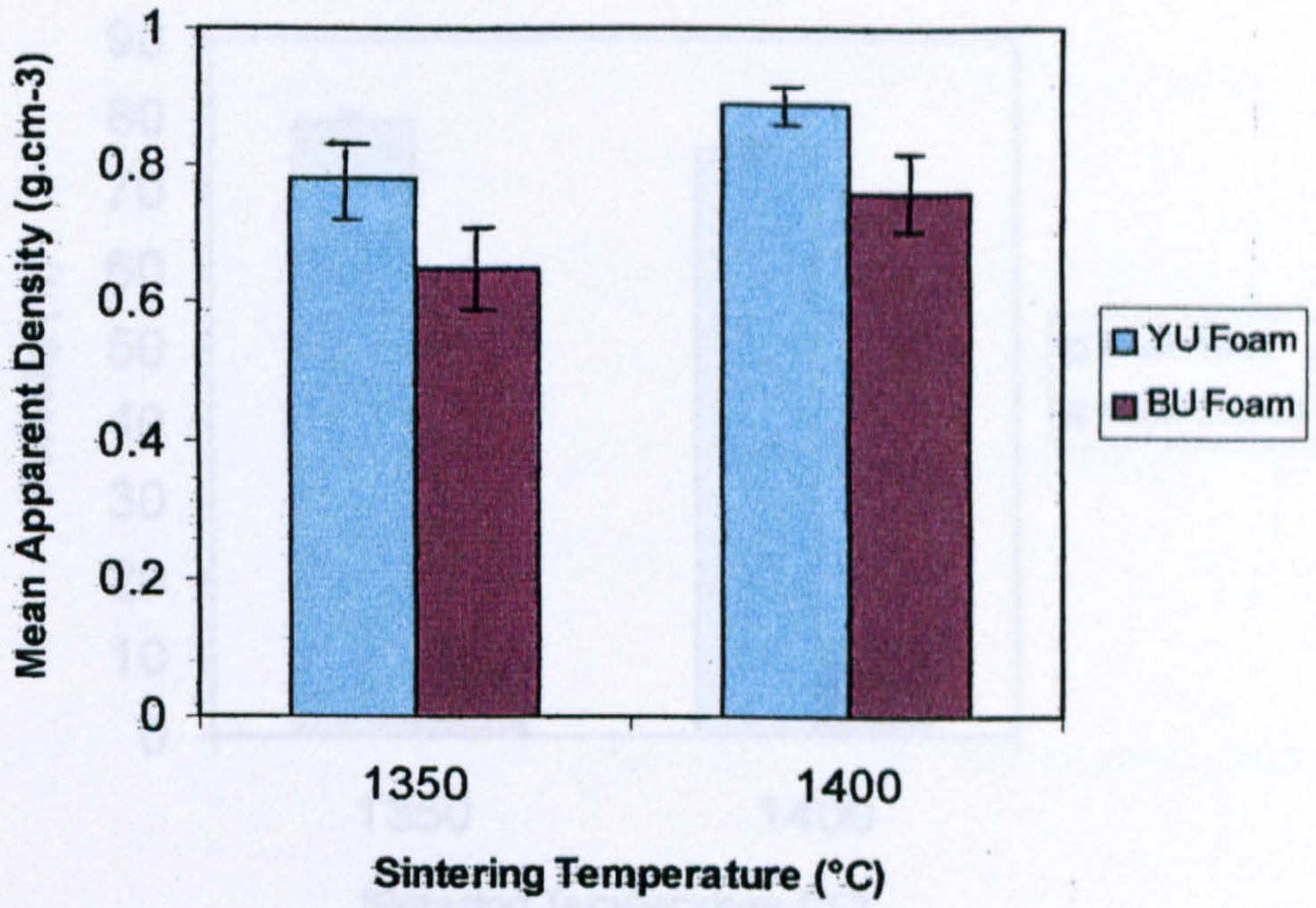


**Figure 8.16** The effect of sintering temperature on the apparent density of YU-/BU-pCAP2-HA

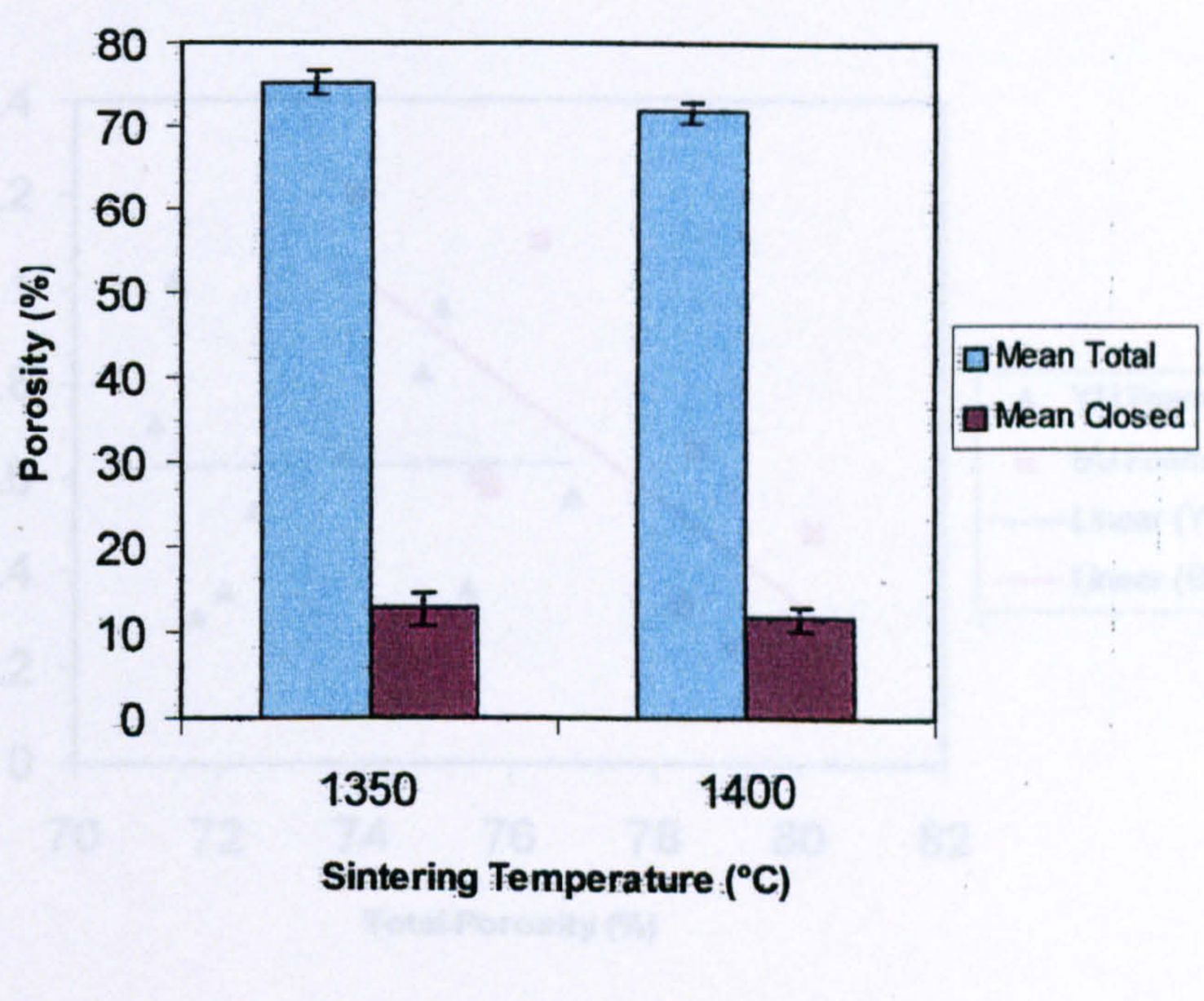


**Figure 8.17** The effect of sintering temperature on the total/closed porosity of YU-pCAP2-HA

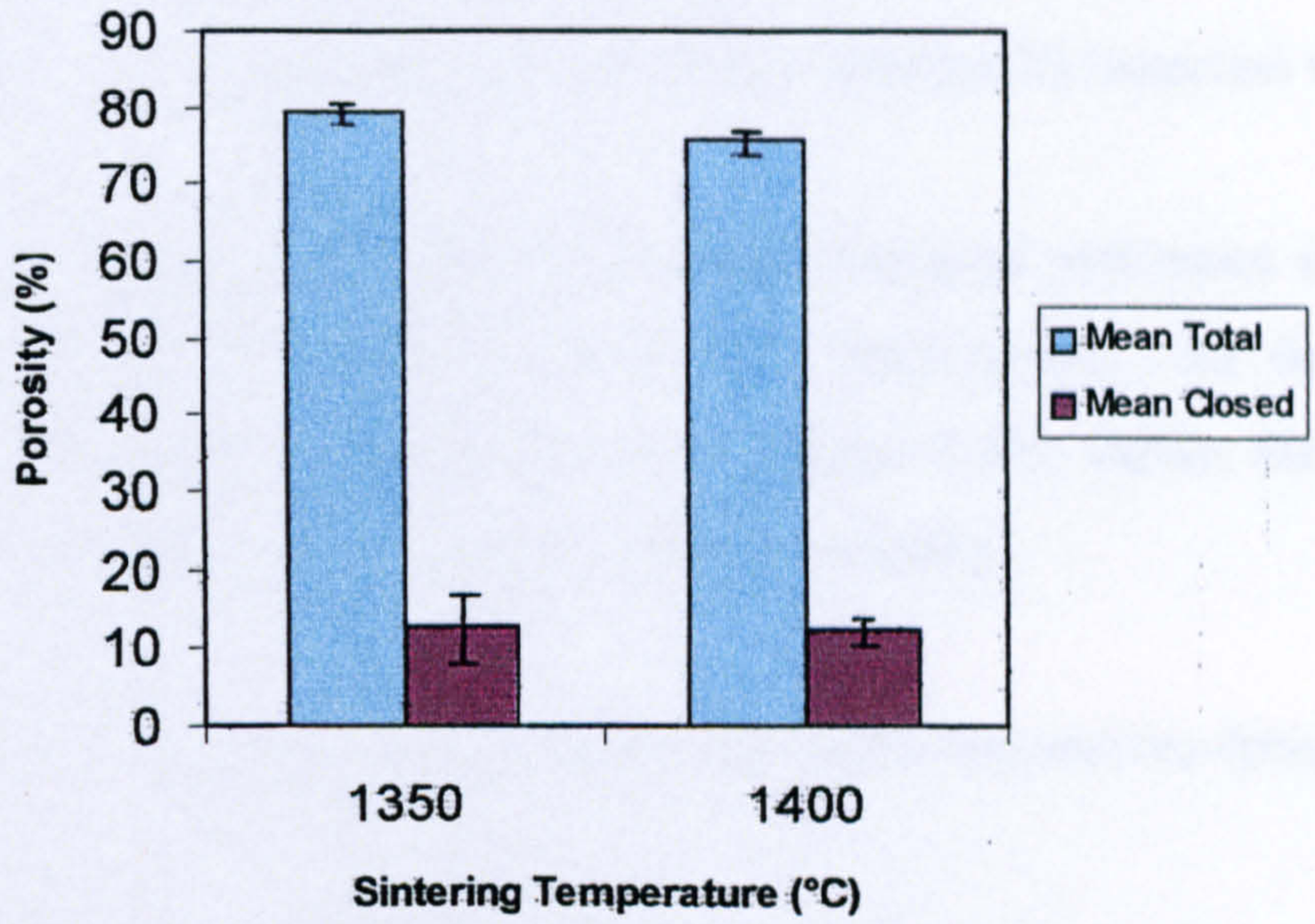


**Figure 8.18** The effect of sintering temperature on the total/closed porosity of BU-pCAP2-HA

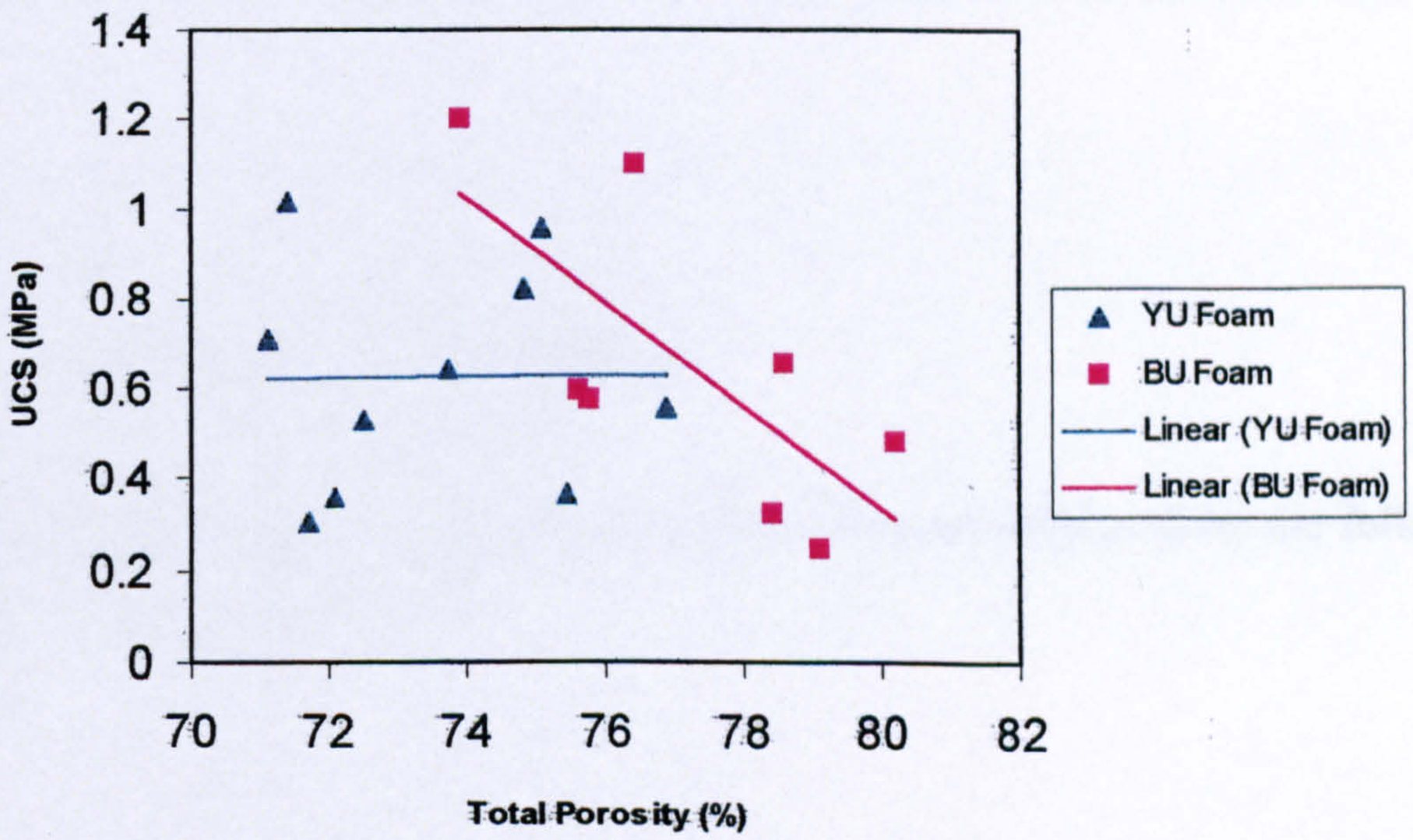


**Figure 8.19** The relationship between strength and total porosity for YU-/BU-pCAP2-HA

Unlike the BU-pCAP2-HA, which increased in strength with increasing sintering temperature (Figure 8.15), the YU-pCAP2-HA experienced a decrease in strength. This

was unusual as the density of both the YU- and BU-pCAP2-HA increased with increasing temperature (Figure 8.16). The densities and strengths of the YU- and BU-pCAP2-HA at 1400°C were 0.89±0.02g.cm$^{-3}$/0.58±0.29MPa and 0.76±0.05g.cm$^{-3}$ /0.76±0.37MPa, which indicated that the weaker samples(YU-species) were more dense.

Both the YU- and BU-pCAP2-HA experienced marginal reductions in total and closed porosity as shown in Figures 8.17 and 8.18, respectively. As the BU-pCAP2-HA decreased in porosity, the UCS increased (Figure 8.19), unlike the YU-pCAP2-HA, which did not appear to have a relationship with porosity.

The following table summarises the behaviour of the two species during the temperature increase:

**Table 8.7** Summary of YU-/BU-pCAP2-HA

| Species | Porosity | Density | Strength |
|---|---|---|---|
| YU-pCAP2-HA | ↓ | ↑ | no change |
| BU-pCAP2-HA | ↓ | ↑ | ↑ |

### 8.2.2.2 Scanning Electron Microscopy

SEM micrographs taken of the batches in this study are displayed on the following page in Figure 8.20 and Figure 8.21.

YU-/BU-pCAP2-HA sintered at 1350°C:

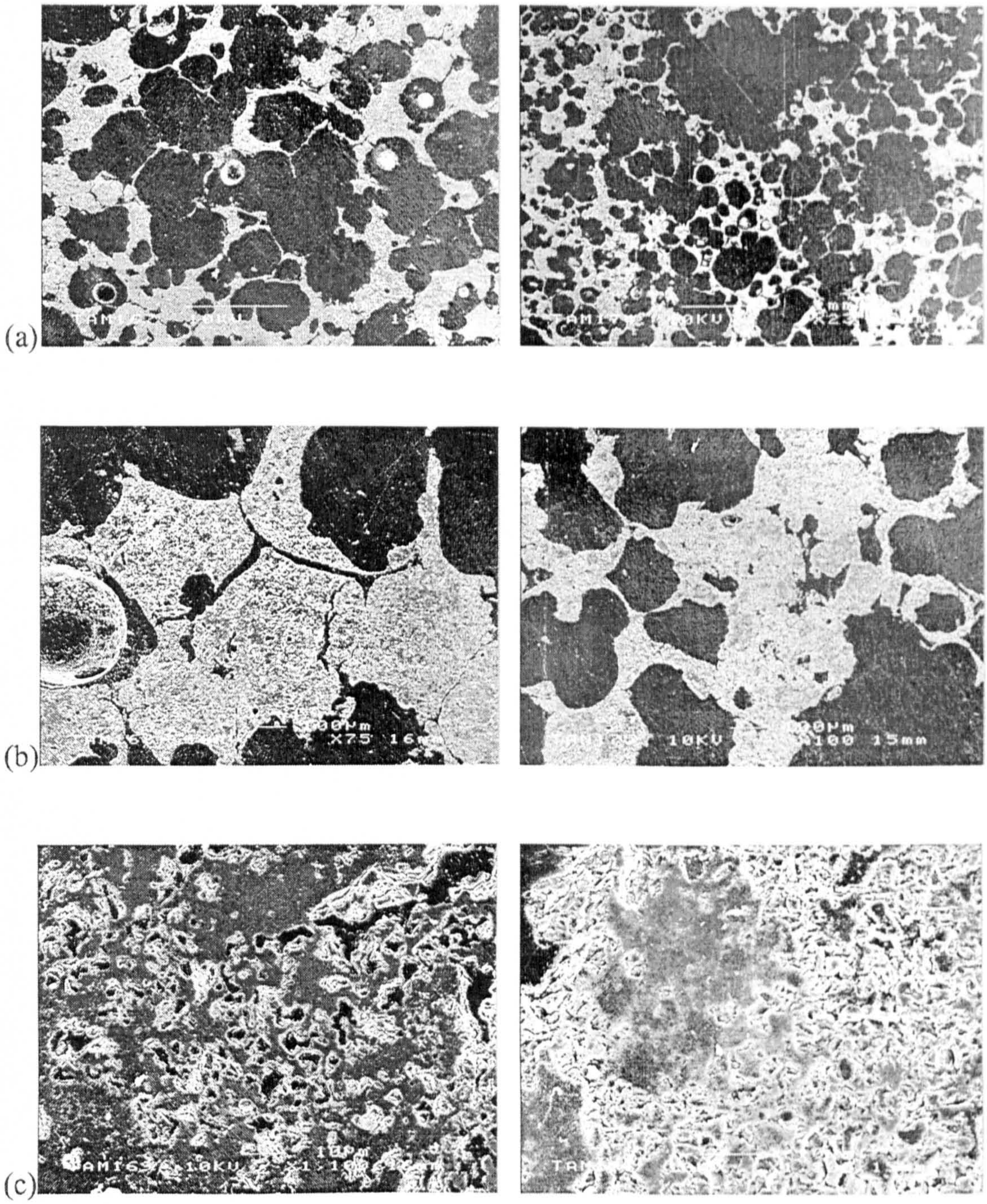


**Figure 8.20** YU-/BU-pCAP2-HA sintered at 1350°C

YU-/BU-pCAP2-HA sintered at 1400°C:

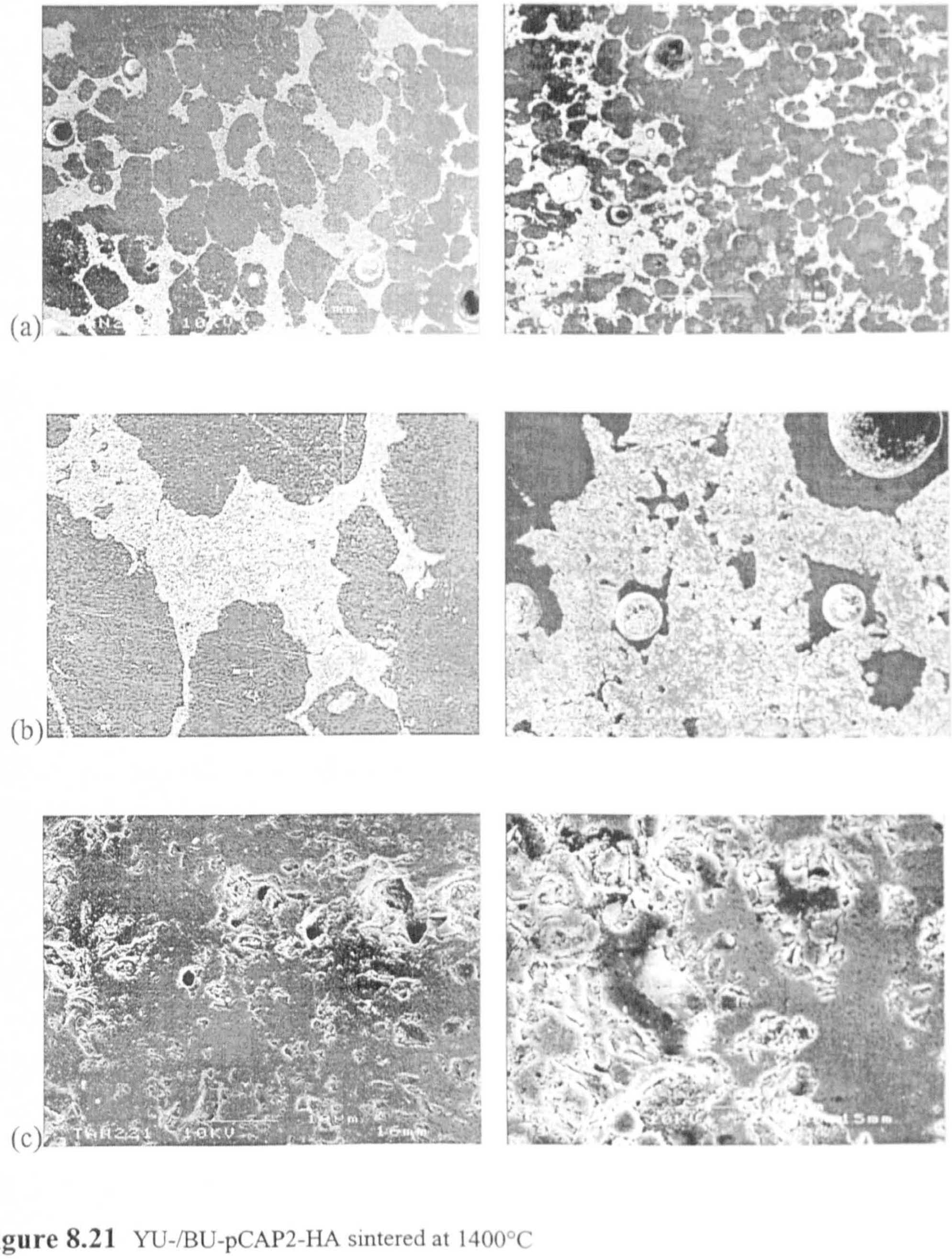


**Figure 8.21** YU-/BU-pCAP2-HA sintered at 1400°C

*Figure 8.20*

At low magnification in image (a), there was a huge difference between the macroporosity of the YU and the BU species. The YU species displayed macroporosity, with some macrocracks within the struts, whereas the BU species displayed what appears to be merged macroporosity into very large pores that were even visible to the eye outside of SEM analysis. At medium magnification in image (b), the YU struts contained some cracks and some porosity, whereas the BU struts lacked structural integrity and appeared thin and porous. At high magnfication in image (c), the struts of both species displayed similar amounts of microporosity.

*Figure 8.21*

Image (a) revealed that the YU-pCAP2-HA experienced a slight reduction in macropore size from 1350°C, with less interconnectivity, but similar-sized struts. Even though the BU-pCAP2-HA appeared to have improved at this temperature in comparison to that of 1350°C in terms of merged macroporosity, it was still much more macroporous than the YU species. At medium magnification in image (b), the YU-pCAP2-HA appeared to display less porosity within the struts in comparison to the BU-pCAP2-HA, but the latter species did experience a reduction in strut porosity in comparison to that of 1350°C. Image (c) showed that at high magnification, both species experienced a reduction in internal microporosity in comparison to their appearance at 1350°C.

## 8.4 DISCUSSION

### 8.4.1 PRODUCTION OF POROUS HA ($_P$HA)

The pilot study revealed that an increase in temperature caused the pHA to decrease in porosity, and increase in strength and density (similar to the findings of Liu(1997,1998) and Rodriguez-Lorenzo et al (1998)). This behaviour was expected, seeing as in Chapter 5, the dense HA (which existed as struts in pHA) experienced increases in strength and density with increasing sintering temperature. As the temperature was increased in this investigation, the pHA struts densified, as shown in Figure 8.5, indicated by the smaller

degree of microporosity within the struts sintered at 1300°C, as compared to those at 1200°C and 1250°C.

The highest mean UCS (2.85±0.51 MPa) and density (1.13±0.08 $g.cm^{-3}$) were obtained at a sintering temperature of 1300°C; the former was comparable to the findings of Holmes et al (1984), where a highest UCS of 2.3-5 MPa was reported. However, this was ~2-11 MPa lower than the values generally reported for porous HA in Table 3.6. The optimal strength of the pHA in this study corresponded to a total porosity of ~64%, with pores sizes of ≤ 600μm. According to the literature, the optimal pore diameter for homogeneous and abundant bone ingrowth was 565μm (Gauthier et al, 1998), with a minimum pore size of 100μm (Klawitter et al, 1971; Hench, 1991). Therefore not only did the batch sintered at 1300°C prove to display optimal mechanical properties, but also potential for bone ingrowth, with minimal resorption (as indicated by the absence of TCP in the as-sintered materials).

The study carried out at optimal sintering conditions revealed that at a sintering temperature of 1300°C, the pHA made with YU foam (YU-pHA) was stronger than the pHA made with BU foam (BU-pHA). However, despite the fact that the YU-HA displayed a mean UCS of 2.19±1.2 MPa, and that of BU-HA was 1.29±0.1.02 MPa, the BU-HA exhibited a similar density toYU-pHA (refer to Figure 8.7). This can be explained by differences in porosity between the two species. The YU-pHA displayed a closed porosity of ~17%, which was higher than that of the BU-pHA(~11%). Furthermore, because both species displayed similar total porosities (~68%), the BU-pHA contained a larger number of open pores. Therefore, the increased number of struts closing the pores in the YU-pHA indicated a larger number of surfaces to absorb stress, hence the higher mean UCS.

Closed porosity is indicative of a greater concentration of struts, as opposed to open porosity, where the struts are eliminated, to allow a passage between each macropore. So, although the presence of closed porosity implied a greater number of potential stress-raisers, it also implied the presence of a greater amount of dense HA (within the greater

number of intact struts) to absorb mechanical stress during testing, hence mechanical properties were improved with increased closed porosity.

The SEM verified the differences in closed porosity between the two species. The BU-pHA contained several, large, merged macropores (Figure 8.8) (≤ 1000μm), as opposed to the many smaller macropores (≤ 600μm) present in the YU-pHA. The macropores in the BU-pHA appeared to merge into large voids, which explains the greater calculated open porosity in comparison to the YU-pHA.

The results indicated that at 1300°C, the YU-pHA displayed more structural and mechanical integrity than BU-pHA, and therefore the YU foam proved to be the more successful polymeric pre-cursor in the production of pHA.

### 8.4.2 PRODUCTION OF POROUS CAP2-HA ($_p$CAP2-HA)

The pilot study revealed that an increase in sintering temperature resulted in an increase in the decomposition of pCAP2-HA, as shown in Table 8.3, from 21 % α-TCP to 38 % α-TCP. This was expected, seeing as the dense HA reinforced with CAP1 in Chapter 6 experienced similar behaviour when subjected to increments of temperature.

As the sintering temperature increased from 1300°C to 1350°C, the density increased (Figure 8.10), and the total porosity decreased (Figure 8.12), as would be expected. However, the closed porosity increased from ~3% to ~17% with increasing sintering temperature (Figure 8.11), indicating superior densification within the struts. This increase in strut density was believed to result in an enhanced ability of the structure to absorb stress during mechanical loading, hence the mean UCS increased from 0.33±0.11 MPa to 0.87±0.34 MPa with increasing closed porosity. The increase in closed porosity as well as the decrease in open porosity is apparent in the macrostructure shown in Figure 8.11.

The pCAP2-HA was unfortunately much weaker than the pHA; the optimal strength/density of the pHA and pCAP2-HA were 2.85±0.51 MPa/1.19±0.08 g.cm$^{-3}$ and 0.87±0.34 MPa/0.84±0.14 g.cm$^{-3}$, respectively.

As a result of the differences in sintering, optimal pHA, showed an average pore size of ≤ 600μm, while the optimal pCAP2-HA appeared to have a larger average pore size of ≤ 800μm (Figure 8.13). Therefore, the pCAP2-HA displayed weaker mechanical properties. During the burn-out and sintering process, it would be expected that after pyrolysis of the pre cursor, the ceramic coating would consolidate and shrink into a positive replica of the polymer foam. The SEM results indicated that the in the case of pCAP2-HA, the ceramic coating did not shrink to the same extent as in the case of pHA, which may reflect a loss of some CAP2 material in the slip, resulting in poor sintering and the increased pore size. Therefore, the differences in strength were attributed to processing complications arising from the solubility of CAP2 in the water/binder mixture, leading to loss of material and inhibited sintering.

The study carried out at optimal sintering conditions revealed that the BU-pCAP2-HA decomposed to α-TCP to a greater extent at 1350°C and 1400°C than the YU-pCAP2-HA did, yet both experienced an increase in decomposition with increasing temperature (Figure 8.13). These results imply that there use of BU foam as a polymeric pre cursor caused the pCAP2-HA to be more reactive at high temperature, hence increasing the loss of $OH^-$ ions that accompanies decomposition, than when produced with YU foam.

As for the mechanical properties, an increase in sintering temperature to 1400°C, caused the YU-pCAP2-HA to experience a decrease in UCS (from 0.66±0.23 MPa to 0.58±0.29 MPa), despite the increase in density (from 0.78±0.04 g.cm$^{-3}$ to 0.89±0.02 g.cm$^{-3}$. Furthermore, the average pore size for both temperatures (≤ 700μm) did not appear to change. As can be seen in Figure 8.19, the volume of porosity had little to no effect on the UCS of the YU-pCAP2-HA. However, Figure 8.18 revealed that the closed porosity decreased from ~13% to ~12%, indicating further densification of struts.

Usually, an increase in density accompanied by a decrease in porosity would indicate better structural/mechanical integrity. Increased densities with accompanying decreased strengths indicate grain growth. This phenomena may have occurred in the struts of the specimens in this study, yet the micrographs in Figures 8.20-8.21 were not etched and therefore could not reveal any details of the grain structures for verification. The specimens in this study, as well as the entire porous investigation, were not etched on the basis that the macrostructure and microporosity within the struts were fundamental to understanding the mechanical properties.

The BU-pCAP2-HA experienced an increase in strength (from 0.46±0.20 MPa to 0.76±0.37 MPa) (Figure 8.15) and density (from 0.65±0.03 $g.cm^{-3}$ to 0.76±0.05 $g.cm^{-3}$) (Figure 8.16) with increasing temperature, with a corresponding decrease in total porosity (from ~79-76%) (Figure 8.19). On comparing the macrostructures of specimens sintered at the two temperatures (Figure 8.20-8.21), it was clear that the average macropore size of the BU-pCAP2-HA decreased with increasing temperature from ≤ 600 μm to ≤ 500μm; furthermore, there appeared to be less mergence of macropores, all of which would be expected to contribute to the increased strength. At 1400°C, the BU-pCAP2-HA was stronger than the YU-pCAP2-HA, whilst at 1350°C, the opposite occurred. These results indicated that the YU-pCAP2-HA reached the end-levels of sintering (i.e. grain growth) at a lower temperature than the BU-pCAP2-HA, which explains the difference in strength between the two species.

Nevertheless, in terms of producing a porous implant with minimal resorption, i.e. less TCP, the YU-pCAP2-HA at 1350°C appeared to be the most ideal candidate because at this sintering temperature, it was stronger and experienced less decomposition to TCP than the BU-pCAP2-HA.

In order to decipher the better porous material, the optimal properties found for pHA (1300°C) and YU-pCAP2-HA (1350°C) are listed in the following table:

**Table 8.8** Summary of optimal pHA and optimal YU-pCAP2-HA

| Material | % α-TCP | Total Porosity (%) | Mean Apparent Density ($g.cm^{-3}$) | Mean UCS (MPa) |
|---|---|---|---|---|
| YU-pCAP2-HA | 17 | 73 | 0.87±0.34 | 0.84±0.14 |
| pHA | 0 | 64 | 2.85±0.5 | 1.13±0.08 |

Therefore, given that the criterion in this investigation for optimal properties were high strength and minimal decomposition, the pHA sintered at 1300°C was the more suitable candidate, under the processing conditions used.

# CHAPTER 9

# EPILOGUE

## 9.1 SUMMARY

The characterization of HA (P201, Plasma Biotal Ltd., U.K.) revealed that the optimal biaxial flexural strength (60±15 MPa; density of 2.88g.cm$^{-3}$) was obtained at a sintering temperature of 1200°C, with no decomposition to TCP. The unusually high Ca/P ratio (1.68-1.73), combined with the CaO found at high temperature, indicated that this commercial powder was not stoichiometric. The BFS value was much lower than the optimal BFS values found for HA in the literature, due to the difference in density, as shown in Table 9.1:

**Table 9.1** Comparison of BFS/Density values of HA

| Author | Flexural Strength (MPa) | Density (g.cm$^{-3}$) |
|---|---|---|
| Parsons (2001) | 60 | 2.88 (9% porosity) |
| Lu et al (1998) | 110 | 3.12 (1% porosity) |
| Tampieri et al (1997) | 130 | — |
| Willman (1996) | <100 | 3.16 (0% porosity) |

However, despite the large strength differences, the P201 HA showed similarities to that of Aoki (1991) with regards to the effect of sintering temperature of the BFS of HA, as shown in Table 9.2. Aoki's HA increased in strength up until 1300°C, and the P201 HA increased until 1200°C, where it decreased sharply. Both sets of data reveal that the largest increase in strength was observed between 1100°C and 1200°C.

**Table 9.2** The effect of sintering temperature on the BFS of HA

| Parsons (2001) | | Aoki (1991) | |
|---|---|---|---|
| Sintering Temp. (°C) | BFS (MPa) | Sintering Temp. (°C) | BFS (MPa) |
| 1000 | 22±7 | — | — |
| 1100 | 28±8 | 1150 | 61±8 |
| 1200 | 60±15 | 1200 | 104±11 |
| 1250 | 21±11 | 1250 | 106±10 |
| 1300 | 11±2 | 1300 | 113±12 |

When sintered with 2.5 wt % CAP1, the HA showed a significant decrease in strength and decomposition to TCP, as indicated by the optimal mechanical properties obtained for CAP1-HA (26.59 MPa) and RI-TCP (73%). Compared to the values found in the literature (Table 9.3) for HA reinforced with 2.5 wt% additive, the optimal BFS of CAP1-HA was very low (unfortunately, no density values were recorded in the comparable literature).

**Table 9.3** Comparison of BFS values of HA reinforced with 2.5 wt% additive

| Author | Sintering Temperature (°C) | Optimal BFS (MPa) |
|---|---|---|
| Parsons (2001) | 1300 | ~27 |
| Santos et al (1992) | 1300 | ~73 |
| Knowles et al (1993) | 1350 | ~124 |
| Tancred et al (1996) | 1250 | ~32 |
| Wang et al (1998) | 1250 | ~91 |

At first, it seemed possible that the presence of TCP was contributing to the poor mechanical properties. However, particle size analysis revealed that the CAP1-HA particle sizes ($d_{0.5}$→21-39μm) were much larger than the grain sizes (~1μm) observed under scanning electron microscopy; it appeared there was a large presence of agglomerates in the composite powder in the green compacts, pre-sintering. The CAP1 particles were much larger than the HA particles pre-milling and judging by the bimodal distribution of the composite powder post-milling, there was a mismatch of particle size between the CAP1 and HA powders. This uneven particle size distribution inhibited the intimate mixing of the powders, which ultimately affected its packing/density in green compact form, and resulted in the presence of agglomerates. The agglomeration resulted in the existence of porosity in the as-sintered composites, which attributed to the decrease in strength in comparison to that of the P201 HA studied in Chapter 5.

In contrast, additions of CAP2 (2.5 wt%) resulted in reinforcement of the HA with an increase in strength to 91.77±17.29 MPa, with much less decomposition to TCP (RI-TCP of 10%). This clarified the assumption that TCP could not have been the reason for CAP1-HA's decreased strength, seeing as it was also present in CAP2-HA which displayed superior mechanical properties. At optimal sintering conditions, the CAP2-HA displayed a higher density (93% theoretical) than the HA (91% theoretical), and better mechanical properties despite the larger grain sizes, which indicates that the increased strength was due to better sintering, which resulted in reduced porosity. The highest BFS recorded for the CAP2-HA was actually found in the 4 wt% composite, which proved to be stronger than the 4 wt% composites of similar systems found in the literature (Table 9.4)

**Table 9.4** BFS of HA reinforced with 4 wt% additive

| Author | Sintering Temperature (°C) | BFS (MPa) |
|---|---|---|
| Parsons (2001) | 1300 | 105±20 |
| Santos et al (1996) | 1350 | 93±27 |
| Knowles et al (1996) | 1250 | ~94 |

The ideal wt% of CAP2 was decided on the basis of high strength and minimal decomposition to TCP. At 1 wt%, the CAP2-HA contained the smallest amount of TCP out of all the wt%'s (6%TCP), however its BFS was also the lowest (74.34±8.59 MPa). The 2.5 wt% composite was much stronger (91.77±17.29

MPa) with slightly more decomposition to TCP (10%). Above 2.5 wt%, the amount of decomposition toTCP increased, therefore it was decided that the 2.5 wt% CAP2-HA fit the mechanical and chemical criteria the best.

After soaking in physiological solution for 30 days, the 2.5 wt% CAP2-HA showed good retention of strength where the CAP2-HA retained 78% of its strength whilst HA only retained 60%. This decrease in bending strength with time is consistent with that found in the literature (Table 9.5) where Xiaodong et al's (1998) composite rods retained 62% of its strength after 4 weeks, which is similar to the 60% of strength retained by the P201 HA after 30 days (~4 weeks). Unfortunately, the data from Table 9.5 refers to HA/PDLLA composite rods; as no literature was found regarding the effect of soaking time on the bending strengths of HA and its glass reinforced composites. However, de With (1981) demonstrated a reduction in strength when performing 3 point bend tests on HA (72-94% dense) in distilled water as opposed to in dry $N_2$ which equated to an average loss in strength of 30±6 %.

**Table 9.5** Effect of soaking time on mechanical properties of HA and HA composites.

| Week | Percentage of Original Strength | | |
|---|---|---|---|
| | HA, Parsons, 2001 | CAP2/HA Parsons, 2001 | HA/PDLLA Xiaodong et al, 1998, |
| 1 | 80% | 69% | - |
| 2 | - | - | 69% |
| 4 | 60% | 76% | 62% |

The presence of TCP in the CAP2-HA increased its resorption in Ringer's solution. This behaviour manifested within the first 24 hours, in which it was assumed that Ca was released into solution and re-precipitated by day 1 (unfortunately, there was no SEM evidence to corroborate this assumption), as opposed to the HA which experienced this behaviour a day later than the CAP2-HA. The CAP2-HA displayed a higher rate of dissolution than the HA due to the presence of TCP, which may be interpreted as detrimental to the mechanical integrity of the material in-vivo, yet 78% of its strength was retained after 30 days. Therefore, under the test conditions, the CAP2-HA showed better potential than the HA used in this study for maintaining mechanical/structural integrity. The amount of TCP was sufficient enough to speed up the precipitation of a Ca-rich layer on the surface of CAP2-HA, but not so large that it disappeared entirely in solution.

Unfortunately, the CAP2-HA was not as successful whence the technology was transferred to porous structures. The pHA was stronger and did not decompose to TCP (with both YU and BU foam), whereas the pCAP2-HA was much weaker and did experience decomposition. Due to the much higher strength of CAP2-HA in dense form, the poor mechanical properties in porous are assumed to be due to the incompatibility of the CAP2-HA powder and the water-based binder system. The solubility of CAP2 in

water may have had a detrimental effect on both the viscosity of the slurry and its wettability with the foam precursor, leading to insufficient retention of the slurry by the foam and hence weaker strengths.

The strengths of the porous structures were generally lower in comparison to the values found in the literature, as shown in Table 9.6, which displays compressive strengths of porous HA (values of porous reinforced HA were not found in the literature). For example, the porosity of the optimal pHA was 64%, yet Sepulveda et al (1999) managed to produce a more porous structure (~80% porosity) with a much higher compressive strength (4.4-4.7MPa), almost twice that of the optimal pHA. These differences in strength highlight the need to carry out further work on the production of porous structures via foam burnout, which is discussed in Section *9.3*.

**Table 9.6** Compressive strengths of porous HA from various authors

| Author | Porosity | Highest Compressive Strength (MPa) |
|---|---|---|
| Parsons (2001) | 64%<br>74% | 2.85<br>0.87 |
| White et al (1986) | 50-75% | 9.25 |
| Holmes et al (1984) | 66% | 2.3-5 |
| Haddock et al (1999) | — | 5.87 |
| Sepulveda et al (1999) | 80%<br>76% | 4.4-4.7<br>7.4 |
| Metsger et al (1999) | — | 9.3 |

Despite the poor compressive strengths that the pHA displayed in comparison to many of those found in the literature, there were similarities in the relationships between strength and porosity, particularly to those of Lui (Figure 9.1).

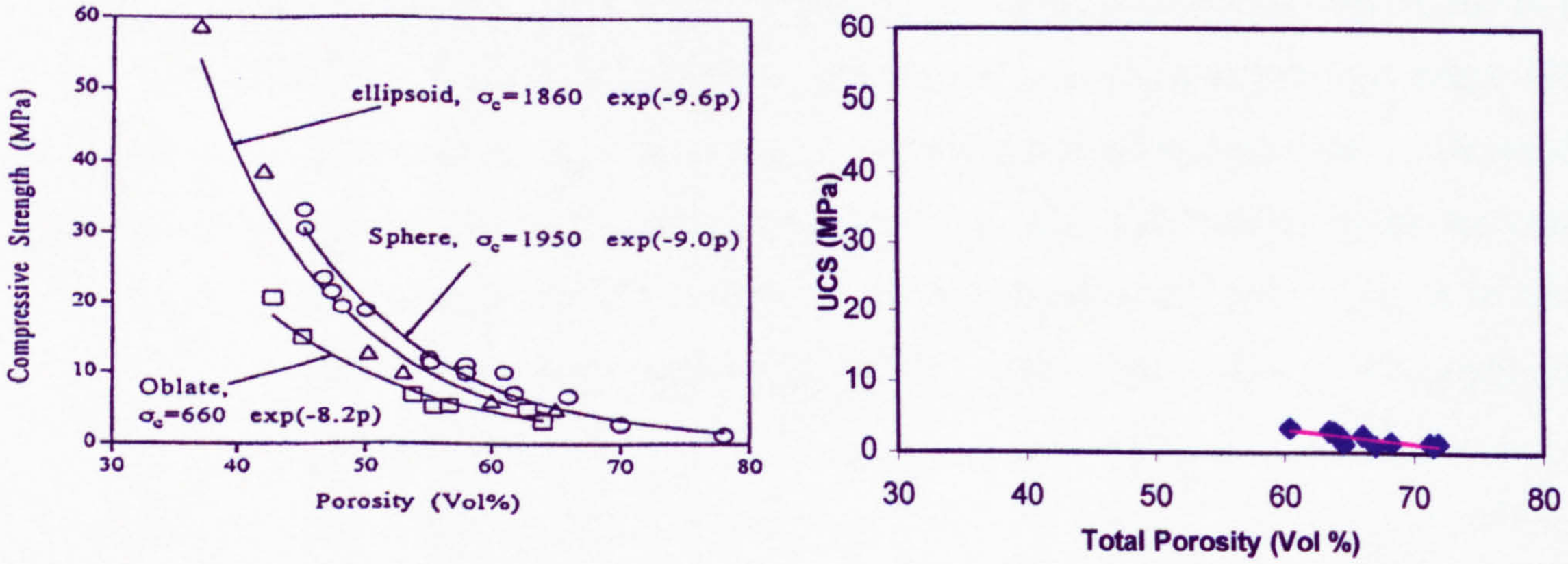


**Figure 9.1** The relationship between strength and total porosity for **(a)** a porous HA ceramic with different pore geometries (Liu, 1996*) **(b)** all pHA specimens

Therefore, although there is room for improvement with regards to the strength of the porous P201 HA, it appeared to follow the porosity-strength trends as those shown in the literature. Unfortunately, there did not appear to be a definite relationship between the strength and porosity of the pCAP2-HA. The pCAP2-HA displayed a similar trend to that of pHA when produced from BU foam only, as shown in Figure 9.2. A comparison of the strength-porosity relationship between the pHA and the pCAP2-HA is shown in Figure 9.3, with some commercial values used as a means of comparison. The UCS values recorded in the investigation in Chapter 8 are marginally lower than some of the commercial values in the same porosity range, as shown in Figure 9.3, which highlights the potential of the porous investigation in this thesis.

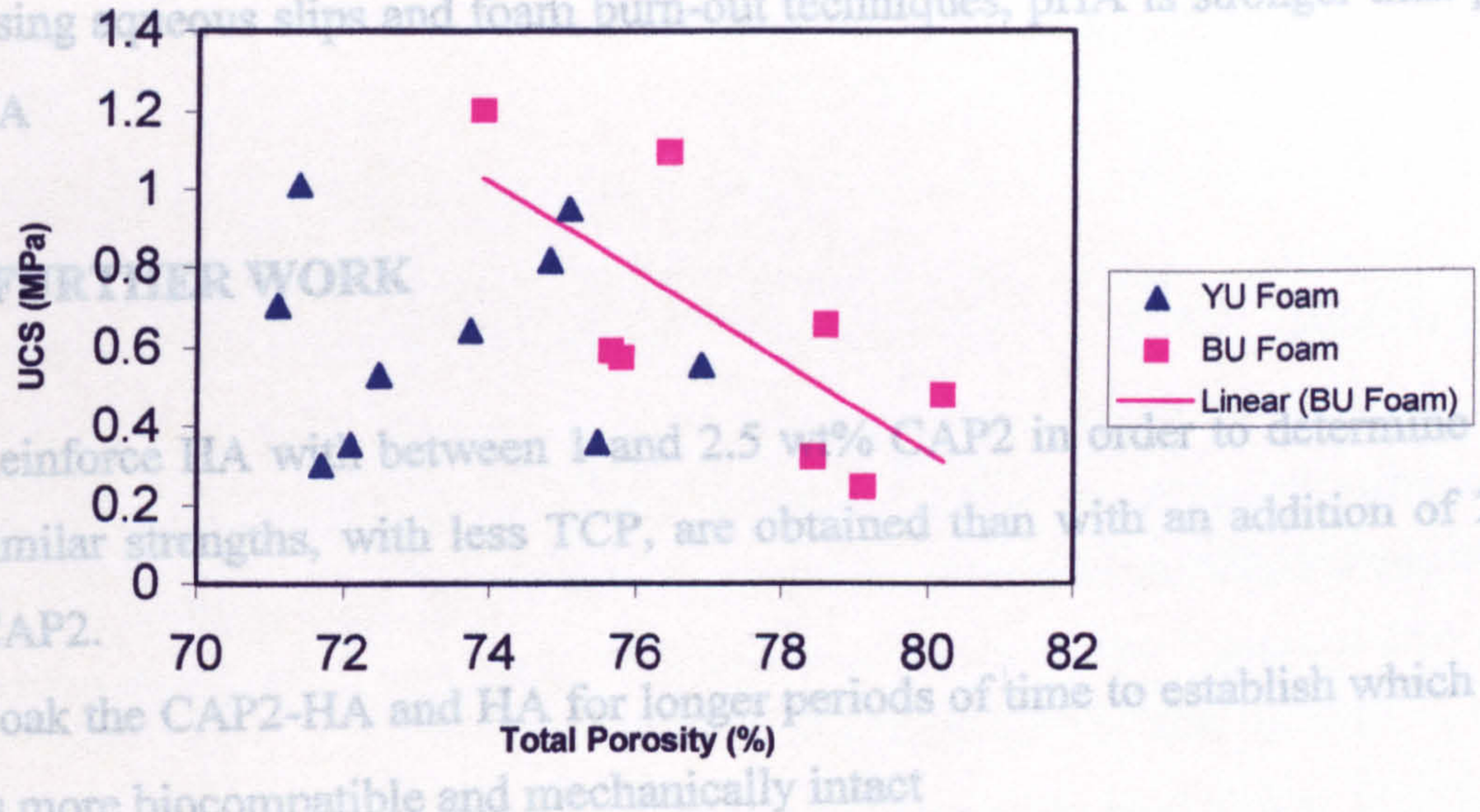


**Figure 9.2** The relationship between strength and total porosity for YU-/BU-CAP2-HA

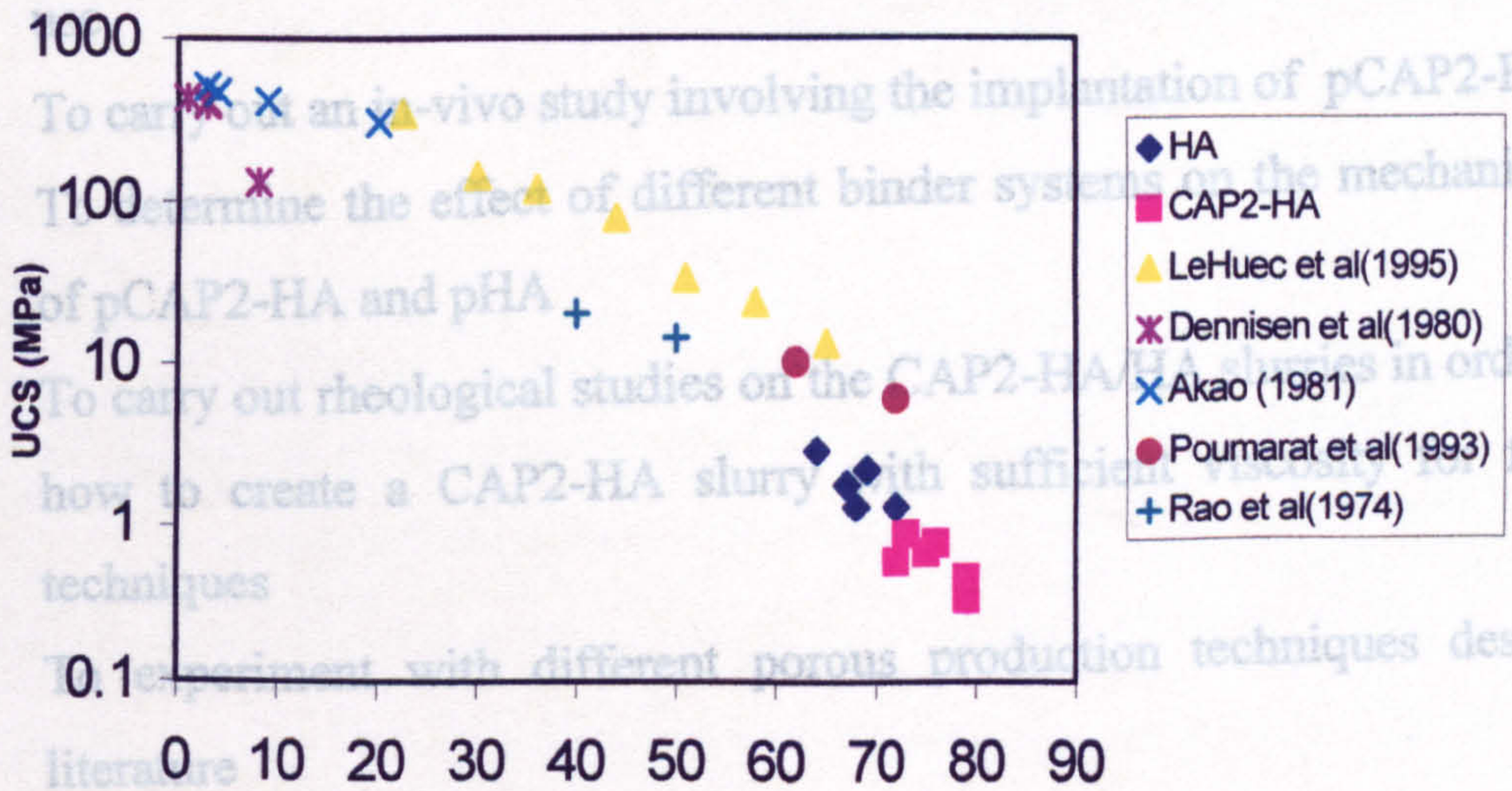


**Figure 9.3** The relationship between strength and porosity for pHA/pCAP2-HA/various commercial specimens

## 9.1 CONCLUSIONS

- CAP1-reinforcement is detrimental to the physical and mechanical properties of HA
- CAP2 improves the mechanical properties of HA with little phase decomposition to TCP
- CAP2-HA is slightly more resorbable, yet still much stronger than HA, as indicated by the difference in dry strengths and the ability of CAP2-HA to retain more strength after soaking in Ringer's solution for 30 days
- Using aqueous slips and foam burn-out techniques, pHA is stronger than pCAP2-HA

## 9.3 FURTHER WORK

- Investigate the effect of milling the additives prior to milling the composite mixture to produce monomodal powder distributions in order to avoid agglomerations in the green compact.
- Reinforce HA with between 1 and 2.5 wt% CAP2 in order to determine whether similar strengths, with less TCP, are obtained than with an addition of 2.5 wt% CAP2.
- Soak the CAP2-HA and HA for longer periods of time to establish which material is more biocompatible and mechanically intact
- Investigate the toxicity of CAP2-HA and HA, as indications of long-term clinical use
- To carry out an in-vivo study involving the implantation of pCAP2-HA
- To determine the effect of different binder systems on the mechanical properties of pCAP2-HA and pHA
- To carry out rheological studies on the CAP2-HA/HA slurries in order to establish how to create a CAP2-HA slurry with sufficient viscosity and wettability for adhering to the foam pre-cursors
- To experiment with different porous production techniques described in the literature

# REFERENCES

**Abrahams I., Knowles J.C.,** Effects of Sintering Conditions on Hydroxyapatite for use in Medical Applications, *J.Mater. Chem.*, 4(2): 185-188, 1994

**Akao M., Aoki H., Kato K. Sato A.,** Dense Polycrystalline b-TCP for Prosthetic Applications, Journal of Materials Science-Materials in Medicine, 17:343-346, 1982

**Andersson O.H., Karlsson K.H.,** Models for Physical Properties and Bioactivity of Phosphate Opal Glasses, *Glastech.Ber.*, 61(10):300-305, 1988

**Andronescu I., Draghici N., Stan E.A., Neagu R.,** Bioactive Glass-ceramics, Revue Roumaine de Chimie, 40(10): 1059-1065, 1995

**Anglin C., Tolhurst P., Wyss U.P., Pichora D.R.,** Glenoid Cancellous Bone Strength and Modulus, Journal of Biomechanics, 32:1091-1097, 1999

**Anselme K., Noel B., Flautre B., Blary M.C., Delecourt C., Descamps M., Hardouin P.,** Association of Porous HA and Bone Marrow Cells for Bone Regeneration, *Bone*, 25(2):515-545, 1999

**Aoki H.,** Science and Medical Applications of HA, *Takayama Press System Centre Co.*, 1991

**Arita I.H., Wilkinson D.S., Mondragon M.A., Castano V.M.,** Chemistry and Sintering Behaviour of Thin Hydroxyapatite Ceramics with Controlled Porosity, *Biomaterials*, 16: 403, 1995

**Benhayoune H., Jallot E., Laquerriere P., Balossier G., Bonhomme P., Frayssinet P.,** Integration of Dense HA Rods into Cortical Bone, *Biomaterials*, 21:235-242, 2000

**Binner J.G.P.,** Production and Properties of Low Densty Engineering Ceramic Foams, *British Ceramic Transactions*, 96(6):247-249, 1997

**Black J., Hastings G.,** Handbook of Biomaterial Properties, *Chapman & Hall*, 1998

**Boccaccini A.R.,** Machinability and Brittleness of Glass-ceramics, *Journal of Materials Processing Technology*, 65:302-304, 1997

**Bonfield W.,** Composites for Bone Replacement, *Journal of Biomedical Engineering*, 10:522-556, 1988

**Bonfield W., Datta P.K.,** Fracture Toughness of Compact Bone, *Journal of Biomechanics*, 9:131-134, 1976

**Brunski J.B.,** Influence of Mechanical Factors at the Bone-Biomaterial Interface, In "The Bone-Biomaterial Interface", *University of Toronto Press*, J.E.Davies, 1991

**Burger W., Richter H.G., Piconi C., Vatteroni R., Cittadini A., Boccalan M.,** New Y-TZP Powders for Medical Grade Zirconia, *Journal of Materials Science-Materials in Medicine*, 8:113-118, 1997

**Burstein F.D., Cohen S.R., Hudgins R., Boydston W.,** The Use of Porous Granular HA in Secondary Orbitocranial Reconstructions, *Plastic Reconstructive Surgery*, 100:869-874, 1997

**Callister Jr. W.D.,** Materials Science and Engineering: An Introduction, Third Edition, *John Whiley & Sons Inc.*,U.S., 1994

**Carter D.R., Giori N.J.,** Effect of Mechanical Stress on Tissue Differentiation in the Bony Implant Bed, In "The Bone-Biomaterial Interface", University of Toronto Press, J.E.Davies, 1991

**Catanese III J., Featherstone J.D.B., Keaveny T.M.,** Characterization of the Mechanical and Ultrastructural Properties of the Heat-Treated Cortical Bone for Use as a Bone Substitute, *Biomaterials*, 45:327-336, 1999

**Cattermole H.C., Fordham J.N., Cunningham J.L.,** Bone Mineral Changes During Tibial Fracture Healing, *Clinical Orthopaedics and Related Research*, 339:190-196, 1997

**Cezayirlioglu H., Bahniuk E., Davy D.T., Heiple K.G.,** Anisotropic Yield Behaviour of Bone Under Combined Axial Force and Torque, Journal of Biomechanics, 18:61-69, 1985

**Chang B-S., Lee C-K., Hong K-S., Youn H-J., Ryu H-S., Chung S-S., Park K-W.,** Osteoconduction of Porous HA with Various Pore Configurations, *Biomaterials*, 21:1291-1298, 2000

**Christel P., Meunier a., Dorlot J., Metal J.,** Biomechanical Compatibility and Design of Ceramic Implants for Orthopaedic Surgery. Bioceramics: Materials Characteristics vs In-vivo Behaviour, *Annals of the New York Academy of Science*, 523: 234-256, 1988

**Clement J., Ekeberg L., Martinez S., Ginebra M.P., Gil F.J., Planell J.A.,** Influence of the Chemical Composition on the Mechanical Properties and In-vitro Solubility of Phosphate Glasses in the System P2O5-CaO-Na2O, *Bioceramics 11*, Eds: LeGeros R.Z. & LeGeros J.P., NY, 1998

**Colgerg A., Frazine R., Sampson K., Villarragu M.L., Didier P.J.,** Mechanical Properties of Rhesus Femoral Cortical Bone as Determined by 3-Point Bending and Ultrasound Tests, *Faseb Journal*, 19(5:2SS):A912, 1999

**Courtney A.C., Hayes W.C., Gibson L.J.,** Age-Related Differences in Post-Yield Damage of Human Cortical Bone. Experiment and Model, *Journal of Biomechanics*, 29(2):257-260, 1996

**Cowin S.C., Van Buskirk W.C., Ashman R.B.,** The Properties of Bone. In: *Handbook of Engineering*, Eds: Skalak A., Chien S., 2-1/2-27, 1986

**Currey J.D.,** Mechanical Properties of Vertebrate Hard Tissues, *Proceedings of the Institution of Mechanical Engineers*, 212 (H): 399-411, 1998

**Currey J.D., Brear K., Zioupos P.,** The Effects of Ageing and Changes in Mineral Content in Degrading the Toughness of Human Femora, *Journal of Biomechanics*, 29(2): 257-260, 1996

**De Groot K.,** Bioceramics of Calcium Phosphate, 1983

**De Groot K.,** Effect of Porosity and Physicochemical Properties on the Stability, Resorption, and Strength of Calcium Phosphate Ceramics, *Annals New York Academy of Sciences*, 227-233, 1987

**De With G., Vandijk H.J.A., Hattu N., Prijs K.,** Preparation, Microstructure and Mechanical Properties of Dense Polycrystalline Hydroxyapatite, *Journal of Materials Science*, 16:1592-1598,1981

**Denissen H., Montanari C., Martinetti R., Van Lingen A., Van den Hooff A.,** Alveolar Bone Response to Submerged Biphosphonate-complexed HA Implants, *Journal of Periodontology*, 71:279-286, 2000

**Ducheyne R., Radin S., King L., Ishikawa K., Kim C.S.,** In-vitro Dissolution and Precipitation of Calcium Phosphate Phases on Various Biomaterials, Bioceramics 4, Eds: Bonfield W., Hastings G., Tanner K.E., London, 1991

**Duskova M., Kozak J., Mazanek J., Smahel Z., Vohradnik M.,** Augmentation of Facial Skeleton with Ceramics in Congenital Disorders and in Post-Traumatic or Post-Operative Deformities, *European Journal of Plastic Surgery*, 23:57-63, 2000

**Engin N.O., Tas A.G.,** Manufacture of Macroporous Calcium Hydroxyapatite Bioceramics, Journal of the European Ceramic Society, 19(13-14): 2569-2572, 1999

**Engstrom A.,** In "*Bone as Tissue*", Eds: Rodahl K., Nicholson J.T., Brown E.M., NY, 1960

**Erts D., Gatherole L.J., Atkins E.D.T.,** Scanning Probe Microscopy of Crystallites in Calcified Collagen, *Journal of Materials Science-Materials in Medicine*, 5:200-206, 1994

**Fabbri M., Celotti G.C., Ravaglioli A.,** Granulates Based on Calcium Phosphate with Controlled Morphology and Porosity for Medical Applications: Physico-Chemical Parameters and Production Techniques, *Biomaterials*, 15(6): 474-477, 1994

**Fernandez-Moran H.,** *Biochim.Biophys.Acta*, 23:260, 1957

**Fitton-Jackson S., Randall J.,** Fibrogenesis and the Formation of Matrix in Developing Bone, In "*Ciba Foundation Symposium on bone Structure and Metabolism*", Eds: Wolstenholme G.E.W., O'Connor C.M., Churchhill, London, 1956

**Fitzgerald T.J., Michaud V.J., Mortensen A.,** Processing of Microcellular SiC foams, *Journal of Materials Science*, 30:1037-1045, 1995

**Flautre B., Anselme K., Delecourt C., Lu J., Hardouin P., Descamps M.,** Histological Aspects in Bone Regeneration of an Association with Porous HA and Bone Marrow Cells, *Journal of Materials Science-Materials in Medecine*, 10:811-814, 1999

**Frame J.,** *InternationalJournal of Oral and Maxillofacial Surgery*, 16:642, 1987

**Fujishiro Y., Hench L.L., Oonishi H.,** Quantitative Rates of In-vivo Bone Generation of Bioglass® and Hydroxyapatite Particles as Bone Graft Substitute, *Journal of Materials Science-Materials in Medicine*, 8:649-652, 1997

**Furakawa T., Matsusue Y., Yasunaga T., Shikinami Y., Okuno M., Nakamura T.,** Biodegradation Behaviour of Ultra-High-Strength HA/Poly(L-Lactide) Composite Rods for Internal Fixation of Bone Fractures, *Biomaterials*, 21: 889-898, 2000

**Galante J., Rostoker W., Ray R.D.,** Physical Properties of Trabecular Bone. *Calif.Tissue.Res.*, 5:236, 1970

**Gaynor-Evans F.,** Mechanical Properties and Histology of Cortical Bone from Younger and Older Men, *Anatomical Records*, 185:1-12, 1975

**Gaynor-Evans F., King A.I.,** Regional Differences in some physical properties of human spongy bone, *Biomechanical Studies of the Musculoskeletal System*, Ed.: Charles C.Thomas, Springfield, 1961, 49

**Gauthier O., Bouler J.M., Aguado E., Pilet P., Daculsi G.,** Macroporous Biphasic Calcium Phosphate Ceramics: Influence of Macropore Diameter and Macroporosity Percentage on Bone Ingrowth, *Biomaterials*, 19:133-139, 1998

**Gibson L.G., Ashby M.F.,** *Cellular Solids*, Pergamon Press, 1988

**Goldschmidt, V.M.,** Skrifter Norke Videnskaps Adad (Oslo), I.Math-Naturwiss., K1(8):7, 1926

**Grant R.A., Horne R.W., Cox R.W.,** New Model for the Tropocollagen Molecule and its Mode of Aggregation, *Nature*, 207:822-826, 1965

**Griffith A.A.,** The Phenomena of Rupture and Flow in Solids, In: , Eds: , 221A(587):163-198, 1920

**Gross U., Strunz V.,** The Interface of Various Glasses and Glass Ceramics with a Bony Implantation Bed, *Journal of Biomedical Materials Research*, 19:251-271, 1985

**Gundle R., Joyner C.J., Triffitt J.T.,** Interactions of Human Osteoprogenitors with Porous Ceramic following Diffusion Chamber Implantation in a Xenogenic Host, *Journal of Materials Science-Materials in Medicine*, 8:519-523, 1997

**Gustow I., Avramov I., Kastner K.,** Glass Formation and Crystallisation, Journal of Non-Crystalline Solids, 123:97-113, 1990

**Haddock S.M., Debes J.C., Nauman E.A., Fong K.E., Arramou Y.P., Keaveny T.M.,** Structure-Function Relationships for Coralline HA Bone Substitute, *Journal of Biomedical Materials Research*, 47:71-78, 1999

**Hancox N.M.,** Biology of Bone, *Cambridge University Press*, Great Britain, ©1972,p.19

**Hanson W., Fernie J.,** An Overview of Glass-Ceramics, *Bulletin (T.W.I.)*, Reprint 438/1/93, 1993

**Hench L.L.,** Ceramic Implants for Humans, *Advanced Ceramic Materials*, 1(4), 1986

**Hench L.L.,** From Concept to Commerce: The Challenge of Technology Transfer in Materials, *MRS Bulletin*, 1990

**Hench L.L.,** Bioceramics:From Concept to Clinic, *Journal of the American Chemical Society*, 74(7):1487-1510, 1991

**Heymann D., Pradal G., Benahmed M.,** Cellular Mechanisms of Calcium Phosphate Ceramic Degradation, *Histology and Histopathology*, 14:871-877, 1999

**Hing K.A., Best S.M., Tanner K.E., Bonfield W., Revell P.A.,** Biomechanical Assessment of Bone Ingrowth in Porous Hydroxyapatite", Journal of Materials Science-Materials in Medicine, 8:731-736, 1997

**Hing K.A., Gibson I.R., Revell P.A., Best S.M., Bonfield W.,** Influence of Phase Purity on the In-vivo Response to Hydroxyapatite, In:Bioceramic 13, Proceedings of the Int. Symposium on Ceramics in Medicine, Eds:Giannini S., Moroni A., Switzerland, pp. 3763-376, 2000

**Hockin H.K., Smith D.T., Jahanmir S.,** Influence of Microstructure on Indentation and Machining of Dental Glass-Ceramics, *Journal of Materials Research*, 11(9):2325-2337, 1996

**Hollinger J.O., Brekke J., Gruskin E., Lee D.,** Role of Bone Substitutes, *Clinical Orthopaedics and Related Research*, 324:55-65, 1996

**Holmes R.E.,** Bone Regeneration Within a Coralline HA Impant, *Bone Regeneration*, 63(5):626-633, 1978

**Holmes R.E.,** A Coralline HA Bone Graft Substitute, *Clinical Orthopaedics and Related Research*, 188:252-262, 1984

**Holmes R.E., Bucholz R.W., Mooney V.,** Porous HA as a Bone Graft Substitute in Diaphyseal Defects:A Histometric Study, *Journal of Orthopaedic Research*, 5:114-121, 1987

**Hoshi A., Watanabe H., Chiba M., Inaba Y.,** Effects of Exercise at Different Ages on Bone Density and Mechanical Properties of Femoral Bone of Aged Mice, *Tohoku Journal of Experimental Medicine*, 185:15-24, 1998

**Huang T.C., Chen H.,** A Study on the Preparation and Gas Permeation of Porous Alumina Supports, *Separation Science and Technology*, 30(10): 2189-2209, 1995

**Huang J., DiSilvio L., Wang M., Tanner K.E., Bonfield W.,** In-vitro Mechanical and Biological Assessment of an HA-Reinforced Polyethylene Composite, *Journal of Materials Science-Materials in Medecine*, 8:775-779, 1997

**Huang J., Wang M., Best S., Tanner K.E., Bonfield W.,** Evaluation of Bioglass® and HA-Reinforced Polyethylene Composites after Ageing in Simulated Body Fluid, *Bioceramics 11*, Eds: LeGeros R.Z. & LeGeros J.P., NY, 1998

**Inman C.L., Warren G.L., Hogan H.A., Bloomfield S.A.,** Mechanical Loading Attenuates Bone Loss due to Immobilisation and Calcium Deficiency, *Journal of Applied Physiology*, 87(1):189-195, 1999

**Inoue O., Ibaraki K., Shimabukuro H., Shingaki Y.,** Solo Implantation of Porous Cuboidal Hydroxyapatite for the Treatment of Simple Bone Cysts, *Bioceramics 4*, Eds: Bonfield W., Hastings G.W., Tanner K.E., 1991

**James P.F., Iqbal Y., Jais U.S., Jordery S., Lee W.E.,** Crystallisation of Silicate and Phosphate Glasses, *Journal of Non-Crystalline Solids*, 219:17-29, 1997

**Jepsen K.J., Davy D.T.,** Comparison of Damage Accumulation Measures in Human Cortical Bone, *Journal of Biomechanics*, 30(9):891-894, 1997

**Jha L.J.,** Preparation and Characterization of Fluoride-Substituted Apatites, *Journal of Materials Science-Materials in Medicine*, 8:185-191, 1997

**Kaneps A.J., Stover S.M., Lane N.E.,** Changes in Canine Cortical and Cancellous Bone Mechanical Properties Following Immobilization and Remobilization with Exercise, *Bone*, 21(5):419-423, 1997

**Kang Q., An Y.H., Friedman R.F.,** Mechanical Properties and Bone Densities of Canine Trabecular Bone, *Journal of Materials Science-Materials in Medicine*, 9:263-267, 1998

**Kay J.F.,** Calcium Phosphate Coatings for Dental Implants, *Dent.Clin.North.Amer.*, 36:1-18, 1992

**Kingery, Bowen & Uhlmann,** Introduction to Ceramics, 2nd Edition, *John Whiley & Sons Inc.*, Canada, 1976

**Klawitter J.J., Hulbert S.F.,** Application of Porous Ceramics for the Attachment of Load Bearing Orthopaedic Applications, *Journal of Biomedical Materials Research Sympsium*, 2:161, 1971

**Knabe C., Gildenhaar R., Berger G., Ostapowicz W., Fitzer R., Radlanski R.J., Gross U.,** Morphological Evaluation of Osteoblasts Cultured on Different Calcium Phosphate Ceramics, *Biomaterials*, 18:1339-1347, 1997

**Knepper M., Milthorpe B.K., Morica S.,** Interdiffusion in Short-Fibre Reinforced HA Ceramics, *Journal of Materials Science-Materials in Medicine*, 9:589-596, 1998

**Knepper M., Morica S., Milthorpe B.K.,** Stability of Hydroxyapatite while Processing Short-Fibre Reinforced HA Ceramics, *Biomaterials*, 18:1523-1529, 1997

**Knese K.H.**, Knochenstruktur als Vaerbundbau. Versuch einer technisehen Deutung der Materialstruktur des Knochens, in Zwanglose Aghandlungen aus dem Gebiet der Normalen und *Pathologischen Anatomie*, W.Bargmann, W.Doerr, Eds., Georg Thieme, Stuttgart, 4, 1988

**Knowles J.**, Development of Hydroxyapatite with Enhanced Mechanical Properties: Effect of High Glass Additions on Mechanical Properties and Phase Stability of Sintered Hydroxyapatite, *British Ceramic Transactions*, 93(3):100-103, 1994

**Knowles J.C., Abrahams I., Bonfield W.**, Effect of Reinforcing Glass Composition on Phase Transformation and Crystallographic Parameters in Hydroxyapatite, *Bioceramics 6*:191-196, Eds: Ducheyne P., Christiansen D., 1993

**Knowles J.C., Bonfield W.**, Development of a Glass-Reinforced HA with Enhanced Mechanical Properties:The Effect of Glass Composition on Mechanical Properties and its Relationship to Phase Changes, *Journal of Biomedical Materials Research*, 27:1591-1598, 1993

**Knowles J.C., Talal S., Santos J.D.**, Sintering Effects in a Glass Reinforced Hydroxyapatite, *Biomaterials*, 17(14):1437-1442, 1996

**Kokubo T, Ito S., Shigematsu M., Sakka S., Yamamuro T.**, Mechanical Properties of New Type of Apatite-Containing Glass-Ceramic for Prosthetic Application, *Journal of Materials Science*, 20:2001-2004, 1985

**Kotha S.P., Walsh W.R., Pan Y., Guzelsu N.**, Varying the Mechanical Properties of Bone Tissue by Changing the Amount of its Structurally Effective Bone Mineral Content, *Bio-Medical Materials and Engineering*, 8:321-334, 1998

**Krajewski A., Ravaglioli A., Roncari E., Pinasco P., Montanari L., Pantieri I.**, A Preliminary Study on the Use of Porous Ceramic Bodies for the Release of Pharmacological Substances, *Bioceramics 11*, Eds: LeGeros R.Z. & LeGeros J.P.), NY, 1998

**Kurata Y., Kushimoto H., Hoshi Y., Yutani Y., Horisawa Y., Sumida M.**, Ceramic Elbow Prosthesis, *Japan Society of Orthopaedic Ceramic Implants*, 3:99-105, 1983

**Kuroyama Y. Higashikata M., Nakamura S., Ohgaki M., Akao M., Aoki H.**, Crystal Chemistry and Biocompatibility of a-TCP produced from b-TCP by a Plasma-Spraying Technique, *Bioceramics 4*, Eds: Bonfield, Hastings, Tanner, London, Butterworth-Heinemann, 65-69, 1991

**Laczka-Osyczka A., Laczka M., Kasugai S., Ohya K.**, Behaviour of Bone Marrow Cells Cultured on Three Different Coatings of Gel-Derived Bioactive Glass-Ceramics at Early Stages of Cell Differentiation, *Journal of Biomedical Materials Research*, 42:433-442, 1998

**Ladizesky N.H., Ward I.M., Bonfield W.**, Hydroxyapatite/High-Performance Polyethylene Fibre Composites for High Load Bearing Bone Replacement Materials, *Journal of Applied Polymer Science*, 65(10):1865-1882, 1997

**Landis W.J., Song M.J., Leith A., McEwen L., McEwen B.F.**, Mineral and Organic Matrix Interaction in Normally Calcifying Tissue Visualised by High Voltage Electron Microscopic Tomography and Graphic Image Reconstruction, *Journal of Structural Biology*, 110:39-54, 1993

**Lawson A.C., Czernuszka J.T.**, Collagen-Calcium Phosphate Composites, *Proceedings of the Institution of Mechanical Engineers*, 212(H):413-425, 1998

**LeGeros R.Z., LeGeros J.P.**, Dense Hydroxyapatite, *An Introduction to Bioceramics*, Eds: Hench L.L., Wilson J., 9:139-180, 1993

**Le Huec J.C., Schaeverbeke T., Clement J., Faber J., Le Rebellr A.,** Influence of Porosity on the Mechanical Resistance of Hydroxyapatite Ceramics under Compressive Stress, *Biomaterials*, 16:113-118, 1995

**Li B., Aspden R.M.,** Composition and Mechanical Properties of Cancellous Bone from the Femoral Head of Patients with Osteoporosis or Osteoarthritis, *Journal of Bone and Mineral Research*, 12(4): 641-651, 1997

**Liao H., Mutrei H., Sjostrom M., Hammarstrom L., Li J.,** Tissue Responses to Natural Artgonite (Margartifa Shell) Implants In-vivo, *Biomaterials*, 21:457-468, 2000

**Lindahl O.,** Mechanical Properties of Dried Defatted Spongy Bone, *Acta.Orthop.Scand.*, 47:11, 1976

**Liu D.M.,** Fabrication and Characterization of Porous Hydroxyapatite Granules, *Biomaterials*, 17(20):1995-1997, 1996

***Liu D.M.,** Porous Hydroxyapatite Bioceramics, *Key Engineering Materials*, 115:209-232, 1996

**Liu D.M.,** Influence of Porosity and Pore Size on the Compressive Strength of Porous Hydroxyapatite Ceramic, *Ceramics International*, 23:135-139, 1997

***Liu D.M.,** Fabrication of Hydroxyapatite Ceramic with Controlled Porosity, *Journal of Materials Science-Materials in Medicine*, 8:227-232, 1997

**Lopes M.A., Santos J.D., Monteiro F.J., Knowles J.C.,** Glass-Reinforced Hydroxyapatite: A Comprehensive Study of the Effect of Glass Composition on the Crystallography of the Composite, *Journal of Biomedical Materials Research*, 39:244-251, 1998

**Lu H., Qu Z., Zhou Y.,** Preparation and Mechanical Properties of Dense Polycrytalline HA through Freeze-Drying, *Journal of Materials Science-Materials in Medicine*, 9:583-587, 1998

**Luo P., Nieh T.G.,** Preparing Hydroxyapatite Powders with Controlled Morphology, *Biomaterials*, 17(20):1996

**Magne P., Belser U.,** Esthetic Improvements and In-vitro Testing of In-Ceram Alumina and Spinell Ceramic, *The International Journal of Prosthodontics*, 10(5):459-466, 1997

**Marra K.G., Szem J.W., Kumta P.N., Dimilla P.A., Weiss L.E.,** In-vitro Analysis of Biodegradable Polymer Blend/HA Composites for Bone Tissue Engineering, *Journal of Biomedical Materials Research*, 47:324-355, 1999

**Martin R.B.,** Bone as a Ceramic Composite Material, *Mat.Science Forum*, 293:5-16, 1999

**Martin R.I., Brown P.W.,** Mechanical Properties of Hydroxyapatite Formed at Physiological Temperature, *Journal of Materials Science: Materials in Medicine*, 6:138-143, 1995

**McCalden R.W., McGeough J.A., Barker M.B., Court-Brown C.M.,** Age-Related Differences in the Tensile Properties of Cortical Bone. The Relative Importance in Changes in Porosity, Mineralisation, and Microstructure, *Journal of Bone and Joint Surgery*, 75-A:1192-1205, 1993

**McConnell D.,** Apatite, *Springer-Verlag*, 1973

**McDermott A.J., Reaney I.M., Lee W.E., James P.F.,** Microscopy of Calcium Phosphate Glass Ceramics, *Institute of Physics Conference Series*, 153:487-490, 1997

**McElhaney J.H., Byars E.F.,** Dynamic Response of Biological Materials, *American Society of Mechanical Engineers Publ.*, 65-WA/HUF 9, 1, 1965

**Metsger D.S., Reiger M.R., Foreman D.W.,** Mechanical Properties of Sintered HA and Tricalcium Phosphate Ceramic, *Journal of Materials Science-Materials in Medicine*, 10:9-17, 1999

**Miyata N., Matsuura W., Kokubo T., Nakamura T.,** Mechanical Behaviour of Bioactive Inorganic Filler-Resin Composite Cements in a Simulated Body Fluid, *Journal of the Ceramic Society*, 107(10): 935-943, 1999

**Murasawa A., Aizawa T., Hanyu T., Wakatsuki H.,** Experience of Alumina Ceramic Total Ankle Prosthesis, *Japan Society of Orthopaedic Ceramic Implants*, 2:177-184, 1982

**Nakamura T., Yamamuro T., Higashi S., Kokubo T., Ito S.,** *Journal of Biomedical Materials Research*, 19:685-698, 1985

**Nicholson P.H.F., Cheng X.G., Lowet G., Boonen S., Davie M.W.J., Dequeker J., Van der Perre G.,** Structural and Material Mechanical Properties of Human Vertebral Cancellous Bone, *Medical Engineering and Physics*, 19(8):729-737, 1999

**Odgaard A., Linde F.,** The Underestimation of Young's Modulus in Compressive Testing of Cancellous Bone Specimens, *Journal of Biomechanics*, 24(8): 691-698, 1991

**Ohgushi H., Dohi Y., Yoshikawa T., Tamai S., Tabata S, Okunaga K., Shibuya T.,** Osteogenic Differentiation of Cultured Marrow Stromal Cells on the Surface of Bioactive Glass-Ceramics, *Journal of Biomedical Materials Research*, 32:341-348, 1996

**Ono I., Tateshita T, Nakajima T., Ogawa T.,** Determinations of Strength of Synthetic HA Ceramic Implants, *Plastic and Reconstructive Surgery*, 102(3):807-813, 1998

**Oonishi H., Hasegawa T.,** Cementless Alumina Ceramic Total Knee Prosthesis, *Japan Society of Orthopaedic Ceramic Implants*, 1:157-160, 1981

**Oreffo R.O.C., Triffit J.T.,** Future Potentials for Using Osteogenic Stem Cells and Biomaterials in Orthopaedics, *Bone*, 25(2):5S-9S, 1999

**Passuti N., Daculsi G., Rogez J.M., Martin S., Bainvel J.V.,** Macroporous Calcium Phosphate Ceramic Performance in Human Spine Fusion, *Clinical Orthopaedics and Related Research*, 248:169-175, 1989

**Pautard F.G.E.,** A Biomolecular Survey of Calcification, In: Calcified Tissues, *Proceedings of the Third European Symposium*, Eds: Fleish H., Blackwood H.J.J., Owen M.,NY, 108-122 1966

**PDF Card No. 9-432, 9-169, 9-348,** *ICDD*, Newton Square, Pennsylvannia, USA

**Pecher P.F.,** Transient Thermal Stress Behaviour in Zirconia-Toughened Alumina, *Journal of the American Ceramic Society*, 64:37-39, 1981

**Peelen J.G.J., Rejda B.V., DeGroot K.,** Preparation and Properties of Sintered Hydroxylapatite, Ceramiurgica Int., 4(2):71-74, 1978

**Piecuch J.F.,** *Journal of Dental Research*, 61(12):1458, 1982

**Piconi C., Maccauro G.,** Zirconia as a Ceramic Biomaterial, *Biomaterials*, 20:1-25, 1999

**Pilliar R.M.,** Quantitative Evaluation of the Effect of Movement at a Porous Coated Implant-Bone Interface. Mechanical Effects on Interfacial Biology, In "*The Bone-Biomaterial Interface*", Ed: Davies J.E., University of Toronto, 34: 380-387, 1991

**Pollack S.R., Salztein R., Peinkowiski D.,** The Electric Double Layer in Bone and its Influence on Stress-Generated Potentials, *Calcified Tissue International*, 36:577, 1984

**Pritchard J.J.,** The General Histology of Bone, In: *The Biochemistry and Physiology of Bone*, 2nd Edition, Ed: Bourne G.H, 1, Academic Press, NY, 1972

**Radin S.R., Ducheyne P.,** Effect of Bioactive Ceramic Composition and Structure on In-vitro Behaviour.III.Porous vs Dense Ceramics, *Journal of Biomedical Materials Research*, 28:1303-1309, 1994

**Radin S.R., Ducheyne P.,** Effect of Serum Protein on Solution-Induced Surface Transformations of Bioactive Ceramics, *Journal of Biomedical Materials Research*, 30:273-279, 1996

**Raynaud S., Champion E., Bernache-Assolant D.,** Synthesis, Sintering, and Mechanical Characteristics of Non-Stoichiometric Apatite Ceramics, *Bioceramics 11*, Eds: LeGeros R.Z. & LeGeros J.P., NY, 1998

**Reaney I.M., James P.F., Lee W.F.,** Effect of Nucleating Agents on the Crystallisation of Ca-P Glasses, *Journal of the American Ceramic Society*, 79(7):1934-1944, 1996

**Rho J.Y., Flaitz D., Swarnakar V., Sacharaya R.,** The Characterization of Broadband Ultrasound Attenuation and Fractal Analysis by Biomechanical Properties, *Bone*, 20(5):497-504, 1997

**Rho J.Y., Kuhn-Spearing L., Zioupos P.,** Mechanical Properties and the Heirarchical Structure of Bone, *Medical Engineering and Physics*, 20:92-102, 1998

**Rice J.C., Cowin S.C., Bowman J.A.,** On the Dependance of the Elasticity and Strength of Cancellous Bone on Apparent Density, *Journal of Biomechanics*, 21:155-168, 1988

**Riqles A., Meunier F.J., Castanet J., Francillon-Vieillot H.,** Comparative Microstructure of Bone, *Bone*, 3:1-78, 1991

**Rodriguez-Lorenzo L.M., Ferreira J.M.F., Vallet-Regi M.,** Processing of Porous HA by Starch Consolidation, *Bioceramics 11*, Eds. LeGeros R.Z. &LeGeros J.P., NY, 1998

**Roy D.M., Linnehan S.K.,** Hydroxyapatite Formed Coral Skeleton Carbonate by Hydrothermal Exchange, *Nature*, 247:220-222, 1974

**Salin V., Jalisi I.J., Lee D., Franks K., Hastings G.W., Knowles J.C., Olsen I.,** The Response of Human Osteoblast Cell Lines to Phosphate-Based Soluble Glasses, *Bioceramics 11*, Eds. LeGeros R.Z. &LeGeros J.P., NY, 1998

**Salyer K., Holmes R., Johns D.,** Replamineform Porous HA as Bone Substitutes in Craneofacial Osseous Reconstruction, *Journal of Dental Research*, 56B:173, 1977

**Sambrook R.M., Binner J.G., Smith R.T., Reochert J.,** Porous Articles, WO/93/04013, 1993

**Santos J.D., Knowles J.C., Morrey S., Monteiro F.J., Hastings G.W.,** Development of a Glass Reinforced Hydroxyapatite with Enhanced Mechanical Properties:Physical Characterization and In-vivo Studies, *Bioceramics 5*, Eds: Yamamuro T., Kokubo T., Nakamura T., Japan, 1992

**Santos J.D., Knowles J.C., Reis R.L., Monteiro F.J., Hastings G.W.,** Microstructural Characterization of Glass-Reinforced Hydroxyapatite Composites, *Biomaterials*, 15(1), 1994

**Santos J.D., Silva P.L., Knowles J.C., Talal S., Monteiro F.J.,** Reinforcement of Hydroxyapatite by Adding $P_2O_5$-CaO Glasses with $Na_2O$, $K_2O$, and MgO, *Journal of Materials Science-Materials in Medicine*, 7:187-189, 1996

**Sax M., Zografou C, Telle R., Kalawrytinos G.,** Properties of Sintered Apatite Ceramics, *Ceramic Processing Science and Technology*, 51:701-705, 1999

**Schoenfeld C.M., Lautenschlager E.P., Meyer P.P.,** Mechanical Properties of Human Cancellous Bone in the Femoral Head, *Med.Biol.Eng.*, 12:313, 1974

**Seidel J., Claussen N., Rodel J.,** Reliability of Alumina Ceramics 2:Effect of Processing, *Journal of the European Ceramic Society*, 17:727-733, 1997

**Sepulveda P., Binner J.G.P., Rogero S.O., Higa O.Z., Bressiani J.C.,** Production of Porous HA by the Gel-Casting of Foams and Cytotoxic Evaluation, *Journal of Biomedical Materials Research*, 50:27-34, 2000

**Shareef M.Y., Messer P.F., Van Noort R.,** Fabrication, Characterization and Fracture Study of a Machinable HA Ceramic, *Biomaterials*, 14(1):69-75, 1993

**Shaw J.,** Materials and Methods, *PhD. Thesis*, Ch.3:99-104, 1996

**Shors E.C., Holmes R.E.,** Porous Hydroxyapatite, In "*An Introduction to Bioceramics*", Eds: Hench L.L., Wilson J., 10:181-198, 1993

**Simske S.J., Ayers R.A., Bateman T.A.,** Porous Materials for Bone Engineering, *Materials Science Forum*, 250:151-182, 1997

**Suchanek W., Yashima M., Kakihan M., Yoshimura M.,** Processing and Mechanical Properties of HA Reinforced with HA Whiskers, *Biomaterials*, 17:1715-1723, 1996

**Suchanek W., Yashima M., Kakihan M., Yoshimura M.,** HA/HA-Whisker Composites without Sintering Additives:Mechanical Properties and Microstructural Evolution, *Journal of the American Ceramic Society*, 80(11):2805-2813, 1997

**Sugita H., Oka M., Toguchida J., Nakamura T., Ueo T., Hayami T.,** Anisotropy of Osteoporotic Cancellous Bone, *Bone*, 24(5): 513-516, 1999

**Tampieri A., Celotti G., Szontagh G., Landi E.,** Sintering and Characterization of HA and TCP Bioceramics with Control of their Strength and Phase Purity, *Journal of Materials Science-Materials in Medicine*, 8:29-37, 1997

**Tancred D.C., McCormack B.A.O., Carr A.J.,** A Quantitative Study of the Sintering and Mechanical Properties of HA/Phosphate Glass Composites, *Biomaterials*, 19:1735-1743, 1996

**Tancred D.C., McCormack B.A.O., Carr A.J.,** A Synthetic Bone Implant Macroscopically Identical to Cancellous Bone, *Biomaterials*, 19:2303-2311, 1998

**Thompson R.C., Yaszemski M.J., Powers J.M., Mikos A.G.,** HA Fibre Reinforced Poly (α-hydroxy ester) Foams for Bone Regeneration, *Biomaterials*, 19:1935-1943, 1998

**Twigg M.V., Richardson J.T.,** Preparation and Properties of Ceramic Foam Catalyst Supports, *Preparation of Catalysts VI*, Ed:, Poncelet G. et al, 1995

**Ueshira T.,** On the Relationship Between the Chemical Components and the Strength of Compact Bone, *J.Kyoto Prefect.Med.Univ.*, 68:923-940, 1960

**Vaughan J.M.,** The Physiology of Bone, *Oxford University Press*, London, 1970

**Wang C.K., Ju C.P., Chern Liu J.H.,** Effect of Doped Bioactive Glass on Structure and Properties of Sintered Hydroxyapatite, *Materials Chemistry and Physics*, 53:138-149, 1998

**Wang X.D., Masilamani N.S., Mabrey J.D., Alder M.E., Agrawal C.M.,** Changes in the Fracture Toughness of Bone May Not be Reflected in its Mineral Density, Porosity, and Tensile Properties, *Bone*, 23(1):67-72, 1998

**Weber J.N., White E.W.,** Carbonate Minerals as Precursors of New Ceramic, Metal, and Polymer Materials for Biomedical Applications, *Mineral Science and Engineering*, 5:151-165, 1973

**Weiner S., Price P.A.,** Disaggregation of Bone into Crystals, *Calcified Tissue International*, 39(6): 365-375, 1986

**Weiner S., Traub W., Wagner H.D.,** Lamellar Bone: Structure-Function Relations, *Journal of Structural Biology*, 126:241-255, 1999

**Wells J.W.,** Scleratina, In "*Treatise on Invertebrate Paleontology*", Eds: Moore R.C., University of Kansas Press, Part F:328, 1967

**Weston T.,** *Atlas of Anatomy*, Marshall Cavendish Books Ltd., 1988

**White S.M., Holmes D.J.S., Miller A., Timmins P.A.,** Collagen-mineral axial relationship in calcified turkey leg tendon by X-ray and nuetron diffraction, *Nature*, 266:421, 1977

**White R.A., Weber J.N., White E.W.,** Replamineform: A New Process for Preparing Porous Ceramic, Metal, and Polymer Prosthetic Materials, *Science*, 176:922-924, 1972

**Williams E.J.A.E., Gaynor-Evans J.R.,** Expanded Ceramic Foam, *Journal of Materials Science*, 31:559-563, 1996

**Wilson J.,Low S.B.,** Bioactive Ceramics for Periodontal Treatment; Comparative Studies in the Patus Monkey, *Journal of Applied of Biomaterials*, 3:123-129, 1992

**Wohl G., Goplen G., Ford J., Novak K., Hurtig M.,** Mechanical Integrity of Subchondral Bone in Osteochondral Autografts and Allografts, *Canadian Journal of Surgery*, 41(3):228-233, 1998

**Wolff J.,** *Pas Destez der Transformation der Knocken*, Hirschwald, Berlin, 1892

**Wolf W.D., Vaidya K.J., Francis L.F.,** Mechanical Properties and Failure Analysis of Alumina-Glass Dental Composites, *Journal of the American Ceramic Society*, 79:1769-1776, 1996

**Xiaodong G., Qixin Z., Jingyuan D.U., Dapin Y., Yahua Y., Shipu L.,** Biodegradation and Mechanical Properties of HA/Poly-D1-lactide Composites for Fracture Fixation, *Journal of Wuhan University of Technology*, 13(4): 9-15, 1998

**Yamamuro T., Takagi H.,** Bone Bonding Behaviour of Biomaterials with Different Surface Characterisitics under Load-Bearing Conditions, In "*The Bone-Biomaterial Interface*", University of Toronto Press, Ed: Davies J.E., 1991

**Yang X., Wang Z.,** Synthesis of Biphasic Ceramics of HA and β-TCP with Controlled Phase Content and Porosity, *J. of Materials Chemistry*, 8(10):2233-2237, 1998

**Ylinen P.,** Filling of Bone Defects with Porous HA Reinforced with Polylactide or Polyglycolide Fibres, *Journal of Materials Science-Materials in Medicine*, 5:522-528, 1994

**Yoshikawa T., Ohgushi H., Nakajima H., Yamada E., Ichijima K., Tamai S., Ohta T.,** In-vivo Osteogenic Durability of Cultured Bone in Porous Ceramics, *Transplantation*, 69(1):128-134, 2000

**Yoshikawa T., Ohgushi H., Tamai S.,** Immediate bone forming capability of prefabricated osteogenic hydroxyapatite, *Journal of Biomedical Materials Research*, 32:481-492, 1996

**Young R.A., Elliot J.C.,** Scale Bases for Several Properties of Apatites, *Archives of Oral Biology*, 11:699-707, 1966

**Zachariasen W.H.,** The Atomic Arrangement of Glass, *Journal of the American Ceramic Society*, 54:3841-3851, 1932

**Zarzycki J.,** Glasses and the Vitreous State, *Cambridge University Press*, 1991

**Zhang R., Ma P.X.,** Poly(α-hydroxyl acids) HA Porous Composites for Bone-Tissue Engineering. I. Preparation and Morphology, *Journal of Biomedical Materials Research*, 44:446-455, 1999

**Zyman Z., Ivanor I., Glushko V., Dedukh N., Malayshkina S.,** Inorganic Phase Composition of Remineralisation in Porous CaP Ceramics, *Biomaterials*, 19:1269-1273, 1998

**Zysset P.K., Guo X.E., Hoffler C.E., Moore K.E.,** Elastic Modulus and Hardness of Cortical and Trabecular Bone Lamellae Measured by Nanoindentation in the Human Femur, *Journal of Biomechanics*, 32:1005-1012, 1999

**Akao M., Aoki H., Kato K.** Mechanical Properties of Sintered Hydroxyapatite for Prosthetic Applications. J. Mater. Sci., **16**, 809-812, **(1981)**.

**Denissen H.W., de Groot K., Driessen A.A., Wolke J.G.C., Peelen J.G.J., van Dijk H.J.A., Gehring A.P., Klopper P.J.** Hydroxyapatite Implants: Preparation, Properties and Use in Alveolar Ridge Preservation. Sci. Ceram., **10**, 63-69, **(1980a)**

**Le Huec J.C. Schaeuerbeke T., Clement D., Faber J., le Rebeller A.** Influence of Porosity on the Mechanical Resistance of Hydroxyapatite Ceramics under Compressive Stress. Biomaterials, **16**, 113-118, **(1995)**.

**Poumarat G., Squire P.** Comparision of Mechanical Properties of Human, Bovine Bone and a New Processed Bone Xenograft. Biomaterials, **14** (5), 337-340, **(1993)**.

**Rao W.R., Boehm R.F.** A Study of Sintered Apatites. J. Dent Res., **35** (6), 1351-1354, **(1974)**.

**de With G., van Dijk H.J.A., Hattu N., Prijs K.** Preparation, Microstructure and Mechanical Properties of Dense Polycrystalline Hydroxyapatite. J. Mater. Sci., **16**, 1592-1598, **(1981)**.

# APPENDICES

## APPENDIX A.1

**Table A.1.1** The mechanical properties and Weibull Modulus of P201 HA sintered at different temperatures

| Batch | Sintering Temperature (°C) | Mean Density ($g.cm^{-3}$) | Mean Biaxial Flexural Strength (MPa) | Weibull Modulus |
|---|---|---|---|---|
| 1 | 1000 | 1.64 ± 0.012 | 22.71 ± 9.14 | 0.43 |
| 2 | 1000 | 1.64 ± 0.023 | 21.56 ± 3.64 | 6.54 |
| 3 | 1100 | 2.02 ± 0.016 | 23.04 ± 6.58 | 3.63 |
| 4 | 1100 | 2.19 ± 0.053 | 33.06 ± 4.95 | 7.06 |
| 5 | 1200 | 2.78 ± 0.038 | 55.76 ± 16.86 | 2.96 |
| 6 | 1200 | 2.97 ± 0.041 | 64.27 ± 11.40 | 5.36 |
| 7 | 1250 | 2.97 ± 0.015 | 16.43 ± 6.25 | 3.90 |
| 8 | 1250 | 3.07 ± 0.015 | 24.63 ± 12.72 | 2.59 |
| 9 | 1300 | 3.05 ± 0.031 | 11.11 ± 2.37 | 5.76 |
| 10 | 1300 | 3.04 ± 0.034 | 11.80 ± 2.44 | 5.68 |

## APPENDIX A.2

**Table A.2.1.** RI-TCP in CAP2-HA with different wt % additive

| Sample ID | 1 wt % | 2.5 wt % | 3.25 wt % | 4 wt % | 5 wt % |
|---|---|---|---|---|---|
| 1 | 4.2 | | | | |
| 2 | 6.3 | | | | |
| 3 | | 8.3 | | | |
| 4 | | 12.5 | | | |
| 5 | | 10.4 | | | |
| 6 | | 8.3 | | | |
| 7 | | | 14.3 | | |
| 8 | | | 12.5 | | |
| 9 | | | | 10.4 | |
| 10 | | | | 20.8 | |
| 11 | | | | 20.8 | |
| 12 | | | | 20.8 | |
| 13 | | | | | 22.9 |
| 14 | | | | | 16.6 |

**Table A.2.2** BFS of CAP2-HA

| Batch | 1 wt % BFS (MPa) | 2.5 wt % BFS (MPa) | 3.25 wt % BFS (MPa) | 4 wt % BFS (MPa) | 5 wt % BFS (MPa) |
|---|---|---|---|---|---|
| 1 | 75.81 ± 4.32 | | | | |
| 2 | 72.87 ± 11.49 | | | | |
| 3 | | 70.74 ± 7.15 | | | |
| 4 | | 101.66 ± 20.99 | | | |
| 5 | | 95.95 ± 8.95 | | | |
| 6 | | 96.62 ± 10.03 | | | |
| 7 | | | 91.09 ± 16.25 | | |
| 8 | | | 94.26 ± 11.3 | | |
| 9 | | | | 101.28 ± 10.08 | |
| 10 | | | | 130.16 ± 20.38 | |
| 11 | | | | 102.54 ± 11.02 | |
| 12 | | | | 89.60 ± 11.57 | |
| 13 | | | | | 87.04 ± 12.50 |
| 14 | | | | | 92.42 ± 10.86 |

**Table A.2.3** Mean density measurements for all CAP2-HA batches

| Batch | 1 wt % D ($g.cm^{-3}$) | 2.5 wt % D ($g.cm^{-3}$) | 3.25 wt % D ($g.cm^{-3}$) | 4 wt % D ($g.cm^{-3}$) | 5 wt % D ($g.cm^{-3}$) |
|---|---|---|---|---|---|
| 1 | 2.94 ± 0.024 | | | | |
| 2 | 2.71 ± 0.033 | | | | |
| 3 | | 2.98 ± 0.064 | | | |
| 4 | | 2.92 ± 0.028 | | | |
| 5 | | 2.95 ± 0.025 | | | |
| 6 | | 2.97 ± 0.01 | | | |
| 7 | | | 2.96 ± 0.041 | | |
| 8 | | | 2.95 ± 0.05 | | |
| 9 | | | | 2.98 ± 0.035 | |
| 10 | | | | 2.93 ± 0.027 | |
| 11 | | | | 2.97 ± 0.016 | |
| 12 | | | | 2.97 ± 0.019 | |
| 13 | | | | | 2.92 ± 0.008 |
| 14 | | | | | 3.14 ± 0.83 |

**Table A.2.4** Weibull modulus values for the BFS of all CAP2-HA batches

| Batch | 1 wt % WM | 2.5 wt % WM | 3.25 wt % WM | 4 wt % WM | 5 wt % WM |
|---|---|---|---|---|---|
| 1 | 21.5 | | | | |
| 2 | 6.6 | | | | |
| 3 | | 11.5 | | | |
| 4 | | 4.9 | | | |
| 5 | | 13.2 | | | |
| 6 | | 11.1 | | | |
| 7 | | | 6.1 | | |
| 8 | | | 9.5 | | |
| 9 | | | | 12.4 | |
| 10 | | | | 6.7 | |
| 11 | | | | 10.29 | |
| 12 | | | | 8.50 | |
| 13 | | | | | 7.6 |
| 14 | | | | | 9.0 |

# APPENDIX A.3

## PHYSICAL PROPERTIES OF A NOVEL GLASS-CERAMIC-REINFORCED HYRDROXYAPATITE COMPOSITE

N.S. Parsons, K.A. Hing, T. Buckland, S.M. Best and W. Bonfield

IRC in Biomedical Materials, Queen Mary and Westfield College, Mile End Road, London E1 4NS, UK

## ABSTRACT

An investigation was performed with the objective of determining the effects of adding calcium-phosphate based materials of varying Ca:P ratios on the sintering characteristics and phase composition of hydroxyapatite. Samples were prepared from a commercially available hydroxyapatite (Plasma Biotal, U.K.) and two Ca-P additives, CAP1 and CAP2. Compacts were then pressed and sintered at 1300°C for 2 hours and characterised by measurements of linear shrinkage, density, and X-ray diffraction. The results were compared with those for pressed and sintered hydroxyapatite, which served as a control. The CAP2-HA underwent a greater degree of shrinkage and densification than both CAP1-HA and as-received HA, demonstrating its potential as a sintering aid. Furthermore, X-ray diffraction patterns demonstrated that there was minimal decomposition of the HA to TCP in the CAP2-HA than in the CAP1-HA, and preliminary strength tests indicated that the CAP2 additions reinforced the HA..

**KEYWORDS:** glass-ceramic, hydroxyapatite

## INTRODUCTION

Hydroxyapatite has been successfully used as a bone substitute material for the past thirty years[1]. However, due to its relatively poor mechanical strength, its use has been limited to non-major load-bearing applications. As a result, attempts have been made to reinforce hydroxyapatite with secondary phase additions such as calcium/phosphate-based glasses[2,3]. However, the improved mechanical properties obtained by secondary-phase reinforcement are often associated with decomposition of the HA to tricalcium phosphate (TCP), which may be undesirable due to the increased solubility of the latter *in-vivo*[4].

The mechanical integrity of dense hydroxyapatite is dependent upon a number of factors, including processing conditions, sample preparation, and the degree of densification during sintering. The present study aims to investigate the effects of varying the Ca:P ratio of the reinforcing secondary phase on the phase composition, densification and mechanical properties of the final composite material.

## MATERIALS AND METHODS

Two Ca-P additives were produced via a melt/crystallisation process of the precursors; material CAP1 had a Ca:P ratio of 0.5 and material CAP2 had a Ca:P ratio of 0.835. The raw materials were combined in a pestle and mortar and placed in a platinum-rhodium crucible for melting in the furnace at 1350°C for ~1 hour, followed by quenching onto a stainless steel plate.

Differential thermal analysis (DTA) was used to determine the thermal behaviour of the Ca-P additives. DTA was carried out using a Setaram Labsys DSC/DTA with a 1600°C sensor rod, at a ramp rate of 10°C.min$^{-1}$ in platinum crucibles, under a nitrogen atmosphere.

X-ray diffractometry (XRD) was performed to determine crystalline phase composition using a Siemens D-5000$^{TM}$ X-ray diffractometer measuring from 25 to 40° 2θ. Intensity data was collected using a scintillation counter, and the results were compared with JCPDS Ca-P standards.

Two composite powders (CAP1-HA and CAP2-HA) were prepared by wet-milling commercial HA in 300 ml of methanol for 24 hours in a ceramic ball mill with 2.5 wt% of the CAP1 and CAP2 additives respectively. The mixed powders were then dried and mechanically sieved through a 75 μm mesh. The resulting composites were uniaxially pressed at 85 MPa in a steel die using 5 g of powder to produce 30 mm diameter discs. The discs were placed in a furnace on an alumina tile and then fired at a rate of 5°C.min$^{-1}$ up to 1300°C , the temperature was held for 2 hours, followed by furnace cooling at a rate of 10°C.min$^{-1}$. As a control, discs were prepared from the as-received commercial HA powder using similar processing conditions.

The resulting sintered discs were characterised by calculating their linear shrinkage and apparent density, taken as an indication of the degree of densification achieved during sintering. XRD was performed to establish the crystalline phases present post-sintering.

All the discs were mechanically tested in biaxial flexure (in their as-sintered, unpolished state), using a concentric ring jig with a load ring diameter of 4 mm and an outer support ring diameter of 17 mm. The specimens were tested to failure on an Instron test machine (Instron 4464) at a crosshead speed of 1mm.min$^{-1}$ using a 2 kN load cell. The flexural strengths (in MPa) were calculated using the peak load at failure and the following relationship:

$$\sigma_{BFS} = \left\{ \left( \frac{3P}{2\pi t^2} \right) \cdot \left( 1.25 \ln \frac{d_s}{d_l} \right) \cdot \left( 0.75 \frac{d_s^2 - d_l^2}{2d^2} \right) \right\}$$

where $\sigma_{BFS}$ is the biaxial flexural strength (BFS) in MPa, $P$ is the load at failure in N, and $d_s$, $d_l$, $d$ and $t$ are the support ring diameter, the loading ring diameter, the specimen diameter and the specimen thickness respectively, in mm. A minimum of nine disks of each material were tested.

## RESULTS

CAP1 remained glassy when quenched, in contrast to CAP2, which crystallised spontaneously on cooling. DTA of the two materials is shown in Figure 1. Regions of interest are identified as A, B, C and D. Point A, at 467.5 °C, shows the onset of the glass transition in CAP1. Point B, at 557.4 °C shows the subsequent peak crystallisation temperature. This is followed by the melting of the crystalline phase, the onset of which is marked by C at 971°C. In CAP2, the crystalline material shows a melting endotherm whose onset is marked by D at 1197 °C. The starting composition of CAP2 (Ca:P ratio of 0.835) suggests that the inflection point at E may be indicative of a residual phosphate-based glass transition, followed by a crystallisation at point F. XRD of CAP2 as prepared, shown in Figure 2, demonstrates the crystalline phase to be $Ca_2P_2O_7$.

Linear shrinkage measurements are given in Table 1, and showed that relative to HA, CAP1-HA produced less shrinkage and CAP2-HA produced more shrinkage. These results are corroborated by the apparent density values, where the mean density of the sintered discs increased when HA was combined with CAP2 and decreased when HA was combined with CAP1.

XRD of the composites, shown in Figure 3, demonstrated the decomposition of HA to TCP in CAP1-HA. The diffraction pattern of CAP2-HA was similar to that of the sintered HA control material; there was minimal decomposition.

Mean BFS of the composites and the HA controls are shown in Figure 4, together with their standard deviations. These preliminary results indicate that additions of CAP1 were detrimental to the mechanical integrity of the composite, where as additions of CAP2 appeared to reinforce the as-received HA.

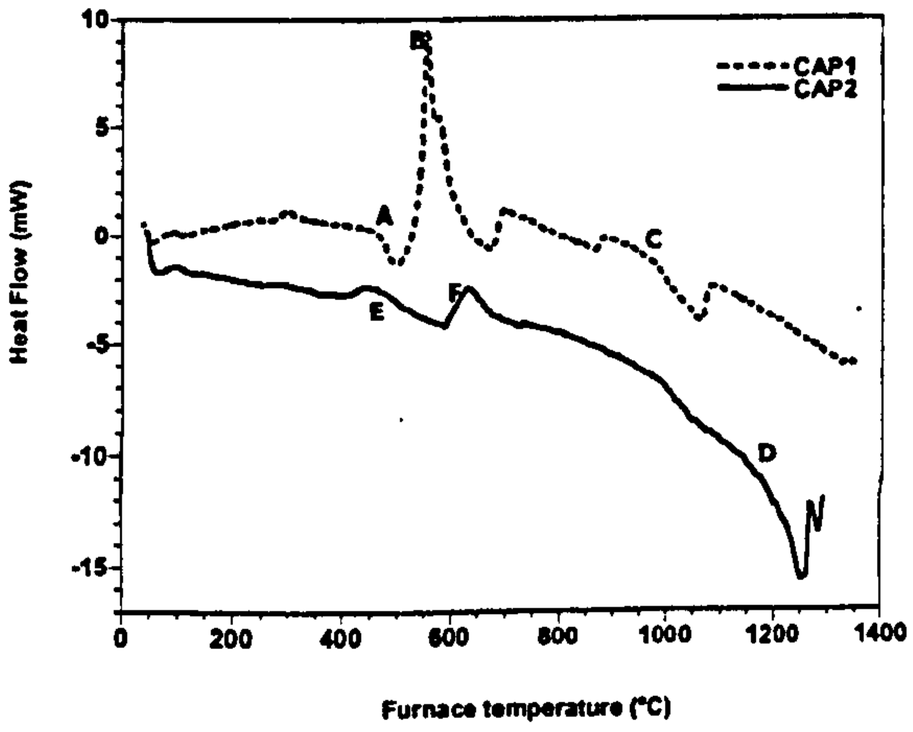


Figure 1: DTA traces for CAP1 and CAP2 materials

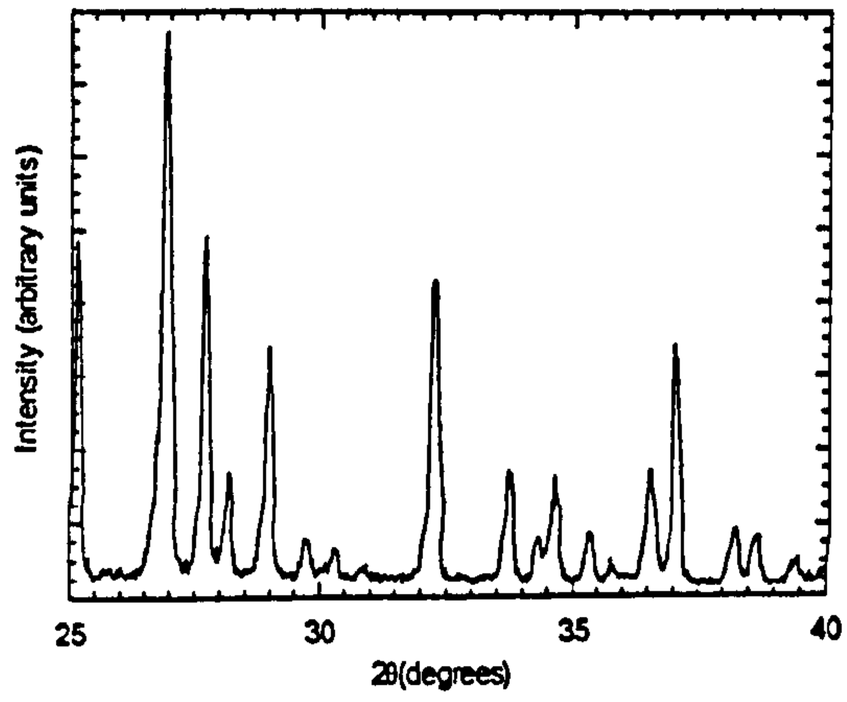


Figure 2: XRD pattern for CAP2, showing peaks characteristic of $Ca_2P_2O_7$

Table 1: Linear shrinkage measurements and mean density measurements of CAP1-HA, HA and CAP2-HA

| | HA | CAP1-HA | CAP2-HA |
|---|---|---|---|
| Linear shrinkage (%) | 18.3 | 13.6 | 19.3 |
| Mean apparent density ± SD ($g.cm^{-1}$) | 2.78 ± 0.04 | 2.54 ± 0.05 | 2.98 ± 0.06 |

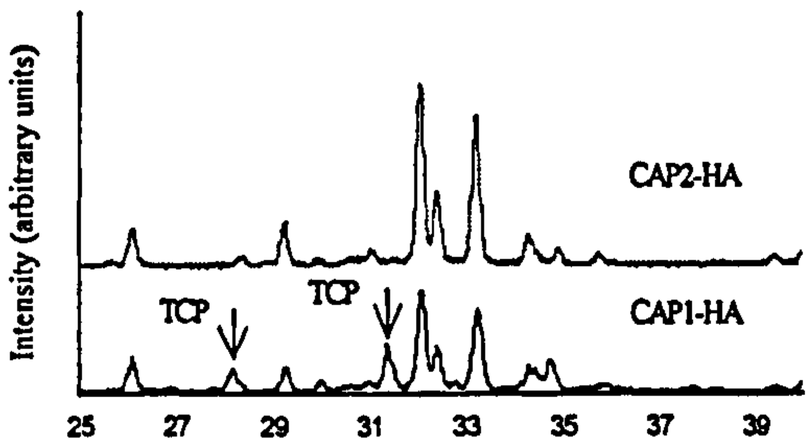


Figure 3: XRD patterns of the two sintered composites, CAP1-HA and CAP2-HA, showing HA decomposition to TCP in CAP1-HA

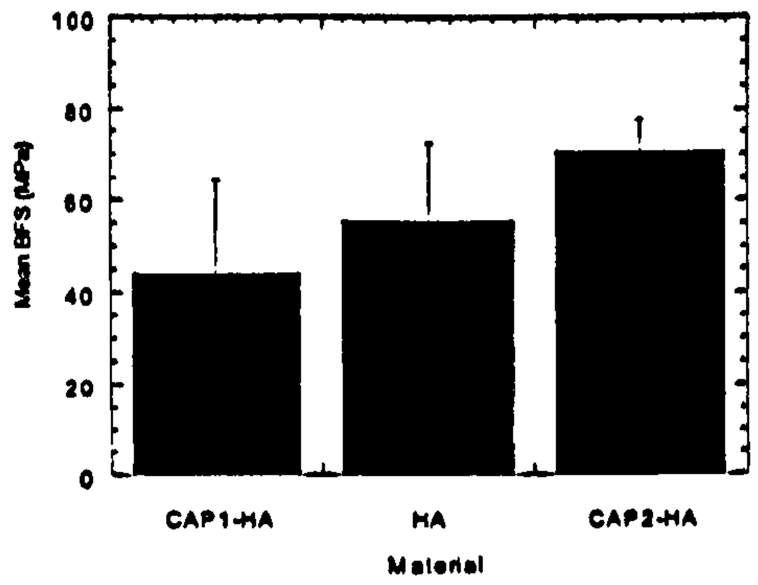


Figure 4: Mean and standard deviations of the biaxial flexural strengths measured for CAP1-HA and CAP2-HA, compared to that of sintered HA controls

## DISCUSSION

XRD of CAP2 (Ca:P ratio of 0.835) showed the presence of $Ca_2P_2O_7$, a crystalline phase with a Ca:P ratio of 1:1. This suggested that there were surplus phosphorus ions present in the material, forming a residual glassy phase (points E and F in Figure 1.) Furthermore, the associated deficiency of Ca ions is greater in CAP1 than CAP2, increasing the driving force for the decomposition of the as-received HA to TCP and CaO in CAP1-HA.

The greater degree of densification of CAP2-HA was attributed to liquid-phase sintering, possibly as a result of differences in viscosity between the liquid phases within the two composites at elevated temperature. This correlates with the mechanical data, whereby the composite that underwent the most densification also appeared to have the highest mean biaxial flexural strength.

## CONCLUSIONS

These results indicate that glass-ceramic reinforcement using a Ca:P ratio of 0.835 (CAP2) suppresses decomposition experienced by glass-reinforced samples with a Ca:P ratio of 0.5 (CAP1). Preliminary mechanical results demonstrated that CAP2 reinforcement resulted in an improvement in mechanical performance over not only the CAP1 samples but also the commercially available HA used in the composites.

## ACKNOWLEDGEMENTS

The support of the Engineering and Physical Sciences Research Council for funding of the IRC in Biomedical Materials is gratefully acknowledged.

## REFERENCES

[1] De Groot K, *Biomaterials* 1980; 1; 47
[2] Lopes MA, Santos JD, Monteiro FJ, Knowles JC, *J. Biomed. Mater. Res.* 1998; 39; 244-251
[3] Santos JD, Knowles JC, Reis RL, Monteiro FJ, Hastings GW, *Biomaterials* 1994; **15** (1)
[4] Eggli PS, Muller W, Schenk RK, *Clin. Orth. Rel. Res.* 1988; **232**; 127-138
[5] Levin EM, Robbins CR, McMurdie HF, "Phase diagrams for ceramicists", *The American Ceramic Society*, Ed. Reser MK, 1964